

A New Multi-Motor Drive System based on Two-Stage Direct Power Converter

Dinesh Kumar, M.Tech

GEORGE GREEN LIBRARY OF
SCIENCE AND ENGINEERING

Submitted to the University of Nottingham for the Degree of Doctor of Philosophy,
February 2011.

Abstract

The two-stage AC to AC direct power converter is an alternative matrix converter topology, which offers the benefits of sinusoidal input currents and output voltages, bidirectional power flow and controllable input power factor. The absence of any energy storage devices, such as electrolytic capacitors, has increased the potential lifetime of the converter.

In this research work, a new multi-motor drive system based on a two-stage direct power converter has been proposed, with two motors connected on the same shaft. A vector control scheme is proposed where each motor has an independent current control loop, but shares a single speed control loop. The two-motor on the same shaft solution has applications in aerospace to increase the availability of the system. The two-stage direct power converter therefore offers the possibility of a cost effective multi-motor drive system.

The feasibility and performance of the proposed multi-motor drive system is demonstrated through simulation results and validated with experimental results from a laboratory prototype.

Acknowledgements

I would like to thank my supervisors, Prof. Patrick Wheeler and Prof. Jon Clare of the Power Electronics, Machine and Control (PEMC) group at the University of Nottingham for their guidance and continuous support throughout the course of this research. I would like to express my sincere gratitude to Prof. Tae-Woong Kim, GyeongSang National University, South Korea for interesting discussion on motor control.

Thanks are due to all my friends and colleagues in the PEMC group for their continuous support and for providing such a pleasant working environment. I would like to especially thank Dr. Lee Empringham, Dr. Meng Yeong Lee, Ms Sudarat Khwan-on and Dr. Qiang Gao for their advices on practical issues, Dr. Liliana de Lillo and Dr. Dang Huy Quoc Si for their invaluable help and encouragement during my study.

Last but not least, my minds and thanks always go to my beloved wife, parents, brother and sister, who have always been enriching my life with their continuous support and love.

Contents

1. Introduction

1.1 Introduction.....	1
1.2 DC-AC Power Conversion.....	2
1.3 AC-DC Power Conversion.....	3
1.4 AC-DC-AC Power Conversions.....	5
1.5 Direct AC-AC Power Conversion.....	7
1.6 Multi-Motor Drive System.....	9
1.7 Research Objective.....	10
1.8 Thesis Outline.....	11

2. Overview of Direct AC-AC Power Conversion

2.1 Introduction.....	13
2.2 Overview of the Conventional Matrix Converter.....	13
2.3 The Two-Stage Direct Power Converter.....	17
2.3.1 Overview.....	17
2.3.2 Space Vector Modulation (SVM) for Two-stage Direct Power Converter.....	18
2.3.2.1 SVM for the Inversion Stage.....	19
2.3.2.2 SVM for the Rectification Stage.....	27

2.3.2.3 Synchronisation between the Rectification and the Inversion stage.....	35
2.3.3 The Bi-directional Switch Cell.....	41
2.3.4 Current Commutation Techniques for Direct Power Converter.....	45
2.3.4.1 The Output Current Direction based Commutation Technique.....	47
2.3.4.2 The Relative Input Voltage Magnitude based Commutation Technique.....	50
2.3.5 The Input Filter.....	52
2.4 Protection Issues for the Two-Stage Direct Power Converter.....	54
2.4.1 Over-Voltage Protection.....	54
2.4.2 The Clamp Circuit.....	55
2.4.3 Protection against Over-Voltage Caused by the LC Filter.....	56
2.5 The Advantages of the Two-Stage Direct Power Converter.....	57
2.6 Simulation Results.....	61
2.7 Conclusions.....	68

3. The Multi-Motor Drive Converter Topology based on Two-Stage Direct Power Converter

3.1 Introduction	69
3.2 Overview of the Multi-Motor Drive System.....	69
3.3 The Circuit Topology for Proposed Multi-Motor Drive Converter Topology.....	73
3.4 The Space Vector Modulation (SVM) for Multi-Motor Drive Converter Topology.....	75

3.5 Simulation Results..... 82
3.6 Conclusions..... 87

4. Multi-Motor Drive System

4.1 Introduction.....88
4.2 The Proposed Multi-Motor Drive System.....89
4.3 Induction Motor Control.....90
4.4 Scalar Control.....91
4.5 Vector Control.....92
 4.5.1 Vector Control of Separately Excited DC Motor93
 4.5.2 Vectors and Torque in Induction Motor.....94
 4.5.3 Vector Control Implementation.....97
 4.5.4 The Flux Angle.....105
 4.5.4.1 Direct Vector Control.....107
 4.5.4.2 Indirect Vector Control.....108
 4.5.5 Current Controller Design.....112
 4.5.6 Speed Controller Design.....113
 4.5.7 Voltage Compensation Terms.....114
4.6 Direct Torque Control.....116
4.7 Indirect Vector Control Scheme for Proposed Multi-Motor Drive
 System.....117
4.8 Simulation Results.....119
 4.8.1 Multi-Motor Drive System with an RL load for one Inverter and an
 Induction Motor for the other Inverter.....119

4.8.2 Multi-Motor Drive System Controlling two Induction Motors.....	125
4.8.3 Multi-Motor Drive System with two Induction Motors on same Shaft.....	132
4.8.4 Multi-Motor Drive System with two Induction Motors on same Shaft with one Motor Disable.....	138
4.9 Conclusions.....	143

5. Prototype Multi-Motor Drive System based on Two-Stage Direct Power Converter

5.1 Introduction.....	144
5.2 Structure of the Prototype Converter.....	144
5.3 Power Converter Design.....	146
5.3.1 Gate Drive Circuit.....	146
5.3.1.1 The Gate Drive Circuit for the Rectification Stage.....	147
5.3.1.2 The Gate Drive Circuit for the Inversion Stage.....	149
5.3.2 The Power Circuit.....	150
5.3.3 Input Filter Design.....	153
5.3.4 Voltage Sign Detection Circuit.....	156
5.3.5 Over-Voltage Clamp Circuit.....	158
5.4 The Control and Interface Circuit.....	159
5.4.1 Control Circuits: DSP and FPGA.....	159
5.4.2 Host PC Interface Board.....	162
5.4.3 The Encoder Interface Board.....	163

5.5 Conclusions.....	166
6. Prototype Practical Results	
6.1 Introduction.....	167
6.2 Experimental Results.....	167
6.2.1 Multi-Drive System based on Two-Stage Direct Power Converter...167	
6.2.2 Proposed Multi-Motor Drive System with Vector Control.....	172
6.3 Conclusions.....	188
7. Conclusions	
7.1 Conclusions.....	189
7.2 Future Work.....	191
Appendix-	
A. Parameters used in Simulation for Two-Stage Direct Power Converter.....	192
B. Parameters used in Simulation for Multi-Motor Drive Converter.....	193
C. Induction Motor Dynamic Equations.....	195
D. Parameters used in Simulation for Multi-Motor Drive System.....	198
E. Experimental Parameters for Multi-Motor Drive System	200

Contents

F. Published Papers.....	202
G. List of Symbols.....	203
Bibliography.....	206

List of Figures

Figure 1.1: A conventional three-phase inverter.....	2
Figure 1.2: Three-phase diode bridge rectifier.....	4
Figure 1.3: Active PWM rectifier.....	5
Figure 1.4: Diode rectifier based AC-DC-AC power converter.....	6
Figure 1.5: Active front end based AC-DC-AC power converter.....	6
Figure 1.6: The basic matrix converter circuit.....	8
Figure 1.7: The two-stage direct power converter circuit.....	9
Figure 1.8: Power converter arrangement for a multi-motor drive system.....	10
Figure 2.1: A three-phase conventional matrix converter circuit.....	15
Figure 2.2: Two-stage direct power converter.....	18
Figure 2.3: The equivalent circuit of the two-stage direct power converter.....	19
Figure 2.4: The equivalent circuit of the inversion stage.....	20
Figure 2.5: Inverter voltage hexagon formed by the valid switching combinations of the voltage source inverter.....	24

Figure 2.6: Output voltage reference vector synthesized in a given sector.....	24
Figure 2.7: The equivalent circuit of the rectification stage.....	28
Figure 2.8: Rectifier current hexagon formed by the valid switching combinations of the current source rectifier.....	32
Figure 2.9: Input current reference vector synthesized in a given sector.....	32
Figure 2.10: The switching pattern for the two-stage direct power converter.....	37
Figure 2.11: Switching combinations of rectification and inversion stages, in case the input current reference vector and out voltage reference vector are in sector 1...	40
Figure 2.12: The diode embedded bi-directional switch cell arrangement.....	42
Figure 2.13: The common emitter bi-directional switch cell arrangement.....	43
Figure 2.14: The common collector bi-directional switch cell arrangement.....	44
Figure 2.15: The reverse blocking IGBT bi-directional switch cell arrangement.....	45
Figure 2.16: A two-phase to single-phase matrix converter.....	47
Figure 2.17: The output current direction based four-step commutation technique.....	49
Figure 2.18: The relative voltage magnitude based four-step commutation technique....	51

Figure 2.19: The input filter configuration.....	52
Figure 2.20: A clamp circuit configuration for the two-stage direct power converter.....	55
Figure 2.21: The two-stage direct power converter topologies with reduced number of switches.....	59
Figure 2.22: A multi-drive system based on the two-stage direct power converter.....	60
Figure 2.23: Two-stage direct power converter with RL load.....	61
Figure 2.24: Simulation waveforms of the rectification stage of the two-stage direct power converter.....	64
Figure 2.25: Simulation waveforms of the inversion stage of the two-stage direct power converter for output frequency of 30Hz.....	66
Figure 2.26: Simulation waveforms of the inversion stage of the two-stage direct power converter for output frequency of 60Hz.....	67
Figure 3.1: The basic structure of a multi-motor drive system.....	70
Figure 3.2: A multi-motor drive converter based on an indirect AC-DC-AC converter ...	71
Figure 3.3: A multi-motor drive converter based on multi-pulse rectifiers.....	72
Figure 3.4: A multi-motor drive converter based on conventional matrix converters.....	73

Figure 3.5: A multi-motor drive converter based on the two-stage direct power converter topology.....	74
Figure 3.6: The switching pattern for the multi-motor drive converter topology.....	78
Figure 3.7: Possible switching pattern for inversion stage.....	79
Figure 3.8: Control hardware block-diagram for multi-motor drive converter.....	81
Figure 3.9 The simulation results for the multi-motor drive converter topology with output frequencies 40Hz and 60Hz.....	86
Figure: 4.1. Simplified block diagram of a two-motor drive system	88
Figure 4.2: The two-motor drive system based on a two-stage direct power converter...	90
Figure 4.3: Voltage versus frequency relation for V/f control.....	92
Figure 4.4: DC motor with inherent vector control.....	93
Figure 4.5: Three-phase induction motor model with position of stator current vector (I_s) and rotor flux vector (Ψ_r).....	95
Figure 4.6: Field orientation, where rotor flux vector (Ψ_r) aligned with field producing current (I_{sd}).....	96
Figure 4.7: d-q representation of AC induction motor.....	98

Figure 4.8: Vector control of induction motor.....99

Figure 4.9: Transformation from three-phase to stationary reference frame.....100

Figure 4.10: Transformation from stationary reference frame to rotating reference
frame.....101

Figure 4.11: Transformation from rotating reference frame to stationary reference
frame.....103

Figure 4.12: Transformation from the stationary reference frame to three-phase
quantities.....104

Figure 4.13: d-q representation of AC induction motor with field producing
current (I_{sd}).....106

Figure 4.14: Schematic for air-gap flux measurement used in the direct vector control of an
induction motor.....107

Figure 4.15: Schematic for flux angle measurement used for indirect vector control of
induction motor.....109

Figure 4.16: Indirect vector field oriented control scheme.....111

Figure 4.17: Block diagram of the design of current controller.....112

Figure 4.18: Block diagram of the speed controller.....113

Figure 4.19: Block diagram of the voltage compensation terms used for the vector control of an induction motor.....	116
Figure 4.20: The indirect vector field oriented control scheme for the proposed multi-motor drive system.....	118
Figure 4.21: The multi-drive converter system with an R-L load on inverter I1 and an induction motor load on inverter I2.....	121
Figure 4.22: Simulation results for multi-drive system when inverter I1 connected with R-L load and inverter I2 connected to an induction motor.....	125
Figure 4.23: The multi-motor drive system with two induction motors.....	127
Figure 4.24: Simulation results for the multi-motor drive system.....	132
Figure 4.25: The multi-motor drive system with two induction motors connected to the same shaft.....	133
Figure 4.26: Simulation results for the multi-motor drive system with two induction motors connected to the same shaft.....	137
Figure 4.27: Simulation results for the multi-motor drive system with motor IM2 disabled after 0.4 seconds.....	142
Figure 5.1: Overall structure of the multi-motor drive converter prototype.....	145
Figure 5.2: The overview of the prototype power converter.....	146

Figure 5.3: Schematic diagram of the gate drive circuit for the bi-directional switch cells.....	147
Figure 5.4: The gate-drive circuit for one of the bi-directional switch cell in the rectification stage.....	149
Figure 5.5: Schematic of the gate drive circuit for unidirectional IGBT switch in the inversion stage.....	150
Figure 5.6: IGBT Switch module SK60GM123 used in the rectification stage.....	151
Figure 5.7: Internal circuit layout of IGBT module SK60GM123.....	151
Figure 5.8: The three-phase IGBT inverter bridge module SK35GD126ET used for the inversion stage.....	152
Figure 5.9: Internal circuit of the three-phase inverter bridge module (SK35GD126ET).....	152
Figure 5.10: Input filter for the multi-motor drive converter topology.....	153
Figure 5.11: Schematic to calculate the transfer function of input filter.....	154
Figure 5.12: Bode plot for input filter transfer function.....	156
Figure 5.13: Schematic diagram for the voltage sign detection circuit.....	157
Figure 5.14: The over-voltage detection circuit.....	159

Figure 5.15: The FPGA board used for the prototype converter.....	160
Figure 5.16: The inputs and outputs connected to the FPGA board.....	161
Figure 5.17: The DSK6713 HP1 daughter card.....	162
Figure 5.18: Incremental encoder signals.....	163
Figure 5.19: Incremental encoder signals with inverted signals.....	164
Figure 5.20: Schematic of encoder interface circuit.....	165
Figure 6.1: Multi-motor drive system with induction motors on each inversion stage.....	168
Figure 6.2: Experimental waveforms for the multi-motor drive converter (output frequency for inverter I1 is 30Hz and output frequency for inverter I2 is 40Hz).....	171
Figure 6.3: The multi-motor drive system with two induction motors connected to the same shaft.....	173
Figure 6.4: Experimental waveforms for the multi-motor drive system with two induction motors connected on same shaft for steady state operation.....	176
Figure 6.5: Experimental waveforms for the multi-motor drive system with two induction motors connected on same shaft for transient operation.....	179
Figure 6.6: Experimental waveforms of the multi-motor drive system when speed reversal.....	183

Figure 6.7: Experimental results for the multi-motor drive system when induction motor
IM2 is disabled at 1.27 second.....187

List of Tables

Table 2.1 Definition of switching states for the voltage source inverter (VSI).....	20
Table 2.2 Switch states, valid switching combinations for the VSI and generated output phase voltages.....	23
Table 2.3 Switch states, valid switching combinations for the current source rectifier (CSR) and generated input phase currents.....	29

Chapter 1

Introduction

1.1 Introduction

Power Electronics has now firmly established its importance as indispensable tool in industrial process applications after decades of technological evolution. Power electronics has tremendous importance in aerospace, textiles, robotics, automobile and energy systems. An important aspect of power electronics applications is energy saving.

The era of modern power electronics began with the invention of the silicon-controlled-rectifier (SCR) by Bell Laboratories in 1956, which was later commercialised by the GE Company in 1958. Since then many new power semiconductor devices have emerged. Power electronic systems today incorporate power semiconductor devices as well as microelectronic integrated circuits [1]. The rapid development of solid-state devices in terms of power rating, improved performance, cost and size helps to expand the use of power electronics in a variety of electrical applications in commercial, industrial, residential, aerospace, telecommunications, transportation and power conversion [2].

The term, 'Converter System', in general, is used to denote a static device that converts AC-DC, DC-AC, DC-DC or AC-AC. A power electronics system consists of one or more power electronic converters and a power electronic converter is made up of some power semiconductor devices controlled by integrated circuits. The switching characteristics of power

1.2. DC-AC Power Conversion

semiconductor devices permit a power electronic converter to shape the input power of one form to output power of some other form [1].

The DC-AC and AC-AC power conversion techniques constitute the foundation of this work; therefore the following sections describe the concept of these techniques.

1.2 DC-AC Power Conversion

A DC-AC power converter is referred to as an inverter. In an inverter circuit a DC power supply is converted to a sinusoidal AC output with variable magnitude, frequency and phase.

Figure 1.1 shows the schematic diagram of a conventional three-phase inverter.

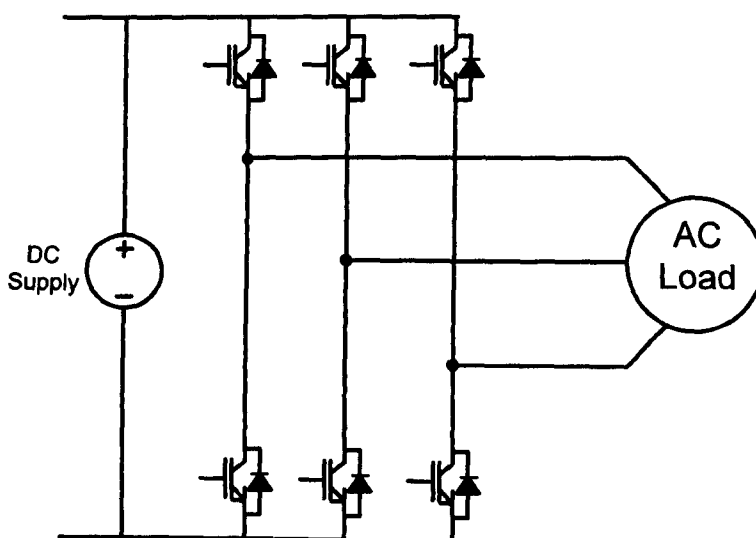


Figure 1.1: A conventional three-phase inverter

1.3. AC-DC Power Conversion

The switching frequency of the inverter is determined by the rate at which the semiconductor devices are switched ON and OFF according to the sequence specified by the modulation strategy such as carrier-based pulse-width modulation or space vector modulation. The output frequency seen by the load is significantly lower than the switching frequency and is an 'average' time weighted waveform formed by the modulation technique in response to a given reference signals[3].

Based on the type of DC power supply used, inverters can be classified into two-types: current source inverters (CSI) and voltage source inverters (VSI). The current source inverter is supplied with a current source. On the other hand, the voltage source inverter is powered from a DC voltage source such as a battery or capacitor.

1.3 AC-DC Power Conversion

A rectifier converts a three-phase AC voltage source to a DC voltage. Simple bi-stable devices, such as the diode or thyristor, can be used for this purpose. Figure 1.2 shows the schematic diagram for a three-phase diode bridge rectifier.

The main advantage of this topology is simple control and low cost, but due to diode bridge rectifier, the supply currents contains large amount of low order harmonics. In addition, diode bridge rectifier can generate only unidirectional power flow; therefore, this topology is not suitable for applications requiring regenerative operation.

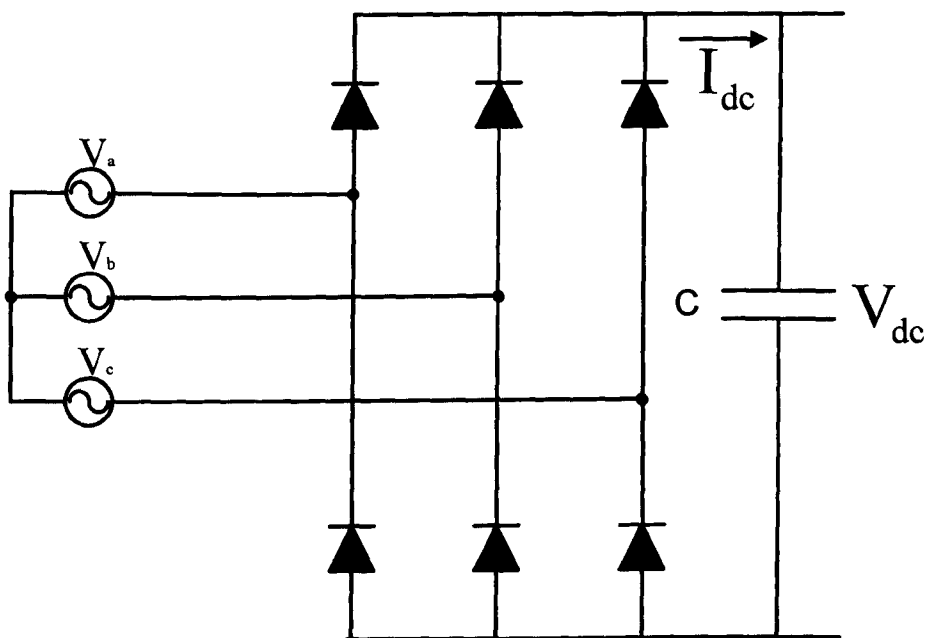


Figure 1.2: Three-phase diode bridge rectifier

An alternate solution is to replace the diode bridge rectifier with an active rectifier (also referred to as active front end) as shown in figure 1.3. The active Pulse Width Modulation (PWM) rectifier provides better input current waveforms, improved input power factor and allows bidirectional power flow. However, by using an active front end, the complexity of control is increased in comparison to the diode bridge rectifier. Also, the use of active devices in the active front end will result in higher losses, increased converter volume and increased cost.

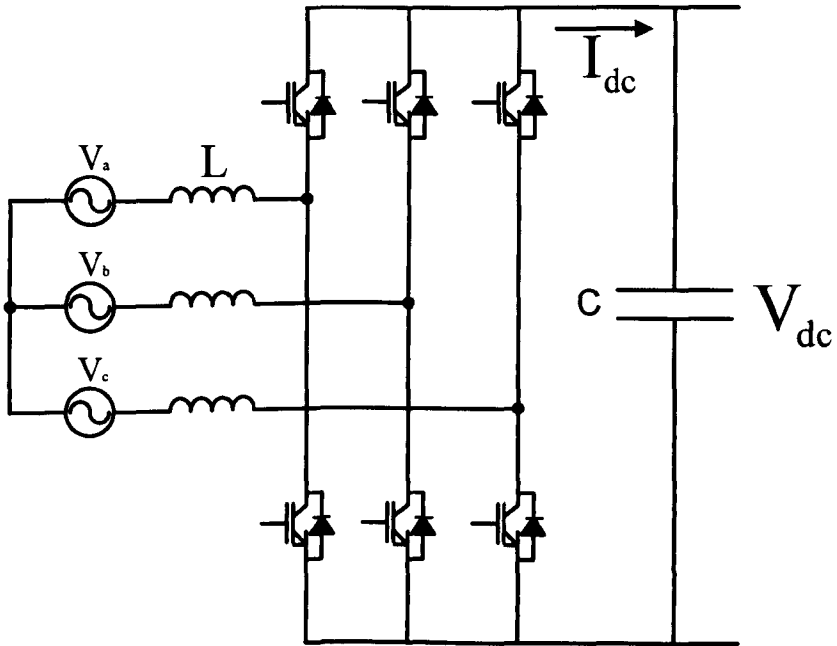


Figure 1.3: Active PWM rectifier

1.4 AC-DC-AC Power Conversions

An AC-DC-AC power converter is one of the most common approaches for AC to AC power conversion. Figure 1.4 shows a diode rectifier based AC-DC-AC power converter and figure 1.5 shows an active front end or back-to-back PWM inverter based AC-DC-AC power converter. In AC-DC-AC power converter the AC power is first converted into DC and stored in a large energy storage element. Then the stored DC energy is converted to the required AC output with variable amplitude and frequency.

1.4. AC-DC-AC Power Conversions

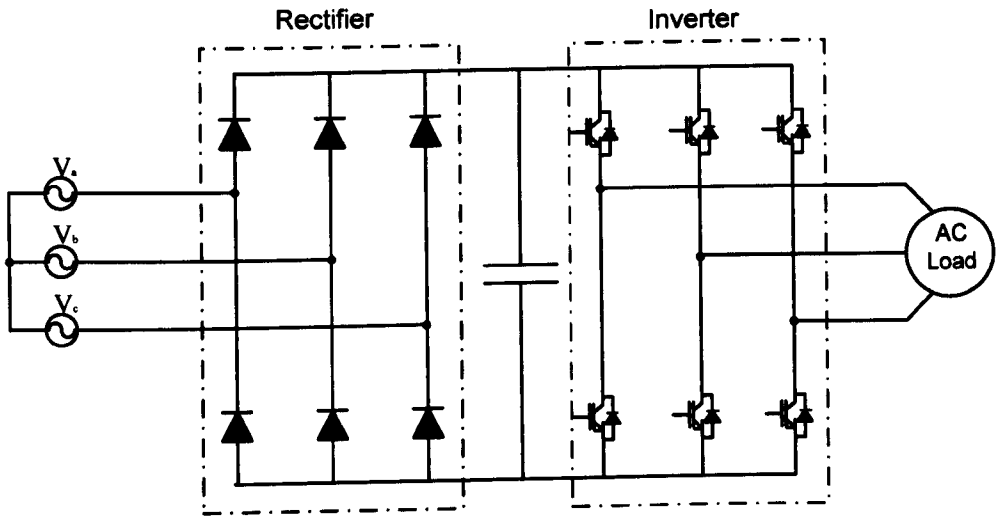


Figure 1.4: Diode rectifier based AC-DC-AC power converter

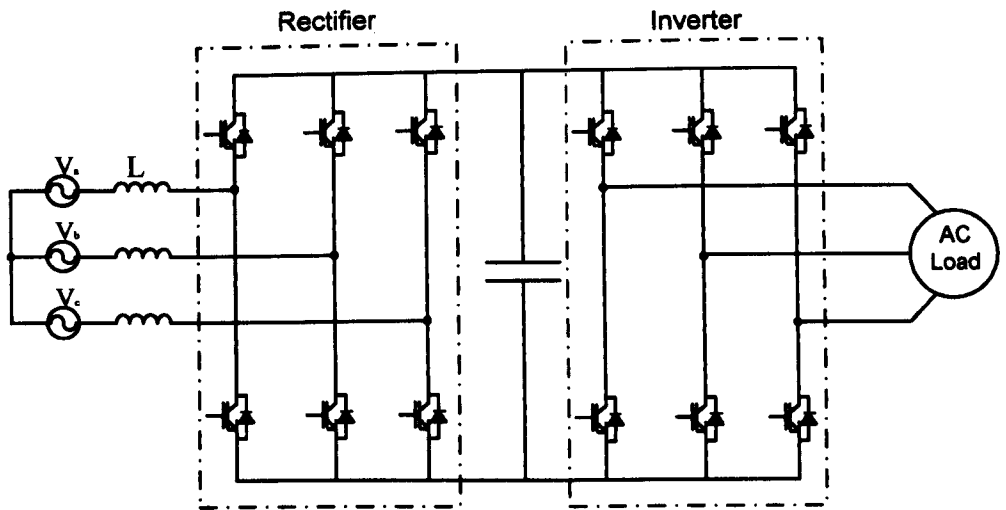


Figure 1.5: Active front end based AC-DC-AC power converter

1.5. Direct AC-AC Power Conversion

The AC-DC-AC converter uses a large energy storage element in the form of an electrolytic capacitor in the intermediate DC-link. Electrolytic capacitors have a short lifetime compare to other electronic components, therefore the overall converter lifetime is reduced. Also these energy storage elements are bulky and unreliable at high temperatures, which limit the converter applications. However, the amount of DC-link energy storage can be reduced as suggested in [4, 5], but this will result in the converter being more sensitive to grid disturbances.

The recent research has focused attention on the direct AC-AC power conversion technology, which eliminate the need for DC-link storage capacitors.

1.5 Direct AC-AC Power Conversion

The direct AC-AC power conversion refers to directly transfer from one form of AC power to another form of AC power without using any energy storage elements. Natural commutated cycloconverters were the first direct AC-AC converter topology [6]. In a cycloconverter, the input AC power is directly transferred into AC at a different frequency without any intermediate DC stage. The technique of cycloconversion was known in Germany in the 1930's, when Mercury-arc rectifiers were used to convert power from 50 Hz to 16.67Hz for railway transportation system. With the development of thyristor in the late 1950's, the first cycloconverter applications were in the variable-speed and constant-frequency supply system for aircraft [1]. The next important application was the variable-frequency induction motor drive [7]. The major advantage of natural commutated cycloconverters is elimination of a bulky DC-link, but the circuit has serious limitations on range of output frequencies and input power factor as well as distortion of the input and output waveforms.

1.5. Direct AC-AC Power Conversion

The improved solution for the above problem is 'Forced Commutated Cycloconverter' or 'Matrix Converter' shown in figure 1.6. This converter topology overcomes most of the limitation of naturally commutated cycloconverter. The matrix converter can generate sinusoidal supply current, adjustable input power factor and variable output voltage with unrestricted frequency from an AC voltage supply. The most important advantage of matrix converter topology is elimination of DC-link energy storage element, which enables the matrix converter to have a compact design that suits many applications like aerospace.

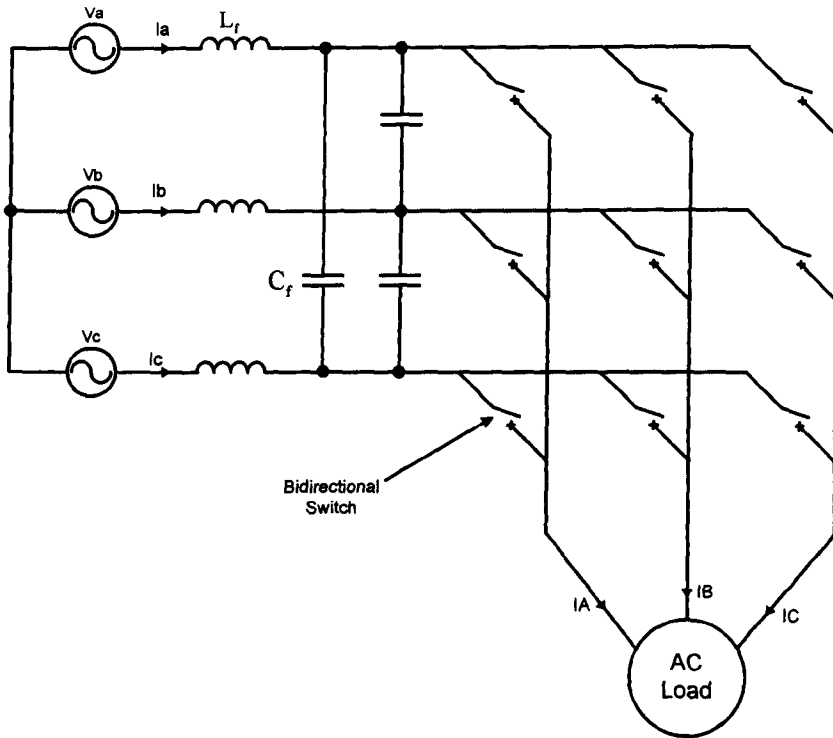


Figure 1.6: The basic matrix converter circuit

1.6 Multi-Motor Drive System

The two-stage direct power converter [8] is another direct AC-AC power conversion topology shown in figure 1.7. The two-stage direct power converter is the indirect form of the matrix converter, therefore it is also known as ‘Indirect Matrix Converter’ in some literature [9]. The two-stage direct power converter provides the same functionality as a conventional matrix converter, but also provides some additional benefits in comparison to conventional matrix converter, for example the possibility of a reduced number of switches as shown in figure 2.21 of Chapter-2 [8] and also offer the possibility of multi-drive systems [9].

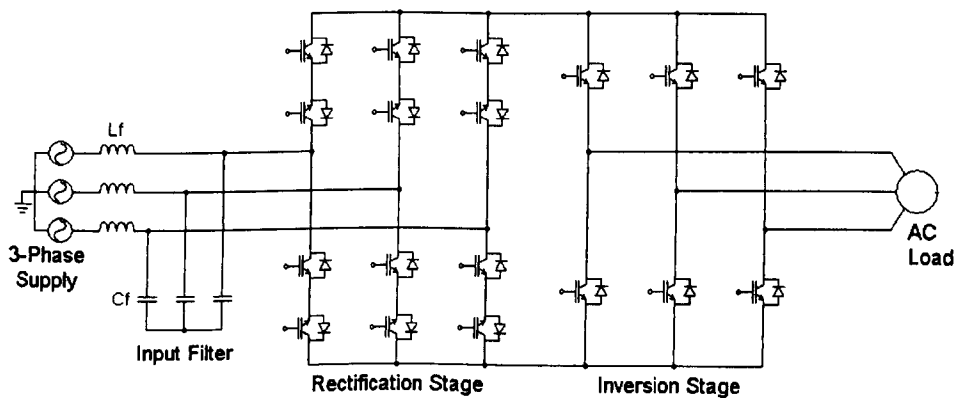


Figure 1.7: The two-stage direct power converter circuit

1.6 Multi-Motor Drive System

The advancement of power electronic applications in industry has changed the focus from issues related to building power converters to issues related to systems development and interaction between different power converters. A number of industrial systems now have several Adjustable Speed Drives (ASD) connected on the same DC-bus in a multi-drive configuration.

1.7. Research Objective

Figure 1.8 shows a schematic for a multi-motor drive system. The AC supply from the main source is rectified and then smother by DC-link capacitor [10].

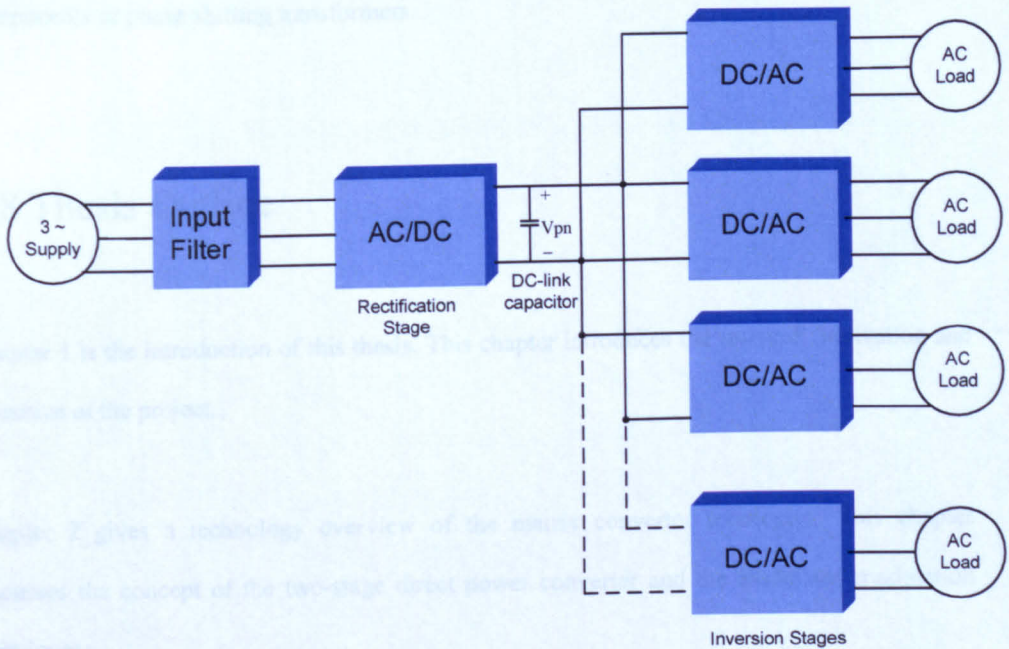


Figure 1.8: Power converter arrangement for a multi-motor drive system

1.7 Research Objective

The limitations of conventional multi-motor drive converter topologies are that they require DC-link components and maybe a phase shifting transformer. The bulky DC-link capacitors have a short life time compared to other power electronic components. As a result the overall converter lifetime is reduced. In application such as aerospace, where weight and volume are critical issues, these bulky DC-link capacitors are a significant disadvantage.

1.8. Thesis Outline

The objective of this research work is the development of multi-motor drive system for industrial and aerospace applications. This research work presents a complete application oriented multi-motor drive system based on the two-stage direct power converter, where two motors can be connected to the same shaft. This topology eliminates the need for any DC-link components or phase shifting transformers.

1.8 Thesis Outline

Chapter 1 is the introduction of this thesis. This chapter introduces the research motivation and objective of the project.

Chapter 2 gives a technology overview of the matrix converter topologies. This chapter discusses the concept of the two-stage direct power converter and the associated modulation techniques.

Chapter 3 discusses the operation principle and modulation strategy for multi-motor drive converter system based on two-stage direct power converter. Simulations results are presented to confirm the ability of the multi-motor drive converter topology.

Chapter 4 presents the proposed application oriented multi-motor drive system. Simulation results are presented to verify the operation of the complete multi-motor drive system.

Chapter 5 presents the hardware implementation for the two-stage direct power converter and multi-motor drive system. This chapter describes the overall structure of the prototype converter

1.8. Thesis Outline

and explains the design of each circuit in detail. The control platform for two-stage direct power converter and multi-motor drive system describe in detail.

Chapter 6 presents the experimental results from two-stage direct power converter prototype including operation as a multi-motor drive system.

Chapter 7 summarises the contribution for this research work and includes some suggestions for future work.

Chapter 2

Overview of Direct AC-AC Power Conversion System

2.1 Introduction

This chapter discusses the conventional matrix converter topology including its operating principles and modulation. This is followed by a detailed discussion about the two-stage direct power converter topology, including a full explanation of the space vector modulation technique and the input filter design. As bi-directional switches are employed in this converter, the switches arrangements, commutation techniques and protection issues are also discussed. The advantages of the two-stage direct power converter over the conventional matrix converter will be described at the end of the chapter.

2.2 Overview of the Conventional Matrix Converter

The basic principle of the matrix converter topology was proposed by Gyugi and Pelly in 1976 [11]. The name “Matrix Converter” arises because the converter consists of a matrix of bi-directional switches. The matrix converter is a direct AC-AC power converter, which can transform any supply frequency into a variable voltage and variable frequency output using the controlled bi-directional switches. The direct AC-AC power conversion principle of a matrix converter gives a distinct structure without any bulky DC-link capacitors. Due to this feature, the matrix converter topology can be implemented with compact size and volume compared to

2.2. Overview of Conventional Matrix Converter

the diode rectifier based Pulse Width Modulation Voltage Source Inverter (PWM-VSI) and the active front end PWM-VSI topologies. The DC-link capacitor typically occupies 30-50% of the total volume of a conventional converter [12]. In addition to its compact design, a matrix converter offers sinusoidal input current waveforms with unity displacement factor. The matrix converter provides an inherent bi-directional power flow capability, so that load energy can be regenerated back to the supply. Due to the absence of any DC-link capacitors the converter life time may be increased and the converter may be designed to operate at high temperature [13].

Figure 2.1 shows the circuit configuration for a three-phase, conventional matrix converter. The converter configuration is a 3 by 3 array of bidirectional switches, which are arranged so that any input line (a, b and c) can be connected to any output line (A, B and C) for any switching period. The switches are controlled in such a way that the average output voltage is a sinusoidal waveform of the required amplitude and frequency.

In a three-phase to three-phase matrix converter there are five hundred and twelve possible switching combinations. For safe commutation of current between bi-directional switches, two basic rules have to be followed to provide safe operation of the converter:

- The input phase must not be shorted, as this causes over-currents
- The output phase must not be open, as this causes over-voltages

These constraints can be expressed as:

$$S_{aj} + S_{bj} + S_{cj} = 1, \quad j \in \{A, B, C\} \quad (2.1)$$

2.2. Overview of Conventional Matrix Converter

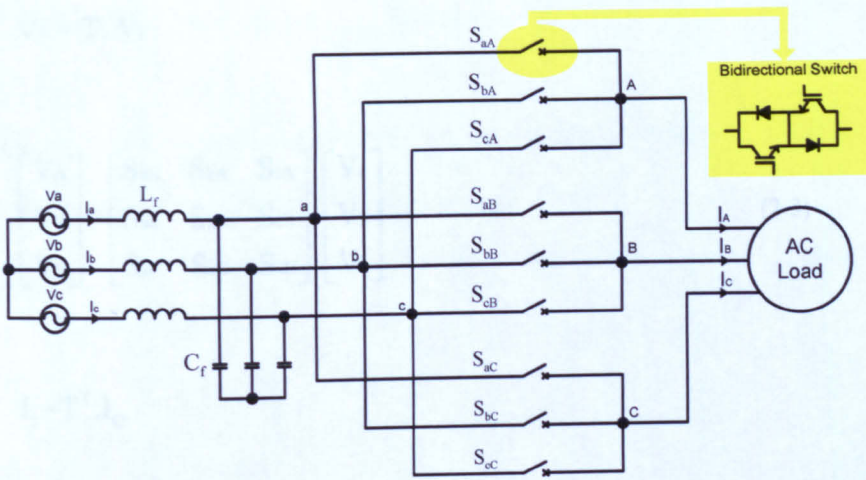


Figure 2.1: A three-phase conventional matrix converter circuit

where, S_{ij} is the switching function for a bidirectional switch, defined as:

$$S_{ij} \begin{cases} 1 & S_{ij} \text{ Closed} \\ 0 & S_{ij} \text{ Open} \end{cases} \quad i \in \{a,b,c\}, \quad j \in \{A,B,C\} \quad (2.2)$$

Using the basic rules mentioned above, the number of legal switches states is reduced to twenty seven. Three letter codes are used to describe which output phase is connected to which input phase. For example the switch state code [bca] refers to the state where the output phase A is connected to input phase b, output phase B is connected to input phase c and output phase C is connected to input phase a.

The instantaneous output voltages and input currents of a matrix converter can be represented by the switch state transfer function matrix, T:

2.2. Overview of Conventional Matrix Converter

$$V_o = T \cdot V_i$$

$$\begin{bmatrix} V_A \\ V_B \\ V_C \end{bmatrix} = \begin{bmatrix} S_{aA} & S_{bA} & S_{cA} \\ S_{aB} & S_{bB} & S_{cB} \\ S_{aC} & S_{bC} & S_{cC} \end{bmatrix} \cdot \begin{bmatrix} V_a \\ V_b \\ V_c \end{bmatrix} \quad (2.3)$$

$$I_i = T^T \cdot I_o$$

$$\begin{bmatrix} I_a \\ I_b \\ I_c \end{bmatrix} = \begin{bmatrix} S_{aA} & S_{aB} & S_{aC} \\ S_{bA} & S_{bB} & S_{bC} \\ S_{cA} & S_{cB} & S_{cC} \end{bmatrix} \cdot \begin{bmatrix} I_A \\ I_B \\ I_C \end{bmatrix} \quad (2.4)$$

where V_a , V_b and V_c are the input phase voltages, V_A , V_B and V_C are output phase voltages; I_a , I_b and I_c are the input currents and I_A , I_B and I_C are the output currents. The elements in the transfer matrix (T_{ij}) represent the switch function from the instantaneous input voltages to the instantaneous output voltages. The values of the elements of the transfer matrix assign in such a way to assure that the output voltages and input currents follow their reference values.

The conventional matrix converter has the following advantages:

- single stage AC-to-AC power conversion
- sinusoidal input currents and output voltages
- bi-directional power flow
- small passive components, which leads to a potential for good power density

2.3. The Two-Stage Direct Power Converter

The matrix converter also has some limitations:

- the voltage transfer ratio is lower than unity (0.866), therefore the circuit has not been considered for standard industrial applications
- nine bi-directional switch modules are needed in matrix converter, increasing cost and complexity

2.3 The Two-Stage Direct Power Converter

2.3.1 Overview

The requirement of large number of bi-directional switch modules in conventional matrix converter topology increases the cost and complexity in terms of commutation of the converter. To overcome this limitation a new idea to build a two-stage direct AC-AC power converter that works in the same way as a conventional matrix converter has been proposed [14, 15, 16]. Figure 2.2 shows the topology of a two-stage direct power converter, which consists of a current source type rectifier (CSR) at the supply side and a voltage source inverter (VSI) at the load side. The rectification stage, with six bi-directional switches, implemented as a three-phase to two-phase matrix converter. The output of the rectification stage is a switching 'DC-link' voltage (V_{pn}).

The inversion stage is a conventional VSI consists of six unidirectional switches. The inversion stage uses the variable DC-link voltage (V_{pn}) to generate the desired output voltage waveforms.

2.3. The Two-Stage Direct Power Converter

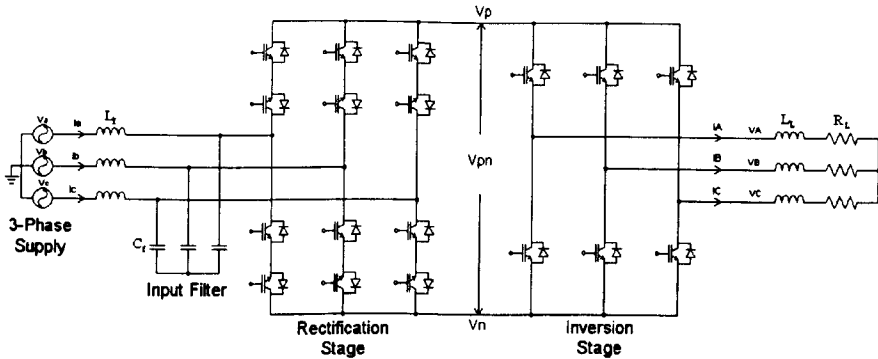


Figure 2.2: Two-stage direct power converter

2.3.2 Space Vector Modulation (SVM) for Two-Stage Direct Power Converter

In order to generate sinusoidal input and output waveforms, the two-stage direct power converter can be modulated using a SVM technique. The circuit of two-stage direct power converter consists of the current source rectifier and voltage source inverter, therefore the method of implementation of the SVM is very similar to one of the proposed methods for a conventional matrix converter. This section describes the implementation of SVM for the two-stage direct power converter using the symbols and conventions shown in figure 2.3.

The SVM implementation for a complete two-stage direct power converter can be divided into three parts:

- modulation of the inversion stage
- modulation of the rectification stage
- synchronization of rectification and inversion stages

2.3. The Two-Stage Direct Power Converter

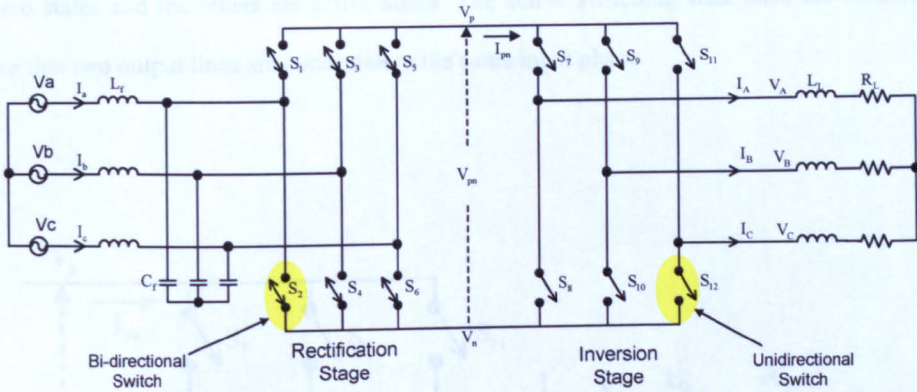


Figure 2.3: The equivalent circuit of the two-stage direct power converter

2.3.2.1 SVM for the Inversion Stage

This section describes the detail explanation of SVM for the inversion stage of the two-stage direct power converter. Consider the inverter part of the converter shown in figure 2.3 operating as a stand alone VSI supplied by a fixed DC source. In this case $V_{pn} = V_p + V_n$ as shown in figure 2.4

The operating status of switches in the inversion stage can be represented by switching states [17]. As shown in Table 2.1, the switching state ‘P’ denotes that the upper switch in the inverter leg is on and the inverter output terminal voltage (V_A , V_B or V_C) is positive, V_{pn} . A ‘O’ denotes that the lower switch in the inverter leg is on and inverter terminal output voltage is zero.

The eight possible switching states for the VSI are shown in Table 2.2. For example, the switching state [PPO] indicates switches S_7 , S_9 and S_{12} in the inverter legs A, B and C respectively are turned ‘ON’ and can conduct. Out of eight switching states, [PPP] and [OOO]

2.3. The Two-Stage Direct Power Converter

are zero states and the others are active states. The active switching state have the common feature that two output lines are connected to the same input phase.

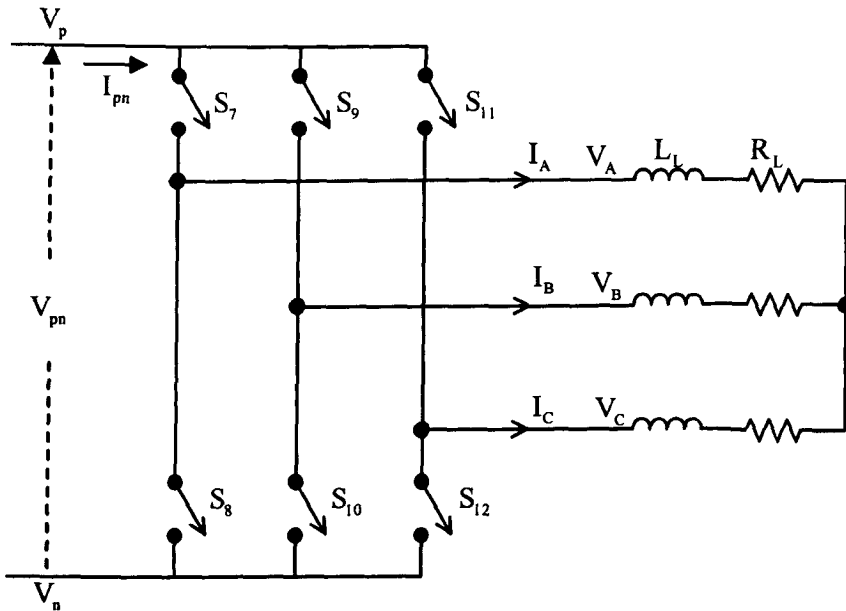


Figure 2.4: The equivalent circuit of the inversion stage

Switching State	Leg A			Leg B			Leg C		
	S_7	S_8	I_{AN}	S_9	S_{10}	I_{BN}	S_{11}	S_{12}	I_{CN}
P	ON	OFF	I_{pn}	ON	OFF	I_{pn}	ON	OFF	I_{pn}
O	OFF	ON	0	OFF	ON	0	OFF	ON	0

Table 2.1 Definition of switching states for the voltage source inverter (VSI)

2.3. The Two-Stage Direct Power Converter

The relationship between switching states and space vectors in a VSI can be derived by first assuming that the operation of the inverter gives a three-phase balanced set of output voltages, therefore:

$$V_A + V_B + V_C = 0 \quad (2.5)$$

where V_A , V_B and V_C are the load phase voltages.

Now the three-phase variables can be transformed equivalent two-phase variables in the α - β reference frame [18]:

$$\begin{bmatrix} V_{\alpha'} \\ V_{\beta'} \end{bmatrix} = \frac{2}{3} \begin{bmatrix} 1 & -\frac{1}{2} & -\frac{1}{2} \\ 0 & \frac{\sqrt{3}}{2} & -\frac{\sqrt{3}}{2} \end{bmatrix} \cdot \begin{bmatrix} V_A \\ V_B \\ V_C \end{bmatrix} \quad (2.6)$$

A space vector can be generally represented in terms of two-phase voltages in the α - β reference frame:

$$\bar{V} = V_{\alpha'} + V_{\beta'} \quad (2.7)$$

$V_{\alpha'}$ and $V_{\beta'}$ can be calculated from equation (2.6) and then substitute into equation (2.7):

$$\bar{V} = \frac{2}{3} [V_A e^{j0} + V_B e^{j2\pi/3} + V_C e^{j4\pi/3}] \quad (2.8)$$

As an example, active switching state [POO], the generated load phase voltages are:

2.3. The Two-Stage Direct Power Converter

$$V_A = \frac{2}{3} V_{pn}, V_B = -\frac{1}{3} V_{pn} \text{ and } V_C = -\frac{1}{3} V_{pn} \quad (2.9)$$

The corresponding space vector, represented by \bar{V}_1 , can be obtained by substituting equation (2.9) in equation (2.8):

$$\bar{V}_1 = \frac{2}{3} V_{pn} e^{j0} \quad (2.10)$$

Following the same procedure, all six active vectors can be derived as:

$$\bar{V}_K = \frac{2}{3} V_{pn} e^{j(K-1)\pi/3} \quad K = 1, 2, \dots, 6 \quad (2.11)$$

The final values of voltage vectors: $\bar{V}_1, \bar{V}_2, \dots, \bar{V}_6$ are shown in Table 2.2.

The zero vectors \bar{V}_0 can be formed using one of two possible switching states [PPP] and [OOO]. Note that zero and active vectors do not move in the reference space and thus they are known as stationary vectors. The reference vector V_{out} rotates along a circular trajectory with the frequency ω_o in the space vector diagram. This reference vector can be expressed as:

$$\bar{V}_{out} = V_{om} e^{j(\omega_o t - \phi_o)} = V_{om} \angle \theta_{out} \quad (2.12)$$

where, V_{om} is the magnitude and θ_{out} is the direction of the reference vector. The variable θ_{out} is equal to $(\omega_o t - \phi_o)$, where $\omega_o t$ is the angle of the output phase voltages and ϕ_o is an arbitrary angle.

2.3. The Two-Stage Direct Power Converter

Switch States	Switching Combinations						Output phase voltage			Space Vector
	S ₇	S ₉	S ₁₁	S ₈	S ₁₀	S ₁₂	V _A	V _B	V _C	
[PPP]	1	1	1	0	0	0	0	0	0	0
[OOO]	0	0	0	1	1	1	0	0	0	0
[POO]	1	0	0	0	1	1	$\frac{2}{3}V_{pn}$	$-\frac{1}{3}V_{pn}$	$-\frac{1}{3}V_{pn}$	$\frac{2}{3}V_{pn}e^{j0}$
[PPO]	1	1	0	0	0	1	$\frac{1}{3}V_{pn}$	$\frac{1}{3}V_{pn}$	$-\frac{2}{3}V_{pn}$	$\frac{2}{3}V_{pn}e^{j\frac{\pi}{3}}$
[OPO]	0	1	0	1	0	1	$-\frac{1}{3}V_{pn}$	$\frac{2}{3}V_{pn}$	$-\frac{1}{3}V_{pn}$	$\frac{2}{3}V_{pn}e^{j\frac{2\pi}{3}}$
[OPP]	0	1	1	1	0	0	$-\frac{2}{3}V_{pn}$	$\frac{1}{3}V_{pn}$	$\frac{1}{3}V_{pn}$	$\frac{2}{3}V_{pn}e^{j\frac{3\pi}{3}}$
[OOP]	0	0	1	1	1	0	$-\frac{1}{3}V_{pn}$	$-\frac{1}{3}V_{pn}$	$\frac{2}{3}V_{pn}$	$\frac{2}{3}V_{pn}e^{j\frac{4\pi}{3}}$
[POP]	1	0	1	0	1	0	$\frac{1}{3}V_{pn}$	$-\frac{2}{3}V_{pn}$	$\frac{1}{3}V_{pn}$	$\frac{2}{3}V_{pn}e^{j\frac{5\pi}{3}}$

Table 2.2 Switch states, valid switching combinations for the VSI and generated output phase voltages

2.3. The Two-Stage Direct Power Converter

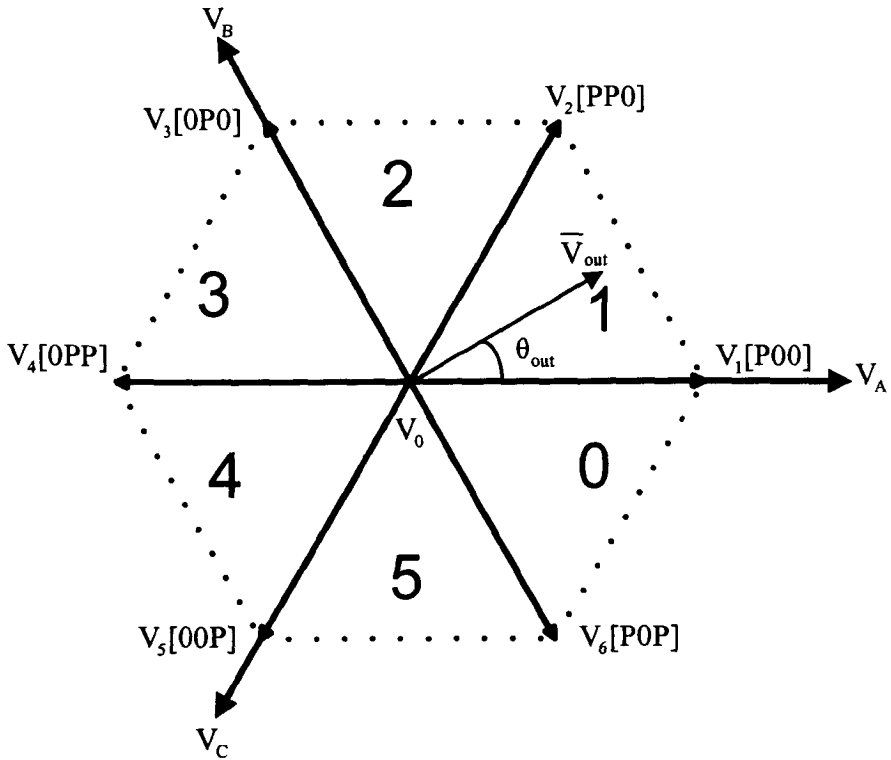


Figure 2.5: Inverter voltage hexagon formed by the valid switching combinations of the voltage source inverter

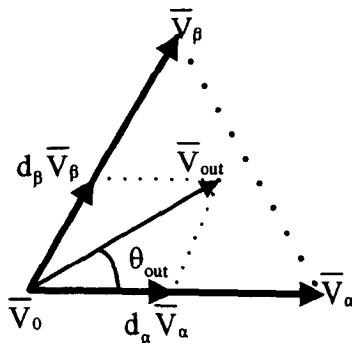


Figure 2.6: Output voltage reference vector synthesized in a given sector

2.3. The Two-Stage Direct Power Converter

The space vector diagram for a VSI is shown in figure 2.5. The eight space vectors can be configured as hexagon in a complex plane and arbitrary output reference vector \bar{V}_{out} lies within the hexagon and can be synthesized by a vector sum out of possible seven output voltage switching states vectors, V_0 to V_6 . The maximum possible amplitude of the output voltage reference vector \bar{V}_{out} is equal to the radius of inner circle of the hexagon which is $\sqrt{3}/2 (= 0.866)$ times the amplitude of active vector. For the two-stage direct power converter the reference output voltage can be generated by applying the SVM method based on the average value of the virtual DC-link.

Figure 2.6 shows the reference vector \bar{V}_{out} within a sector of the output voltage reference hexagon. \bar{V}_{out} can be synthesized by using the two adjacent active vectors, \bar{V}_α and \bar{V}_β with a duty cycle d_α and d_β respectively. Assuming that the sampling period T_s is sufficiently small, the reference vector \bar{V}_{out} can be considered to be constant during each sample period.

Therefore the volt-second balancing equations is:

$$\bar{V}_{out} T_s = \bar{V}_\alpha T_\alpha + \bar{V}_\beta T_\beta + \bar{V}_0 T_0 \quad (2.13)$$

$$\text{where } T_s = T_\alpha + T_\beta + T_0$$

T_α , T_β and T_0 are the switching times for the vectors \bar{V}_α , \bar{V}_β and \bar{V}_0 respectively.

$$\text{As, } \bar{V}_{out} = V_{om} e^{j\theta_{out}}, \bar{V}_\alpha = V_{pn} e^{j2\pi/3}, \bar{V}_\beta = V_{pn} e^{j4\pi/3} \text{ and } \bar{V}_0 = 0; \quad (2.14)$$

2.3. The Two-Stage Direct Power Converter

By substituting equation (2.14) into (2.13) and separating the real and imaginary parts:

$$\begin{aligned} \text{Re: } \quad V_{om}(\cos\theta)T_s &= \frac{2}{3}V_{pn}T_\alpha + \frac{1}{3}V_{pn}T_\beta \\ \text{Im: } \quad V_{om}(\sin\theta)T_s &= \frac{1}{\sqrt{3}}V_{pn}T_\beta \end{aligned} \quad (2.15)$$

Solving the equation (2.15) with $T_s = T_\alpha + T_\beta + T_o$ gives:

$$\begin{aligned} T_\alpha &= \frac{\sqrt{3}T_s V_{om}}{V_{pn}} \cdot \sin\left(\frac{\pi}{3} - \theta_{out}\right) \\ T_\beta &= \frac{\sqrt{3}T_s V_{om}}{V_{pn}} \cdot \sin\theta_{out} \quad \text{for } 0 \leq \theta < \pi/3 \end{aligned} \quad (2.16)$$

$$T_o = T_s - T_\alpha - T_\beta$$

Equation (2.16) can be expressed in terms of modulation index; m_1 :

$$\begin{aligned} T_\alpha &= m_1 \cdot T_s \cdot \sin\left(\frac{\pi}{3} - \theta_{out}\right) \\ T_\beta &= m_1 \cdot T_s \cdot \sin\theta_{out} \quad \text{for } 0 \leq \theta < \pi/3 \end{aligned} \quad (2.17)$$

$$T_o = T_s - T_\alpha - T_\beta$$

$$\text{where } m_1 = \frac{\sqrt{3}V_{om}}{V_{pn}} \quad (2.18)$$

2.3. The Two-Stage Direct Power Converter

Equation (2.17) is then manipulated to give the duty cycles:

$$d_{\alpha} = m_1 \cdot \sin\left(\frac{\pi}{3} - \theta_{\text{out}}\right)$$

$$d_{\beta} = m_1 \cdot \sin\theta_{\text{out}} \quad \text{for } 0 < \theta < \pi/3 \quad (2.19)$$

$$d_o = 1 - d_{\alpha} - d_{\beta}$$

where:

$$\frac{T_{\alpha}}{T_s} = d_{\alpha}, \quad \frac{T_{\beta}}{T_s} = d_{\beta} \quad \text{and} \quad \frac{T_o}{T_s} = d_o$$

The inverter duty cycles are synchronized with the rectification stage to give the complete switching pattern for the two-stage direct power converter.

2.3.2.2 SVM for the Rectification Stage

This section introduces SVM for the rectification stage of the two-stage direct power converter. Consider the rectifier part of the circuit shown in figure 2.3 as a stand alone CSR loaded with a DC current source I_{pn} , as shown in figure 2.7.

The rectification stage can be considered as a three-phase to two-phase matrix converter. The two output phases should provide a unipolar voltage whilst avoiding any short circuit of the supply. Therefore, the switching combinations of the rectification stage limited to the nine

2.3. The Two-Stage Direct Power Converter

shown in Table 2.3. For example, the switching state [ab] indicates switches S_1 and S_4 in the rectifier legs are turned 'ON' and can conduct. Out of nine switching states, [aa], [bb] and [cc] are zero switching states and the other set are active states.

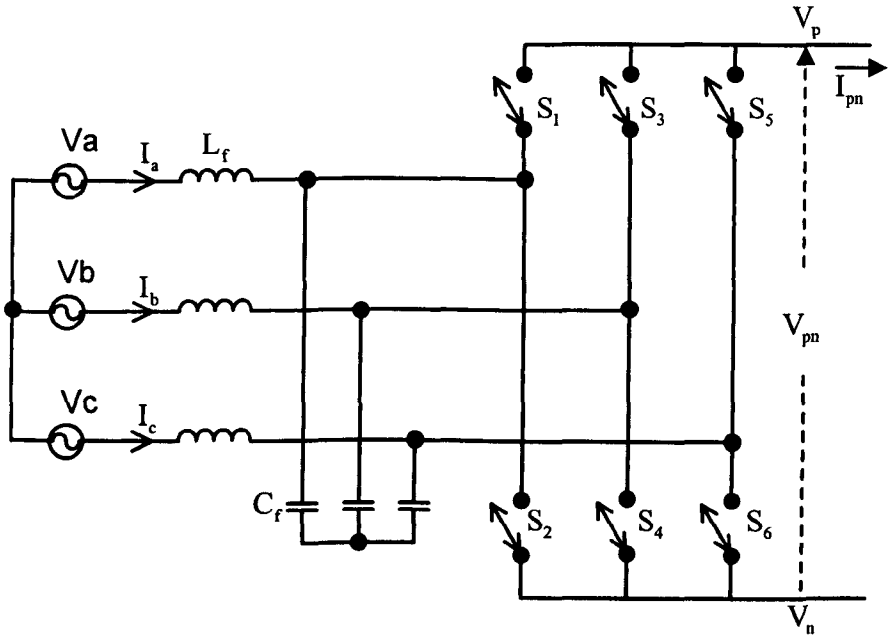


Figure 2.7: The equivalent circuit of the rectification stage

The relationship between the switching states and space vectors for the rectification stage can be derived by first assuming that the operation of the rectifier gives a three-phase balanced set of input current waveforms, therefore:

$$I_a + I_b + I_c = 0 \quad (2.20)$$

where I_a , I_b and I_c are the three input phase currents.

2.3. The Two-Stage Direct Power Converter

Switch States	Switching Combinations						Input Currents			Space Vector
	S ₁	S ₂	S ₃	S ₄	S ₅	S ₆	I _a	I _b	I _c	
[aa]	1	1	0	0	0	0	0	0	0	0
[bb]	0	0	1	1	0	0	0	0	0	0
[cc]	0	0	0	0	1	1	0	0	0	0
[ab]	1	0	0	1	0	0	I _{pn}	-I _{pn}	0	$\frac{2}{\sqrt{3}} I_{pn} e^{j\frac{\pi}{6}}$
[ac]	1	0	0	0	0	1	I _{pn}	0	-I _{pn}	$\frac{2}{\sqrt{3}} I_{pn} e^{j\frac{\pi}{6}}$
[bc]	0	0	1	0	0	1	0	I _{pn}	-I _{pn}	$\frac{2}{\sqrt{3}} I_{pn} e^{j\frac{\pi}{2}}$
[ba]	0	1	1	0	0	0	-I _{pn}	I _{pn}	0	$\frac{2}{\sqrt{3}} I_{pn} e^{j\frac{5\pi}{6}}$
[ca]	0	1	0	0	1	0	-I _{pn}	0	I _{pn}	$\frac{2}{\sqrt{3}} I_{pn} e^{-j\frac{5\pi}{6}}$
[cb]	0	0	0	1	1	0	0	-I _{pn}	I _{pn}	$\frac{2}{\sqrt{3}} I_{pn} e^{-j\frac{\pi}{2}}$

Table 2.3: Switch states, valid switching combinations for the current source rectifier (CSR) and generated input phase currents

2.3. The Two-Stage Direct Power Converter

The three-phase current variables can be transformed to equivalent two-phase variables in the α - β reference frame:

$$\begin{bmatrix} I_{\alpha'} \\ I_{\beta'} \end{bmatrix} = \frac{2}{3} \begin{bmatrix} 1 & -\frac{1}{2} & -\frac{1}{2} \\ 0 & \frac{\sqrt{3}}{2} & -\frac{\sqrt{3}}{2} \end{bmatrix} \begin{bmatrix} I_a \\ I_b \\ I_c \end{bmatrix} \quad (2.21)$$

A space vector can be generally represented in terms of two-phase currents in the α - β reference frame:

$$\bar{I} = I_{\alpha'} + I_{\beta'} \quad (2.22)$$

$I_{\alpha'}$ and $I_{\beta'}$ can be calculated from equation (2.21) and then substituted in equation (2.22):

$$\bar{I} = \frac{2}{3} [I_a e^{j0} + I_b e^{j2\pi/3} + I_c e^{j4\pi/3}] \quad (2.23)$$

As an example, the active switching state [ab], the generated input currents are:

$$I_a = I_{pn}, I_b = I_{pn} \text{ and } I_c = 0 \quad (2.24)$$

The corresponding space vector, represented by \bar{I}_1 , can be obtained by substituting equation (2.24) in equation (2.23):

2.3. The Two-Stage Direct Power Converter

$$\bar{I}_1 = \frac{2}{\sqrt{3}} I_{pn} \cdot e^{-j\pi/6} \quad (2.25)$$

The same procedure is applied to calculate the rest input current space vectors $\bar{I}_2, \bar{I}_3, \dots, \bar{I}_6$. The final values of these input current space vectors are shown in Table 2.3.

The zero vectors \bar{I}_0 can be formed using one of three possible switching states [aa], [bb] and [cc]. Note that the zero and active vectors do not rotate, and are known as stationary vectors. The reference vector \bar{I}_{in} rotates along a circular trajectory with the frequency ω_i . This reference vector can be expressed as:

$$\bar{I}_{in} = I_{im} e^{j(\omega_i t - \phi_i)} = I_{im} \angle \theta_{in} \quad (2.26)$$

where I_{im} is the magnitude and θ_{in} is the direction of the reference vector. The variable θ_{in} is equal to $(\omega_i t - \phi_i)$, where $\omega_i t$ is the angle of the output phase voltages and ϕ_i is an arbitrary angle.

Figure 2.8 shows the space vector diagram for the CSR. The nine space vectors can be configured as a hexagon in a complex plan and the arbitrary input reference vector \bar{I}_{in} lies within the hexagon and can be synthesized by a vector sum out of nine possible input currents switching space vectors, I_0 to I_6 .

Figure 2.9, shows the reference vector \bar{I}_{in} within a sector of the input current reference hexagon. \bar{I}_{in} can be synthesized by using the two adjacent active vectors \bar{I}_7 and \bar{I}_8 with duty

2.3. The Two-Stage Direct Power Converter

cycles d_7 and d_8 respectively. Assuming that the sampling time T_s is sufficiently small, the reference vector \bar{I}_{in} can be considered to be constant during each sample period.

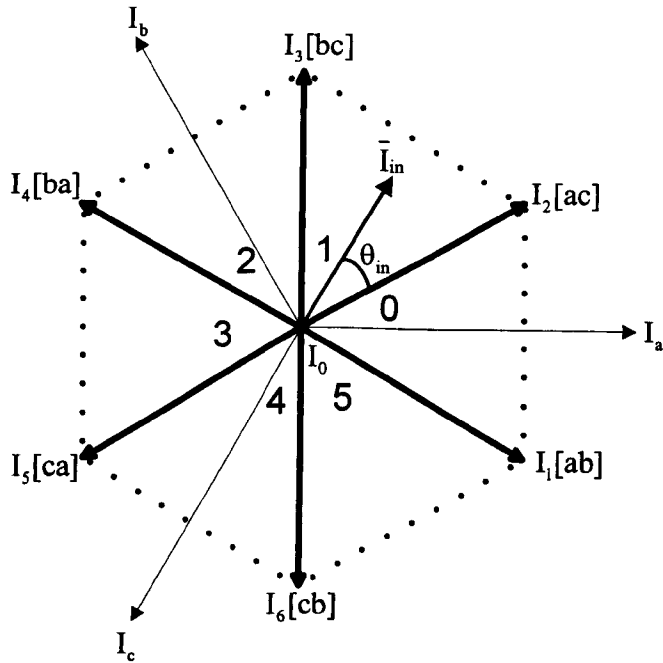


Figure 2.8: Rectifier current hexagon formed by the valid switching combinations of the current source rectifier

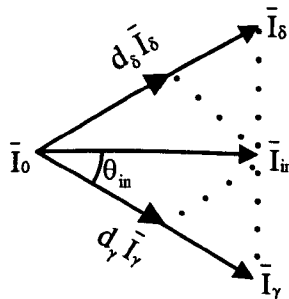


Figure 2.9: Input current reference vector synthesized in a given sector

2.3. The Two-Stage Direct Power Converter

Therefore, the current-second balancing equation is:

$$\bar{I}_{in} \cdot T_S = \bar{I}_\gamma \cdot T_\gamma + \bar{I}_\delta \cdot T_\delta + \bar{I}_0 \cdot T_0 \quad (2.27)$$

where $T_S = T_\gamma + T_\delta + T_0$

T_γ , T_δ and T_0 are the switching times for the vectors \bar{I}_γ , \bar{I}_δ and \bar{I}_0 respectively.

$$\bar{I}_{in} = I_{in} e^{j\theta_{in}}, \bar{I}_\gamma = \frac{2}{\sqrt{3}} I_{pn} e^{-j\pi/6}, \bar{I}_\delta = \frac{2}{\sqrt{3}} I_{pn} e^{j\pi/6} \text{ and } \bar{I}_0 = 0 \quad (2.28)$$

By substituting equation (2.28) into (2.27) and separating the real and imaginary parts, the final value of T_γ , T_δ and T_0 can be obtained as::

$$T_\gamma = \frac{\sqrt{3} T_S I_{in}}{I_{pn}} \sin\left(\frac{\pi}{3} - \theta_{in}\right)$$

$$T_\delta = \frac{\sqrt{3} T_S I_{in}}{I_{pn}} \sin\theta_{in} \quad \text{for } 0 \leq \theta < \pi/3 \quad (2.29)$$

$$T_0 = T_S - T_\gamma - T_\delta$$

2.3. The Two-Stage Direct Power Converter

Equation (2.28) can then be expressed in terms of a modulation index; m_R :

$$T_\gamma = m_R \cdot T_s \cdot \sin\left(\frac{\pi}{3} - \theta_{in}\right)$$

$$T_\delta = m_R \cdot T_s \cdot \sin\theta_{in} \quad \text{for } 0 \leq \theta < \pi/3 \quad (2.30)$$

$$T_o = T_s - T_\gamma - T_\delta$$

$$\text{where } m_R = \frac{I_{im}}{I_{pn}} \quad (2.31)$$

Equation (2.29) is then manipulated to give the duty cycles:

$$d_\gamma = m_R \cdot \sin\left(\frac{\pi}{3} - \theta_{in}\right)$$

$$d_\delta = m_R \cdot \sin\theta_{in} \quad \text{for } 0 < \theta < \pi/3 \quad (2.32)$$

$$d_o = 1 - d_\gamma - d_\delta$$

where:

$$\frac{T_\gamma}{T_s} = d_\gamma, \quad \frac{T_\delta}{T_s} = d_\delta \quad \text{and} \quad \frac{T_o}{T_s} = d_o$$

2.3. The Two-Stage Direct Power Converter

The rectification duty cycles are then used with the inversion state duty cycles to calculate the switching pattern of the two-stage direct power converter. The following section will describe the synchronization between the rectification and inversion stages for the modulation of complete two-stage direct power converter.

2.3.2.3 Synchronisation between the Rectification and the Inversion Stage

This section describes the combined modulation pattern for the complete two-stage direct power converter, using the proposed modulation schemes described in section 2.3.2.1 and 2.3.2.2 for the rectification and the inversion stage.

For the two-stage direct power converter topology, the rectification stage is modulated to supply the maximum average DC-link voltage in order to allow the maximum overall voltage transfer ratio. To achieve this, the modulation index for the rectification stage, m_R , is set to unity and the input displacement factor is set so that the currents are in phase with the supply voltages. To simplify the overall modulation of the two-stage direct power converter, only the modulation on the inversion stage produces zero vectors. The zero vectors in the rectification stage are not used and therefore the rectification switching sequence consists of only two adjacent currents vectors \bar{I}_γ and \bar{I}_δ . The duty cycles d_γ and d_δ for the rectification stage are determined by using equation (2.32) and then adjusted using (2.33) to occupy the whole of the switching period:

$$d_\gamma^R = \frac{d_\gamma}{d_\gamma + d_\delta}, \quad d_\delta^R = \frac{d_\delta}{d_\gamma + d_\delta} \quad (2.33)$$

2.3. The Two-Stage Direct Power Converter

The average DC-link voltage can then be calculated:

$$V_{\text{pn-avg}} = (d_{\gamma}^R \bar{V}_{\gamma} + d_{\delta}^R \bar{V}_{\delta}) \quad (2.34)$$

With the maximum DC-link voltage, $V_{\text{pn-avg}}$ supplied by the rectification stage, the modulation on the inversion stage controls the overall voltage transfer ratio. The maximum DC-link voltage, $V_{\text{pn-avg}}$ is used to compensate the modulation index of the inversion stage, m_1 :

$$m_1 = \frac{\sqrt{3} \cdot V_{\text{om}}}{V_{\text{pn-avg}}} \quad (2.35)$$

By selecting the appropriate vectors and determining their duty cycles, the modulation pattern combines the switching states of the rectification stage (\bar{I}_{γ} and \bar{I}_{δ}) and the inversion stage (\bar{V}_{α} , \bar{V}_{β} and \bar{V}_0) uniformly, producing the switching pattern for the complete two-stage direct power converter shown in figure 2.10. Consider an example where the input current vector \bar{I}_{in} and the output voltage vector \bar{V}_{out} both located in sector 1 of their space vector hexagon. The selected active current vectors for the rectification stage are \bar{I}_2 (\bar{I}_{γ}) and \bar{I}_3 (\bar{I}_{δ}) while the voltage vectors \bar{V}_{α} , \bar{V}_{β} and \bar{V}_0 are selected for the inversion stage.

2.3. The Two-Stage Direct Power Converter

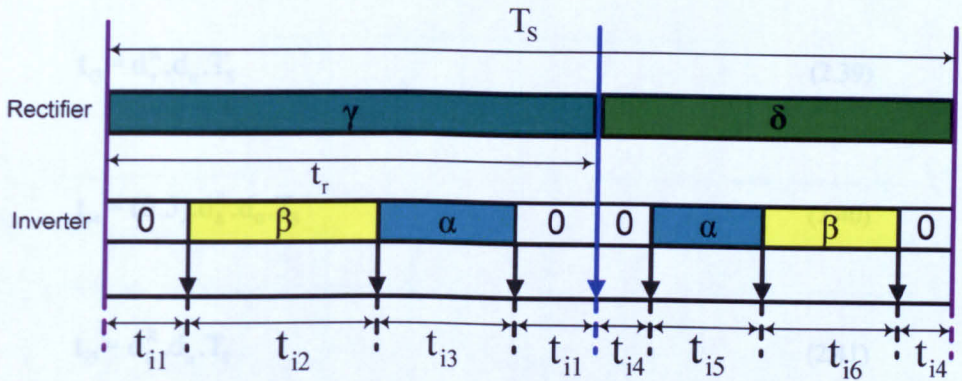


Figure 2.10: The switching pattern for the two-stage direct power converter

The minimum switching transition between each vector can be ensured by using the double-sided switching sequence for the selected voltage vectors. The switching sequence in this case is: $0-\beta-\alpha-0-0-\alpha-\beta-0$. The time interval for each vector in this switching sequence can be determined by using the following equations:

For the rectification stage:

$$t_r = d_\gamma^R \cdot T_s \quad (2.36)$$

For the inversion stage:

$$t_{i1} = 0.5 \cdot d_\gamma^R \cdot d_0 \cdot T_s \quad (2.37)$$

$$t_{i2} = d_\gamma^R \cdot d_\beta \cdot T_s \quad (2.38)$$

2.3. The Two-Stage Direct Power Converter

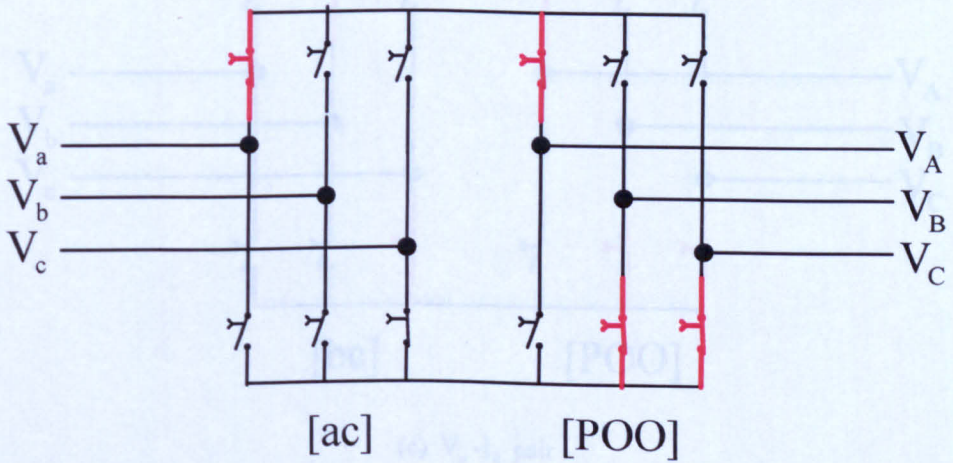
$$t_{i3} = d_{\gamma}^R \cdot d_{\alpha} \cdot T_S \quad (2.39)$$

$$t_{i4} = (0.5) \cdot d_{\delta}^R \cdot d_0 \cdot T_S \quad (2.40)$$

$$t_{i5} = d_{\delta}^R \cdot d_{\alpha} \cdot T_S \quad (2.41)$$

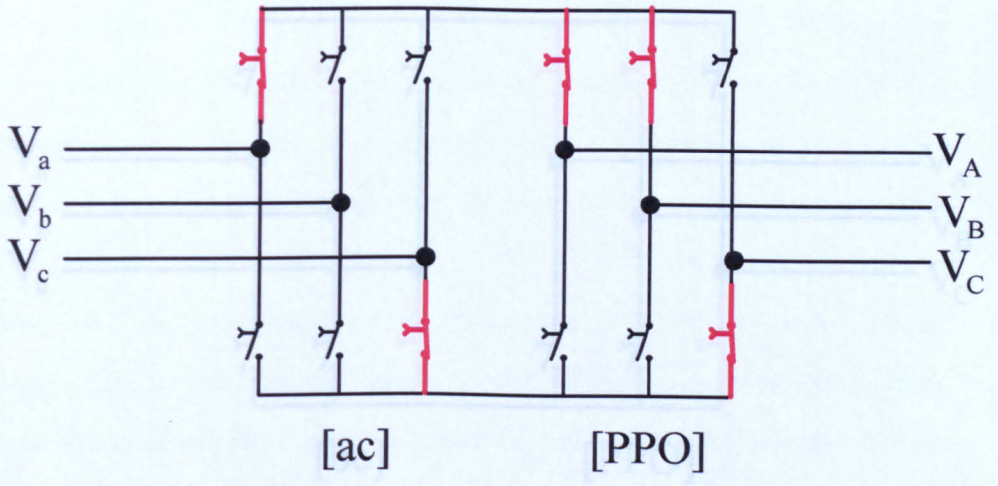
$$t_{i6} = d_{\delta}^R \cdot d_{\beta} \cdot T_S \quad (2.42)$$

The switching combinations of the two-stage direct power converter for this example are shown in figure 2.11.

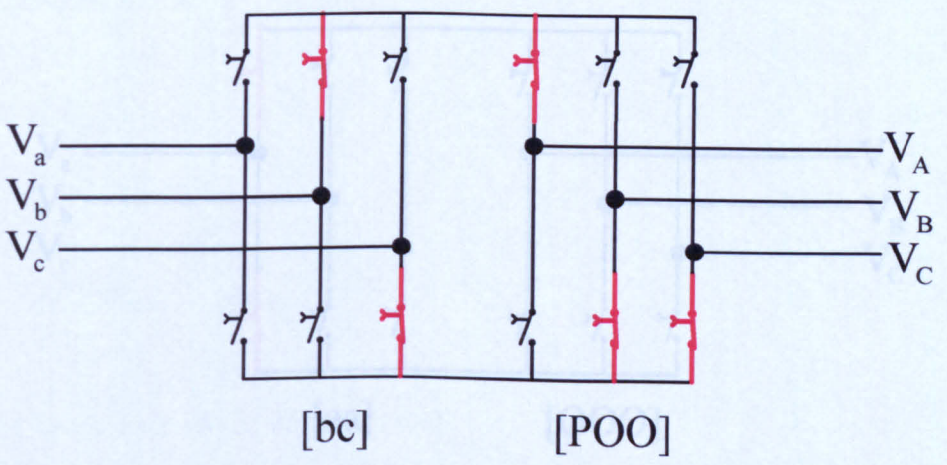


(a) V_{α} - I_{γ} pair

2.3. The Two-Stage Direct Power Converter



(b) V_β - I_γ pair

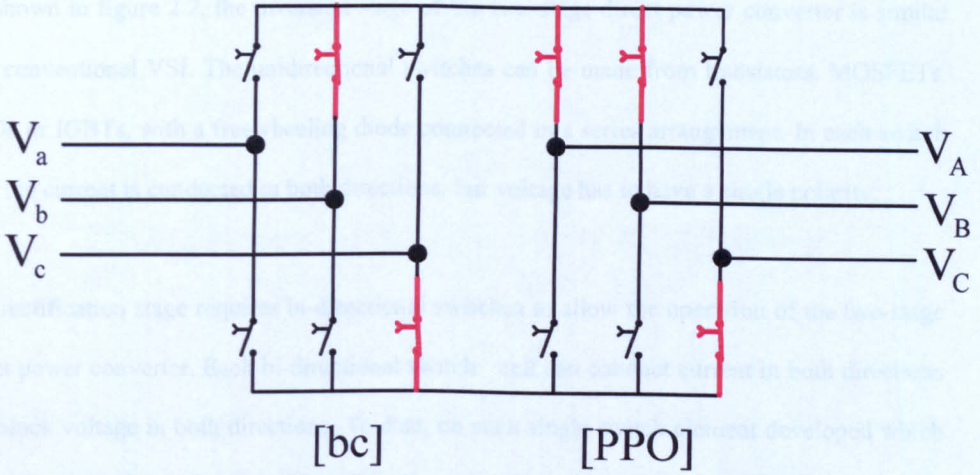


(c) V_α - I_δ pair

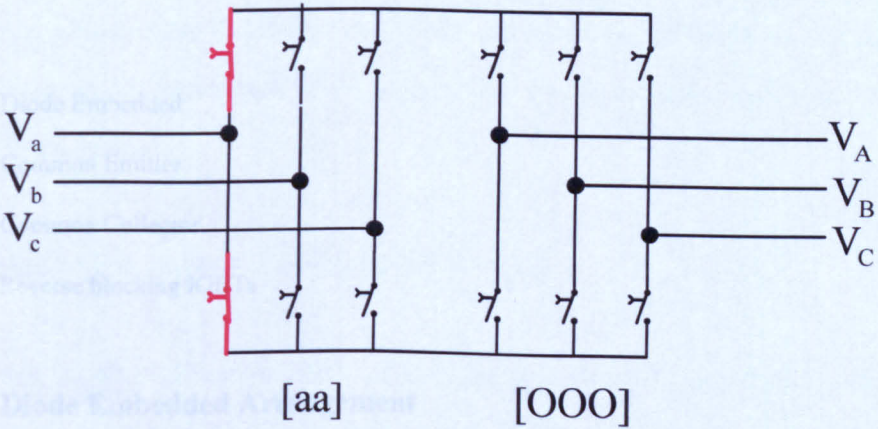
Figure 2.17: Switching combinations of two-legs and three-legs, in case the input current reference vector and the voltage reference vector are in sector 1

2.3. The Two-Stage Direct Power Converter

2.3.3 The Bi-directional Switch Cell



(d) V_β - I_δ pair



(e) V_0 - I_0 pair

Figure 2.11: Switching combinations of rectification and inversion stages, in case the input current reference vector and out voltage reference vector are in sector 1

2.3.3 The Bi-directional Switch Cell

As shown in figure 2.2, the inversion stage of the two-stage direct power converter is similar to a conventional VSI. The unidirectional switches can be made from transistors, MOSFETs, GTOs or IGBTs, with a freewheeling diode connected in a series arrangement. In each switch cell, the current is conducted in both directions, but voltage has to have a single polarity.

The rectification stage requires bi-directional switches to allow the operation of the two-stage direct power converter. Each bi-directional switch cell can conduct current in both directions and block voltage in both directions. To date, no such single switch element developed which has bi-directional switch capabilities. Therefore, the bi-directional switch has to be constructed using available discrete semiconductor devices.

There are four types of bi-directional switch cell arrangements which are commonly used in direct power converters:

- Diode Embedded
- Common Emitter
- Common Collector
- Reverse blocking IGBTs

(i) The Diode Embedded Arrangement

The diode embedded bi-directional switch cell arrangement is shown in figure 2.12. This cell consists of an IGBT which is connected at the centre of a single-phase diode bridge [19]. This switch cell has the characteristics of a true AC-switch: conducting current and blocking voltage in both directions.

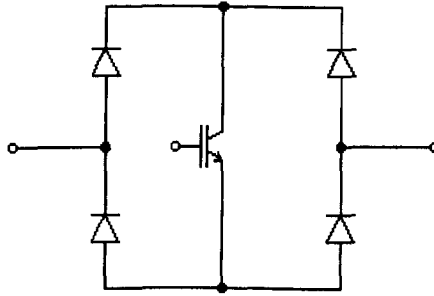


Figure 2.12: The diode embedded bi-directional switch cell arrangement

When the switch cell conducts; the current flows through one of the diodes at the input side, through the IGBT and through the opposite diode at the output side of the switch cell. The on-state voltage drop across this switch cell therefore equals two diode and one IGBT voltage drop. The control of the switch cell is limited to either 'ON' or 'OFF' by using the IGBT gate.

The requirement of a single gate drive circuit per switch cell is the advantage of this arrangement. Also only one IGBT is required to carry the current in both directions. The high conduction losses are the limitation of this arrangement, as each conduction path uses three semiconductor devices.

(ii) The Common Emitter Arrangement

The common emitter bi-directional switch cell arrangement is shown in figure 2.13. This cell consists of two IGBTs and two diodes which are connected in an anti-parallel arrangement. The function of diodes is to provide the reverse voltage blocking capability and the use of two IGBTs gives the independent control of the current direction within the switch cell. When the switch cell conducts the current flows through one IGBT and diode; T1 and D2 conduct during positive half cycle, T2 and D1 conduct during negative half cycle.

2.3. The Two-Stage Direct Power Converter

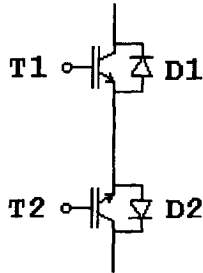


Figure 2.13: The common emitter bi-directional switch cell arrangement

The advantage of this switch arrangement, compared to diode embedded switch cell arrangement, is that only two devices conduct current at any instant in time so the conduction losses are lower.

The limitation of this switch arrangement is the requirement of two gate drive circuits to operate the IGBTs. Due to the common emitter arrangement only one isolated power supply is required for each bi-directional switch cell. Hence, to construct the rectification stage using common emitter bi-directional switch cells will require six isolated power supplies.

(iii) The Common Collector Arrangement

The common collector bi-directional switch cell arrangement is shown in figure 2.14. This cell is similar to the common emitter switch cell where two IGBTs connected with two anti-parallel diodes, but in this cell the IGBTs are connected in such a way that both share a common collector.

2.3. The Two-Stage Direct Power Converter

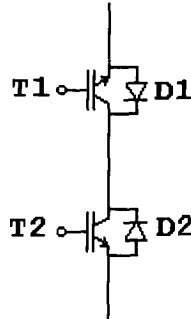


Figure 2.14: The common collector bi-directional switch cell arrangement

The common collector switch cell arrangement has the same conduction losses as the common emitter bi-directional switch cell arrangement. The advantage of this switch cell arrangement, compared to common emitter switch cell, is that the number of isolated power supplies required for the gate drive circuits can be reduced to five for the rectification stage of the two-stage direct power converter. This is possible only if the inductance between the devices sharing the same isolated power supply is low. This is the case for matrix converter modules where all bi-directional switches are integrated in one package [20]. However, as the power levels increase, the stray inductance of the individual bi-directional switches becomes more significant. For higher power converters it is desirable to package the IGBTs into individual bi-directional switches. Hence the common emitter configuration is usually preferred for higher power converters.

(iv) The Reverse Blocking IGBTs Arrangement

The anti-parallel reverse blocking IGBT bi-directional switch cell arrangement is shown in figure 2.15 [21]. In this switch arrangement the number of discrete semiconductor devices further reduced for the construction of the bi-directional switch cell. The main feature of the

2.3. The Two-Stage Direct Power Converter

reverse blocking IGBTs (RB-IGBT) is its reverse voltage blocking capability, which eliminates the use of diodes.

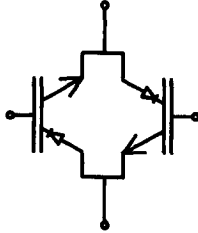


Figure 2.15: The reverse blocking IGBT bi-directional switch cell arrangement

The advantage of this switch arrangement is that the conduction losses are lower than for the other bi-directional switches arrangements. Practically, the limitation of this switch arrangement is that intrinsic diode associated with the IGBT has poor reverse recovery characteristics which can significantly increase the switching losses.

2.3.4 Current Commutation Techniques for Direct Power Converters

The non-ideal characteristics of the semiconductor devices cause a delay in switching, especially during turn-off. This delay may result short circuit when two switching devices change states. As a result, a large current could flow through a switch and damage the circuit. Hence, a specific commutation technique is required for the safe operation of the switches. The most common commutation techniques are the 'dead time' and 'overlap' commutation.

In dead time current commutation, small time gap is introduced between when the outgoing switch is turned 'OFF' and the incoming switch is turned 'ON'. During this time, both

2.3. The Two-Stage Direct Power Converter

incoming and outgoing switches are in the 'OFF' state. In the case of the two-stage direct power converter, the rectification stage uses the bi-directional switch cells, where no natural freewheeling path is available. Therefore, dead time can cause large over voltage across the semiconductors device due to absence of a path for the inductive load current. Hence, the dead time current commutation is not suitable for the rectification stage of two-stage direct power converter.

However, the inversion stage has a freewheeling diode connected in anti-parallel with each switching device, so a current path is always available for the energy stored in the load. Hence, the dead time commutation technique can be applied to each leg of the inversion stage.

In the overlap current commutation technique, the incoming switch is turned 'ON' before the outgoing switch is turned 'OFF'. This will cause a line to line short circuit during the overlap period resulting in the potential destruction of the converter. The short circuit current can be limited by adding an extra inductor in series to each supply phase. However, this would not be a sensible design as the converter input need to be capacitive in nature.

To commutate the current between bi-directional switch cells of the rectification stage, a complex commutation technique is required due to the lack of any natural freewheeling paths. The rectification stage is a three-phase to two-phase matrix converter where the input lines must never be short-circuited and the output lines must never be open-circuited. The most suitable bi-directional switch cells for use in the rectification stage are the common-emitter and the common collector switch arrangements shown in figures 2.13 and 2.14. The four-step commutation technique can be applied to commutate the current in these bi-directional switch cells. The implementation of the four-step commutation depends upon the output current direction or the relative input voltage magnitude. The following subsection describes the two variations of the four step commutation technique: the output current direction based

2.3. The Two-Stage Direct Power Converter

commutation technique [22] and the relative input voltage magnitude based commutation technique [19].

A two-phase to single-phase matrix converter, as shown in figure 2.16, is used to explain the principles of the four-step commutation process. The common emitter bi-directional switch cell arrangement is used as an example, but the methods can also be applied to a common collector switch cell arrangement.

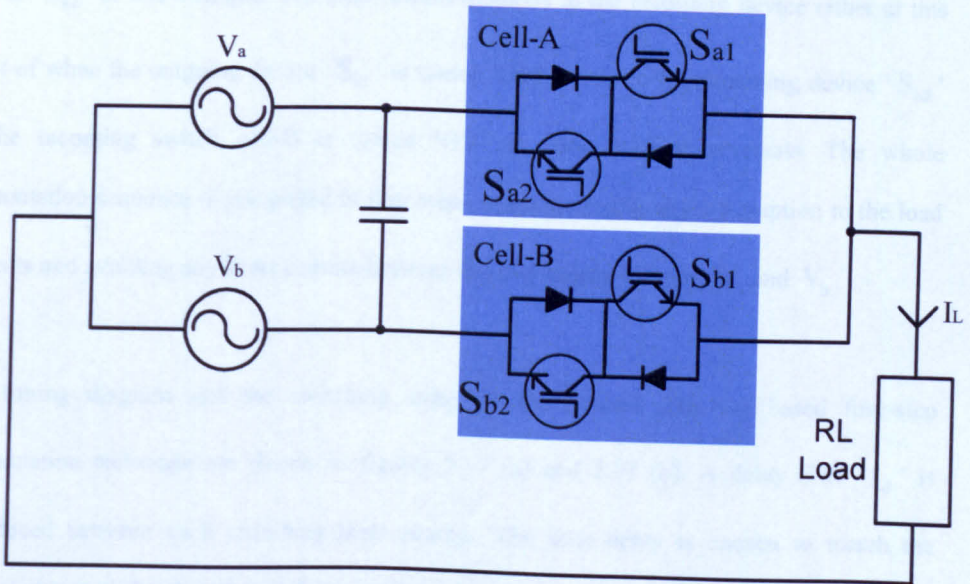


Figure 2.16: A two-phase to single-phase matrix converter

2.3.4.1 The Output Current Direction based Commutation Technique

In the output current direction based commutation technique, the four-step switching pattern depends on the direction of the load current (I_L). To implement this technique, the bi-directional switch cell must be designed in such a way as to allow the direction of the current flow in each switch cell to be controlled.

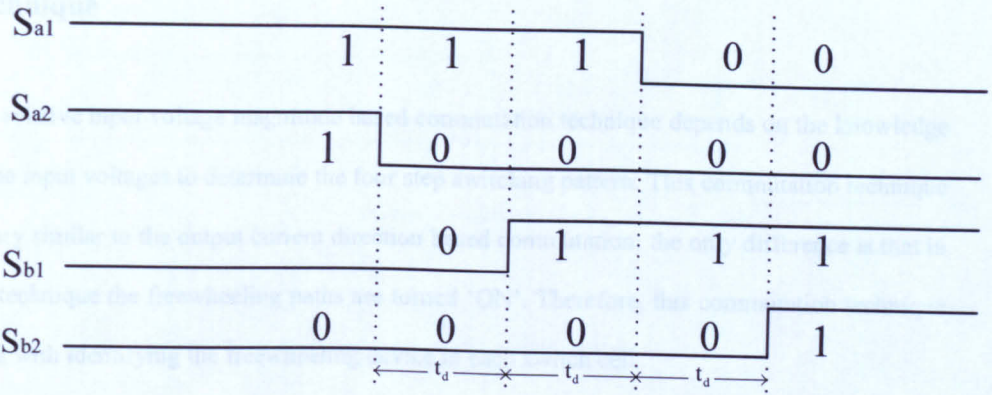
2.3. The Two-Stage Direct Power Converter

Figure 2.16 shows a two-phase to single-phase matrix converter, representing the two switch cells (A and B). In steady state, both of the devices in cell-A are initially 'ON' allowing the current to flow in both directions. The following explanation assumes that the load current is flowing in the direction where $I_L > 0$. When a commutation to cell-B is required, the current direction is used to determine which device in the outgoing switch cell-A is not conducting. This device is then turned off. In this case, device ' S_{a2} ' is not conducting so it is turned 'OFF'. The device that will conduct the current in the incoming switch cell-B is then turned 'ON', device ' S_{b1} ' in this example. The load current transfers to the incoming device either at this point of when the outgoing device ' S_{a1} ' is turned 'OFF'. Finally the remaining device ' S_{b2} ' in the incoming switch cell-B is turned 'ON' to allow current reversals. The whole commutation sequence is completed in four steps without causing any interruption to the load currents and avoiding any short circuits between the two supply sources, V_a and V_b .

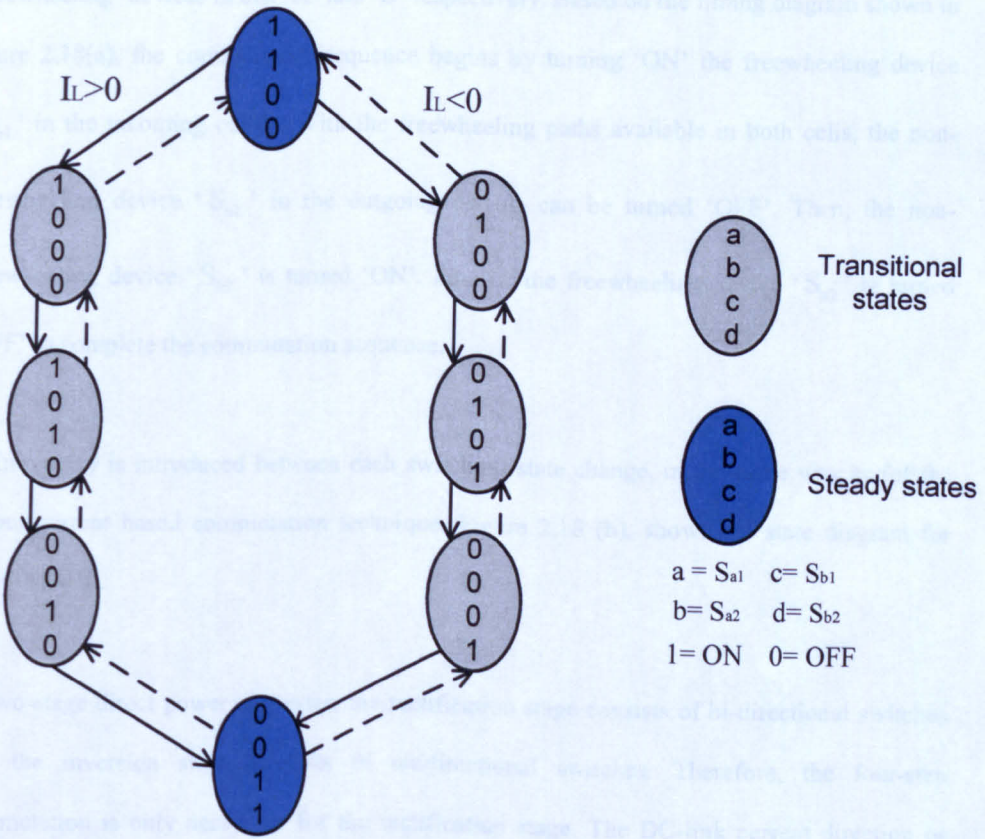
The timing diagram and the switching state for the current direction based four-step commutation technique are shown in figures 2.17 (a) and 2.17 (b). A delay time ' t_d ' is introduced between each switching state change. The time delay is chosen to match the characteristics of the chosen switching devices.

The current direction based commutation technique is dependant on the information of the load current direction. If a current transducer is used, it is not always possible to determine the direction of the current accurately; especially when the variation of the load current is very fast or the current level is very low in a high power converter. An accurate method to determine the direction of the current in a bi-directional switch arrangement was proposed in [23], but this method requires additional hardware and increases the complexity of the converter.

2.3. The Two-Stage Direct Power Converter



(a) The timing diagram for $I_L > 0$



(b) The states diagram

Figure 2.17: The output current direction based four-step commutation technique

2.3.4.2 The Relative Input Voltage Magnitude based Commutation Technique

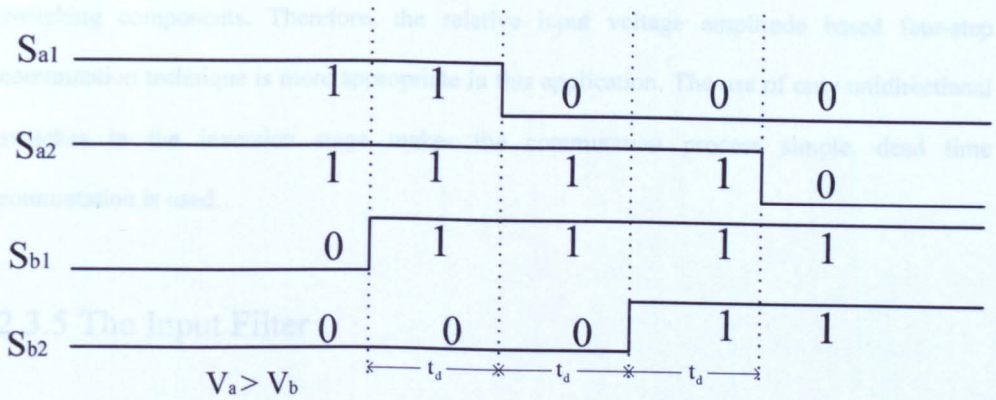
The relative input voltage magnitude based commutation technique depends on the knowledge of the input voltages to determine the four step switching pattern. This commutation technique is very similar to the output current direction based commutation; the only difference is that in this technique the freewheeling paths are turned 'ON'. Therefore, this commutation technique starts with identifying the freewheeling device in each switch cell.

Referring to figure 2.16, for the case where $V_a > V_b$, the device ' S_{a2} ' and ' S_{b1} ' are the 'freewheeling' devices in cell 'A' and 'B' respectively. Based on the timing diagram shown in figure 2.18(a), the commutation sequence begins by turning 'ON' the freewheeling device ' S_{b1} ' in the incoming cell-B. With the freewheeling paths available in both cells, the non-freewheeling device ' S_{a1} ' in the outgoing cell-A, can be turned 'OFF'. Then, the non-freewheeling device ' S_{b2} ' is turned 'ON'. Finally, the freewheeling device ' S_{a2} ' is turned 'OFF' to complete the commutation sequence.

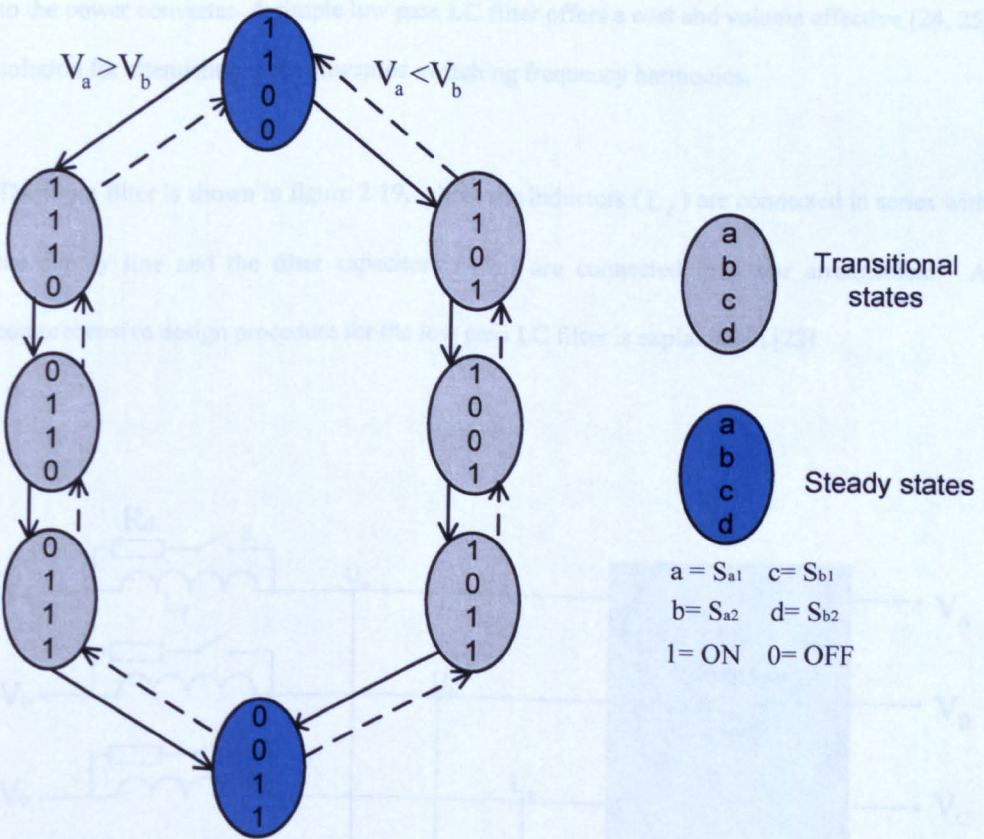
A time delay is introduced between each switching state change, in the same way as for the output current based commutation technique. Figure 2.18 (b), shows the state diagram for when $V_a > V_b$.

In two-stage direct power converter, the rectification stage consists of bi-directional switches and the inversion stage consists of unidirectional switches. Therefore, the four-step commutation is only necessary for the rectification stage. The DC-link current direction or relative magnitude of the input supply voltage can be used to implement the four-step commutation in the rectification stage.

2.3. The Two-Stage Direct Power Converter



(a) The timing diagram for $V_a > V_b$



(b) The states diagram

Figure 2.18: The relative voltage magnitude based four-step commutation technique

2.3. The Two-Stage Direct Power Converter

The accurate detection of current direction is difficult due to presence of high frequency switching components. Therefore, the relative input voltage amplitude based four-step commutation technique is more appropriate in this application. The use of only unidirectional switches in the inversion stage makes the commutation process simple, dead time commutation is used.

2.3.5 The Input Filter

The input current waveforms of the two-stage direct power converter contain switching frequency harmonics. These input current harmonics can be reduced by adding an input filter to the power converter. A simple low pass LC filter offers a cost and volume effective [24, 25] solution for attenuating these unwanted switching frequency harmonics.

The input filter is shown in figure 2.19, where the inductors (L_f) are connected in series with the supply line and the filter capacitors (C_f) are connected in a star arrangement. A comprehensive design procedure for the low pass LC filter is explained in [22].

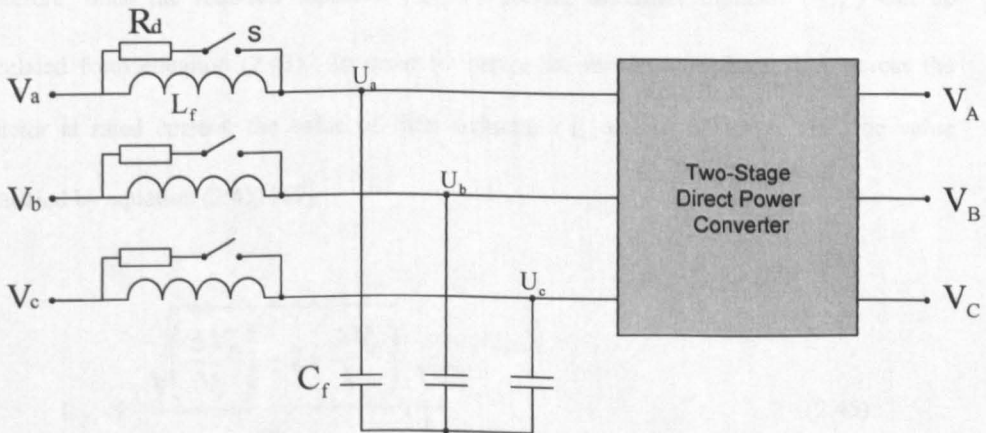


Figure 2.19: The input filter configuration

2.3. The Two-Stage Direct Power Converter

The resonant frequency (ω_o) for the input filter design can be described by following relationship:

$$\omega_o = \frac{1}{\sqrt{L_f C_f}} \quad (2.43)$$

In order to design a low pass filter, the resonant frequency (ω_c) must be lower than the switching frequency to provide considerable attenuation at the switching frequency.

The maximum filter capacitor ($C_{f,max}$) can be determined using the equation given below [19]:

$$C_f < C_{max} = \frac{P_{out} \cdot \tan(\phi_{i,max})}{3 \cdot V_i^2 \cdot \omega_i} \quad (2.44)$$

where P_{out} is the output power of the converter and $\phi_{i,max}$ is the maximum acceptable displacement factor. V_i and ω_i are the magnitude and frequency of the supply voltage. Therefore, once the required capacitor (C_f) selected, the filter inductor (L_f) can be calculated from equation (2.43). In order to ensure the minimum voltage drop across the inductor at rated current, the value of filter inductor (L_f) must be lower than the value calculated by equation (2.45) [19]:

$$L_f \leq \frac{\sqrt{\left(\frac{\Delta V_l}{V_r}\right)^2 - 2 \cdot \left(\frac{\Delta V_l}{V_r}\right)}}{\omega_i} \cdot \frac{V_r}{I_r} \quad (2.45)$$

2.4. Protection Issues for the Two-Stage Direct Power Converter

where ΔV_l is the maximum voltage drop across the filter inductor; V_r and I_r are the rated supply phase voltage and current respectively.

To design a low pass filter for direct power converter, a compromise between capacitor and inductor's size has to be made. The capacitor offer the high input power factor, but requires a large inductor to achieve the required cutoff frequency. However, the maximum permissible voltage drop (ΔV_l) limits the size of the inductor.

2.4 Protection Issues for the Two-Stage Direct Power Converter

One of most desirable feature of two-stage direct power converter is that it does not require any energy storage components; therefore no electrolytic capacitors are used. However, the absence of any energy storage components may cause over-current when the emergency shutdown of converter circuit or may be over-voltage during power-up procedure. Therefore, the protection circuit is implemented with the converter circuit to avoid any over-voltage or over-current during any abnormal situation. This section will describe the various protection circuit associated with the two-stage direct power converter circuit.

2.4.1 Over-Voltage Protection

In a two-stage direct power converter over-voltages can appear when the converter is disabled either from the input side or from the load side. At the input side, the over-voltage can occur due to line perturbations or transients due to the input filter during the power-up procedure. Over-voltage at the load side can occur due to the unexpected shut down of the converter, for

2.4. Protection Issues for the Two-Stage Direct Power Converter

example in an over-current situation. When all the bi-directional switches are turned 'OFF' there is no freewheeling path for the current to discharge the stored energy within the load inductance, causing an over-voltage. Therefore an additional protection circuit is required to protect the converter circuit from any damage. A clamp circuit is the most appropriate solution to avoid the over-voltage on input and the load side of the converter. The next section describes the clamp circuit for the two-stage direct power converter circuit.

2.4.2 The Clamp Circuit

The clamp circuit is a protection circuit used to protect the converter from over voltage either from the input side or from the load side [26]. The clamp circuit consists of eight fast recovery diodes with a clamp capacitor (C_c) and resistor (R_c) connected in parallel, as shown in figure 2.20.

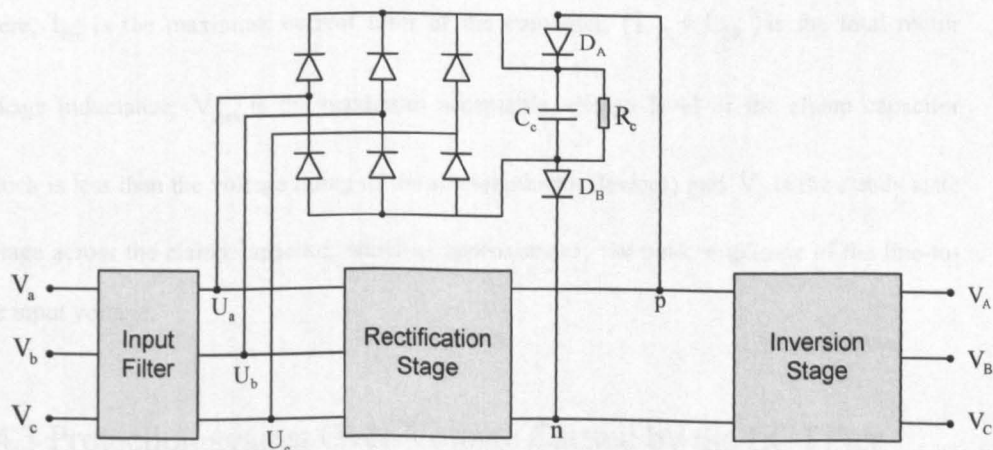


Figure 2.20: A clamp circuit configuration for the two-stage direct power converter

2.4. Protection Issues for the Two-Stage Direct Power Converter

During an over voltage situation on the input side, the fast recovery diodes provides the path for the current, which charge up the capacitor. The energy stored in the clamp capacitor is then dissipated by the resistor R_c . Two-anti-parallel diodes are connected to the inversion stage.

During over voltage situation on load side, diodes (D_A and D_B) provides a freewheeling path for the inductive load current charging up the clamp capacitor, which is then discharge by the parallel connected resistor.

A comprehensive analysis for the designing of the clamp circuit for matrix converters in induction motor applications was discussed in 1996[22]. The value of clamp capacitor (C_c) can be estimated by using the following equation:

$$C_c = \frac{3}{2} \frac{I_{lim}^2 (L_{\delta S} + L_{\delta R})}{V_{max}^2 - V_{ll}^2} \quad (2.46)$$

where, I_{lim} is the maximum current limit of the converter, $(L_{\delta S} + L_{\delta R})$ is the total motor leakage inductance; V_{max} is the maximum acceptable voltage level of the clamp capacitor (which is less than the voltage rating of the semiconductor devices) and V_{ll} is the steady state voltage across the clamp capacitor, which is approximately the peak amplitude of the line-to-line input voltage.

2.4.3 Protection against Over-Voltage Caused by the LC Filter

The low pass LC filter is used to filter out the input current harmonics, but this can cause some disruption during the power-up of the two-stage direct power converter due to start-up transients.

2.5. The Advantages of the Two-Stage Direct Power Converter

A method is suggested in [25] to avoid over-voltage problem by connecting a damping resistor 'R_d' with a switch 'S' in parallel with the inductor 'L_f' as shown in figure 2.19. The damping resistor 'R_d' has to be smaller than the choke reactance at the cut-off frequency:

$$R_d \leq 2\pi f_c L_f \quad (2.47)$$

The switch 'S' is at the closed position during the power-up. Due to small value of the damping resistance R_d, most of the current flows through it instead of the inductors which improve the waveforms during power-up process. Once the filter and the clamp capacitors are fully charged to the supply voltage, switch 'S' is turned 'OFF'.

2.5 The Advantages of the Two-Stage Direct Power Converter

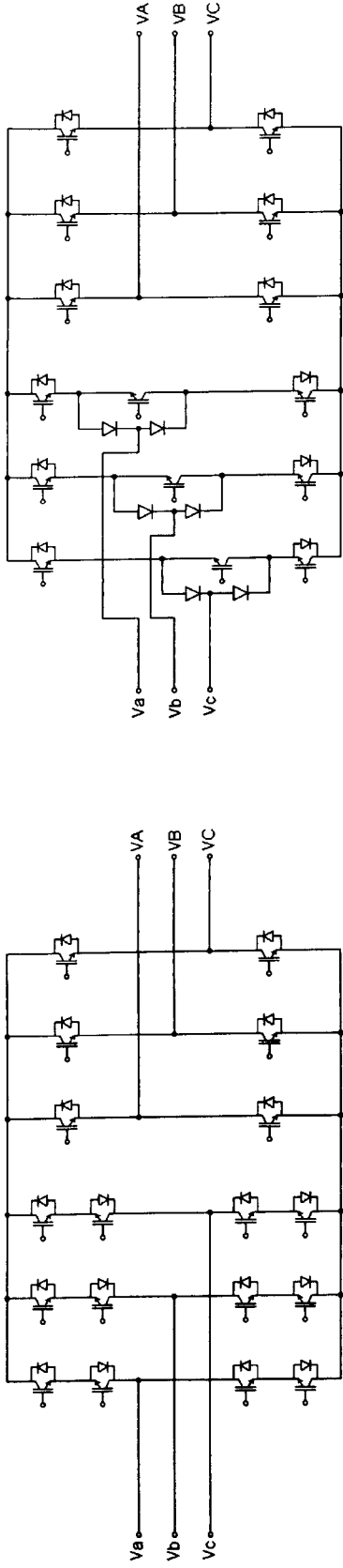
The two-stage direct power converter offers the similar advantages to the conventional matrix converter, such as bidirectional power flow, sinusoidal input currents and unity input power factor. However, in some applications, the two-stage direct power converter may be preferred over the conventional matrix converter due to:

- The reduced number of bi-directional switching devices
- The cost effective multi-drive systems

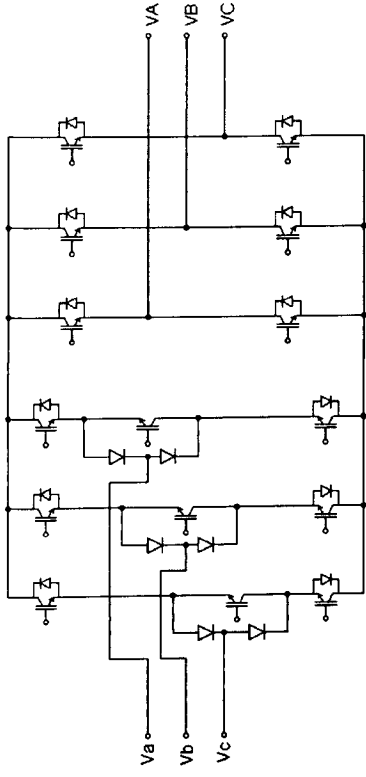
(i) Reduced Number of Bi-Directional Switching Devices

The possibility of reducing the total number of semiconductor switching devices required for the two-stage direct power converter topology has been presented in [9]. These topologies are known as the “Sparse Matrix Converters”. Figure 2.21 shows the various topologies with reduced number of switches. However, the sparse matrix converter required reduced number of switching devices, but still able to provide unity input power factor, sinusoidal input current and load voltages similar to the conventional matrix converter. Also, due to reduced number of switches, the sparse matrix converter offers a direct power converter with simple in design and cheaper in cost.

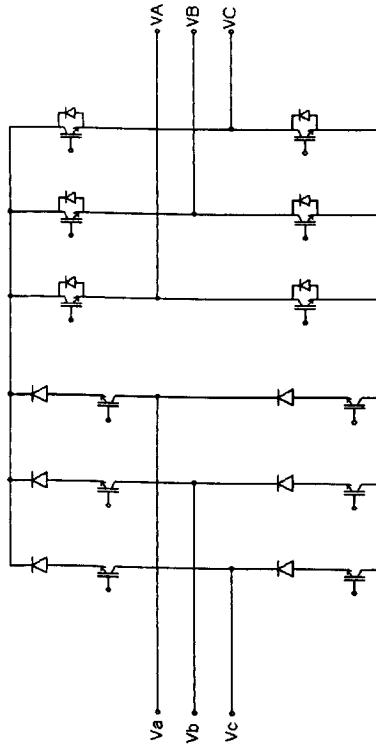
The switch reducing process is performed at the rectification stage as shown in figure 2.21. In case of Very Sparse (VSMC) and Ultra Sparse Matrix Converter (USMC), the rectification stage is in unidirectional nature, therefore, these two topologies are not suitable for regenerative operation and the minimum load power factor of the VSMC and USMC is limited to 0.866 [9, 27]. In case of Sparse Matrix Converter (SMC), the reduced number of semiconductors switches will not affect the regeneration capability of the converter, but the conduction losses will be higher due to requirement of more semiconductors devices for conducting the DC-link current.



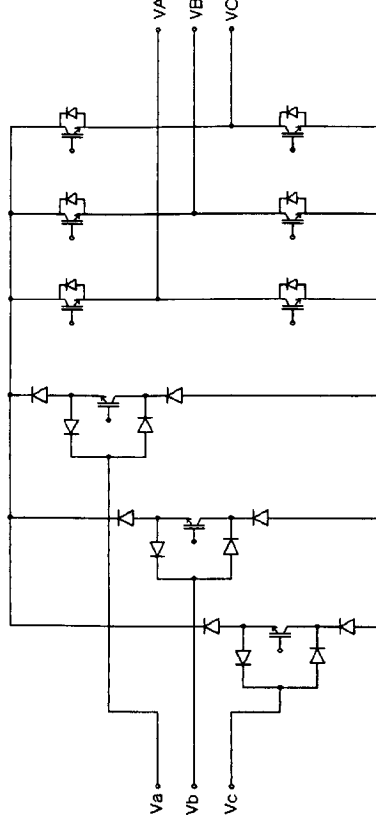
(a) The two-stage direct power converter



(b) The sparse matrix converter



(c) The very sparse matrix converter



(d) The ultra sparse matrix converter

Figure 2.21: The two-stage direct power converter topologies with reduced number of switches

(ii) The Cost Effective Multi-Drive System

In a multi-drive system a single rectification stage can be shared by several inversion stages using common DC-link energy storage components [28]. This concept provides a cost effective multi-drive system due to sharing of the rectification stage. Therefore a common DC-link without energy storage components may be an alternative. The two-stage direct power converter offers an attractive option for the multi-drive system, which eliminates the use of any energy storage in DC-link. Figure 2.22 shows the block diagram of a multi-drive system based on the two-stage direct power converter [10].

In this multi-drive concept, the rectification stage is shared by many loads without using any DC-link energy storage components, which results a reduction of numbers of active and passive components. Therefore, this concept provides the cost effective and weight/volume effective multi-drive system. The multi-motor drive converter topology based on the two-stage direct power converter is discussed in chapter 3.

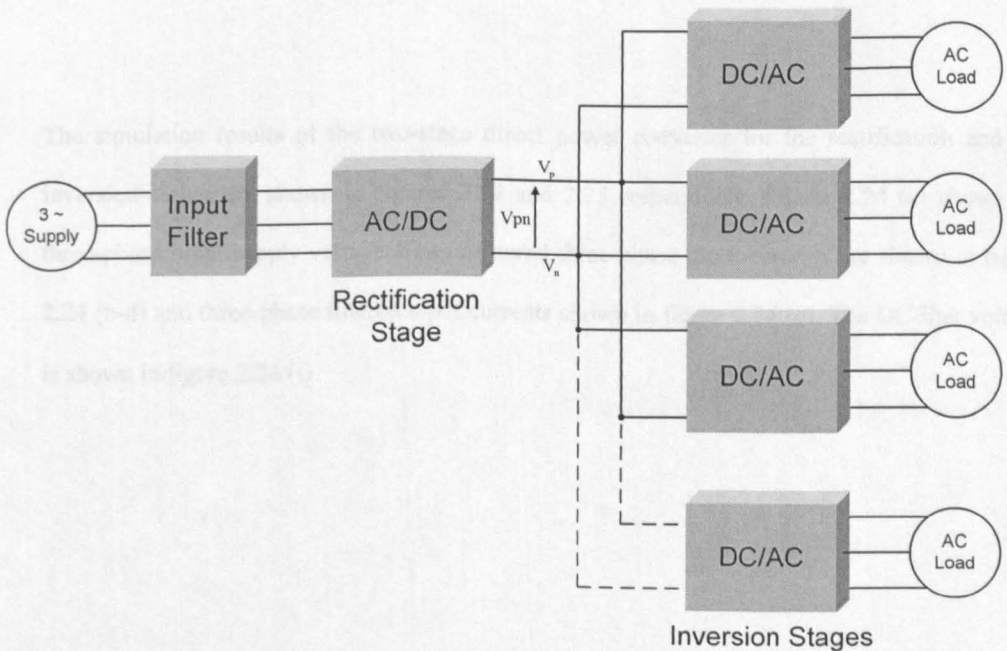


Figure 2.22: A multi-drive system based on the two-stage direct power converter

2.6 Simulation Results

The two-stage direct power converter shown in figure 2.23 has been simulated by using 'SABER', based on the specification presented in Appendix 'A'.

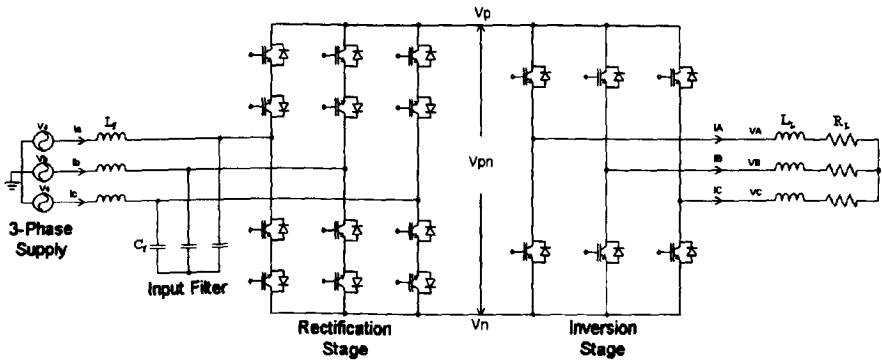
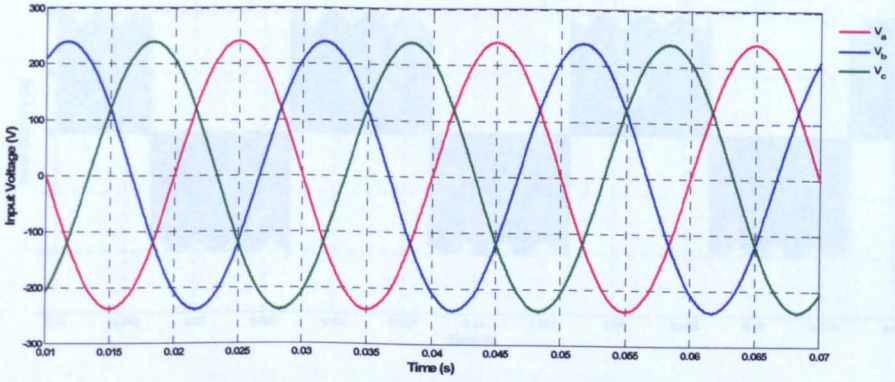


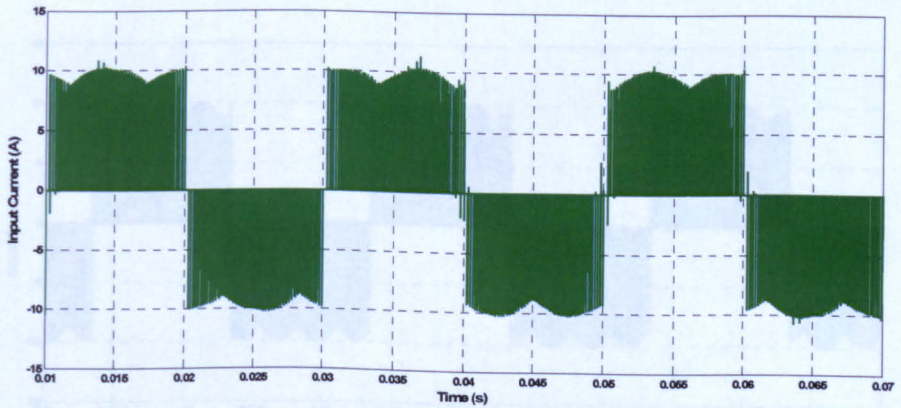
Figure 2.23: Two-stage direct power converter with RL load

The simulation results of the two-stage direct power converter for the rectification and the inversion stages are shown in figures 2.24 and 2.25 respectively. Figure 2.24 (a) shows the three-phase input supply voltage. The unfiltered three-phase input currents are shown in figure 2.24 (b-d) and three-phase filtered input currents shown in figure 2.24 (e). The DC-link voltage is shown in figure 2.24 (f).

2.6. Simulation Results

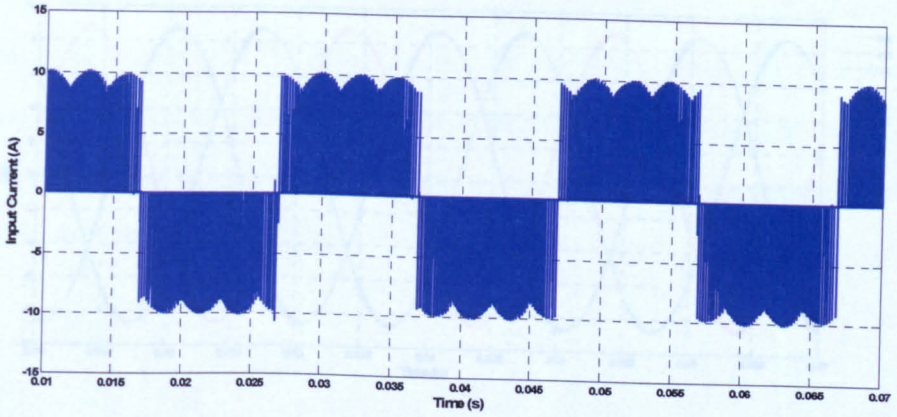


(a) The input phase voltages

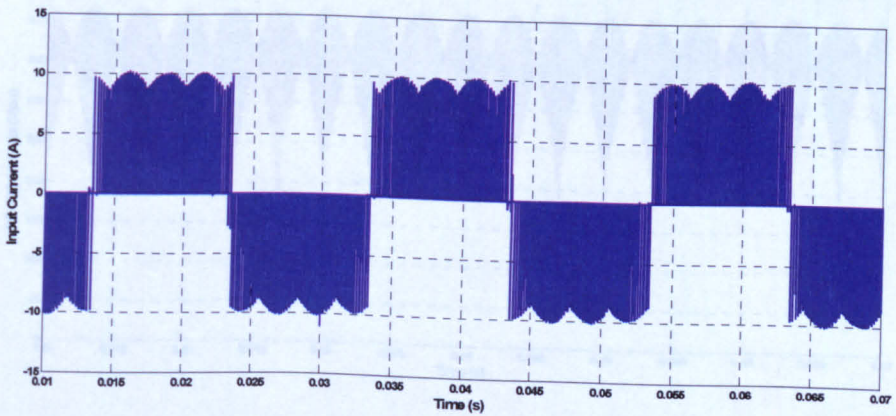


(b) The unfiltered input current, i_a

2.6. Simulation Results



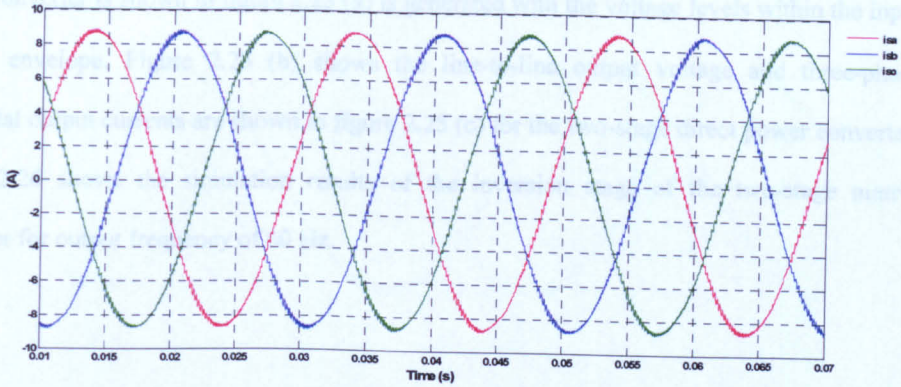
(c) The unfiltered input current, i_b



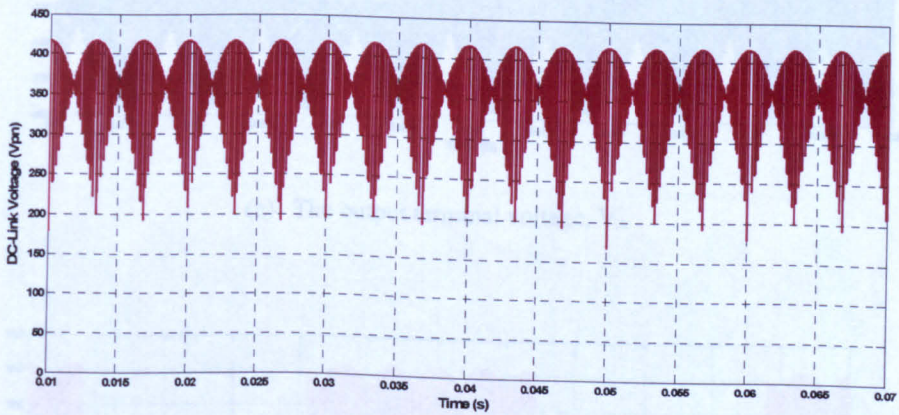
(d) The unfiltered input current, i_c

2.6. Simulation Results

Figure 2.24 shows the simulation results of the inversion stage for the two-stage direct power converter for output frequency 30 Hz. The output terminal voltage, V_{pn} , of the two-stage direct power converter is shown in Figure 2.25. The output current, i_{pn} , of the two-stage direct power converter is shown in Figure 2.26. The output voltage, V_{pn} , of the two-stage direct power converter is shown in Figure 2.27. The output current, i_{pn} , of the two-stage direct power converter is shown in Figure 2.28.



(e) The filtered three-phase input currents

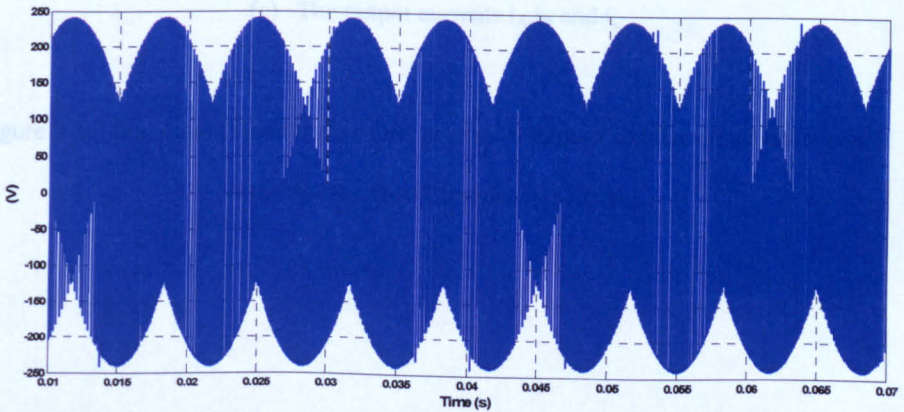


(f) The DC-link voltage, V_{pn}

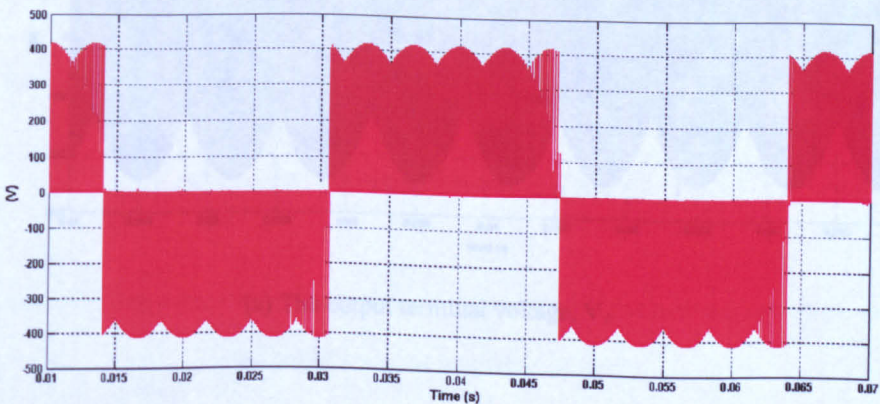
Figure 2.24: Simulation waveforms of the rectification stage of the two-stage direct power converter

2.6. Simulation Results

Figure 2.25 shows the simulation results of the inversion stage for the two-stage direct power converter for output frequency 30 Hz. The output terminal voltage, V_A , of the two-stage direct power converter is shown in figure 2.25 (a) is generated with the voltage levels within the input voltage envelope. Figure 2.25 (b) shows the line-to-line output voltage and three-phase sinusoidal output currents are shown in figure 2.25 (c) for the two-stage direct power converter. Figure 2.26 shows the simulation results of the inversion stage of the two-stage matrix converter for output frequency of 60 Hz.

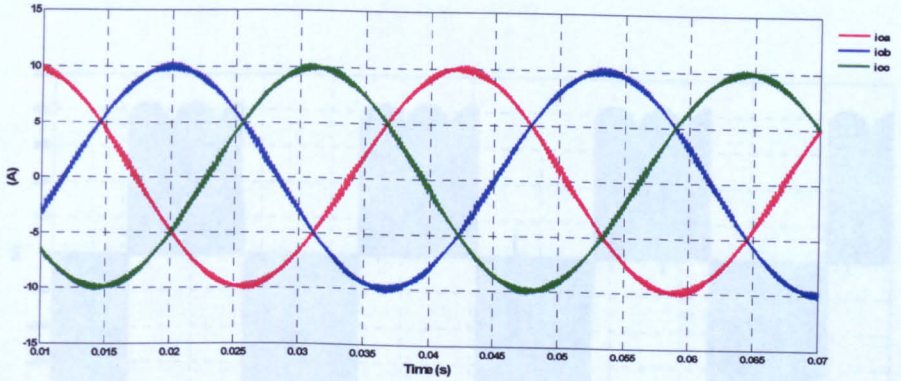


(a) The output terminal voltage, V_A



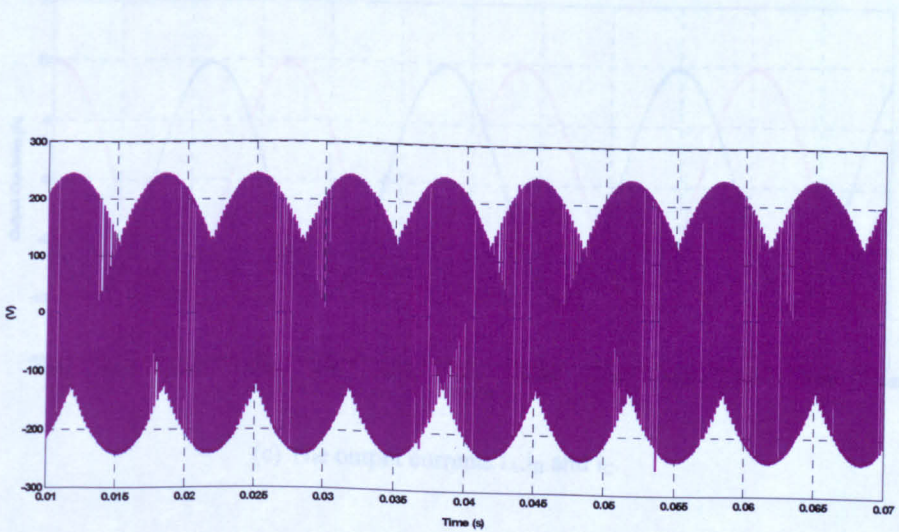
(b) The line-to-line output voltage, V_{AB}

2.6. Simulation Results



(c) The output currents i_A, i_B and i_C

Figure 2.25: Simulation waveforms of the inversion stage of the two-stage direct power converter for output frequency of 30Hz.

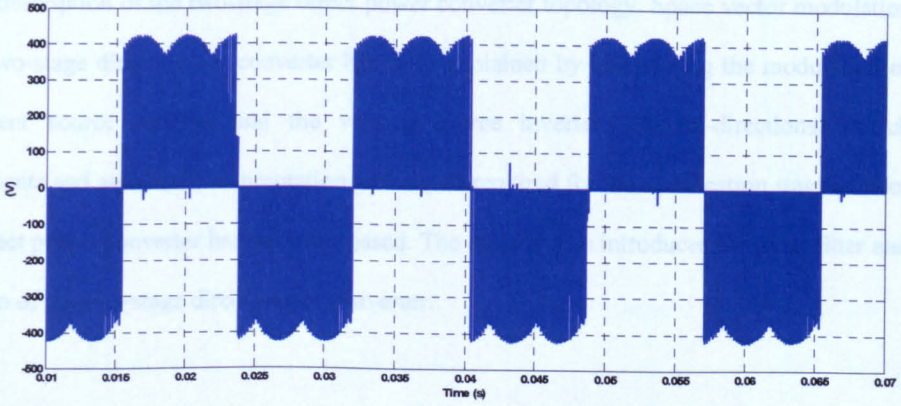


(a) The output terminal voltage, V_A

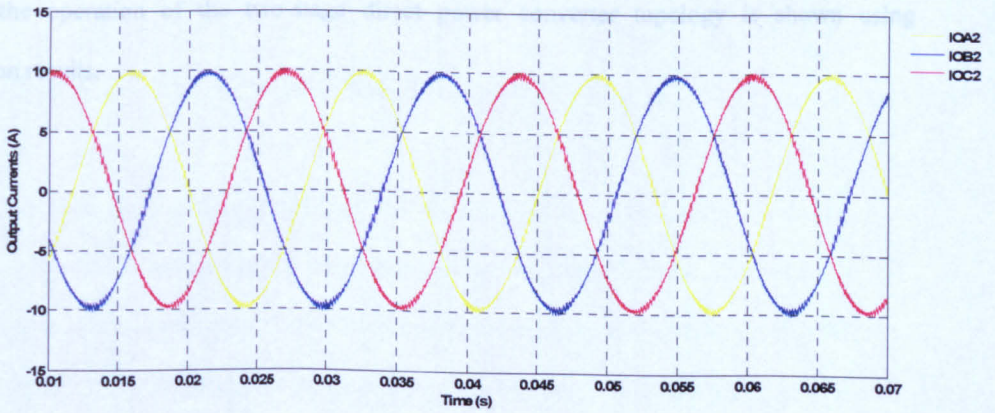
2.6. Simulation Results

2.7 Conclusions

This chapter has given a basic overview of the conventional matrix converter topology and the detailed description of the two-stage direct power converter topology. The advantages of the two-stage direct power converter over the conventional matrix converter are reviewed, which clarify the advantages of the two-stage direct power converter over the conventional matrix converter in some applications.



(b) The line-to-line output voltage, V_{AB}



(c) The output currents i_A, i_B and i_C

Figure 2.26: Simulation waveforms of the inversion stage of the two-stage direct power converter for output frequency of 60Hz.

2.7 Conclusions

This chapter has given a basic overview of the conventional matrix converter topology and the detailed description of the two-stage direct power converter topology. Space vector modulation for the two-stage direct power converter has been explained by considering the modulation of the current source rectifier and the voltage source inverter. The bi-directional switch arrangements and associated commutation techniques required for the rectification stage of two-stage direct power converter has been discussed. The chapter also introduces the input filter and protection of the two-stage direct power converter.

The advantages of the two-stage direct power converter over the conventional matrix converter are reviewed, which clarifies the preference of the two-stage direct power converter over the conventional matrix converter in some applications.

Finally the operation of the two-stage direct power converter topology is shown using simulation results.

Chapter 3

The Multi-Motor Drive Converter Topology based on the Two-stage Direct Power Converter

3.1 Introduction

This chapter discusses the basic concept of the multi-motor drive system and gives a brief description of some possible multi-motor drive converter topologies. A weight/volume effective multi-motor drive converter topology based on the two-stage direct power converter is introduced. The circuit configuration and space vector modulation technique for the proposed multi-motor drive converter topology are also discussed.

3.2 Overview of the Multi-Motor Drive System

The adjustable speed drive (ASD) technology has significantly matured due to the continue development in the power semiconductor devices and in the low cost of control processors [29]. The revolutions in ASD's with large electromechanical systems have been replaced with more compact and efficient power electronic equipment. A recent trend is to integrate the power electronics with the electrical motor in order to produce an efficient and flexible single unit [8]. As the output performances of the ASD have continued to improve, the research trends for the ASD have focused more on the interaction with the utility grid.

3.2. Overview of the Multi-Motor Drive System

A motor drive usually consists of an indirect power converter with a rectifier and an inverter. The function of the rectifier is to convert the AC into DC and then the inverter converts the DC into AC at adjustable frequency and voltage. Normally each motor has its own inverter to permit independent control, but the rectifier can be shared between multiple inverters [28].

Figure 3.1 shows the basic structure of a multi-motor drive topology, where the common rectifier can use, for example, a six-pulse, twelve-pulse or active front end topology feeding all the individual inverters. The individual inverters may have different power ratings and may even have different performance requirements. The multi-motor drive systems often allow some of the motors to regenerate via the common DC-link, independent of the type of the rectifier used.

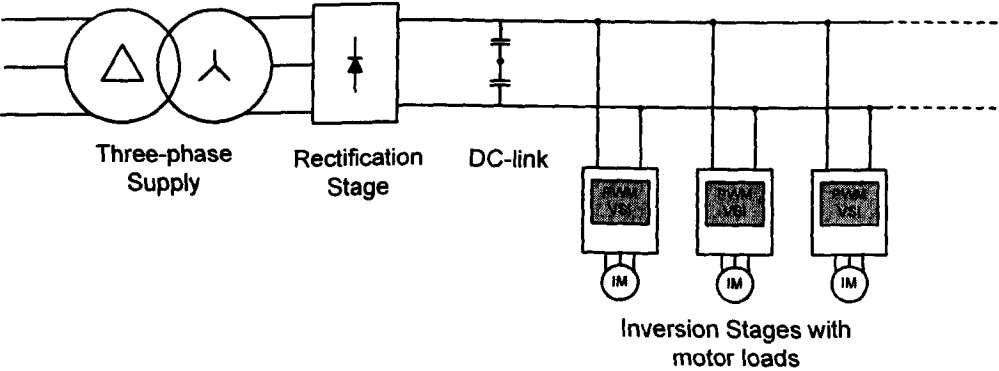


Figure 3.1: The basic structure of a multi-motor drive system

The multi-motor drive topology can be used in many industrial applications, for example textile factories, electric/hybrid vehicles, paper mills, oil-pumping and aerospace applications. The multi-motor drive concept has offered an attractive approach to reduce the cost and size of the converter system [30].

3.2. Overview of the Multi-Motor Drive System

Figure 3.2 and 3.3 show the some of possible multi-motor drive topologies with converters using DC-link capacitors [31]. The multi-motor drive topology shown in figure 3.2 establishes the common DC-bus voltage to feed the two inverter-motor units through a single Voltage Source Rectifier (VSR). This multi-motor drive system utilises the VSR in a cost effective and viable way because the cost and size of the VSR is shared by the multiple loads.

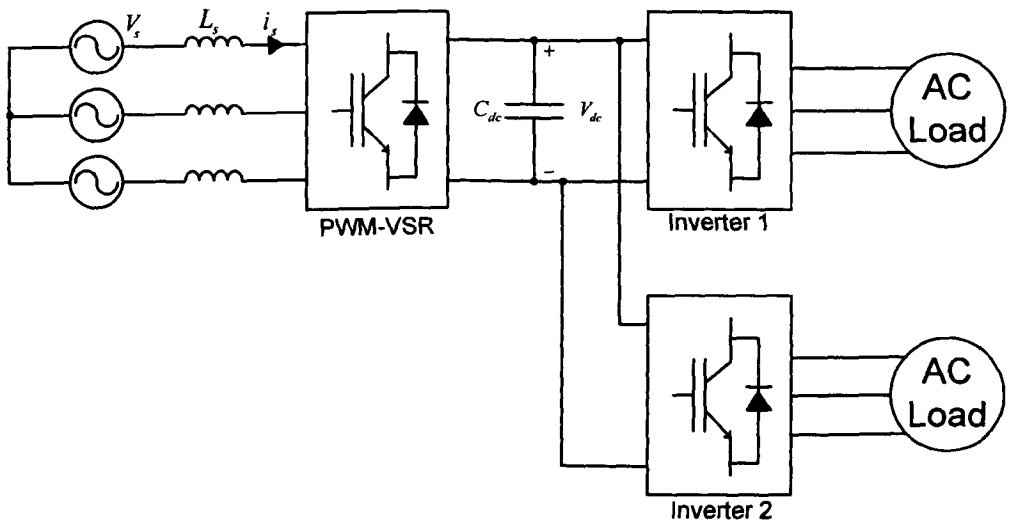


Figure 3.2: A multi-motor drive converter based on an indirect AC-DC-AC converter

In the multi-motor drive topology shown in figure 3.3 a phase-shifting transformer is used to split the three phase voltage into two phase shifted versions which are then rectified and recombined. This topology offers the reduction of ripple in DC link voltage and minimizes the harmonics in the supply currents.

3.2. Overview of the Multi-Motor Drive System

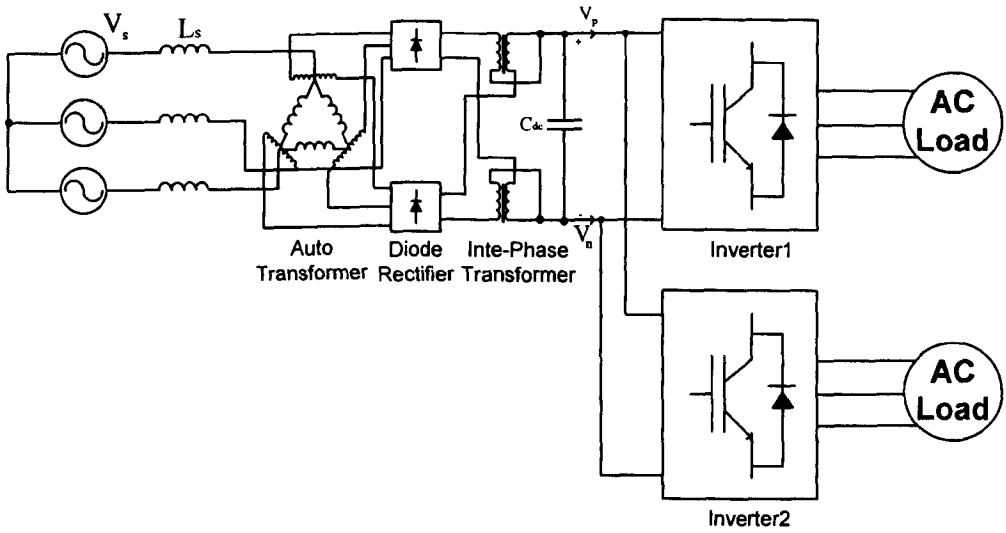


Figure 3.3: A multi-motor drive converter based on multi-pulse rectifiers

The limitation of the above topologies is that they require DC-link capacitors and maybe a phase-shifting transformer. The bulky DC-link capacitors have a short life time compared to the other devices in the converter. In applications such as aerospace, where weight and volume are critical issues, these DC-links have significant disadvantages. The matrix converter has no bulky DC-link components; hence the topology has the potential for a significant improvement in power density.

The possibility of a multi-motor drive system for automotive applications has been investigated in [32]. This automotive system consists of four matrix converters driving four induction motors, one for each wheel. In this solution, the number of semiconductor devices is high and the only advantage is that the converters may share a common input filter. A multi-motor drive system based on a conventional matrix converter is shown in figure 3.4.

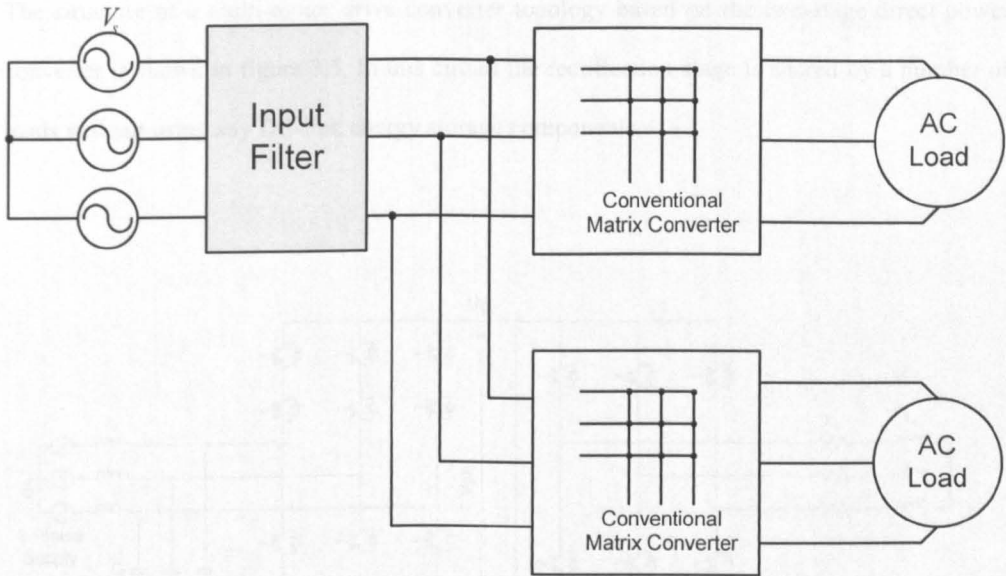


Figure 3.4: A multi-motor drive converter based on conventional matrix converters

The two-stage direct power converter offers an attractive option for the multi-motor drive converter, which eliminates the use of energy storage in a DC-link and results a reduction of numbers of active and passive components. A multi-motor drive converter topology based on the two-stage direct power converter is discussed in next section.

3.3 The Circuit Topology for Proposed Multi-Motor Drive Converter Topology

It is possible to use the two-stage direct power converter to develop a compact multi-motor drive power converter [8]. The two-stage direct power converter has no DC-link energy storage and the resulting topology has the potential for a significant improvement in power density.

3.3. The Circuit Topology for Proposed Multi-Motor Drive Converter Topology

The structure of a multi-motor drive converter topology based on the two-stage direct power converter is shown in figure 3.5. In this circuit the rectification stage is shared by a number of loads without using any DC-link energy storage components.

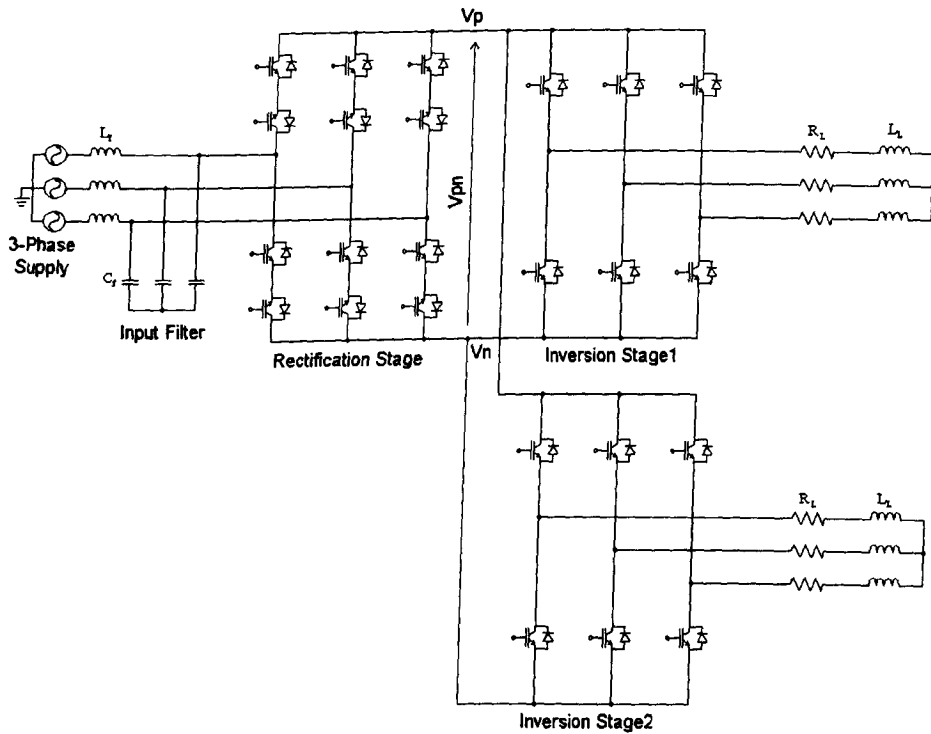


Figure 3.5: A multi-motor drive converter based on the two-stage direct power converter topology

3.4 The Space Vector Modulation (SVM) for Multi-Motor Drive Converter Topology

In order to draw sinusoidal input currents from the supply, the average output power must be constant. The output power is constant in the case of a stable, symmetrical and sinusoidal load. By using the two-stage direct power converter, it is possible to connect several inversion stages to the same variable DC-link, assuming that the switching patterns of the inversion stages are synchronized with the rectification stage. In each stage a combination of vectors is produced to synthesis a reference vector of a given amplitude and angle. After determining the vectors and their duty cycles, the modulation pattern of the multi-drive converter topology then combines the switching states of both stages uniformly so that a correct balance of the input currents and output voltages can be obtained for each switching period, as described in section 2.3.2.

The space vector modulation for the multi-drive converter topology can be derived from the modulation of the two-stage direct power converter. In the rectification stage, the zero vectors are eliminated and each inversion stage uses the zero vectors as per their requirements. As zero vectors are not used in the rectification stage, the rectification switching sequence consists of only two adjacent currents vectors (\bar{I}_γ , \bar{I}_δ). The duty cycles d_γ and d_δ for the rectification stage are determined using equations (2.32) and then adjusted:

$$d_\gamma^R = \frac{d_\gamma}{d_\gamma + d_\delta}, \quad d_\delta^R = \frac{d_\delta}{d_\gamma + d_\delta} \quad (3.1)$$

The average DC-link voltage is then recalculated to give the new value of the modulation index of the 'n' inversion stage (general case):

3.4. The SVM for Multi-Motor Drive Converter Topology

$$V_{pn_avg} = (d_{\gamma}^R \bar{V}_{\gamma} + d_{\delta}^R \bar{V}_{\delta}) \quad (3.2)$$

$$m_1^n = \frac{\sqrt{3} \cdot V_{om}}{V_{pn_avg}} \quad (3.3)$$

In order to minimize the transition between each vectors, the inverter stages use a double-sided switching sequence: 0- β - α -0-0- α - β -0. The duty-cycles of active switching vectors for the 'n' inversion stage are:

$$d_{\alpha}^n = m_1^n \cdot \sin\left(\frac{\pi}{3} - \theta_{out}^n\right) \quad (3.4)$$

$$d_{\beta}^n = m_1^n \cdot \sin(\theta_{out}^n) \quad (3.5)$$

Therefore, the duty-cycles for the switching sequences of any 'n' inversion stage are as follow:

$$d_0^n = d_{\gamma}^R [1 - (d_{\alpha}^n + d_{\beta}^n)] \quad (3.6)$$

$$d_1^n = d_{\gamma}^R \cdot d_{\alpha}^n \quad (3.7)$$

$$d_2^n = d_{\gamma}^R \cdot d_{\beta}^n \quad (3.8)$$

$$d_3^n = d_{\delta}^R \cdot d_{\beta}^n \quad (3.9)$$

3.4. The SVM for Multi-Motor Drive Converter Topology

$$d_4^n = d_8^R \cdot d_\beta^n \quad (3.10)$$

$$d_5^n = d_8^R [1 - (d_\alpha^n + d_\beta^n)] \quad (3.11)$$

The time interval for each vector in this switching sequence can be determined by using the following equations:

For the rectification stage:

$$t_r = d_\gamma^R \cdot T_s \quad (3.12)$$

For any of 'n' inversion stage:

$$t_{i0}^n = d_0^n \cdot T_s \quad (3.13)$$

$$t_{i1}^n = d_1^n \cdot T_s \quad (3.14)$$

$$t_{i2}^n = d_2^n \cdot T_s \quad (3.15)$$

$$t_{i3}^n = d_3^n \cdot T_s \quad (3.17)$$

$$t_{i4}^n = d_4^n \cdot T_s \quad (3.18)$$

$$t_{i5}^n = d_5^n \cdot T_s \quad (3.19)$$

3.4. The SVM for Multi-Motor Drive Converter Topology

The synthesis of the switching pattern for the rectification stage and the two inversion stages are shown in figure 3.6.

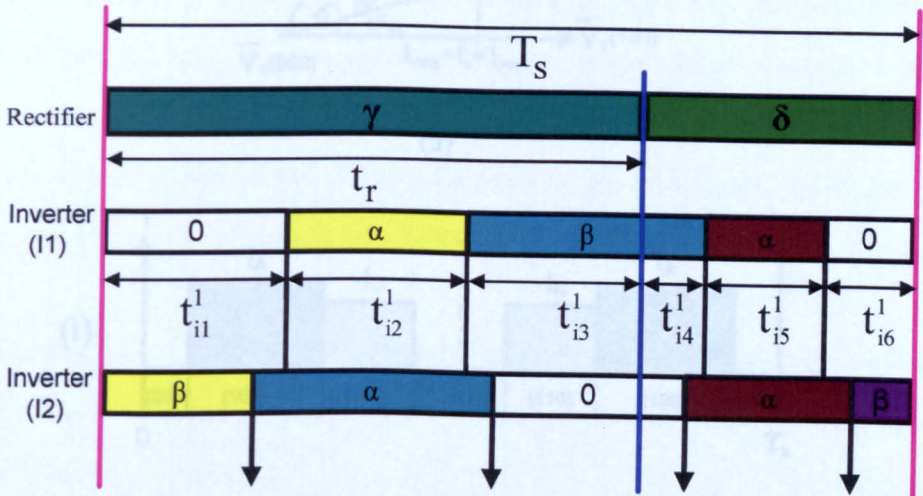
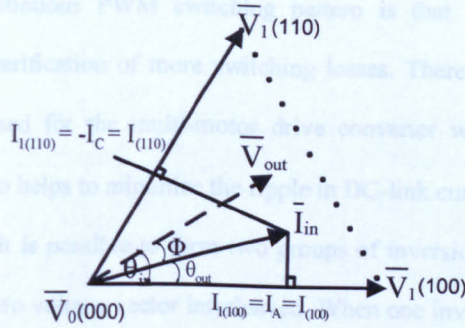


Figure 3.6: The switching pattern for the multi-motor drive converter topology

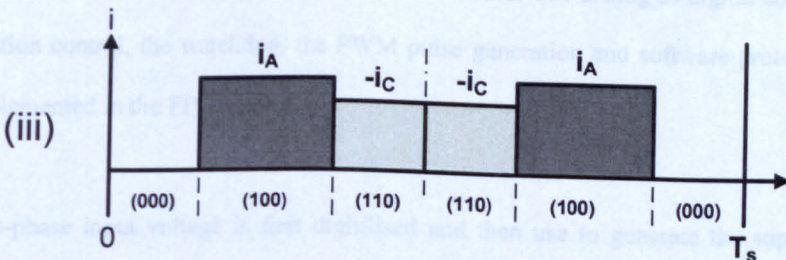
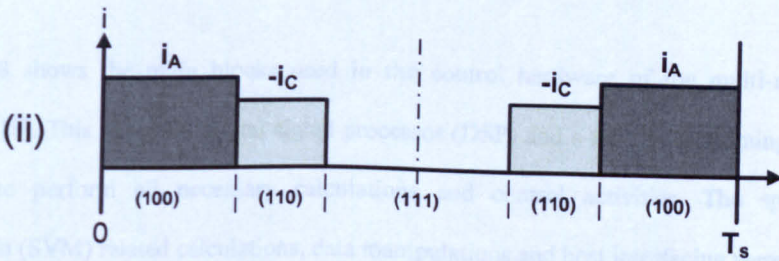
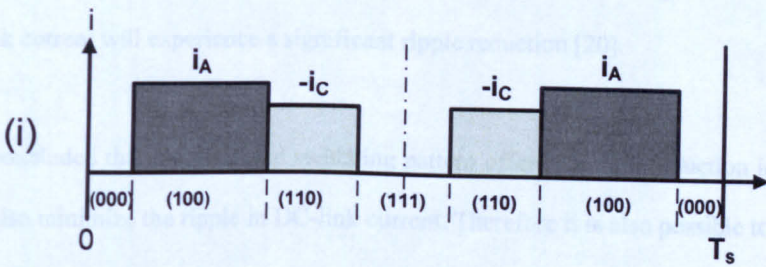
The switching pattern shown in figure 3.6 is different from the switching pattern used for two-stage direct power converter shown in figure 2.10 of Chapter-2. The switching pattern for inverter stage presented in figure 2.10 is known as the continuous PWM switching pattern which uses the multiple zero voltage vectors. A discontinuous PWM switching pattern is used for multi-motor converter shown in figure 3.6. Some of possible switching pattern for inversion stage are shown in figure 3.7 (b) when the output voltage reference vector is in sector-1 as in figure 3.7(a):

3.4. The SVM for Multi-Motor Drive Converter Topology

The advantage of continuous PWM voltage modulation is that it gives the better quality waveforms with the sacrifice of more switching losses. Therefore a discontinuous PWM switching pattern is used in this converter which not only reduces the switching losses but also helps to minimize the DC-link current. In the proposed multi-motor drive converter, it is possible to use the space vector modulation (SVM) based calculation. This calculation is done by using the reference vector position. The required output voltage reference vector \vec{V}_{out} is produced by the inverter stage switching pattern, which will have their zero DC-link current at the same time another inverter produce a vector by synchronizing with the rectifier stage switching pattern as shown in figure 3.6. The sum of



(a)



(b)

Figure 3.7: Possible switching pattern for inversion stage, (a) Output voltage reference vector position, (b) for (i) Continuous PWM switching pattern and (ii, iii) Discontinuous PWM switching patterns

3.4. The SVM for Multi-Motor Drive Converter Topology

The advantage of continuous PWM switching pattern is that it gives the better quality waveforms with the scarification of more switching losses. Therefore a discontinuous PWM switching pattern is used for the multi-motor drive converter which not only reduces the switching losses but also helps to minimize the ripple in DC-link current. In the proposed multi-motor drive converter, it is possible to form two groups of inversion stages switching pattern, which will have their zero voltage vector interleaved. When one inverter has to produce a zero-vector causing zero DC-link current at the same time another inverter produce a active vector by synchronizing with the rectification switching pattern as shown in figure 3.6. The sum of two DC-link current will experience a significant ripple reduction [20].

It may be concluded that the proposed switching pattern offers not only reduction in switching losses but also minimize the ripple in DC-link current. Therefore it is also possible to reduce the size of input filter components.

Figure 3.8 shows the main blocks used in the control hardware of the multi-motor drive converter [8]. This require a digital signal processor (DSP) and a field programming gate array (FPGA) to perform all necessary calculations and control activities. The space vector modulation (SVM) related calculations, data manipulations and host interfacing were performed in Texas Instruments standard TMS320C6713 DSP board. The analog to digital controller, the commutation control, the watchdog, the PWM pulse generation and software protection items were implemented in the FPGA board.

The three-phase input voltage is first digitilised and then use to generate the supply current reference angle for the space vector modulation of rectification stage. The required output frequency is used to generate the output voltage reference angle for the inversion stages. The DC-link voltage (V_{pn}) generated by rectification stage is used to develop the space vector modulation for inversion stages as shown in figure 3.8.

3.4. The SVM for Multi-Motor Drive Converter Topology

3.5 Simulation Results

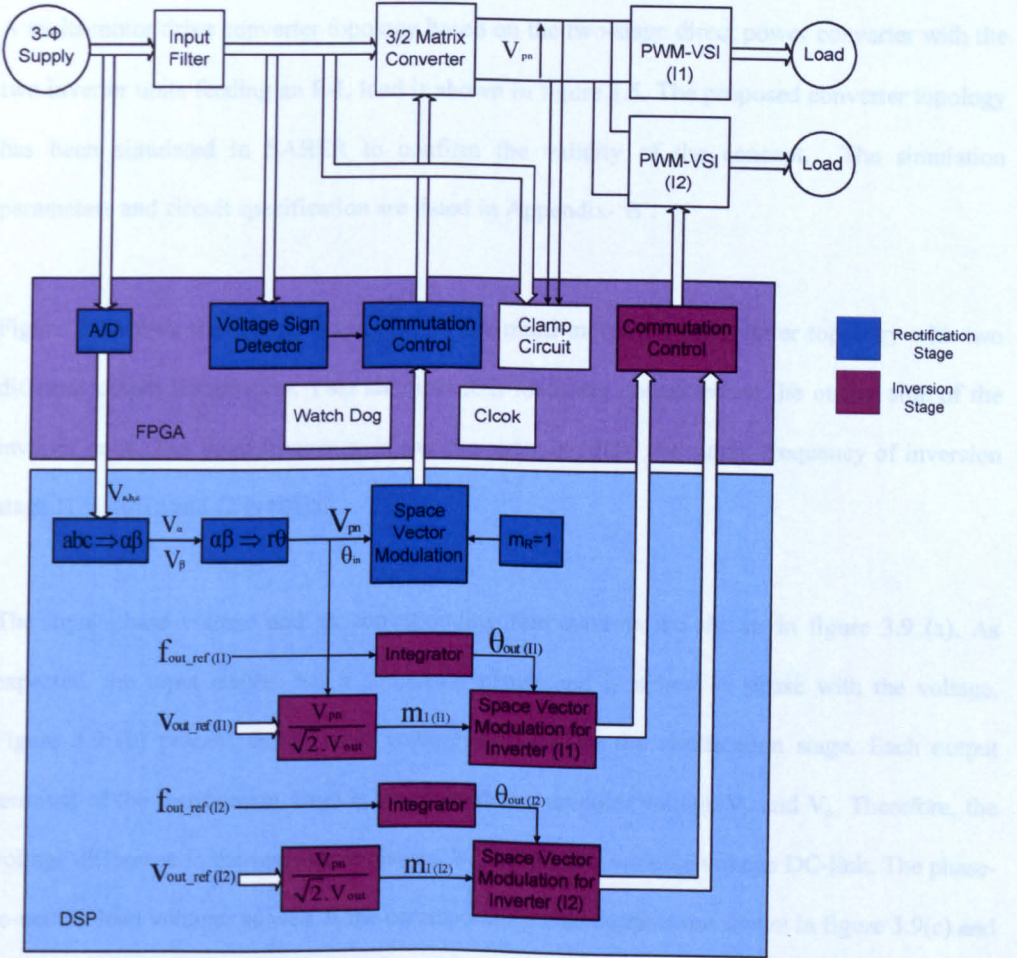


Figure 3.8: Control hardware block-diagram for multi-motor drive converter

3.5 Simulation Results

A multi-motor drive converter topology based on the two-stage direct power converter with the two inverter units feeding an R-L load is shown in figure 3.5. The proposed converter topology has been simulated in SABER to confirm the validity of the concept. The simulation parameters and circuit specification are listed in Appendix-'B'.

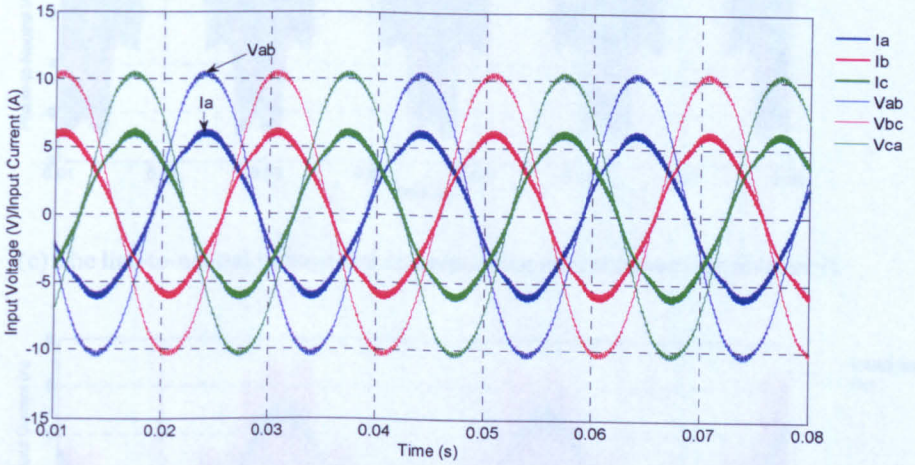
Figure 3.9 shows the simulation results for the multi-motor drive converter topology with two different output frequencies. Two identical R-L loads are connected on the output side of the inverter units. The input frequency of the converter is 50Hz, the output frequency of inversion stage I1 is 40Hz and I2 is 60Hz.

The input phase voltage and its corresponding line currents are shown in figure 3.9 (a). As expected, the input current has a sinusoidal nature and is almost in phase with the voltage. Figure 3.9 (b) present the DC-link voltage provided by the rectification stage. Each output terminal of the rectification stage is maintained at a unipolar voltage V_p and V_n . Therefore, the voltage difference in the two output phages, V_{pn} becomes a variable voltage DC-link. The phase-to-neutral load voltages as well as the corresponding load currents are shown in figure 3.9(c) and (d) for Inverter I1 and Inverter I2 respectively. The results in figure 3.9 show the performance of the multi-motor dive converter on the grid side. The three input currents are sinusoidal, balanced and in phase with the voltage.

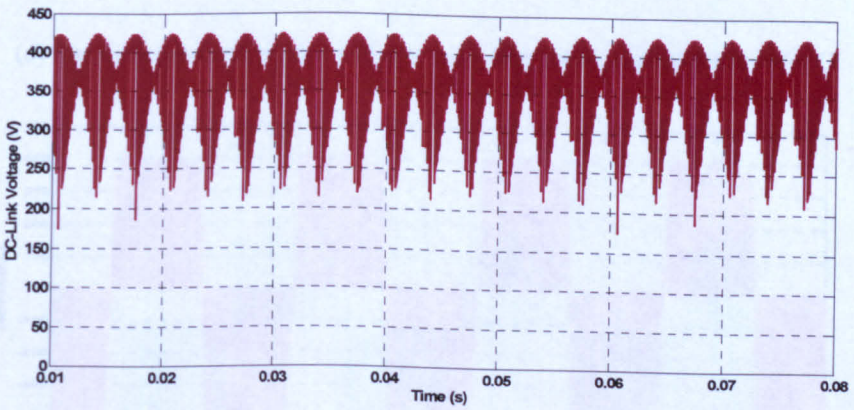
The output performance of the multi-motor drive converter is shown by the waveforms of the line-to-line output voltages and three-phase output currents for inverter I1 and inverter I2 in figure 3.9 (e-l).

3.5. Simulation Results

The below simulation results prove that the multi-motor drive converter topology is capable of producing the unrestricted output frequency with sinusoidal input and output currents.

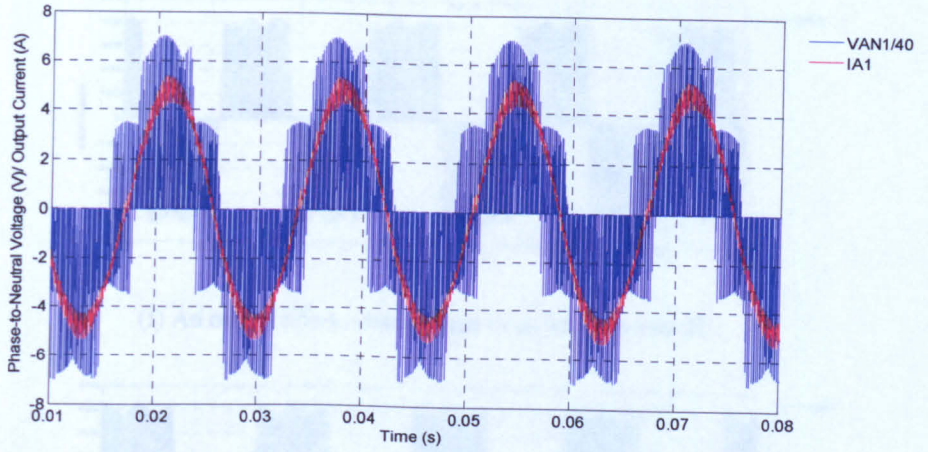


(a) Three-phase input phase voltages and line currents

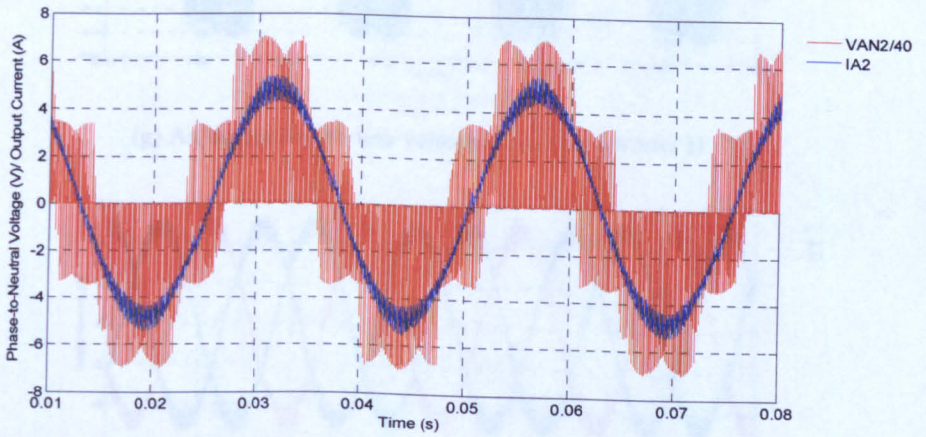


(b) DC-link voltage

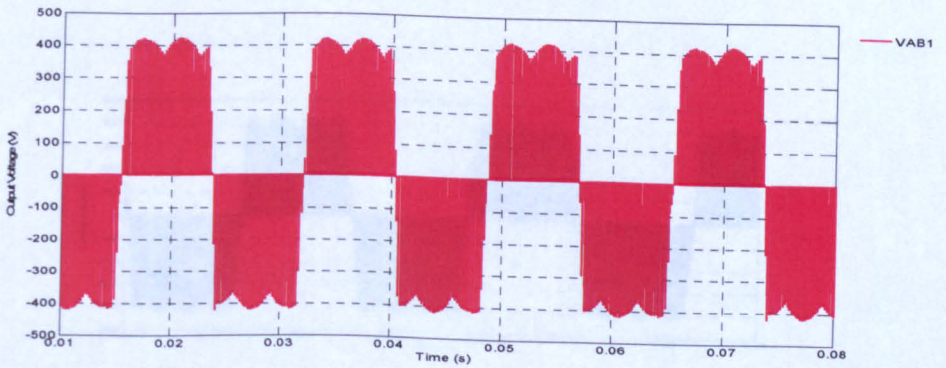
3.5. Simulation Results



(c) The line-to-neutral voltage and corresponding output current for inverter I1

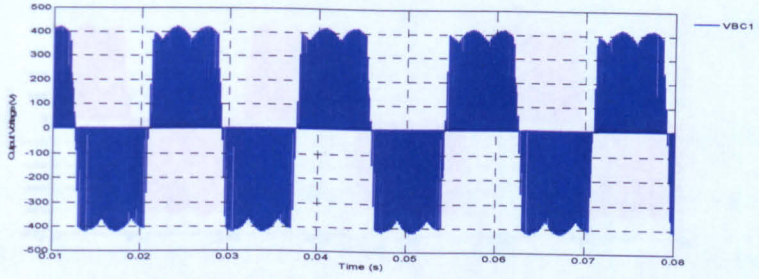


(d) The line-to-neutral voltage and corresponding output current for inverter I2

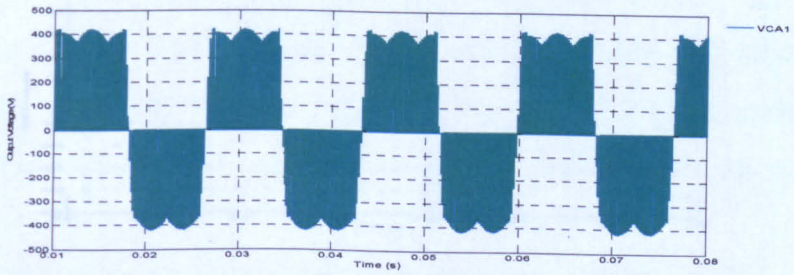


(e) An output line-to-line voltage (V_{AB1}) for inverter I1

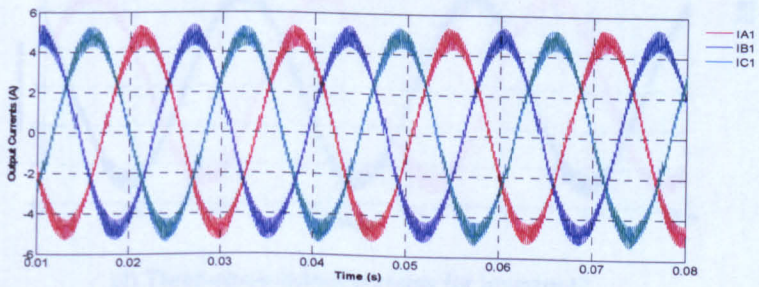
3.5. Simulation Results



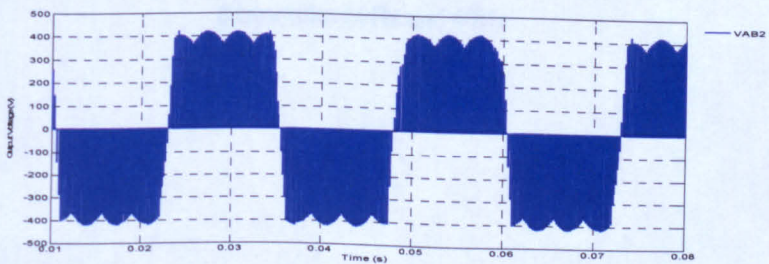
(f) An output line-to-line voltage (V_{BC1}) for inverter I1



(g) An output line-to-line voltage (V_{CA1}) for inverter I1

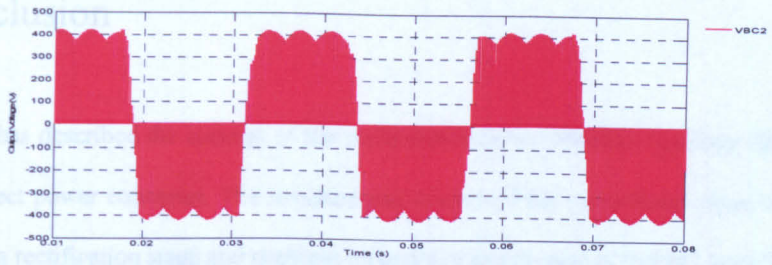


(h) Three-phase output currents for inverter I1

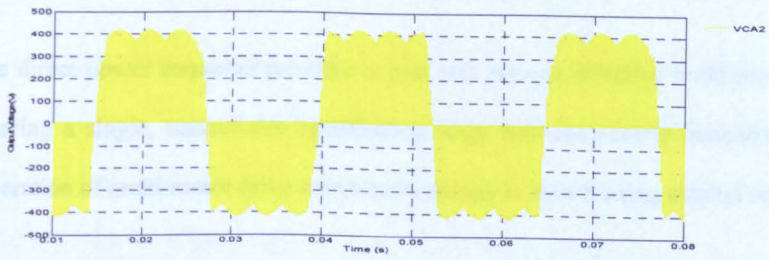


(i) An output line-to-line voltage (V_{AB2}) for inverter I2

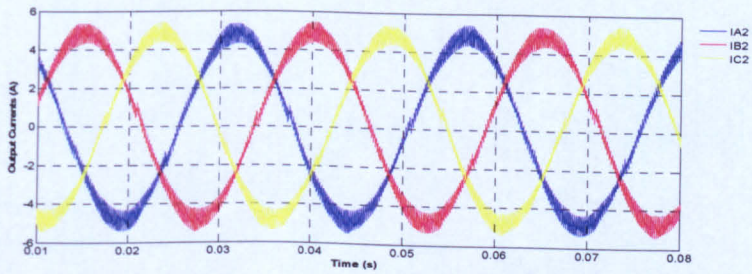
3.5. Simulation Results



(j) An output line-to-line voltage (V_{BC2}) for inverter I2



(k) An output line-to-line voltage (V_{CA2}) for inverter I2



(l) Three-phase output currents for inverter I2

Figure 3.9: The simulation results for the multi-motor drive converter topology with output frequencies 60Hz and 40Hz

3.6 Conclusion

This chapter has described the concept of the multi-motor drive converter topology based on a two-stage direct power converter. The structure and control of the multi-motor drive converter consisting of a rectification stage and multiple inversion stages to supply the AC loads based on the two-stage matrix converter approach are explained.

The two-stage direct power converter provides a cost and volume effective multi-motor drive system by sharing a single, controllable rectification stage between several inversion stages. Finally the operation of multi-motor drive converter topology is shown using simulation results.

Chapter 4

Multi-Motor Drive System

4.1 Introduction

This chapter deals with the control and simulation of the proposed multi-motor drive system, where two motors are connected on same shaft. This type of multi-motor drive system can be used in many industrial and aerospace applications [31]. Figure 4.1 shows the overall configuration of the multi-motor drive system with a common motor shaft.

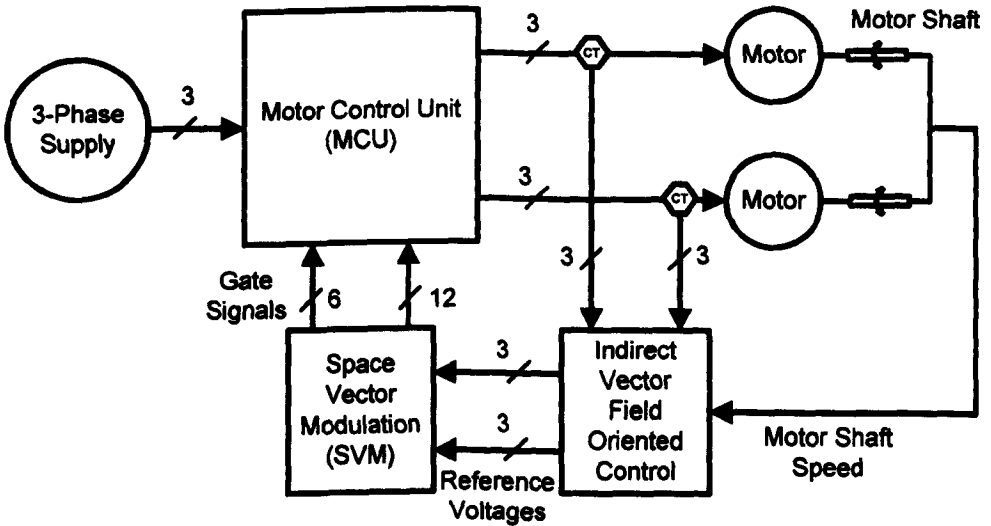


Figure: 4.1. Simplified block diagram of a two-motor drive system

4.2. The Proposed Multi-Motor Drive System

The system supply is a three-phase fixed voltage supply which is converted to a three-phase, variable voltage and frequency source by the Motor Control Unit (MCU). In a conventional system, the MCU could be based on a multi-pulse rectifier system which contains a DC-link capacitor and phase-shifting transformer. Both these components are quite large both in terms of weight and volume. It is unlikely that the size or mass of either of these components will be reduced significantly in the future [33]. As weight and volume are at a premium in aerospace applications any modifications that can be made to reduce these are welcome.

4.2 The Proposed Multi-Motor Drive System

In the proposed multi-motor drive system a conventional MCU can be replaced by a two-stage direct power converter based multi-drive system which eliminates the need for DC-link energy storage and a phase shifting transformer. The power circuit for the proposed multi-motor drive system is shown in figure 4.2.

In this system one input port is connected to the three-phase power supply and the two output ports are connected to the two motors which are on the same shaft [31]. The cost of the rectification stage is therefore shared by both motor drives. So far few publications [8, 28] presented a multi-motor drive system, but this is the first time where the performance of the multi-motor drive system tested with two motor on same shaft. A new modified vector control technique is developed to control the two-motors on same shaft as shown in figure 4.20. The proposed vector control technique is very similar to classical vector field oriented control scheme [34], but in this a single speed control loop is used to gives the torque producing current which is being halved to give the reference for two current control loops for each motor.

4.3. Induction Motor Control

Induction motors are used in this project, therefore the next section will introduce the control scheme for these induction motors.

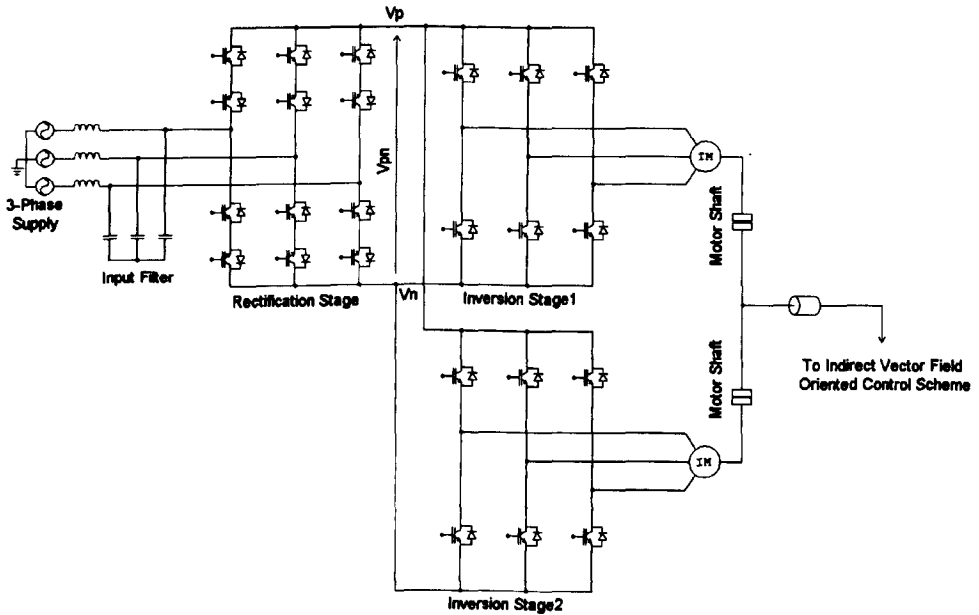


Figure 4.2: The two-motor drive system based on a two-stage direct power converter

4.3 Induction Motor Control

Induction motors are popular in many industrial appliances. Induction motors have the advantages of simple and rugged design, low cost, low maintenance and can have a direct connection to an AC power source [35].

4.4. Scalar Control

When operated directly from the line voltage (50Hz utility input at essentially a constant voltage), an induction motor operates at approximately constant speed.

However, in many applications (for example fans, compressors, pumps and blowers etc) speed control of induction motor is required. The commonly used speed control techniques for induction motors can be classified using the following categories [35]:

- Open loop, Scalar control (V/f control)
- Vector control (Indirect torque control)
- Direct torque control (DTC)

4.4 Scalar Control

In this type of control, the air-gap flux (ϕ) is kept constant by controlling the stator voltage (V) and stator frequency (f), hence the V/f ratio is maintained as a constant. Since only the magnitude of the voltage and the frequency are controlled, this technique is known as scalar control [35]. During low speed operation the stator voltage and frequency both approach zero and this low voltage will be seen across the stator resistance. This will effect the air-gap flux (ϕ), which will not be maintained at the required level, hence the maximum available torque will decrease. This problem can be avoided by boosting the stator voltage to a level in order to compensate stator resistance voltage drop, as shown in figure 4.3.

This V/f control method offers the advantages such as low cost, simple design and requires very little knowledge of the motor design variables. The major disadvantage of this method is poor dynamic performance; hence V/f control is not used in applications where high dynamic performance is required.

4.5. Vector Control

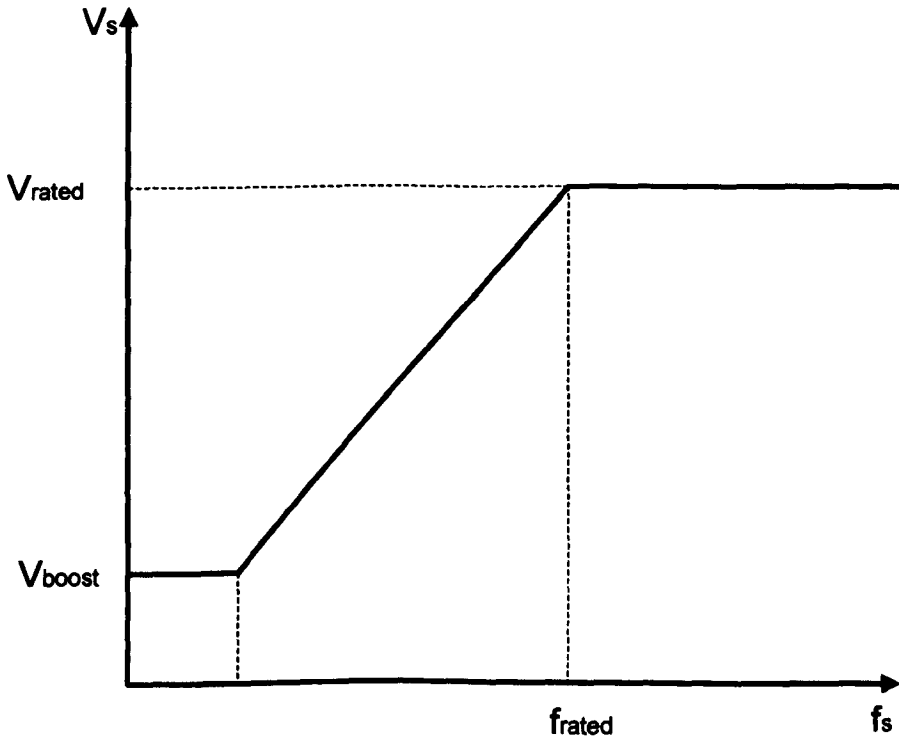


Figure 4.3 Voltage versus frequency relation for V/f control

4.5 Vector Control

In vector or field oriented control, the magnitude and phase alignment of the vector variables are controlled. Vector control was invented at the beginning of the 1970s and the demonstration that an induction motor can be controlled in the same way as a separately excited DC motor brought renaissance in the high performance of control of AC drives [36]. Therefore, the following section will first describe the vector control concept for a separately excited DC

4.5. Vector Control

motor and then the analogy between a three-phase induction motor with a separately excited DC motor.

4.5.1 Vector Control of Separately Excited DC Motor

Vector control of an induction motor is analogous to the control of the separately excited DC motor. In a DC motor, as shown in figure 4.4, the field flux (Ψ_f) produced by the field current (I_f) is perpendicular to the armature flux (Ψ_a) produced by the armature current (I_a).

The torque developed by the separately excited DC motor is [51]:

$$T \propto (I_a \times \Psi_f) \tag{4.1}$$

$$T \propto I_a \Psi_f \sin\theta$$

Since $\theta = 90^\circ$ all the time

$$T \propto I_a I_f \tag{4.2}$$

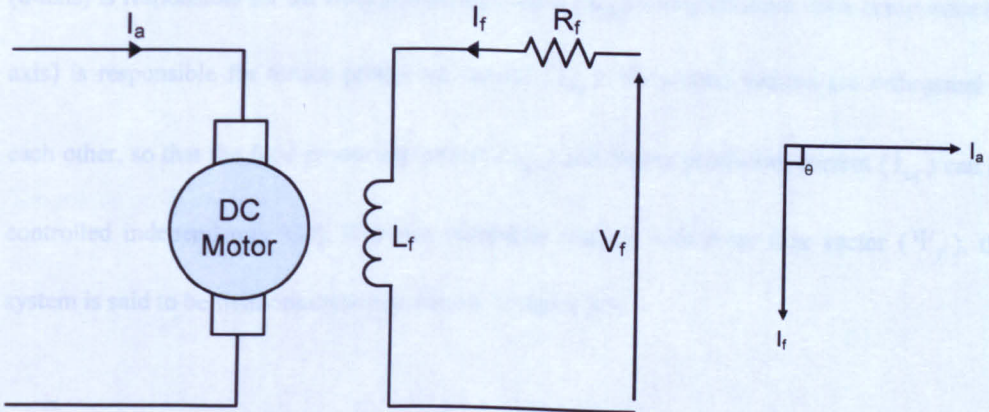


Figure 4.4: DC motor with inherent vector control

4.5. Vector Control

Where, T is the electrical torque developed by the DC motor. The armature current (I_a) and field current (I_f) are inherently decoupled (or independent), therefore it is possible to control the torque by controlling the armature current and keeping the field current constant.

4.5.2 Vectors and Torque in Induction Motor

The same vector concept can be applied to an induction motor. Under three-phase sinusoidal conditions, the current vector I_s has constant magnitude and rotates at a constant speed (ω_e) as shown in figure 4.5. The rotor flux (Ψ_r) is developed by the flux linkage in three-phase rotor coils.

The rotor flux vector Ψ_r rotates at ω_{sl} relative to rotor and rotates at ω_e ($\omega_r + \omega_{sl} = \omega_e$) relative to stator. Therefore, both I_s and Ψ_r rotate at ω_e . In the steady state situation, a constant angle θ exists between I_s and Ψ_r as shown in figure 4.5.

The current vector I_s can be resolved into d-q components (I_{sd}, I_{sq}). The direct axis component (d-axis) is responsible for the field producing current (I_{sd}) and quadrature -axis component (q-axis) is responsible for torque producing current (I_{sq}). These two vectors are orthogonal to each other, so that the field producing current (I_{sd}) and torque producing current (I_{sq}) can be controlled independently [30]. If d-axis current is aligned with rotor flux vector (Ψ_r), the system is said to be field orientation as shown in figure 4.6.

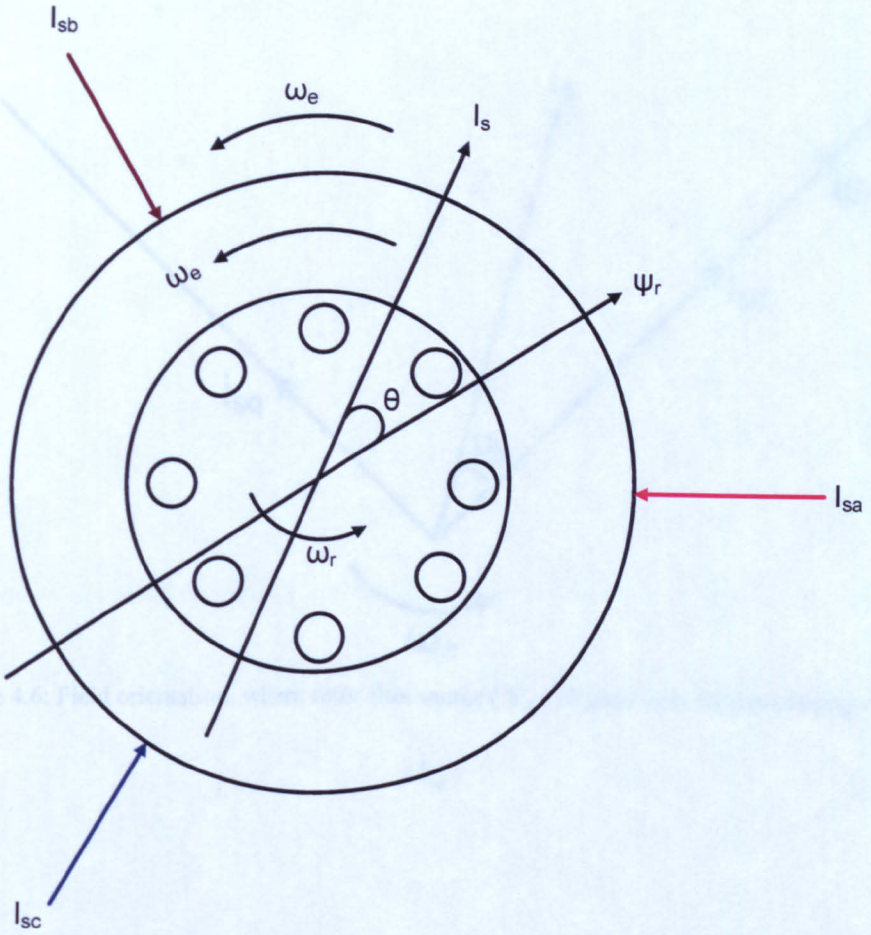


Figure 4.5: Three-phase induction motor model with position of stator current vector (I_s) and rotor flux vector (Ψ_r)

The torque produced by induction motor can be given as:

$$T = k(i_s \times \Psi_r) \quad (4.3)$$

$$T = k |I_s| |\Psi_r| \sin\theta \quad (4.4)$$

4.5. Vector Control

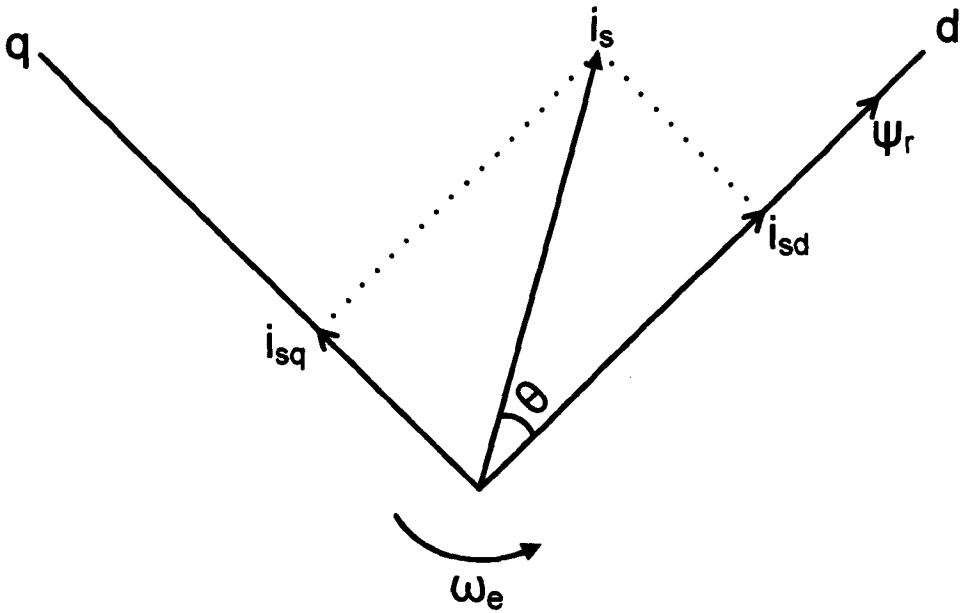


Figure 4.6: Field orientation, where rotor flux vector (Ψ_r) aligned with field producing current (I_{sd})

If I_{sq} at 90° to Ψ_r then equation (4.4) becomes:

$$T = k\Psi_r I_{sq} \tag{4.5}$$

Ψ_r is, in fact, Ψ_{rd} , because Ψ_r is oriented on the d-axis.

$$T_e = kI_{sq} \Psi_{rd} \tag{4.6}$$

If $\Psi_{rd} = L_o I_{mrd}$

$$T_e = kL_o I_{mrd} I_{sq} \tag{4.7}$$

4.5. Vector Control

Since, $I_{mrd} = I_{sd}$, equation (4.7) becomes:

$$T_e = k_t I_{sd} I_{sq} \quad (4.8)$$

Where,

$$k_t = \frac{2}{3} \left(\frac{P}{2} \right) \frac{L_o^2}{Lr} \quad (4.9)$$

This shows that under a constant field current (I_{sd}), the electromagnetic torque is directly proportional to the torque current (I_{sq}). This is shown in equation (4.10):

$$T_e \propto I_{sd} I_{sq} \quad (4.10)$$

Referring to the DC machine torque equation (4.2), the direct-axis current I_{sd} is analogous to field current I_f (the flux producing current) and the quadrature-axis current I_{sq} is analogous to armature current I_a (the torque producing current).

4.5.3 Vector Control Implementation

To implement the vector control for an induction motor, the stator currents are transformed to the stationary and rotating reference frames as required. A three-phase induction machine can be represented by an equivalent two-phase machine using direct (d) and quadrature (q) axis for both stator and rotor as shown in figure 4.7. I_A , I_B and I_C are the stator currents of

4.5. Vector Control

induction motor. $I_{s\alpha}$ and $I_{s\beta}$ represent the direct and quadrature axes currents in the stationary reference frame. I_{sd} and I_{sq} are the direct and quadrature axis currents in the rotating reference frame.

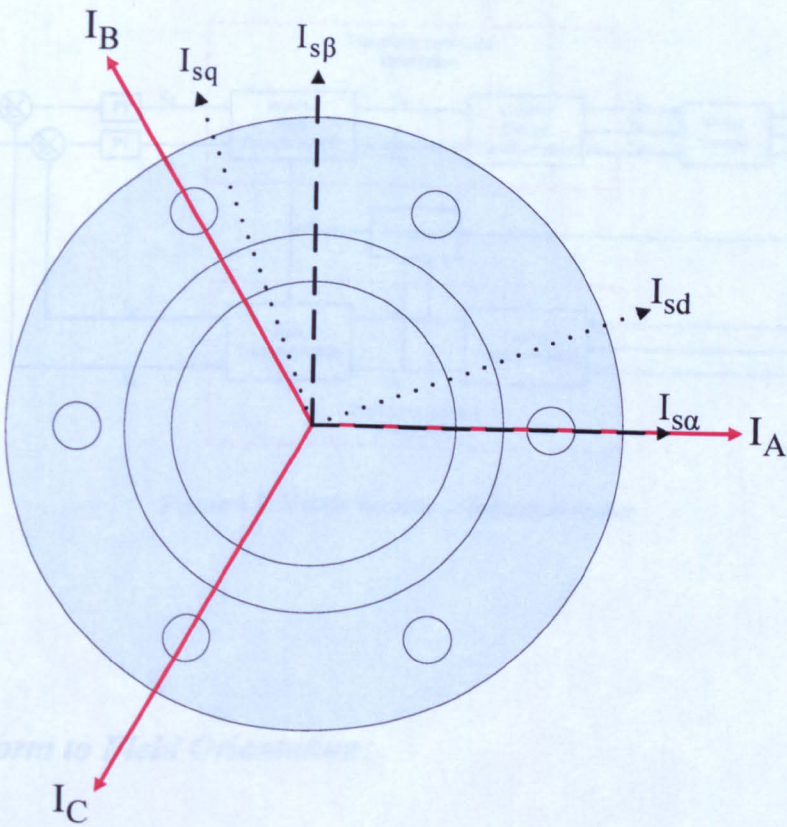


Figure 4.7: d-q representation of AC induction motor

The vector control implementation for the induction motor drive is shown in figure 4.8. The three-phase stator currents are first transformed into the direct and quadrature components of the rotating reference frame. The resulting error terms are then transformed back to three-phase quantities and applied to motor.

4.5. Vector Control

Transform to $\alpha\beta$:

The vector control implementation process can be divided into two parts:

- Transform to field orientation and
- Transform from field orientation.

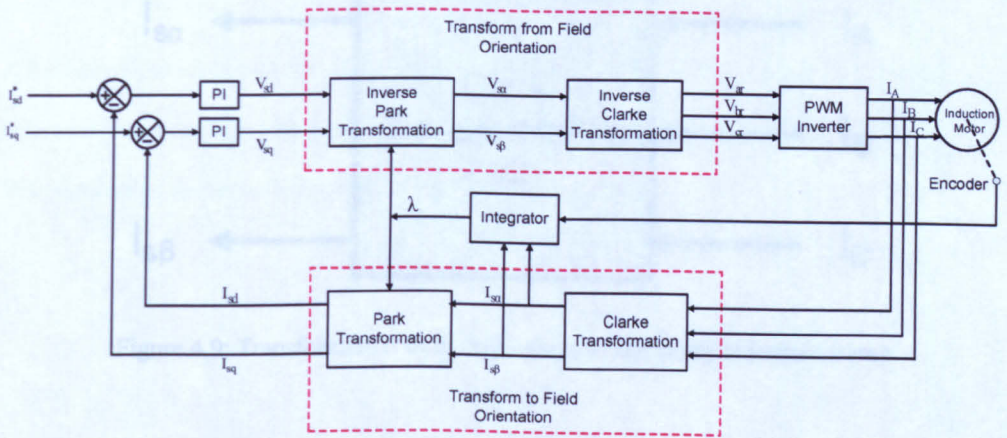


Figure 4.8: Vector control of induction motor

Transform to Field Orientation:

A three to two ($3/2$) phase transformation is used to transform the instantaneous line quantities (A, B, C) into stator reference frame ($\alpha\beta$) and then followed by a vector rotation from stator reference frame ($\alpha\beta$) to rotating reference frame (dq). This can be achieved using the following two stages:

4.5. Vector Control

Transformation to $\alpha\beta$:

This section describes a transformation that can be used to transform the three-phase quantities into the stationary reference frame ($\alpha\beta$). This transformation process is shown by figure 4.9.

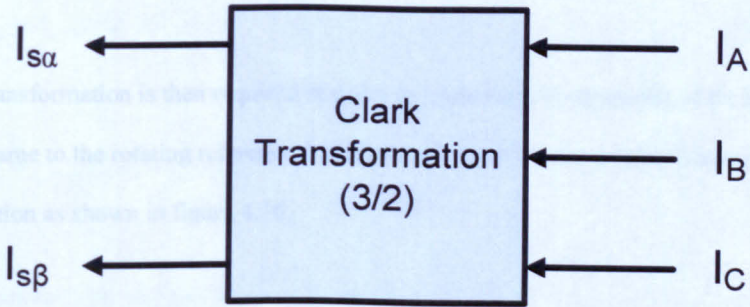


Figure 4.9: Transformation from three-phase to stationary reference frame

The stator current vector of induction motor can be written as:

$$I_s = I_A + I_B e^{j\frac{2\pi}{3}} + I_C e^{j\frac{4\pi}{3}} \quad (4.11)$$

$$I_s = I_{s\alpha} + jI_{s\beta} \quad (4.12)$$

Substitute the equation (4.12) into equation (4.11) and then separating the real and imaginary parts to obtain the values of $I_{s\alpha}$ and $I_{s\beta}$ as shown below:

$$I_{s\alpha} = \frac{3}{2} I_A \quad (4.13)$$

4.5. Vector Control

$$I_{s\beta} = \frac{\sqrt{3}}{2} I_B - \frac{\sqrt{3}}{2} I_C \quad (4.14)$$

The mathematical transformation for this process is known as the “Clarke Transformation”. will be

Transformation from $\alpha\beta$ to dq :

A further transformation is then required in order to relate these components of the stationary reference frame to the rotating reference frame of the rotor. This can be achieved using the Park Transformation as shown in figure 4.10.

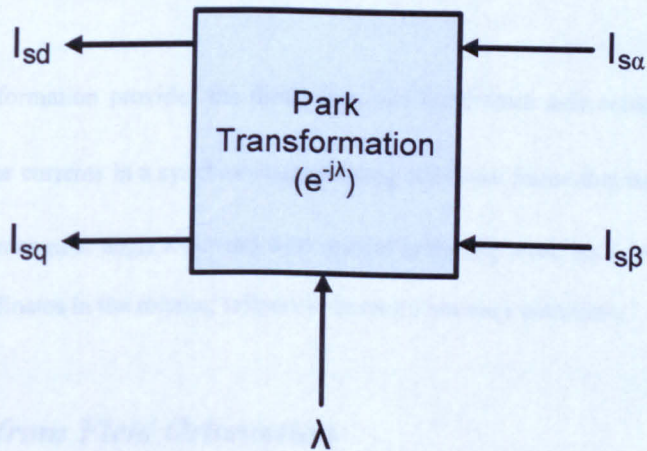


Figure 4.10: Transformation from stationary reference frame to rotating reference frame

If the rotor flux angle (λ) between stationary reference frame and rotating reference frame is known, then the transformation from stationary reference frame ($\alpha\beta$) to rotating reference frame (dq) can be obtained as follows:

4.5. Vector Control

$$I_s e^{-j\lambda} = (I_{s\alpha} + jI_{s\beta})(\cos\lambda - j\sin\lambda) = I_{sd} + jI_{sq} \quad (4.15)$$

By separating the real and imaginary parts of equation (4.15), the final values of I_{sd} and I_{sq} will be:

$$I_{sd} = I_{s\alpha} \cos\lambda + I_{s\beta} \sin\lambda \quad (4.16)$$

$$I_{sq} = -I_{s\alpha} \sin\lambda + I_{s\beta} \cos\lambda \quad (4.17)$$

Where, λ represents the angular position of the rotor flux.

The Park Transformation provides the direct axis and quadrature axis components (I_{sd} and I_{sq}) of the stator currents in a synchronously rotating reference frame that rotate at an angular velocity ω and an angular angle λ ($\lambda = \omega t$) with respect to the α - β axes. As a result, in the steady state, these coordinates in the rotating reference frame do not vary with time.

Transform from Field Orientation

The transformation from the rotating reference frame (dq) to three-phase quantities is required in the implementation of vector control of an induction motor. For this the quantities in rotating reference frame (dq) are first transform into the stationary reference frame ($\alpha\beta$) and then to three-phase quantities. This can be achieved using the following two stages:

4.5. Vector Control

Transformation from dq to $\alpha\beta$:

This section describes a transformation that can be used to transform the quantities in the rotating reference frame (dq) to the stationary reference frame ($\alpha\beta$). By using this transformation real stationary quadrature voltages can be obtained. This transformation process is known as Inverse Park Transformation, as shown in figure 4.11.

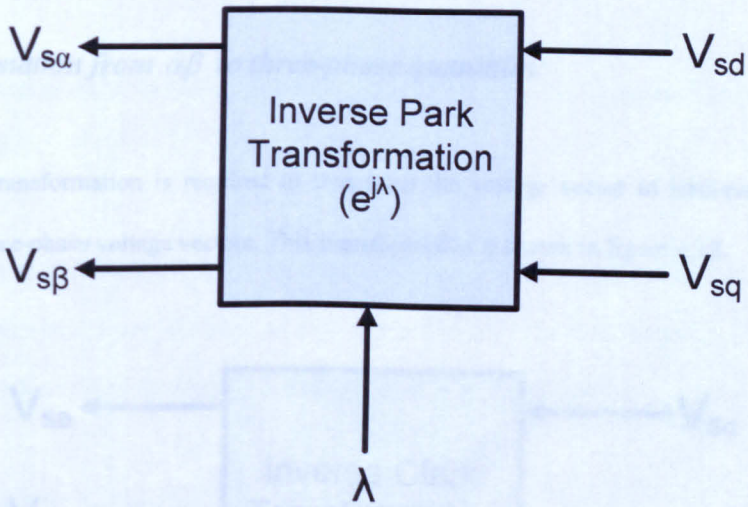


Figure 4.11: Transformation from rotating reference frame to stationary reference frame

The two to three phase transformations can be achieved using:

$$\mathbf{V}_s = (V_{s\alpha} + jV_{s\beta}) = (V_{sd} + jV_{sq})e^{j\lambda} \quad (4.18)$$

$$\mathbf{V}_s = (V_{s\alpha} + jV_{s\beta}) = (V_{sd} + jV_{sq})(\cos\lambda + j\sin\lambda) \quad (4.19)$$

4.5. Vector Control

By separating the real and imaginary parts of equation (4.19), the value of $V_{s\alpha}$ and $V_{s\beta}$ can be obtained:

$$V_{s\alpha} = V_{sd} \cos\lambda - V_{sq} \sin\lambda \quad (4.20)$$

$$V_{s\beta} = V_{sd} \sin\lambda + V_{sq} \cos\lambda \quad (4.21)$$

Transformation from $\alpha\beta$ to three-phase quantities:

A further transformation is required to transform the voltage vector in stationary reference frame to three-phase voltage vectors. This transformation is shown in figure 4.12.

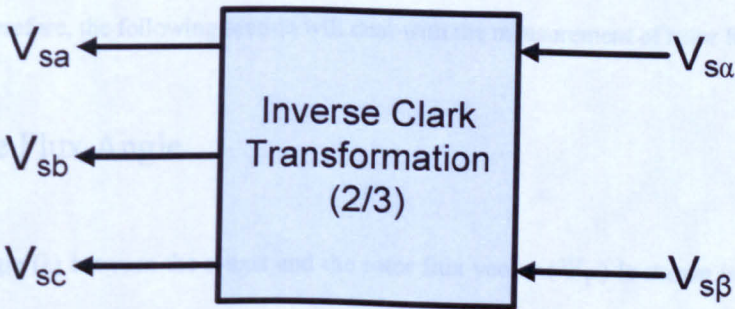


Figure 4.12: Transformation from the stationary reference frame to three-phase quantities

The $\alpha\beta$ to three-phase transformation can be obtained by solving equations (4.13) and (4.14)

in terms of voltages together with $V_{sa} + V_{sb} + V_{sc} = 0$;

4.5. Vector Control

$$V_{sa} = \frac{2}{3} V_{sa} \quad (4.22)$$

$$V_{sb} = -\frac{1}{3} V_{sa} + \frac{1}{\sqrt{3}} V_{sp} \quad (4.23)$$

$$V_{sc} = -\frac{1}{3} V_{sa} - \frac{1}{\sqrt{3}} V_{sp} \quad (4.24)$$

The mathematical transformation of above process is known as the “Inverse Clark Transformation”.

As shown in above section, the correct measurement of rotor flux angle (λ) is important in the Park Transformation and the Inverse Park Transformation to complete the transformation process. Therefore, the following section will deal with the measurement of rotor flux angle (λ).

4.5.4 The Flux Angle

The flux angle (λ) between the α -axis and the rotor flux vector (Ψ_r) is shown in figure 4.13. The flux angle (λ) is used to produce the correct field orientation by ensuring the alignment of I_{sd} with the Ψ_r .

The d-q frame rotates at a frequency, ω_e . This gives the following equation:

$$\omega_e(t) = \frac{d}{dt} \lambda(t) \quad (4.25)$$

4.5. Vector Control

$$\lambda(t) = \int \omega_e(t) dt \quad (4.26)$$

To implement direct vector control the rotor flux angle (λ) is obtained by directly measuring the air-gap flux in the machine. The air-gap flux can be measured by using the Hall effect sensors, which are mounted in the air-gap. Figure 4.14 shows that the Hall effect sensors are arranged in electrical quadrature which provides the air-gap flux along the axis of Ψ .

The flux angle (λ) can be either measured directly using the sensors embedded in the motor or derived indirectly. These two methods lead to two vector control techniques:

- Direct vector control
- Indirect vector control

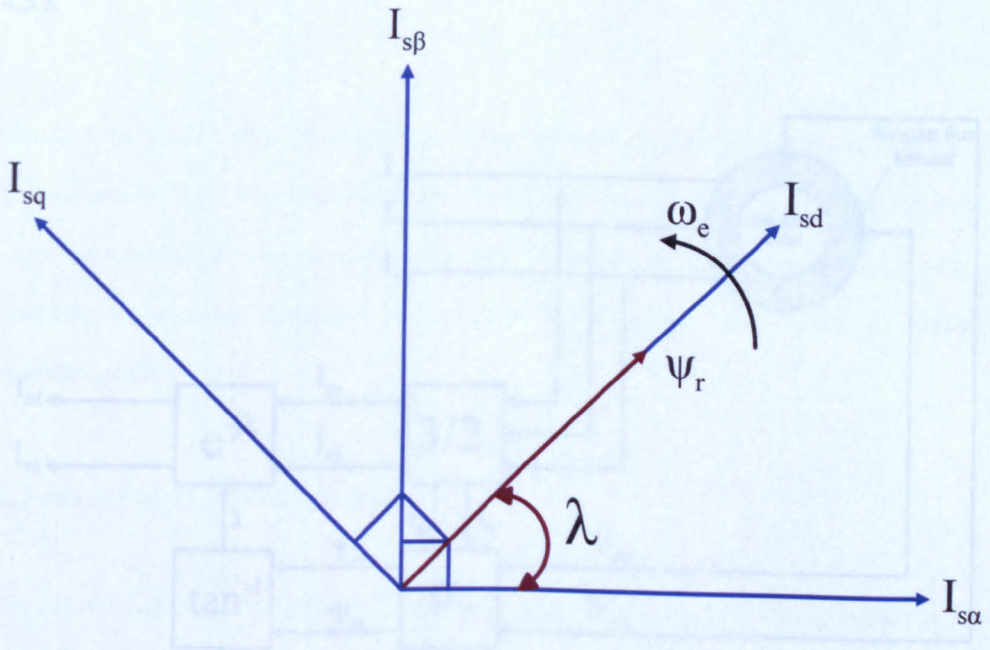


Figure 4.13: d-q representation of AC induction motor with field producing current (I_{sd})

Figure 4.14: Schematic for air-gap flux measurement used in direct vector control of an induction motor.

4.5.4.1 Direct Vector Control

To implement direct vector control the rotor flux angle (λ) is calculated by directly measuring the air-gap flux in the machine. The air-gap flux can be measured by using the Hall Effect sensors, which are mounted in the air-gap. Figure 4.14 shows that the Hall Effects sensors are arranged in electrical quadrature which provides the air-gap flux linkage in the form of $\Psi_{o\alpha}$ and $\Psi_{o\beta}$ [37].

The rotor flux linkage ($\Psi_{r\alpha}, \Psi_{r\beta}$) can be calculated from these air-gap flux linkages ($\Psi_{o\alpha}, \Psi_{o\beta}$) using the equations (4.27) and (4.28) respectively [51]. The three-phase stator currents (I_A, I_B, I_C) are referred to the stator stationary frame ($I_{s\alpha}, I_{s\beta}$), as discussed in section 4.5.3.

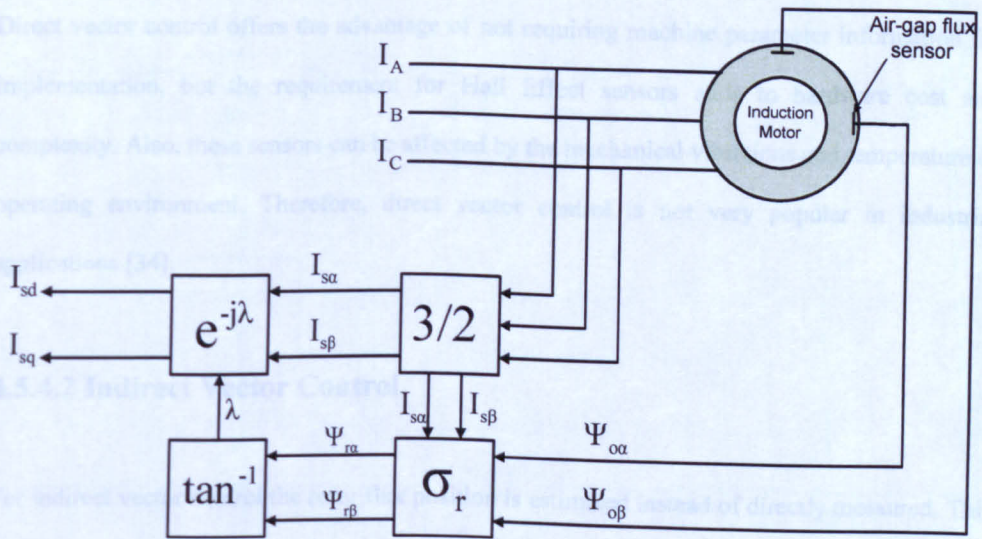


Figure 4.14: Schematic for air-gap flux measurement used in the direct vector control of an induction motor

4.5. Vector Control

$$\Psi_{ra} = (1 + \sigma_r) \Psi_{\sigma a} - L_o I_{sa} \quad (4.27)$$

$$\Psi_{rp} = (1 + \sigma_r) \Psi_{\sigma p} - L_o I_{sp} \quad (4.28)$$

where, $\sigma_r = \frac{L_r - L_o}{L_o}$, σ_r is Leakage co-efficient, L_r is rotor inductance and L_o is mutual inductance.

The rotor flux angle (λ) can be calculated using:

$$\lambda = \tan^{-1} \left(\frac{\Psi_{rp}}{\Psi_{ra}} \right) \quad (4.29)$$

Direct vector control offers the advantage of not requiring machine parameter information for implementation, but the requirement for Hall Effect sensors adds to hardware cost and complexity. Also, these sensors can be affected by the mechanical vibrations and temperature of operating environment. Therefore, direct vector control is not very popular in industrial applications [34].

4.5.4.2 Indirect Vector Control

For indirect vector control the rotor flux position is estimated instead of directly measured. This method is also known as slip frequency control, because the instantaneous rotor flux angle (λ) depends on the slip frequency (ω_{sl}) and motor shaft speed (ω_e). The rotor flux position information can be derived by measuring the rotor speed using a shaft mounted encoder. Figure

4.5. Vector Control

4.15, shows the schematic for measurement of rotor flux angle (λ) for use in indirect vector control. The slip frequency (ω_{sl}) can be accurately estimated using the reference d-q axis currents (I_{sd}^*, I_{sq}^*) and rotor time constant, (τ_r) [51]:

$$\omega_{sl} = \frac{I_{sq}^*}{\tau_r I_{sd}^*} \quad (4.30)$$

where, $\tau_r = \frac{L_r}{R_r}$

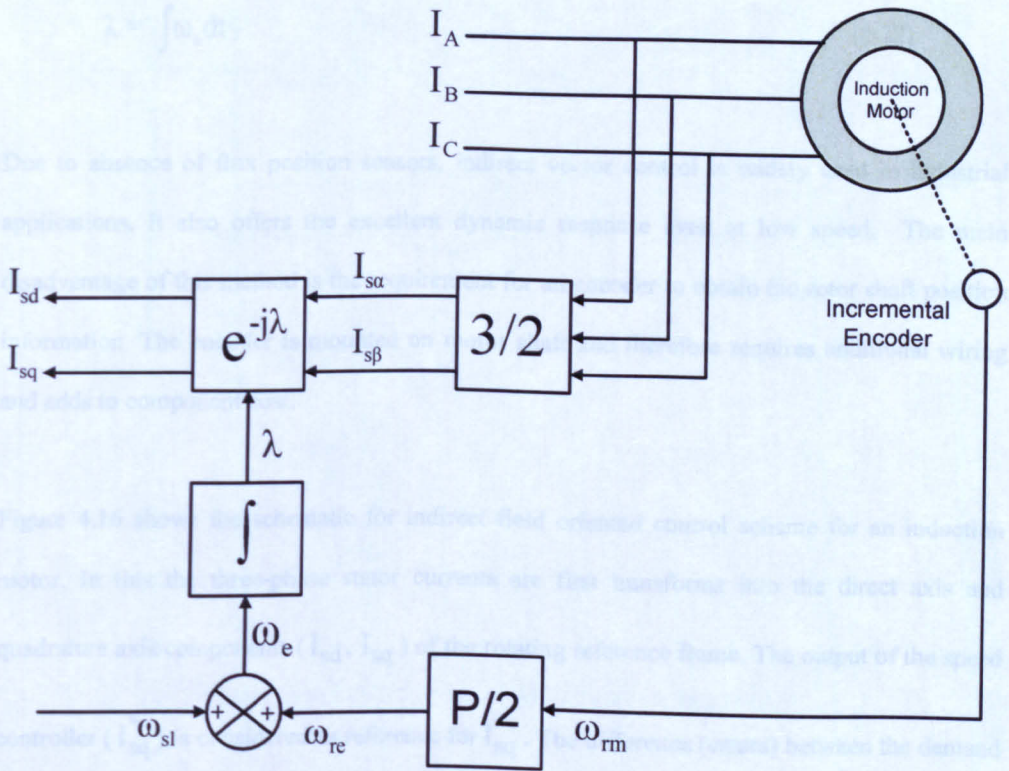


Figure 4.15: Schematic for flux angle measurement used for indirect vector control of induction motor

4.5. Vector Control

The motor speed obtained using an incremental encoder is the mechanical speed (ω_m) of the motor, which is then multiplied by motor pole pair to convert to electrical rad/sec (ω_{re}). The electrical speed (ω_e) can then be obtained by adding the slip speed (ω_{sl}) and the measured electrical speed (ω_{re}) as shown in equation (4.31):

$$\omega_e = \omega_{sl} + \omega_{re} \quad (4.31)$$

The rotor flux angle is obtained by integrating the electrical speed (ω_e):

$$\lambda = \int \omega_e dt \quad (4.32)$$

Due to absence of flux position sensors, indirect vector control is widely used in industrial applications. It also offers the excellent dynamic response even at low speed. The main disadvantage of this method is the requirement for an encoder to obtain the rotor shaft position information. The encoder is mounted on motor shaft and therefore requires additional wiring and adds to component cost.

Figure 4.16 shows the schematic for indirect field oriented control scheme for an induction motor. In this the three-phase stator currents are first transforms into the direct axis and quadrature axis components (I_{sd} , I_{sq}) of the rotating reference frame. The output of the speed controller (I_{sq}^*) is considered as reference for I_{sq} . The difference (errors) between the demand value (I_{sd}^* , I_{sq}^*) and actual value (I_{sd} , I_{sq}) of the direct and quadrature axis current components are input to the current controllers. The outputs of the current controllers are

4.5. Vector Control

summed with voltage compensation terms. Then the output terms (V_{sd}^* , V_{sq}^*) that are referenced to the rotating reference frame are transformed back to the three-phase reference voltages (V_{ra}^* , V_{rb}^* , V_{rc}^*) for the PWM generation. The design of speed controller and current controllers will be discussed in the sections 4.5.5 and 4.5.6 respectively. The voltage compensation terms will be described in section 4.5.7.

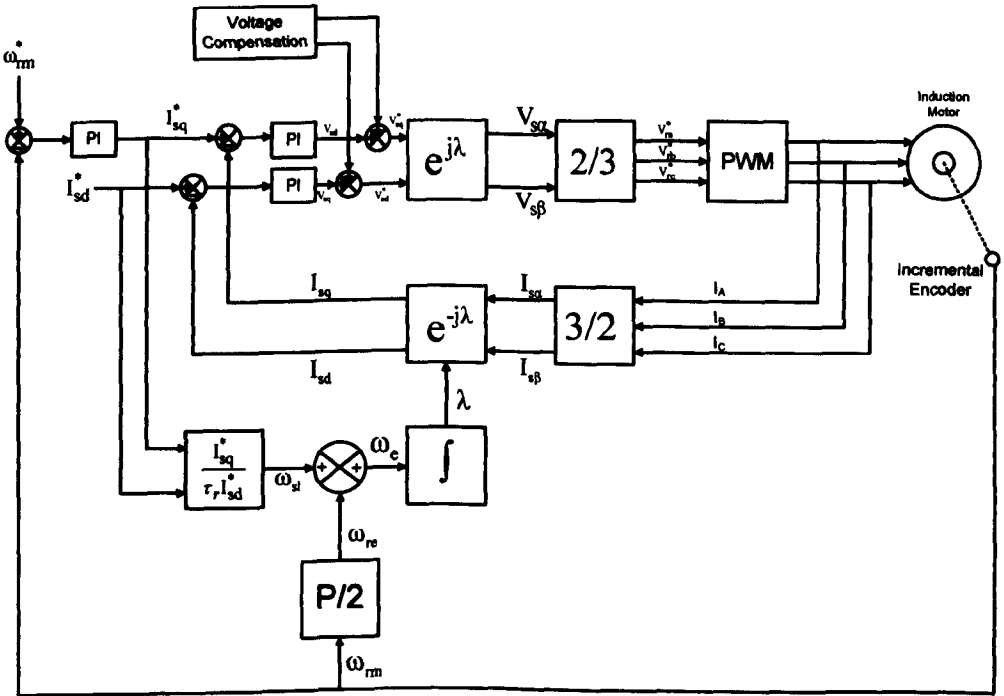


Figure 4.16: Indirect vector field oriented control scheme

4.5. Vector Control

4.5.5 Current Controller Design

The block diagram shown in figure 4.17 is common to both the torque producing current (I_{sq}) and the field producing current (I_{sd}) controller, since both are governed by the same armature time constant (τ_s). The armature time constant (τ_s) is defined as the ratio between the motor leakage co-efficient (σL_s) and the stator resistance (R_s).

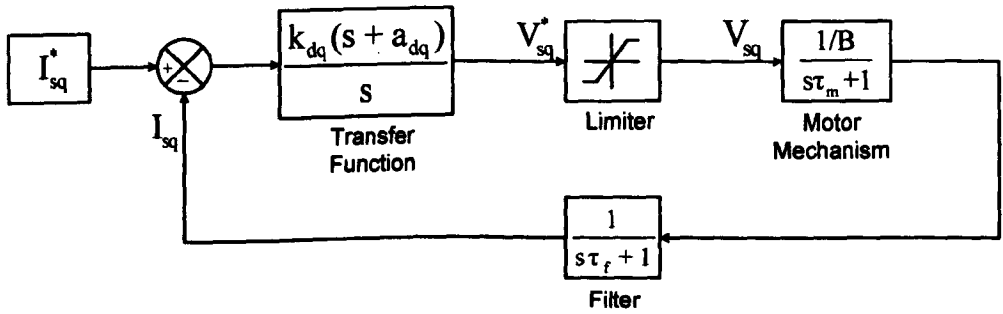


Figure 4.17: Block diagram of the design of current controller

The current controller loop includes the PI controller, a limiter which represents the maximum phase voltage that can be obtained from the converter (V_{sq}) and the stator characteristics of the induction motor with stator resistance (R_s) and motor leakage co-efficient (σL_s).

The motor leakage co-efficient (σL_s) can be calculated using:

$$\sigma L_s = \frac{L_s L_r - L_o^2}{L_r} \quad (4.33)$$

4.5. Vector Control

Where L_s is the stator self inductance, L_r is the rotor self inductance and L_0 is the mutual inductance.

The current control is the inner control loop and speed control is outer control loop. The bandwidth of the current controller is between 1/5 and 1/10 times the converter switching frequency. To drive the motor in stable mode, the bandwidth of the current control loop has to be at least ten times faster than that of speed control loop.

4.5.6 Speed Control Loop Design

The schematic block diagram of the speed controller is shown in figure 4.18. The speed error is the difference between the demand speed (ω_{re}^*) and actual speed (ω_{re}). The speed error is then passed through a PI controller, which gives the output in the form of the demanded torque producing current. The demanded torque producing current (I_{sq}^*) is kept within a defined range using a limiter. The measured value of the torque producing current (I_{sq}), with torque constant (k_t), is used to produce the electrical torque as shown in equation (4.8).

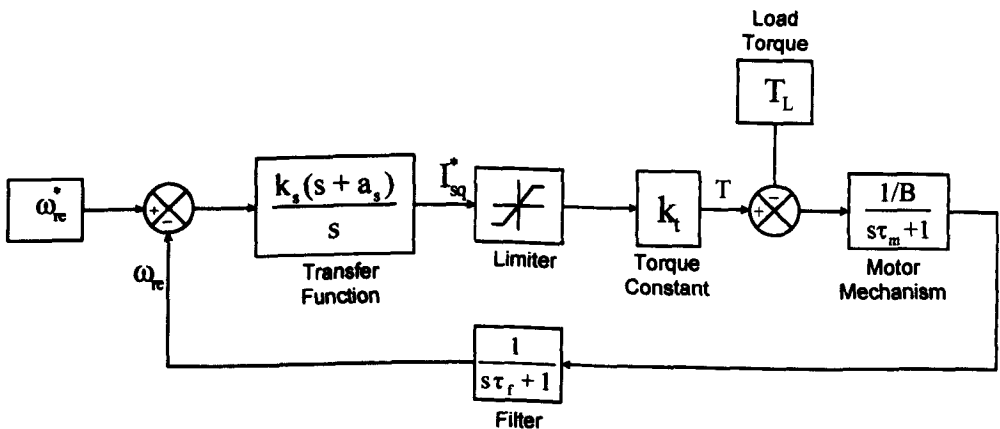


Figure 4.18: Block diagram of the speed controller

4.5. Vector Control

The mechanical dynamics of the motor are defined by:

$$T = T_L + J s \omega_{re} + B \omega_{re} \quad (4.34)$$

$$\text{and } \tau_m = \frac{J}{B}$$

where J is moment of inertia and B is rotational friction of the motor and load. The bandwidth of the speed control loop is normally 1/10 of the current control loop bandwidth.

4.5.7 Voltage Compensation Terms

To improve the performance of the current control loop, compensation voltages are added with the output of the current controllers. The voltage compensation terms can be derived from the stator equations as given in Appendix-'C'.

$$V_{sd} = R_s I_{sd} + \sigma L_s \frac{d}{dt} I_{sd} - \omega_c \sigma L_s I_{sq} + \frac{L_o}{L_r} \frac{d}{dt} \Psi_{rd} \quad (4.35)$$

$$V_{sq} = R_s I_{sq} + \sigma L_s \frac{d}{dt} I_{sq} + \omega_c \sigma L_s I_{sd} + \omega_c \frac{L_o}{L_r} \Psi_{rd} \quad (4.36)$$

Therefore the voltage compensation terms are:

$$V_{sdc} = -\omega_c \sigma L_s I_{sq} + \frac{L_o}{L_r} \frac{d}{dt} \Psi_{rd} \quad (4.37)$$

4.5. Vector Control

$$V_{sqc} = \omega_e \sigma L_s I_{sd} + \omega_e \frac{L_0}{L_r} \Psi_{rd} \quad (4.38)$$

$$\text{where, } \Psi_{rd} = L_0 I_{mrd} \quad (4.39)$$

For steady state condition: $I_{mrd} = I_{sd}^*$, then equation (4.39) became:

$$\Psi_{rd} = L_0 I_{sd}^* \quad (4.40)$$

Substitute the equation (4.40) in equation (4.35) and (4.36) as:

$$V_{sdc} = -\omega_e \sigma L_s I_{sq} + \frac{L_0^2}{L_r} \frac{d}{dt} I_{sd}^* \quad (4.41)$$

$$V_{sqc} = \omega_e \sigma L_s I_{sd} + \omega_e \frac{L_0^2}{L_r} I_{sd}^* \quad (4.42)$$

These voltage compensation terms are added to the output of each current controller to get the reference voltages V_{sd}^* and V_{sq}^* as shown in figure 4.19.

4.6. Direct Torque Control (DTC)

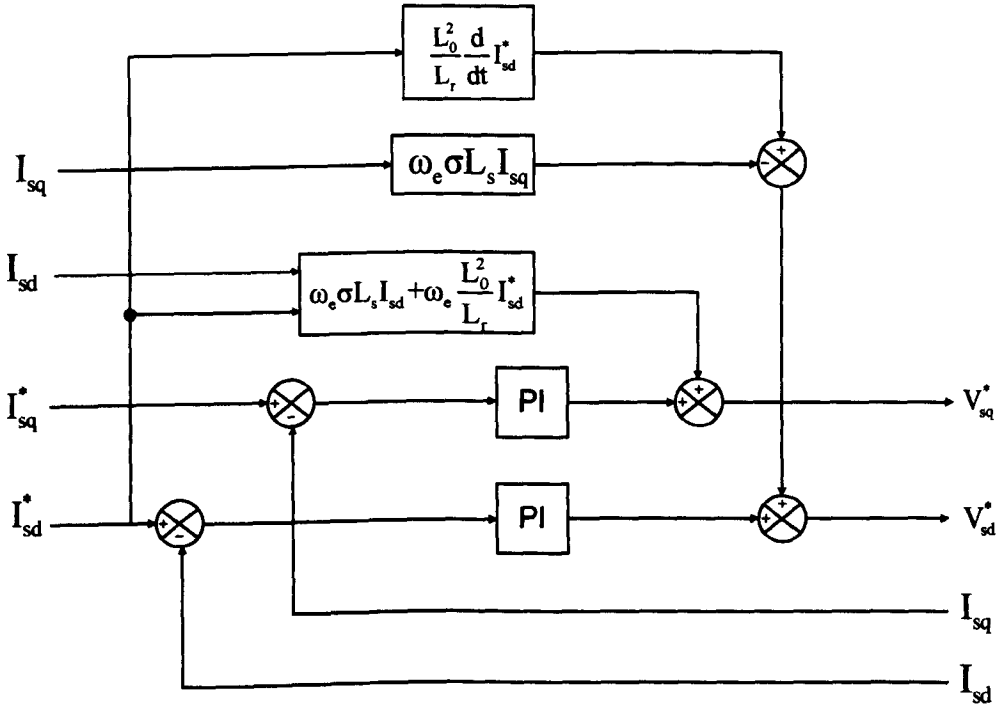


Figure 4.19: Block diagram of the voltage compensation terms used for the vector control of an induction motor

4.6 Direct Torque Control (DTC)

The difference between the traditional vector control methods and DTC is that DTC has no fixed switching pattern. The switches in the inverter are controlled according to load requirement; hence DTC response is extremely fast due to elimination of fixed switching patterns in the converter modulation [35].

4.7 Vector Control Scheme for Proposed Multi-Motor Drive System

Induction motors are most widely used motors in industrial motion control and domestic appliances due to their reliability, robustness and simplicity. The major limitation of induction motors is poor dynamic behavior because of rotor flux is in relative with stator flux, which depends on slip speed, and hence both are not always orthogonal position. In order to overcome this problem, an indirect vector field oriented control technique can be used for the speed control of induction motors [34].

Figure 4.20 shows the block diagram of the vector control scheme for the proposed multi-motor drive system where the three-phase currents for each machine and the rotor position are measured. The motor speed (ω_{re}) is measured by determining the rate of change of the position encoder and comparing this to the demanded speed (ω_{re}^*). The resulting speed error is then processed by a proportional-integral (PI) controller to produce the reference for the torque producing current (I_{sq}^*).

In this control scheme the three-phase stator currents (I_{A1}, I_{B1}, I_{C1}) and (I_{A2}, I_{B2}, I_{C2}) are transformed to stationary two-axis currents, ($I_{s\alpha1}, I_{s\beta1}$) and ($I_{s\alpha2}, I_{s\beta2}$) using the Clark transformation. These two-axis currents are then transformed into the rotating d-q axis currents, (I_{sd1}, I_{sq1}) and (I_{sd2}, I_{sq2}) using the Park Transformation. In order to calculate the rotating d-q axis current, the value of flux angle is needed. This angle is determined by integrating the sum of the rotor position signal and the reference slip position obtained using equation (4.25). The transformation of the d-q axis values back to the instantaneous stator reference frame by using the Inverse Park Transformation [18].

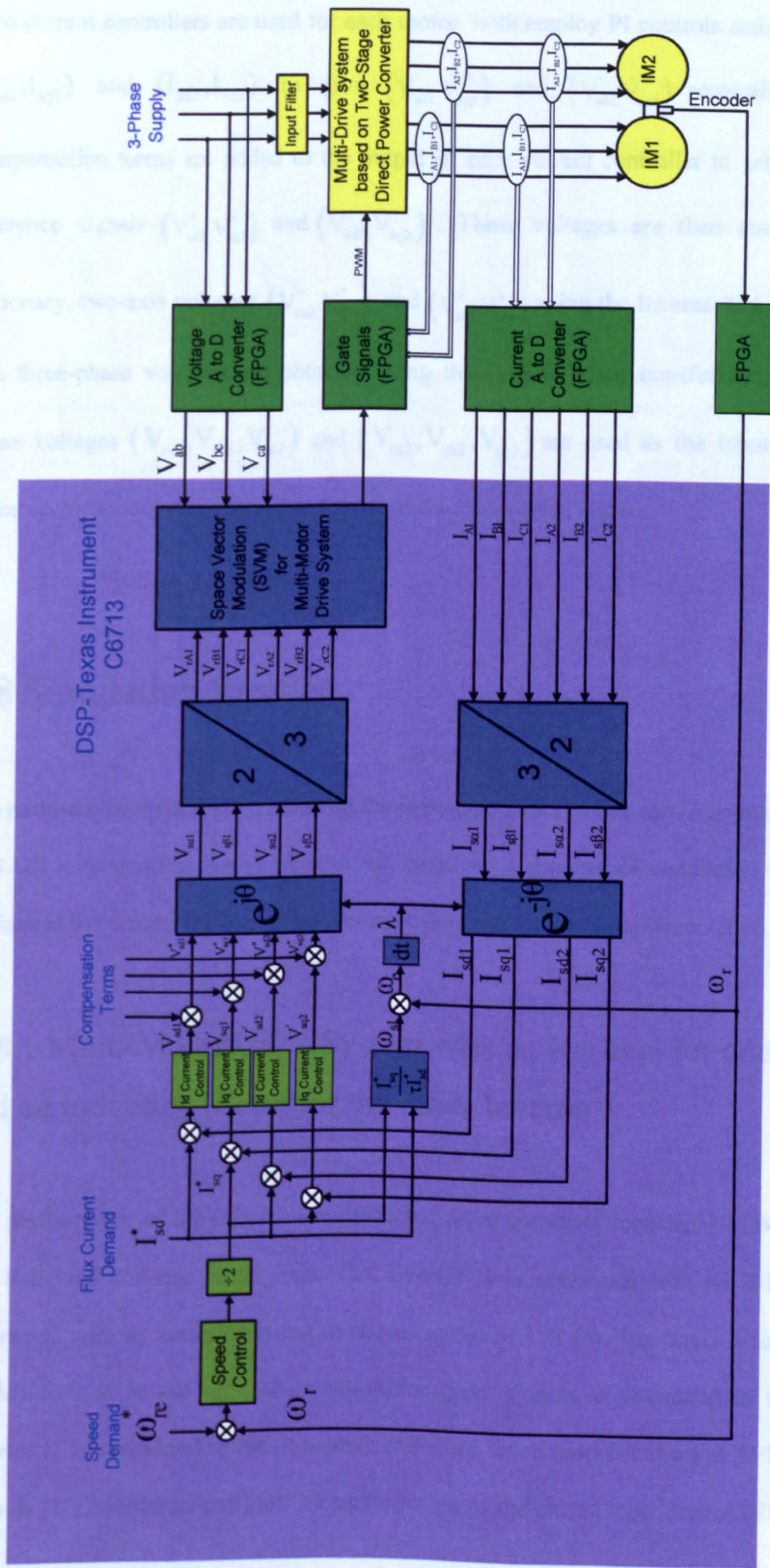


Figure 4.20: The Indirect vector field oriented control scheme for the proposed multi-motor drive system

4.8. Simulation Results

Two current controllers are used for each motor, both employ PI controls acting as the error in (I_{sd1}, I_{sq1}) and (I_{sd2}, I_{sq2}) to give (V'_{sd1}, V'_{sq1}) and (V'_{sd2}, V'_{sq2}) respectively. Voltage compensation terms are added to the output of each current controller to get the d-q voltage reference signals (V^*_{sd1}, V^*_{sq1}) and (V^*_{sd2}, V^*_{sq2}) . These voltages are then converted into the stationary, two-axis voltages (V^*_{sa1}, V^*_{sb1}) and (V^*_{sa2}, V^*_{sb2}) using the Inverse Park Transformation. The three-phase voltages are obtained using the Inverse Clark transformation. These three-phase voltages $(V_{ra1}, V_{rb1}, V_{rc1})$ and $(V_{ra2}, V_{rb2}, V_{rc2})$ are used as the input signals for the space vector modulation algorithm for the multi-motor drive system.

4.8 Simulation Results

The multi-motor drive system based on the two-stage direct power converter has been simulated in SABER to confirm the validity of the concept. A number of simulation tests have been performed to confirm the correct operation of the vector control implementation.

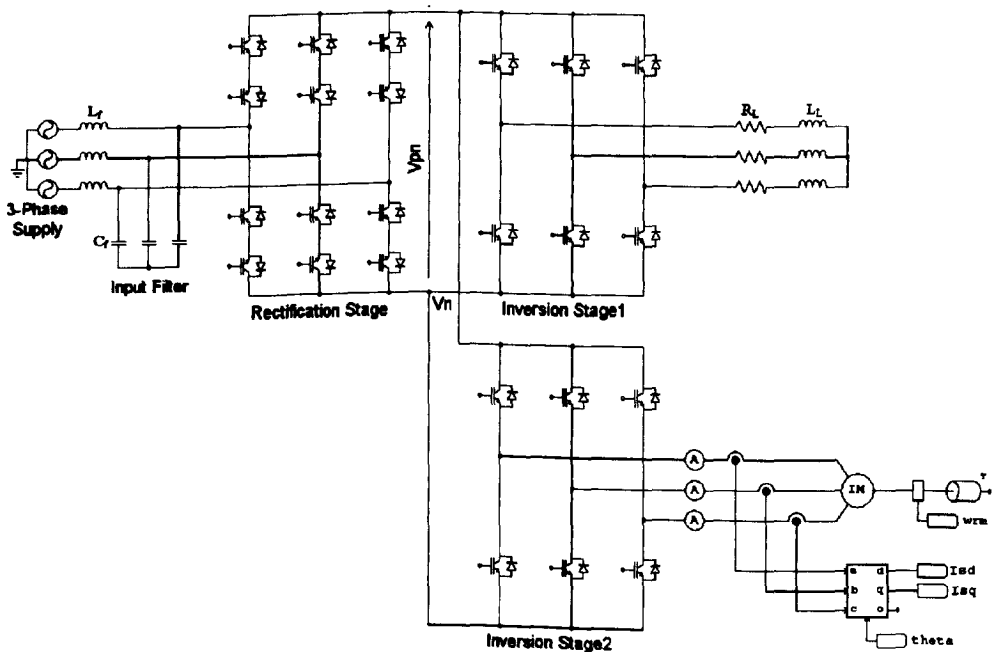
4. 8.1 Multi-Motor Drive System with an RL load for one Inverter and an Induction Motor for the other Inverter

The performance of the proposed multi-motor drive converter topology has been tested with one R-L load and one motor load. The inverter I1 is connected with an R-L load and the inverter I2 with an induction motor as shown in figure 4.21 (a). The Space Vector Modulation (SVM) is used to modulate the multi-motor drive system as discussed in Chapter-3. The inverter I1 is connected to the R-L load; therefore, open loop control and SVM are used for inverter I1. In order to analyse the performance of the closed loop control of the inverter I2,

4.8. Simulation Results

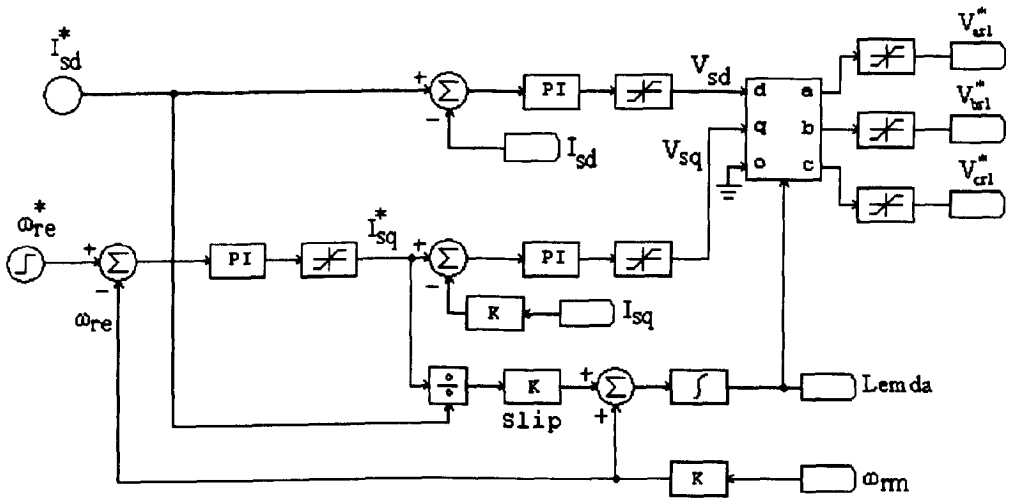
the vector field oriented control scheme is used to control the induction motor, as shown in figure 4.21 (b). The output currents (I_{A2} , I_{B2} , I_{C2}) of the inverter I2 are used to calculate the d-q axis currents (I_{sd} , I_{sq}). The d-q axis currents are then used to calculate the reference voltages (V_{ra2} , V_{rb2} , V_{rc2}) as shown in figure 4.21 (b). The simulation parameters are listed in Appendix 'D'.

The simulation results for the multi-drive converter system are shown in figure 4.22. The closed loop vector performance for inverter I2 is shown in figure 4.22. Figure 4.22 (a) shows the three-phase supply voltage for the multi-drive converter. Figure 4.22 (b) shows the dynamic performance of the induction motor driving acceleration from standstill to 82 rad/sec with no-load torque. Figure 4.22 (c) shows the set of sinusoidal, balanced input currents obtained at the supply side of the converter. It is noted that at 0.1 second the motor starts accelerating, therefore it require more supply current until it reaches steady state position. The supply currents remain constant during steady state operation.



(a) Multi-motor drive converter circuit

4.8. Simulation Results



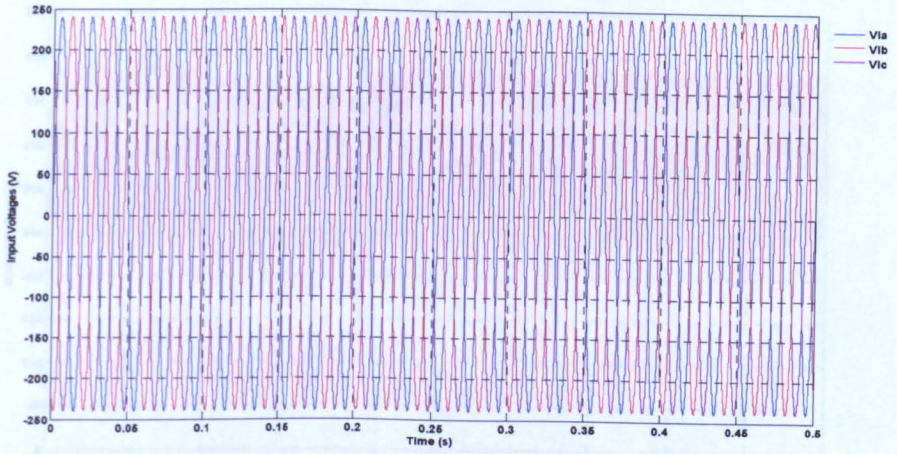
(b) Vector control scheme for Inverter I2

Figure 4.21: The multi-motor drive converter system with an R-L load on inverter I1 and an induction motor load on inverter I2

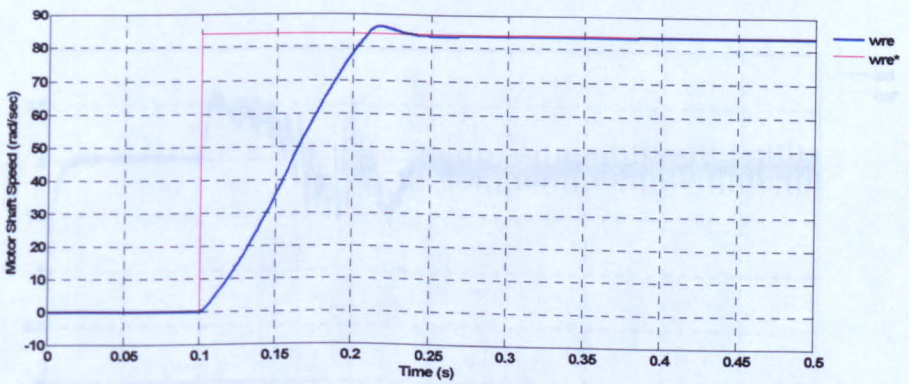
Figure 4.22 (d) present the 'DC-link' voltage provided by the rectification stage. Each output terminal of the rectification stage is maintained with a unipolar voltage waveforms V_p and V_n . Therefore, the voltage difference in the two output phages, V_{pn} becomes a variable DC-link voltage.

The field producing current (I_{sd}) is maintained a constant level during steady state speed, as shown in figure 4.22 (e). The reference of the field producing current (I_{sd}^*) is maintained 2.0A and the torque producing current (I_{sq}^*) has a maximum value of 10.0A, as shown in figure 4.22 (f). The output performance of the multi-motor drive system with open loop and closed loop vector control is shown by the three-phase output currents and line-to-line output voltage waveforms for inverter I1 and I2 in figure 4.22 (g) to (j).

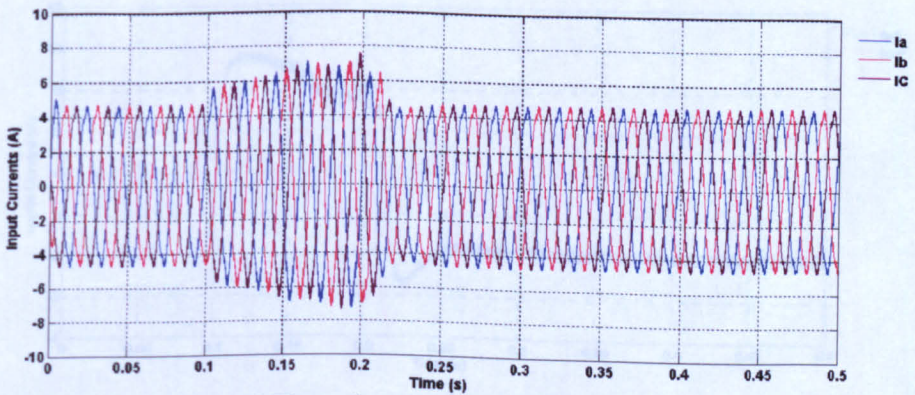
4.8. Simulation Results



(a) Three-phase input voltages

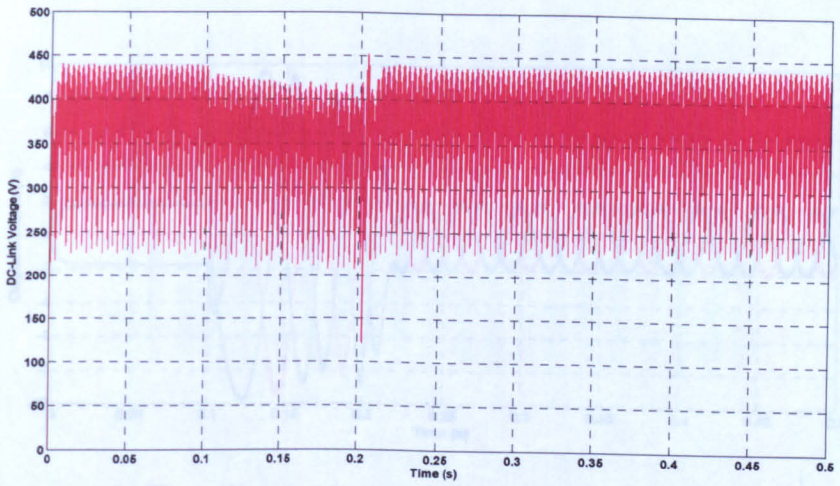


(b) Motor shaft speed connected on Inverter I2

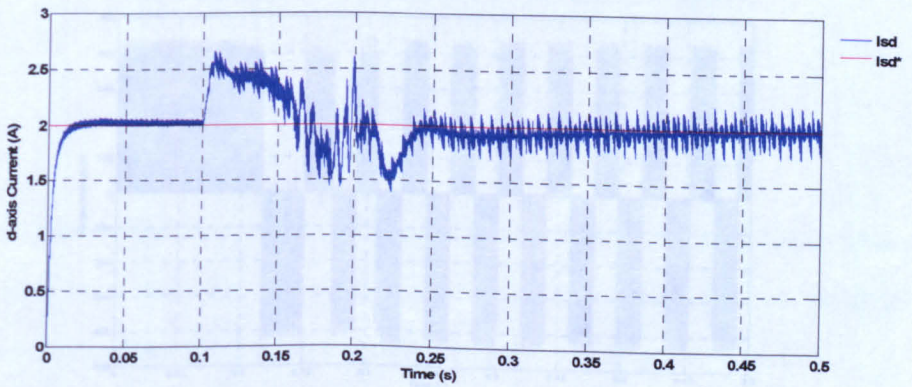


(c) Three-phase input currents (I_a , I_b , I_c)

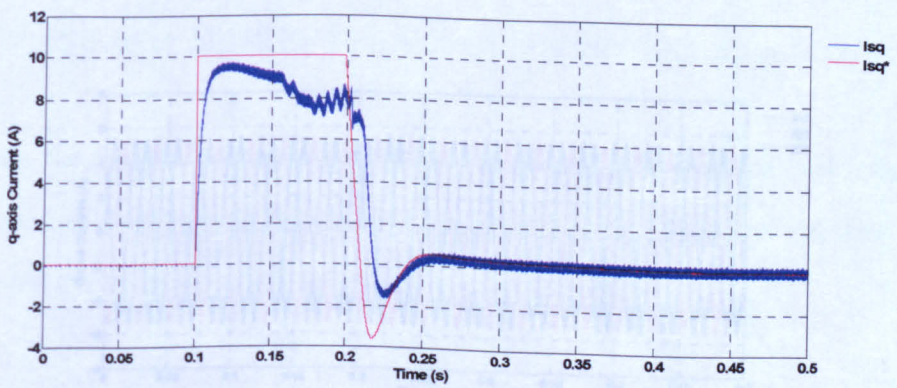
4.8. Simulation Results



(d) DC-link voltage (V_{pn})

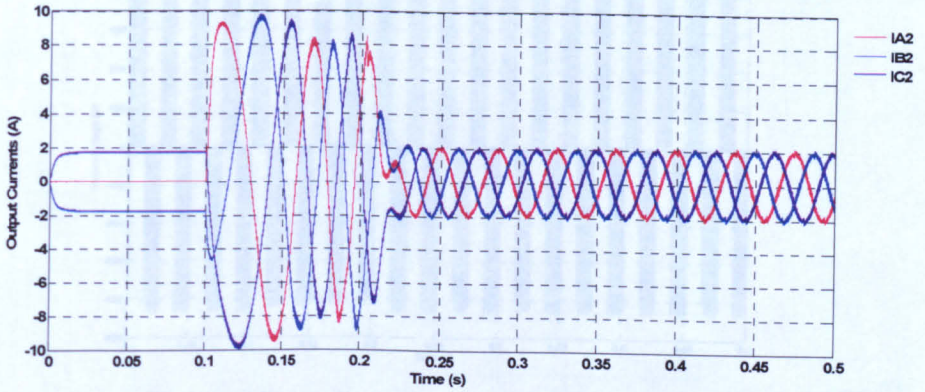


(e) d-axis current for induction motor

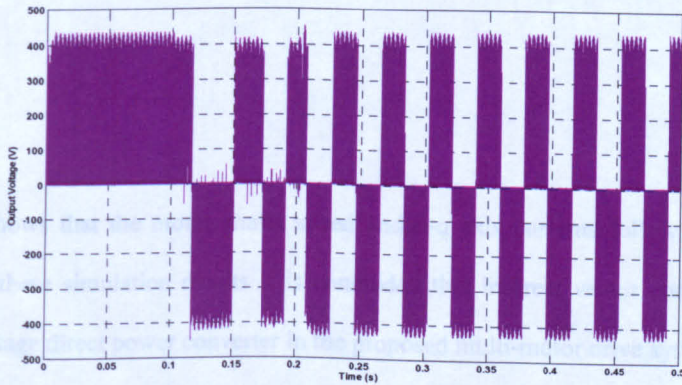


(f) q-axis current for induction motor

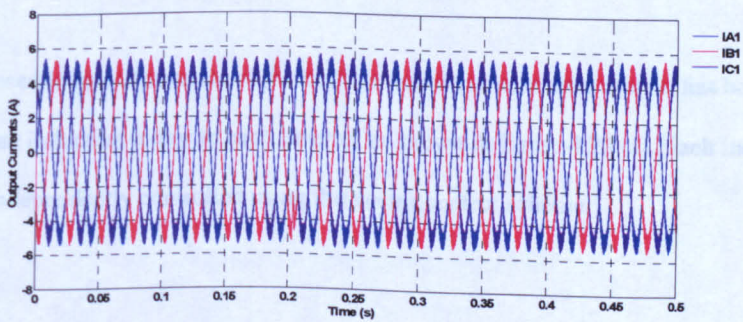
4.8. Simulation Results



(g) Three-phase output currents (I_{A2} , I_{B2} , I_{C2}) for inverter I2

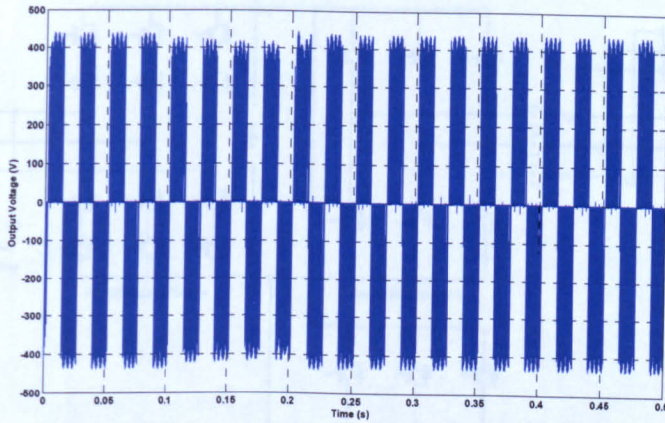


(h) Output line-to-line voltage (V_{AB2}) for inverter I2



(i) Three-phase output currents (I_{A1} , I_{B1} , I_{C1}) for inverter I1

4.8. Simulation Results



(j) Output line-to-line voltage (V_{AB1}) for inverter I1

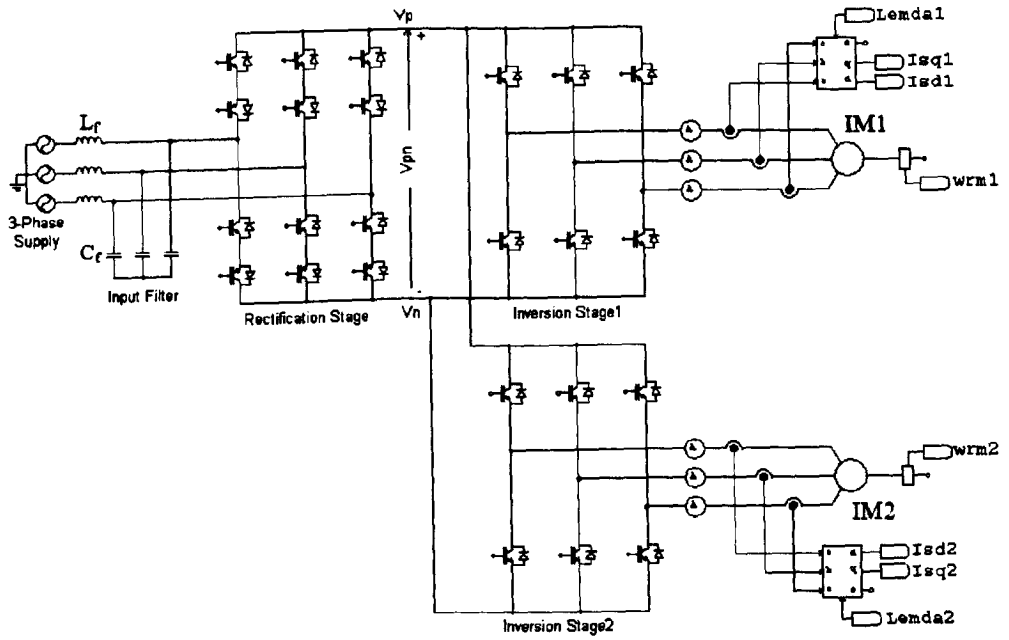
Figure 4.22: Simulation results for multi-motor drive system when inverter I1 connected with R-L load and inverter I2 connected to an induction motor

Figure 4.22 shows that the motor shafts speed and d-q axis currents follow their references values. From these simulation results it is concluded that indirect vector control works well with the two-stage direct power converter in the proposed multi-motor drive system.

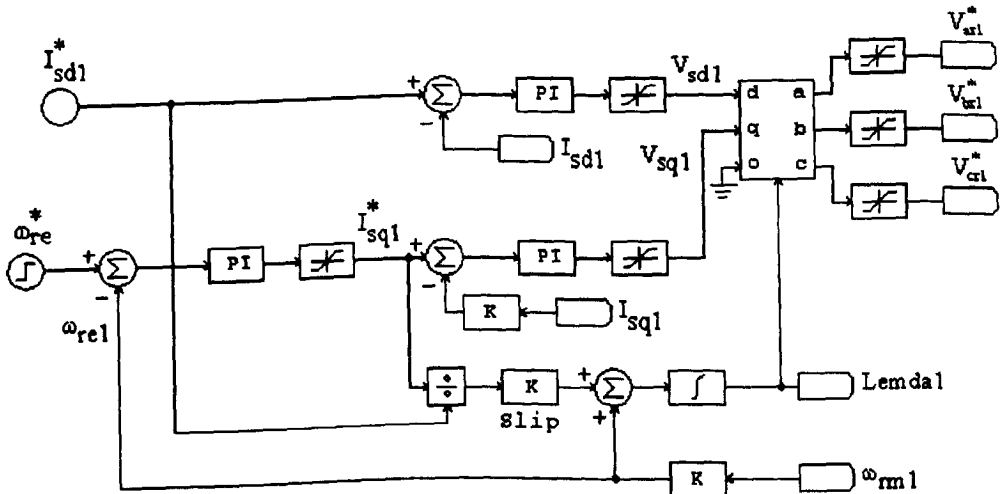
4.8.2 Multi-Motor Drive System Controlling two Induction Motors

In this case, closed loop performance of the multi-motor drive converter system has been tested by connecting an induction motor to each inverter as shown in figure 4.23 (a). Each induction motor is then independently controlled using the vector control scheme.

4.8. Simulation Results

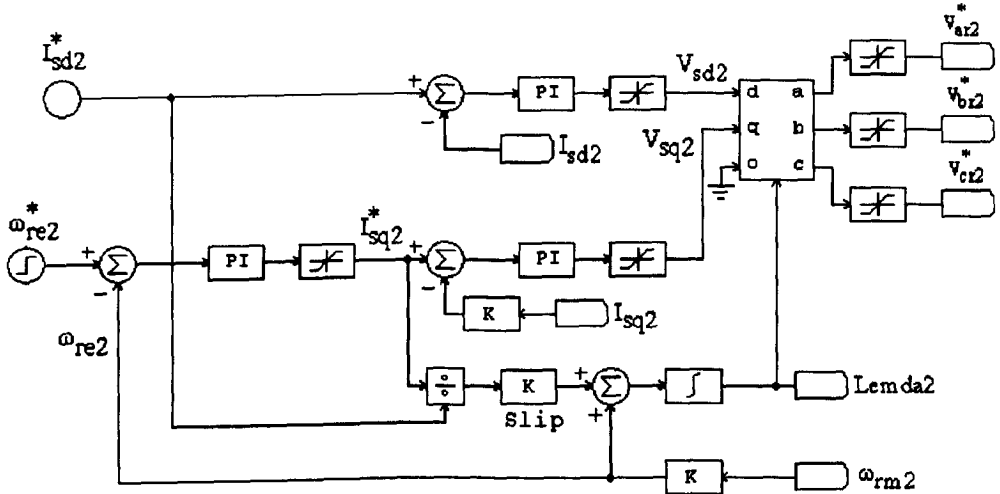


(a) The multi-motor drive converter



(b) The vector control scheme for motor IM1

4.8. Simulation Results



(c) The vector control scheme for motor IM2

Figure 4.23: The multi-motor drive system with two induction motors

Figure 4.23 (b) shows the vector control scheme for the multi-motor drive system for induction motor IM1. The output currents (I_{A1} , I_{B1} , I_{C1}) are used to calculate the d-q currents (I_{sd1} , I_{sq1}). The reference voltages (V_{m1} , V_{r1} , V_{c1}) for space vector modulation are calculated from the d-q axis reference currents (I_{sd1}^* , I_{sq1}^*).

In this test, the control of induction motor IM1 is run from 0.1 to 0.5 second and at 0.55 second motor IM2 started. Figure 4.24 (a) and (b) shows the reference and actual value of motor shaft speeds, ω_{re1} and ω_{re2} , for induction motor IM1 and IM2 respectively.

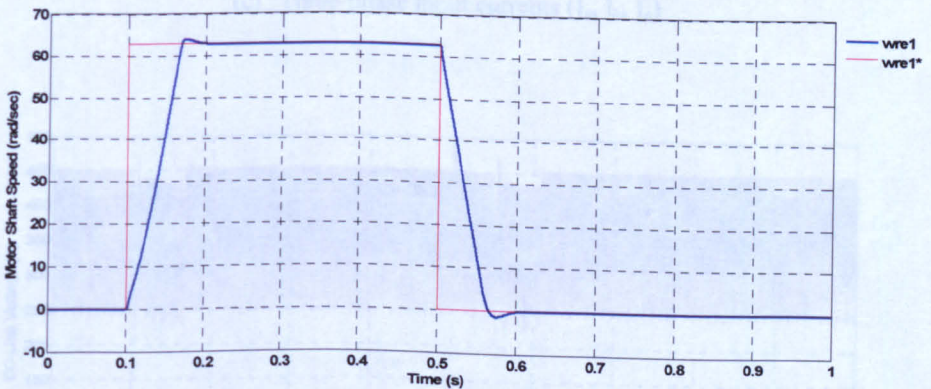
The sinusoidal input currents (I_a , I_b , I_c) and DC-link voltage (V_{pn}) for the multi-motor drive system are shown in figure 4.24 (c) and (d) respectively. It is noted that the value of three-

4.8. Simulation Results

phase input currents is high during the acceleration mode of IM1 and IM2 at 0.1 sec and 0.55 sec respectively.

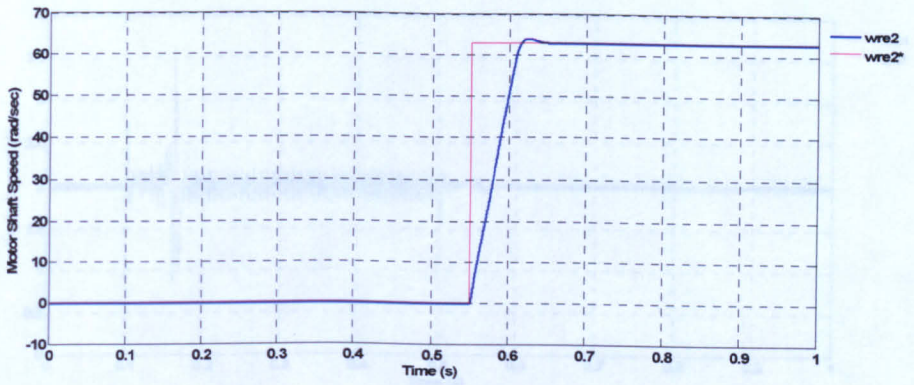
Figure 4.24 (e, f) shows the field producing current (I_{sd}) for induction motors IM1 and IM2 respectively. As explained in section 4.5.2, the field producing current or d-axis current (I_{sq}) is maintained at a constant level. For this simulation, the reference for the field producing current (I_{sd}^*) is 2.0 A. IM1 is run from 0.1 to 0.5 second; figure 4.24 (e) shows that the actual value of d-axis current follow the reference during this interval

Figure 4.24 (g, h) presents the torque producing current (I_{sq}) for induction motors IM1 and IM2 respectively. It is noticed that during the step transient (acceleration and deceleration mode), the torque producing current (I_{sq}) reaches to the maximum limit 10.0 A as shown in figure 4.24 (g). The output performance of the multi-motor drive system is shown in figure 4.24 (i-l)

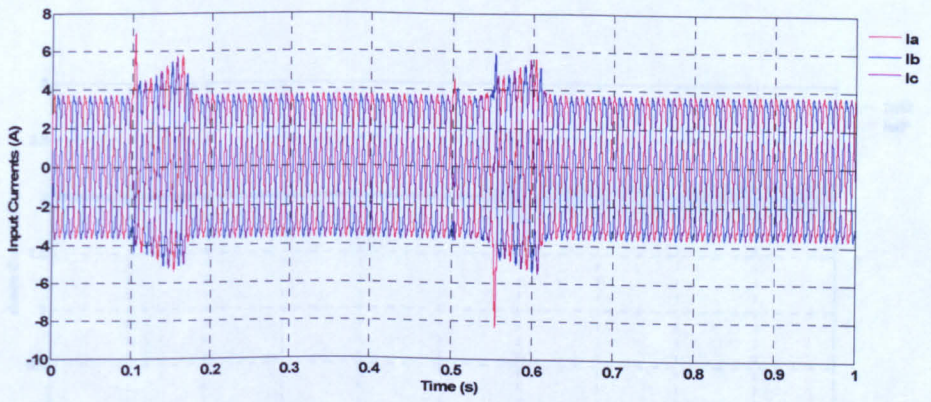


(a) Shaft speed of motor(IM1)

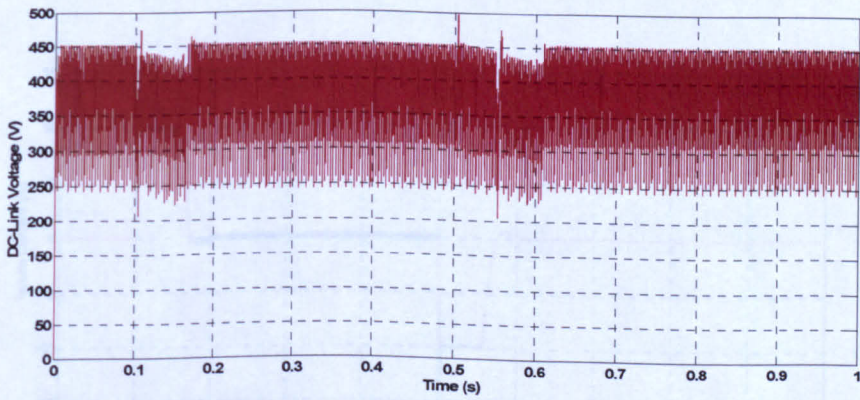
4.8. Simulation Results



(b) Shaft speed of motor IM2

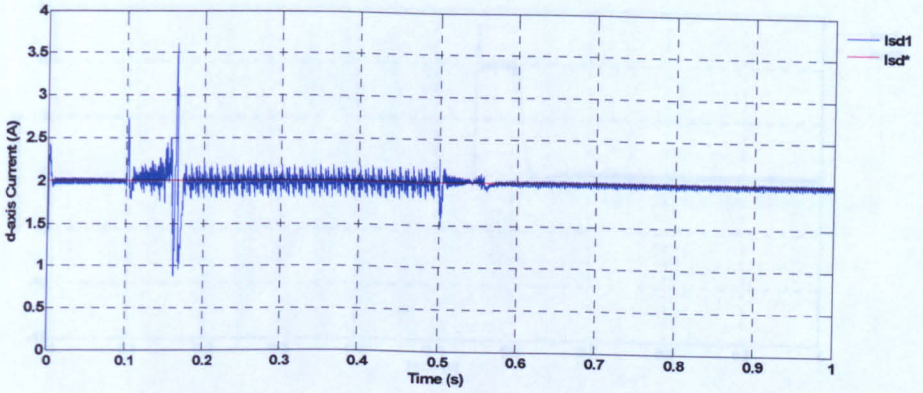


(c) Three-phase input currents (I_a , I_b , I_c)

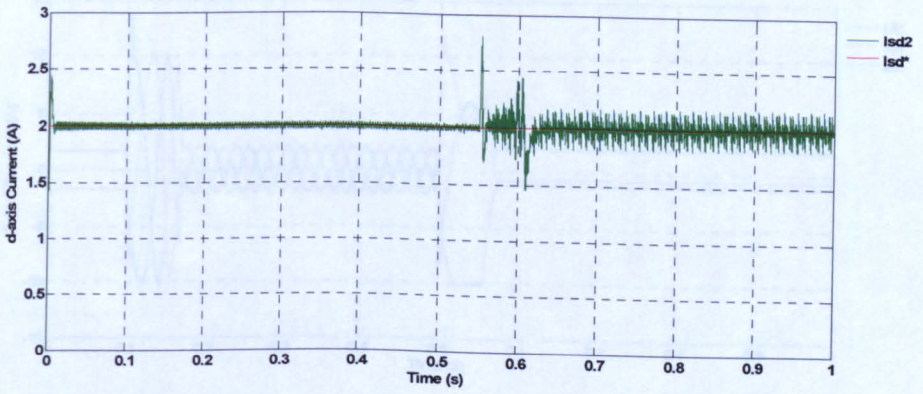


(d) DC-link voltage (V_{pn})

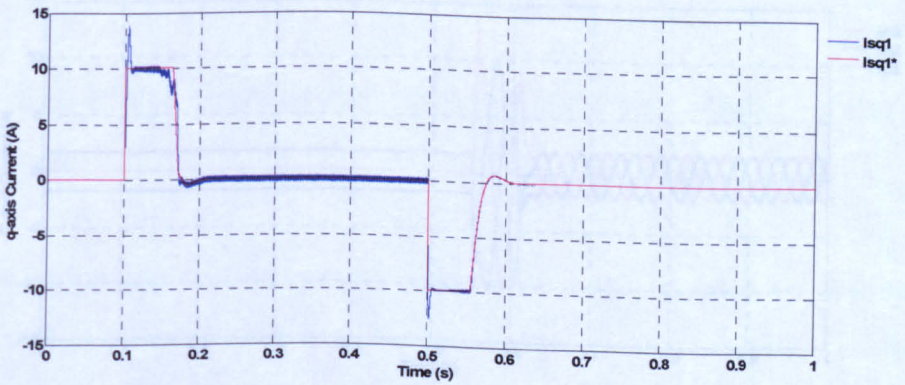
4.8. Simulation Results



(e) d-axis current for motor IM1

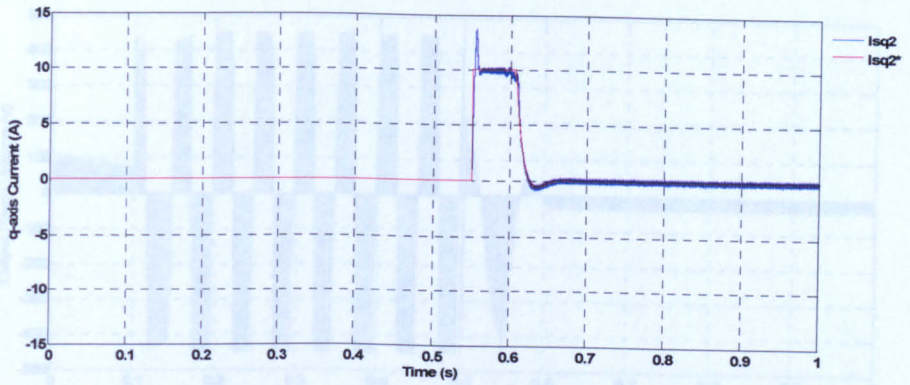


(f) d-axis current for motor IM2

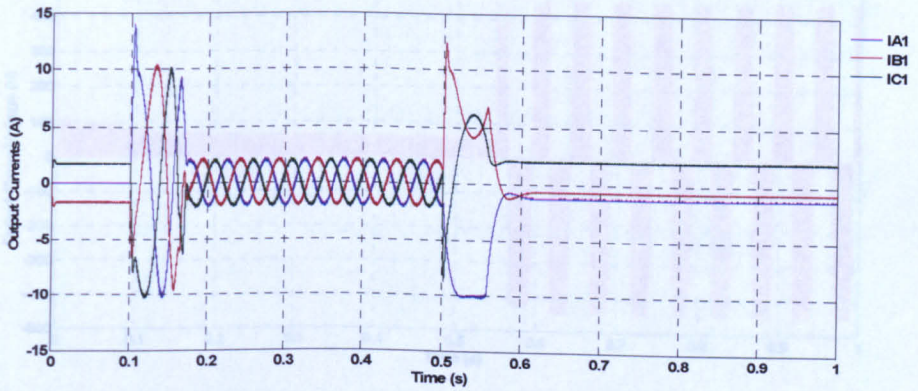


(g) q-axis current for motor IM1

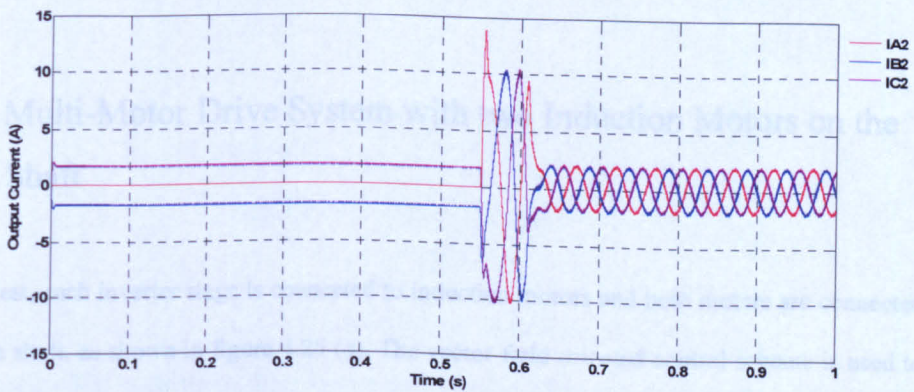
4.8. Simulation Results



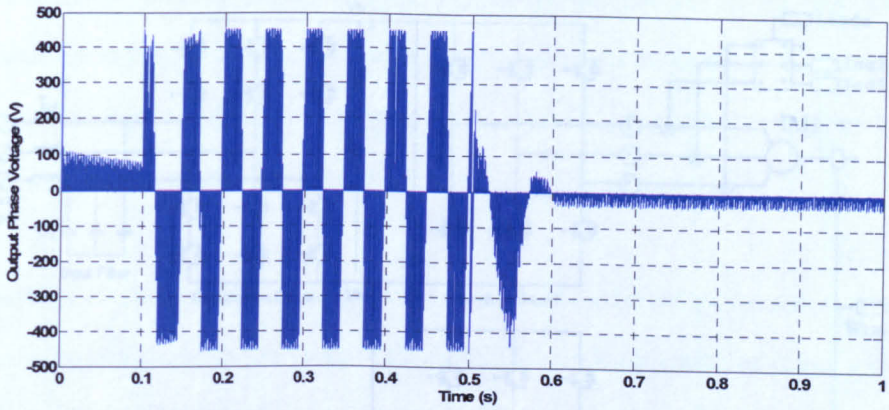
(h) q-axis current for motor IM2



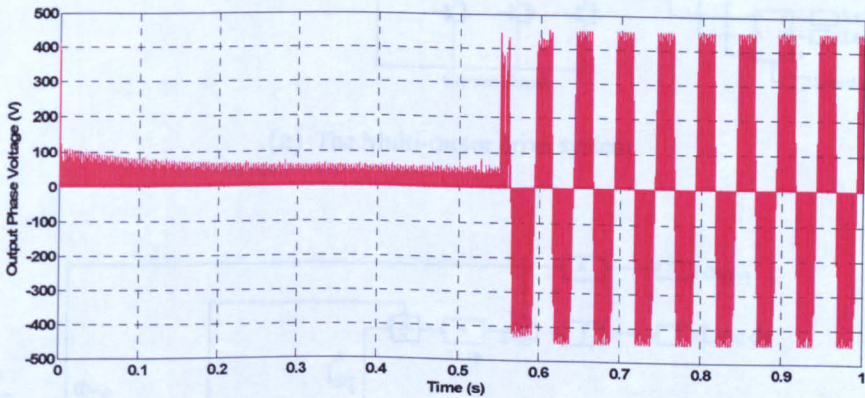
(i) Output currents (I_{A1} , I_{B1} , I_{C1}) for motor IM1



(j) Output currents (I_{A2} , I_{B2} , I_{C2}) for motor IM2



(k) One output line-to-line voltage (V_A) for motor IM1



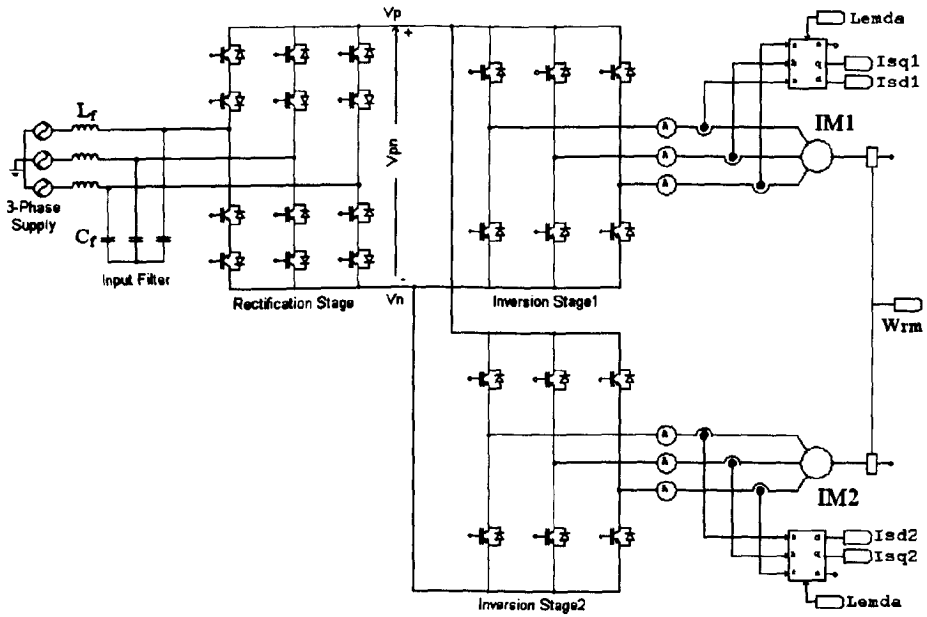
(l) One output line-to-line voltage (V_A) for motor IM2

Figure 4.24: Simulation results for the multi-motor drive system

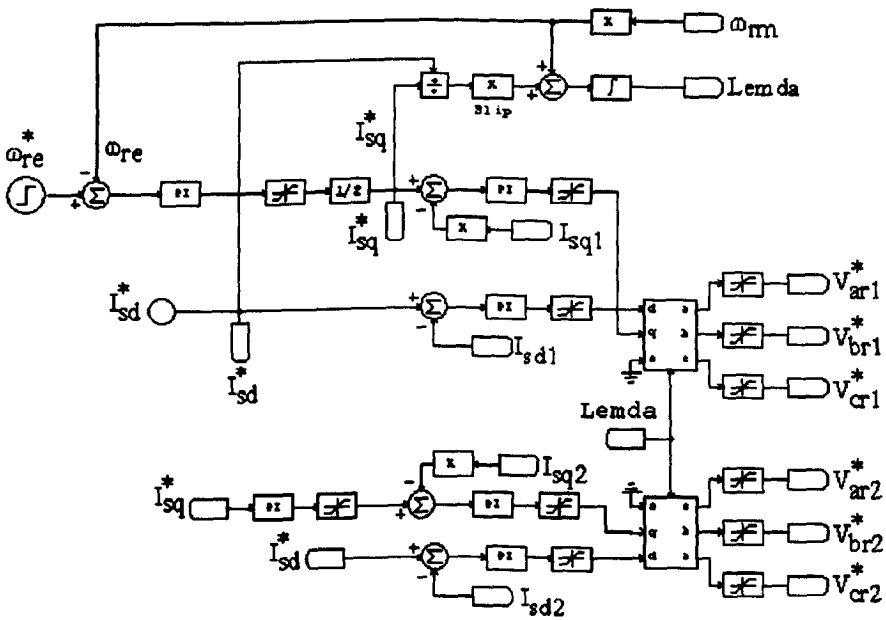
4.8.3 Multi-Motor Drive System with two Induction Motors on the same Shaft

In this test, each inverter stage is connected to induction motors and both motors are connected on same shaft, as shown in figure 4.25 (a). The vector field oriented control scheme is used to control the motor shaft speed is shown in figure 4.25 (b).

4.8. Simulation Results



(a) The Multi-motor drive system



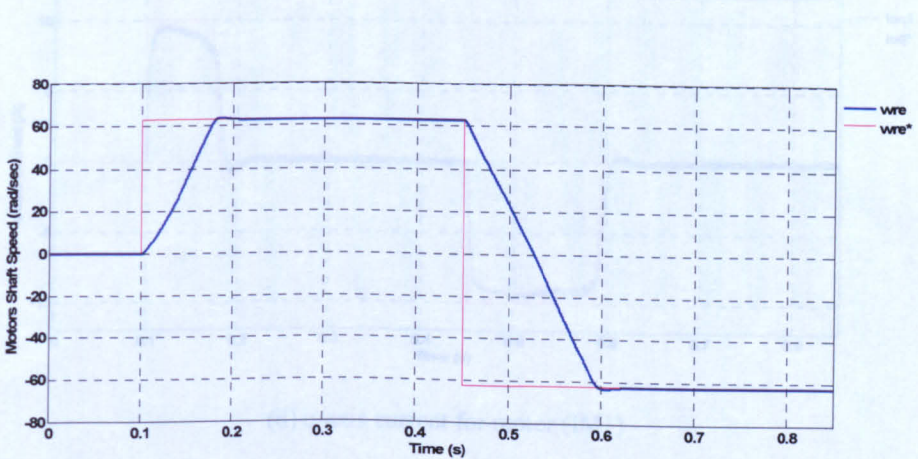
(b) Vector control scheme

Figure 4.25: The multi-motor drive system with two induction motors connected to the same shaft

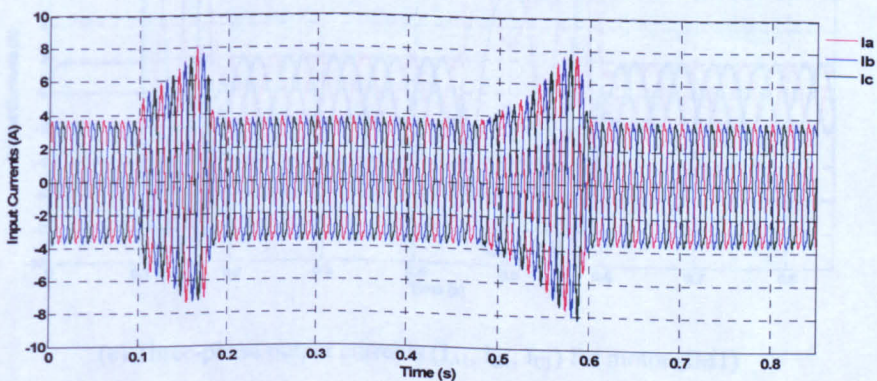
4.8. Simulation Results

This vector control scheme is slightly different from the scheme shown in the previous section. Each motor has an independent current control loop. The reference for these two current control loops is derived from a single speed control loop, the required torque producing current being halved to give the reference for each motor.

The feasibility of the proposed multi-motor drive system is confirmed by simulation. Figure 4.26 shows the waveforms for the motor shaft speed, d-axis currents, input and output currents and output voltages, for a speed reversal from 62rad/sec to -62rad/sec. The simulation results show that the actual speed and d-q axis currents follow their respective references.

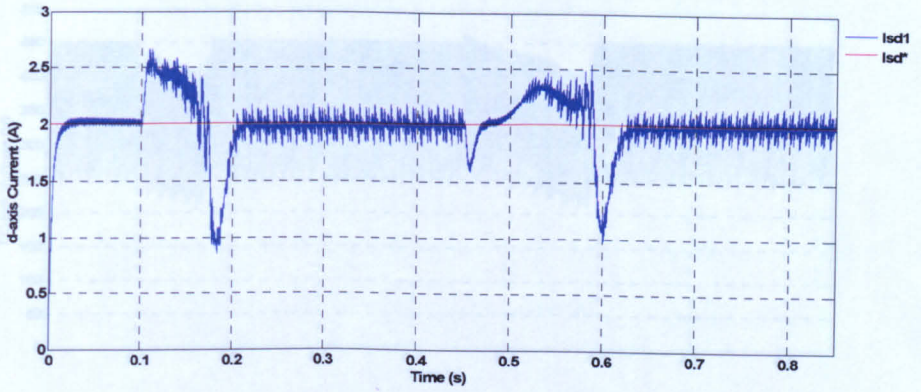


(a) Motor shaft speed

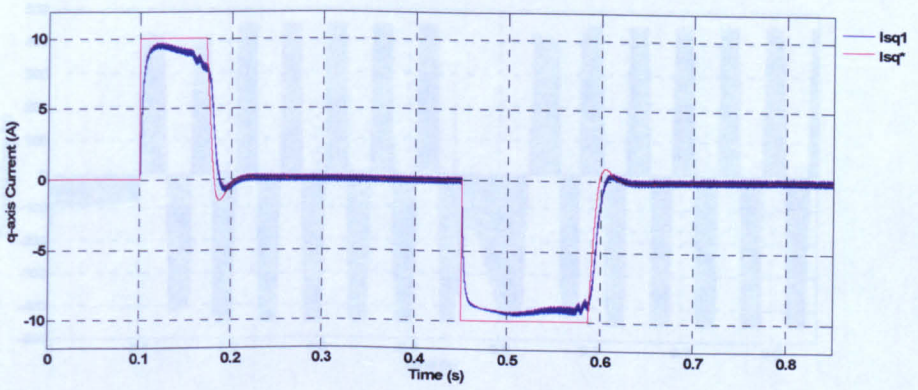


(b) Three-phase input currents (I_a , I_b , I_c)

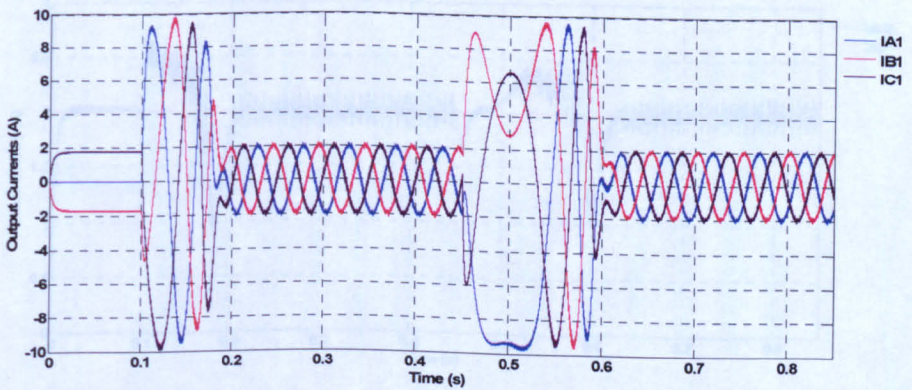
4.8. Simulation Results



(c) d-axis current for motor (IM1)

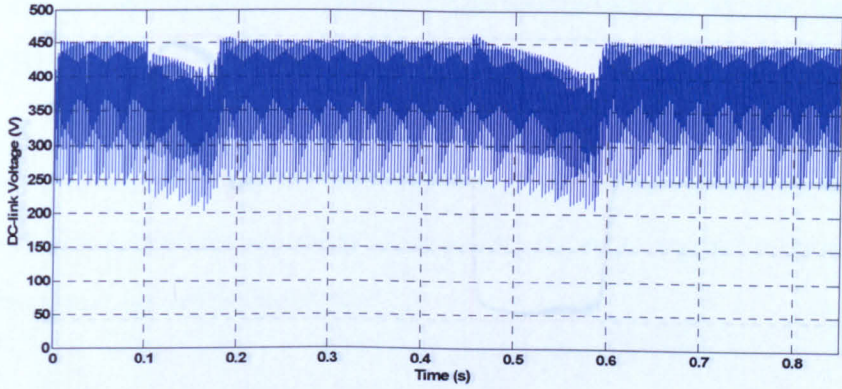


(d) q-axis current for motor (IM1)

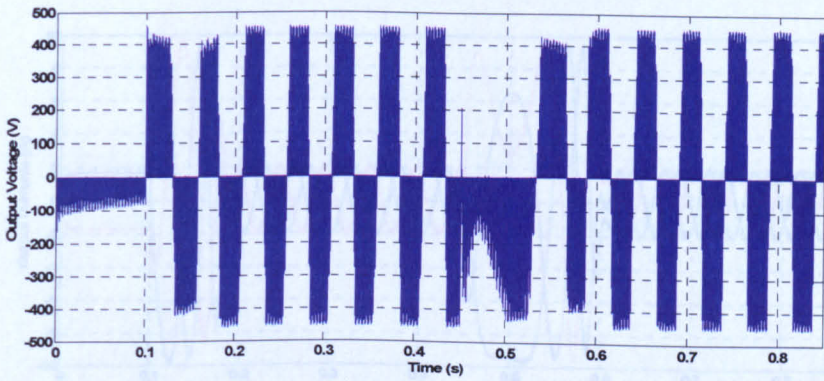


(e) Three-phase output currents (I_{A1} , I_{B1} , I_{C1}) for motor (IM1)

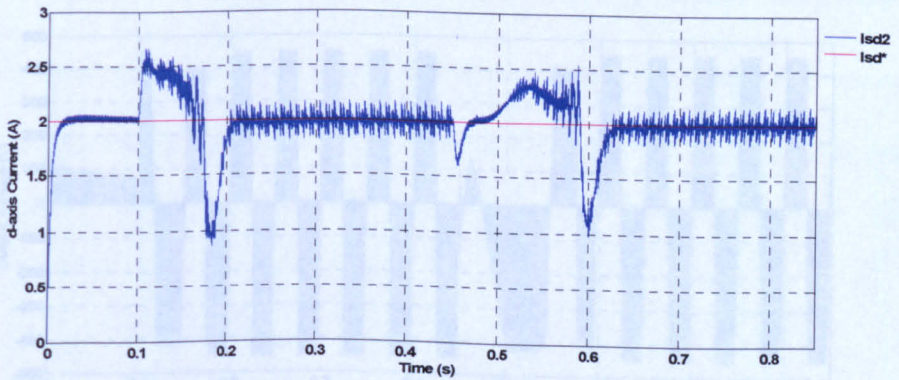
4.8. Simulation Results



(f) DC-link voltage waveforms (V_{pn})



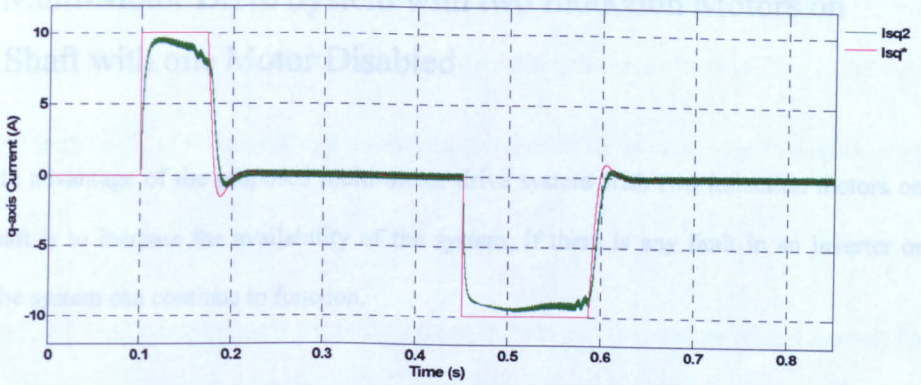
(g) One output line-to-line voltage (V_{AB1}) for motor (IM1)



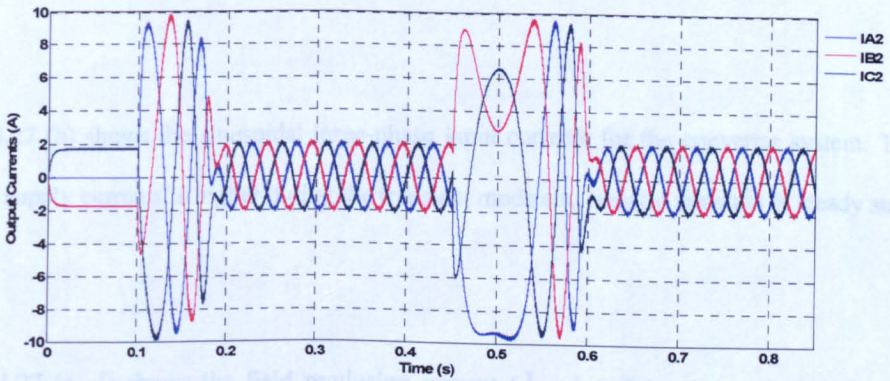
(h) d-axis current for motor (IM2)

Figure 4.26: Simulation results for the multi-motor drive system with two induction motors connected to the same shaft

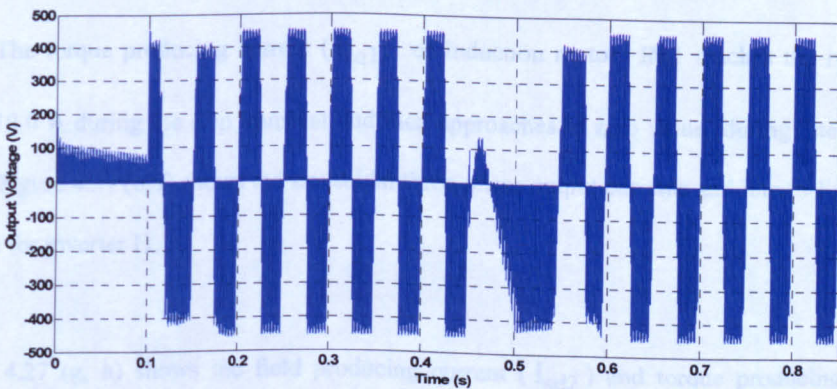
4.8. Simulation Results



(i) q-axis current for motor (IM2)



(j) Three-phase output currents (I_{A2} , I_{B2} , I_{C2}) for motor (IM2)



(k) One output line-to-line voltage (V_{AB2}) for motor (IM2)

Figure 4.26: Simulation results for the multi-motor drive system with two induction motors connected to the same shaft

4.8.4 Multi-Motor Drive System with two Induction Motors on same Shaft with one Motor Disabled

The main advantage of the proposed multi-motor drive system with two induction motors on same shaft is to increase the availability of the system. If there is any fault in an inverter or motor, the system can continue to function.

Figure 4.27 shows the simulation results for the multi-drive system, after 0.4 seconds motor IM2 is disabled. Figure 4.27 (a) shows that the motor shaft speed follows the reference speed well.

Figure 4.27 (b) shows the sinusoidal three-phase input currents for the converter system. The value of supply currents is higher during the transient mode and remains constant at steady state mode.

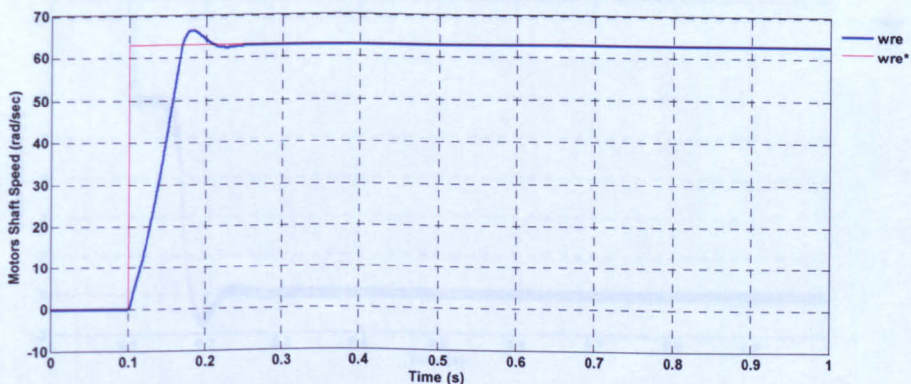
Figure 4.27 (c, d) shows the field producing current (I_{sd1}) and torque producing current (I_{sq1}) for induction motor IM1. The field producing current (I_{sd1}) is maintained a constant level. The torque producing current (I_{sq1}) of induction motor IM1 reaches the maximum limit 10.0 A during the step transient and then approaches to zero value during steady state mode. Figure 4.27 (e, f) shows the sinusoidal three-phase output currents and line-to-line output voltage for inverter I1.

Figure 4.27 (g, h) shows the field producing current (I_{sd2}) and torque producing current (I_{sq2}) for induction motor IM2. The torque producing current (I_{sq2}) of induction motor IM2 reaches the maximum limit 10.0 A during the step transient and then approaches to zero value

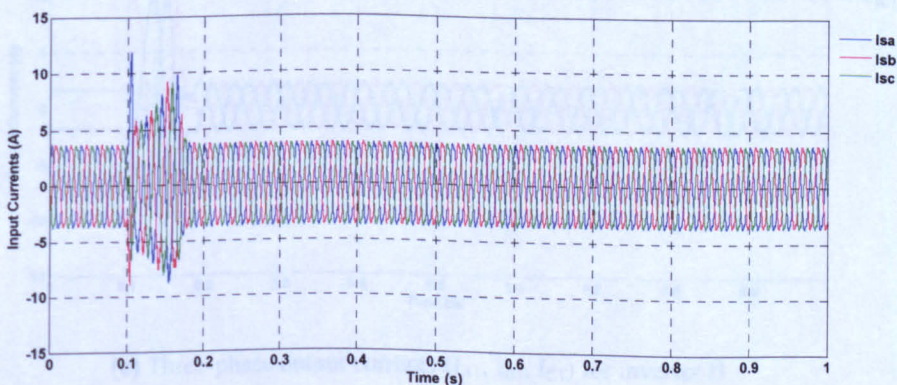
4.8. Simulation Results

during steady state mode. At 0.4 second motor IM2 is disabled, therefore torque producing current (I_{sq2}) remain zero even if shaft speed recover the reference speed by IM1. The field producing current (I_{sd2}) is maintained a constant level until 0.4 sec and after that approaches to zero value.

Figure 4.27 (i) and (j) shows the three-phase output current and line-to-line output voltage for inverter I2. These results shows that when motor IM2 disabled at 0.4 second, the value of output currents and output voltage approaches to zero.

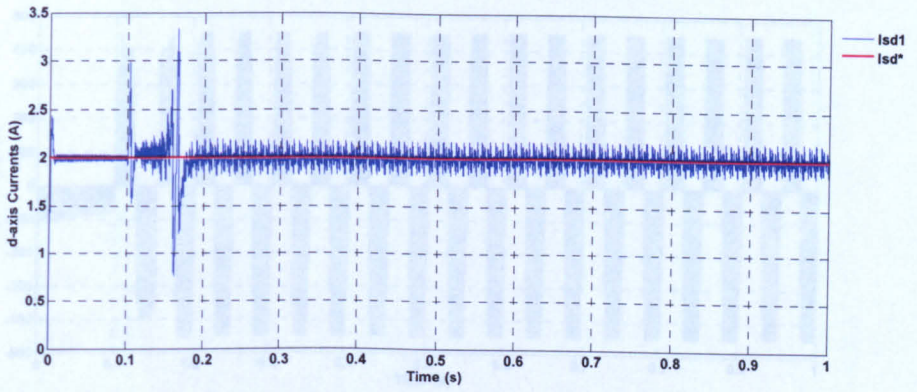


(a) The motor shaft speed

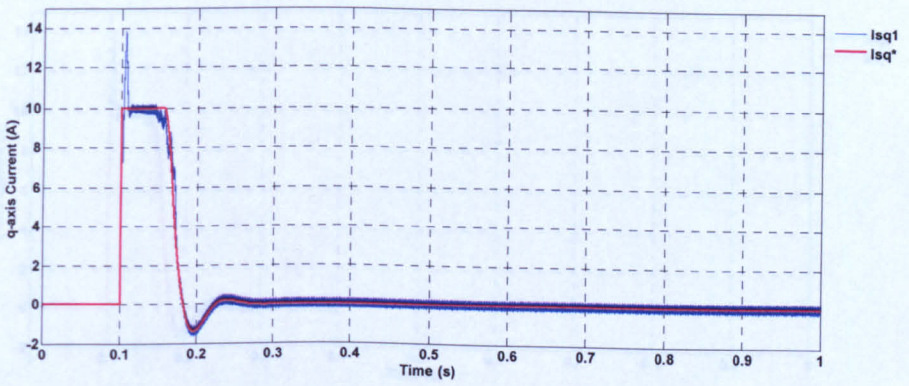


(b) Three-phase input currents (I_a , I_b , I_c)

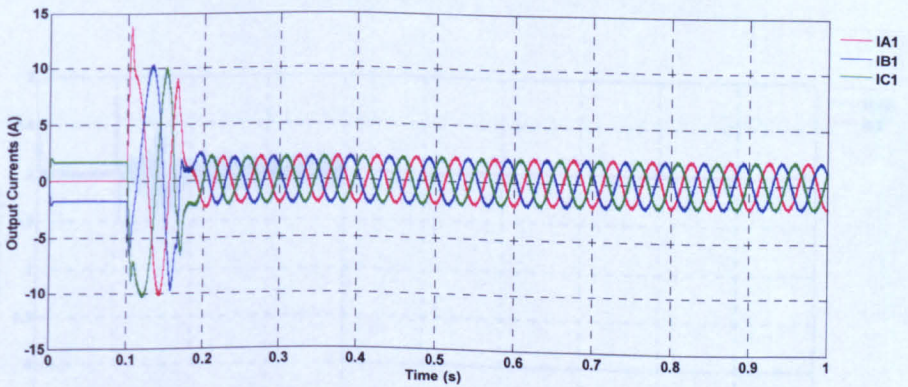
4.8. Simulation Results



(c) d-axis current for motor IM1

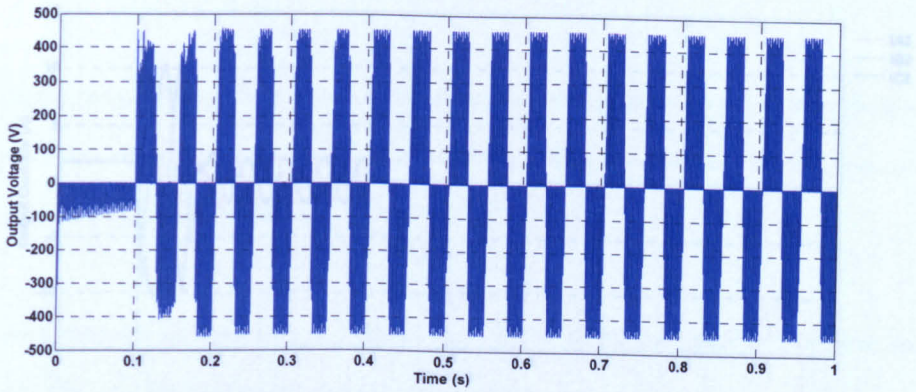


(d) q-axis current for motor IM1

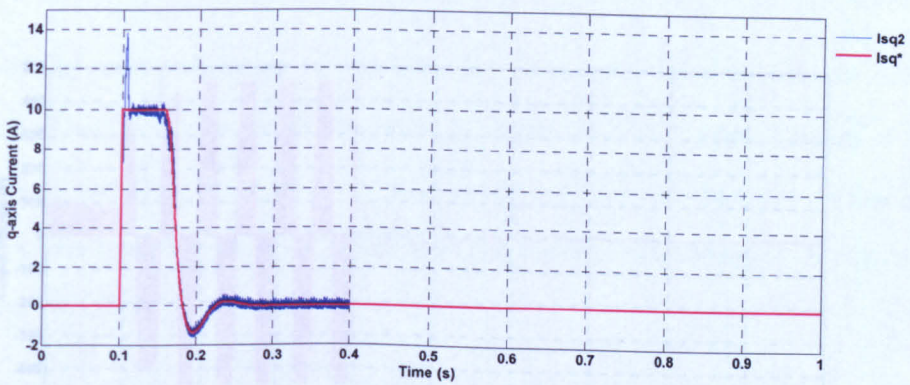


(e) Three-phase output currents (I_{A1} , I_{B1} , I_{C1}) for inverter I1

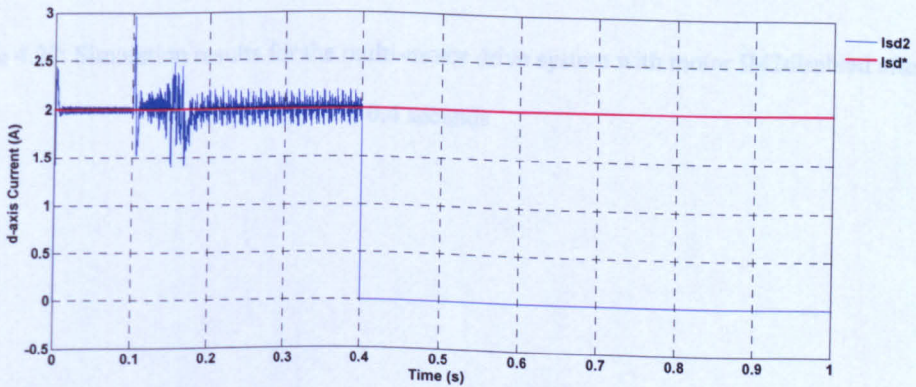
4.8. Simulation Results



(f) An output line-to-line voltage (V_{AB1}) for inverter I1

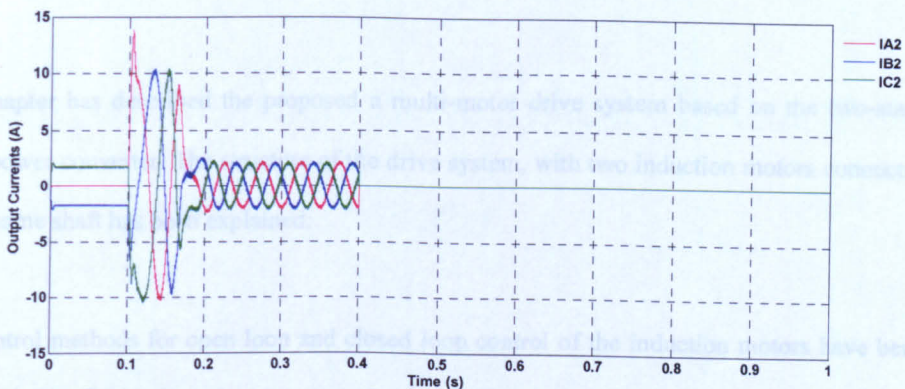


(g) q-axis current for motor IM2

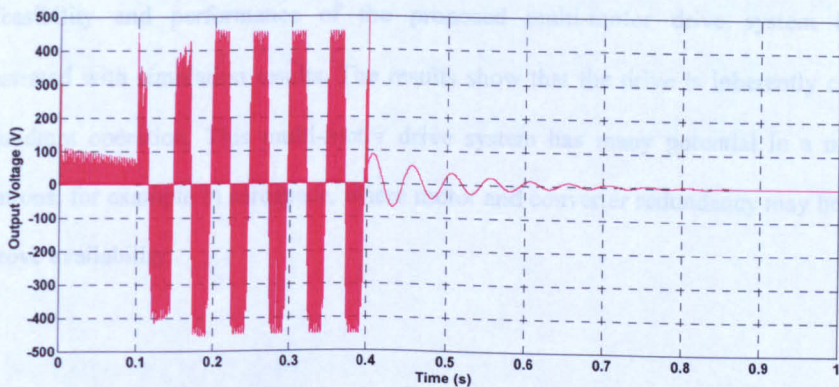


(h) d-axis current for motor IM2

4.9 Conclusions



(i) Three-phase output currents (I_{A2} , I_{B2} , I_{C2}) for inverter I2



(j) An output line-to-line voltage (V_{AB1}) for inverter I2

Figure 4.27: Simulation results for the multi-motor drive system with motor IM2 disabled after 0.4 seconds

4.9 Conclusions

This chapter has described the proposed a multi-motor drive system based on the two-stage direct power converter. The structure of the drive system, with two induction motors connected on the same shaft has been explained.

The control methods for open loop and closed loop control of the induction motors have been described. The field oriented vector control scheme for the proposed multi-motor drive system has been developed.

The feasibility and performance of the proposed multi-motor drive system has been demonstrated with simulation results. The results show that the drive is inherently capable of four quadrant operation. This multi-motor drive system has many potential in a number of applications, for example in aerospace, where motor and converter redundancy may be required to improve availability.

Chapter 5

Prototype Multi-Motor Drive System based on Two-Stage Direct Power Converter

5.1 Introduction

The performance of the multi-motor drive system has been evaluated using a SABER simulator, as described in chapter 4. In order to validate the simulation results a laboratory prototype has been designed. This chapter describes the hardware implementation for this prototype. The chapter starts with a description of the overall structure of the prototype and then gives a detailed explanation of the design of each circuit used.

5.2 Structure of the Prototype Converter

The overall structure of the laboratory prototype is shown in figure 5.1. The construction of the laboratory prototype can be categorised as follows:

- (i) Converter power circuit
- (ii) Control platform
- (iii) Interface circuits

5.2. Structure of the Prototype Converter

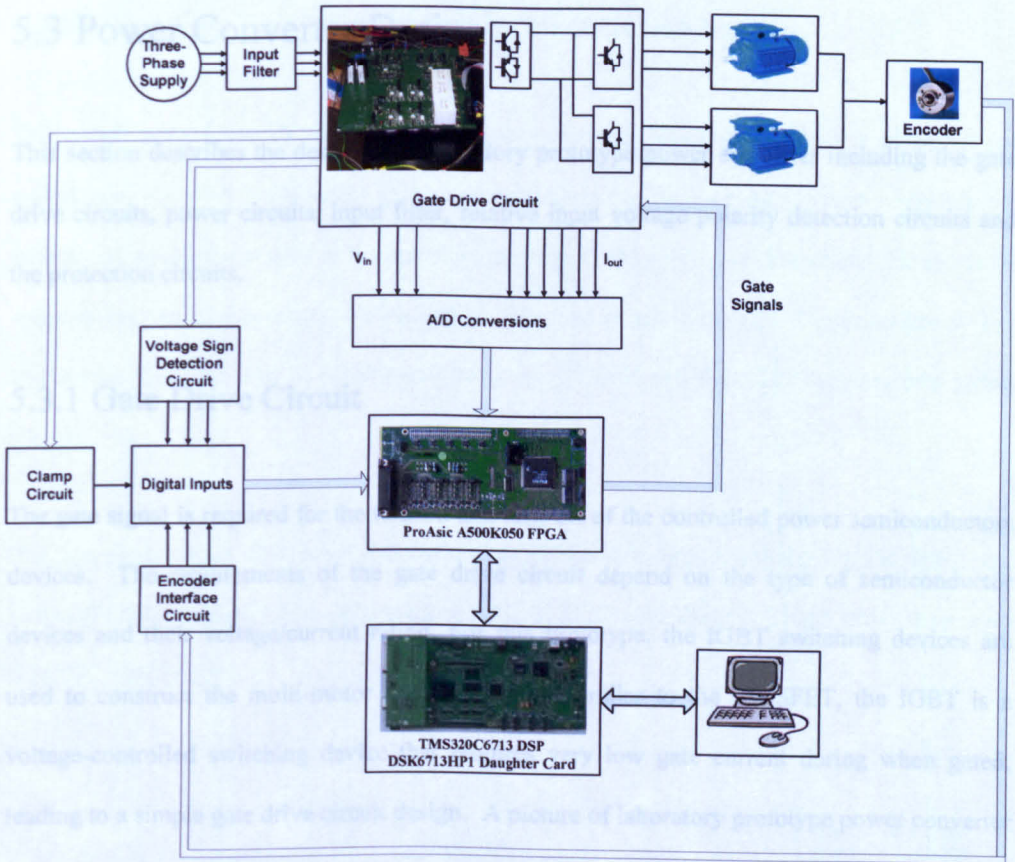


Figure 5.1: Overall structure of the multi-motor drive converter prototype

The first section of this chapter describes the design and construction of the power converter. This includes a detail description of the main circuits, such as the gate drives, power assembly, input filter, relative input voltage polarity detection and the protection circuits.

The second section of this chapter describes the implementation of the control platform and interface including the Digital Signal Processor (DSP), Field Programmable Gate Array (FPGA) board, interface board, encoder interface board and measurement board and sensors.

5.3 Power Converter Design

This section describes the design of a laboratory prototype power converter including the gate drive circuits, power circuits, input filter, relative input voltage polarity detection circuits and the protection circuits.

5.3.1 Gate Drive Circuit

The gate signal is required for the turn-on and turn-off of the controlled power semiconductor devices. The requirements of the gate drive circuit depend on the type of semiconductor devices and their voltage/current rating. For this prototype, the IGBT switching devices are used to construct the multi-motor drive converter. Similar to the MOSFET, the IGBT is a voltage-controlled switching device that requires very low gate current during when gated, leading to a simple gate drive circuit design. A picture of laboratory prototype power converter is shown in figure 5.2.

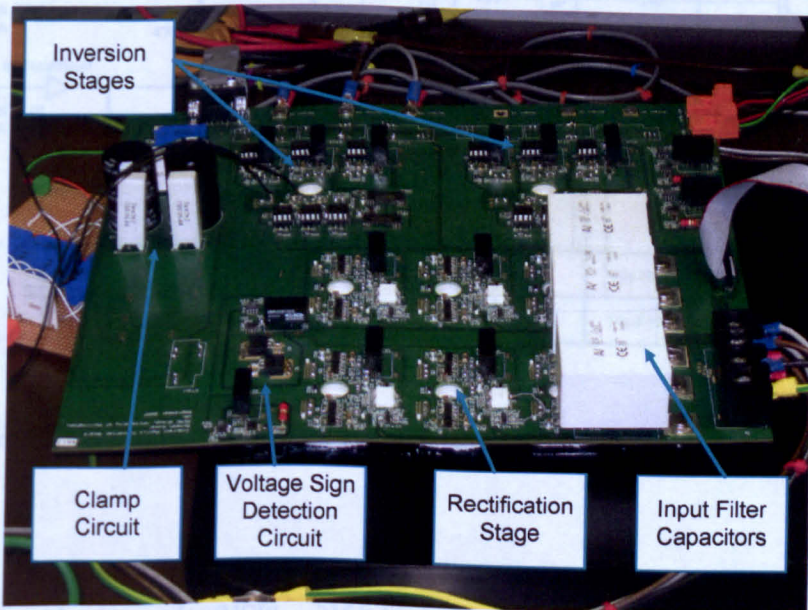


Figure 5.2: The overview of the prototype power converter

5.3. Power Converter Design

5.3.1.1 The Gate Drive Circuit for the Rectification Stage

The rectification stage of the proposed power converter topology requires a bi-directional switch cell. Figure 5.3 shows the gate drive schematic for the common-emitter bi-directional switch cell arrangement used in the rectification stage of the prototype. The choice for choosing common-emitter bi-directional switch cell is discussed in section 2.3.3. The common-emitter bi-directional switch cell is constructed using two IGBTs and therefore requires two gating signals.

The gate drive circuit consists of four main components: the dc/dc converter (DCP020515), the buffer (SN74LVC1G07), the opto-coupler (HCPL-315J) and the NPN/PNP drive transistors (FZT790A/FZT690B).

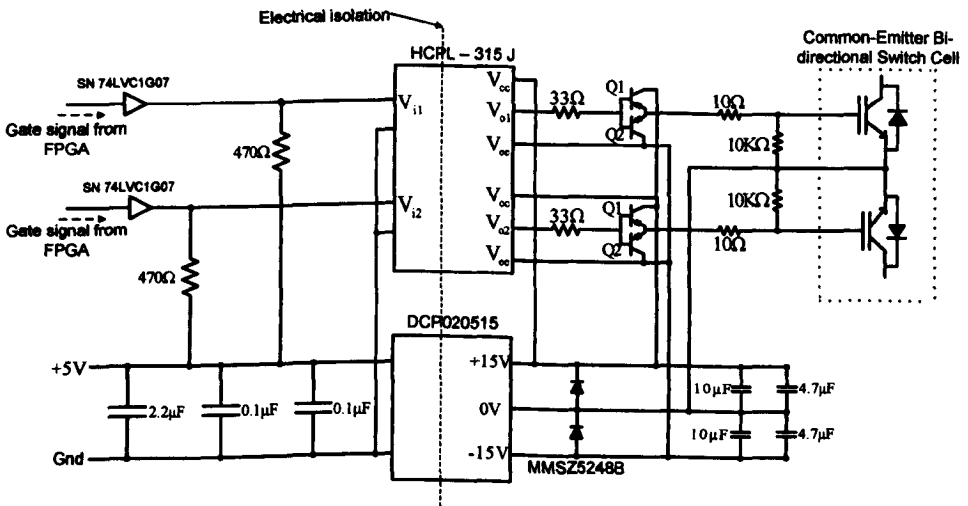


Figure 5.3: Schematic diagram of the gate drive circuit for the bi-directional switch cells

A dual-channel opto-coupler (HCPL – 315J) is used to provide the electrical isolation between the low power and high power sides of the gate drive. Both side of the opto-coupler are

5.3. Power Converter Design

powered by an isolated DC supply (DCP020515DU), as shown in figure 5.3. The dc/dc converter (DCP020515DU) generates a dual supply +15V and -15V derived from a 5V supply voltage. The +5V is common with the input side of the opto-coupler and $\pm 15V$ is common with output side of the opto-coupler.

A buffer chipset (SN74LVC1G07) is used to buffer each input channel and to provide the required current to drive the opto-coupler. A 470Ω pull-up resistor is connected between the 5V supply voltage and the open collector pin of the output buffer.

As mentioned earlier, four-step current commutation is used to pass the current between the bi-directional switches. Based on the turn-on and turn-off time of the switching devices, a suitable time gap is introduced between each switch state. If this time gap is too long, the switching time required to complete the commutation sequence will be increased and that will affect the converter output waveforms. To overcome this problem, the turn-on and turn-off time of the IGBT have to be minimised. This can be done by using the two complementary push-pull amplifier, formed with two discrete NPN and PNP transistor (FZT790A and FZT690B) [38]. The output of this push-pull amplifier is fed to the IGBT gate through the gate resistor (10Ω). A value of 10Ω was selected so that commutation between phases would occur in as short a time as possible. It is also noted that if the gate circuit fails and a voltage is applied on the power circuit, the IGBT may be destroyed due to the Miller effect [39]. In order to avoid this destruction, a resistor ($10K\Omega$) is placed between the gate and emitter. Figure 5.4 shows the photograph of the gate drive circuit for one of the bi-directional switch cells used in the rectification stage of the converter.

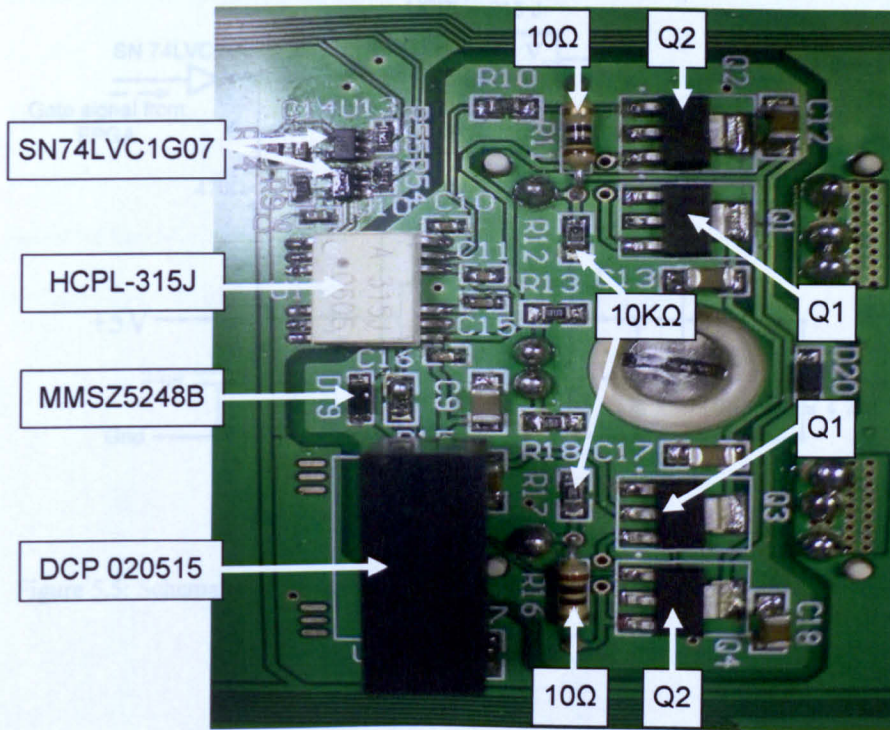


Figure 5.4: The gate-drive circuit for one of the bi-directional switch cell in the rectification stage

5.3.1.2 The Gate Drive Circuit for the Inversion Stage

The inversion stages use unidirectional switches; a schematic of the gate drive circuit used for the unidirectional switch is shown in figure 5.5. Compared to figure 5.3, the gate drive circuit for unidirectional switch is simpler because only one gate signal is required. Due to the presence of a natural freewheeling path (through the anti-parallel diode) for each IGBT, a simple dead-time current commutation technique, as discussed in section 2.3.5, can be used for the unidirectional switches.

5.3. Power Converter Design

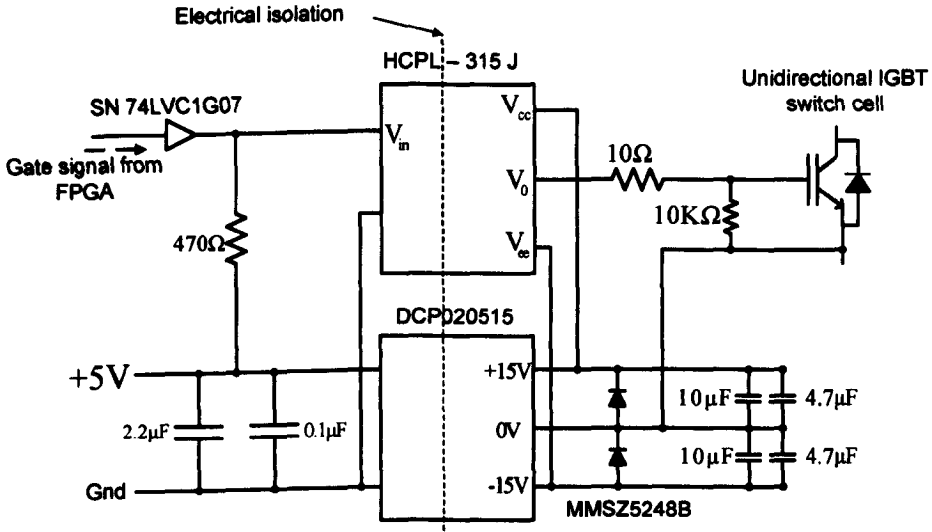


Figure 5.5: Schematic of the gate drive circuit for unidirectional IGBT switch in the inversion stage

In the gate drive circuit a single channel opto-coupler (HCPL-312) is used to provide the electrical isolation. An isolated power supply (DCP020515) is used to provide the supply to the opto-coupler. A buffer chipset (SN74LVC1G07) is used for input channel of the opto-coupler. The output of the opto-coupler is fed to the IGBT module through the gate drive resistor (10Ω) and a $10K\Omega$ resistor is placed between the gate and emitter in the bottom layer of Printed Circuit Board (PCB) to avoid the problem associated with the Miller effect.

5.3.2 The Power Circuit

For the experimental verification of the proposed multi-motor drive topology, a 7.5kW laboratory prototype was built. The power circuit consists of six IGBT bidirectional switch

5.3. Power Converter Design

modules (SK60GM123) [40] for the rectification stage and two three-phase inverter bridge modules (SK35GD126ET) for the inverter stage [41].

The IGBT (SK60GM123) module for the rectification stage is shown in figure 5.6. This module is rated at 1200V and 60A and uses the common emitter configuration. The internal circuit layout of the SK60GM123 IGBT module is shown in figure 5.7, where the common emitter configuration consists of two IGBTs connected with two ant-parallel diodes.

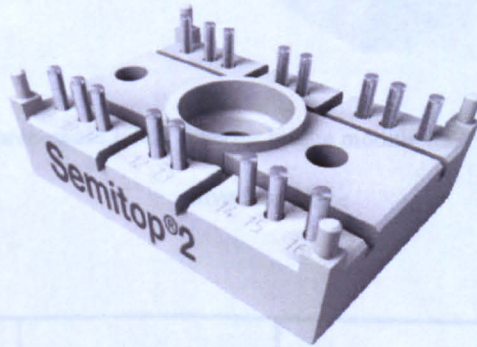


Figure 5.6: IGBT Switch module SK60GM123 used in the rectification stage

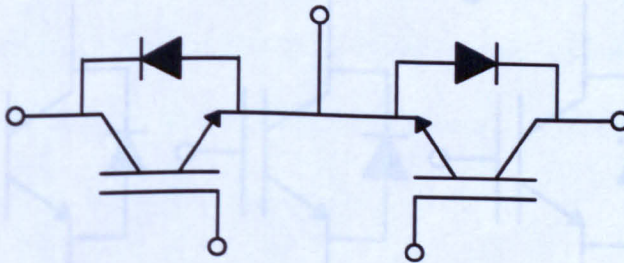


Figure 5.7: Internal circuit layout of IGBT module SK60GM123

5.3. Power Converter Design

A three-phase inverter bridge module (SK35GD126ET) is shown in figure 5.8. This module is used for each inversion stage and is rated at 1200V and 40A. Figure 5.9 shows the circuit of the three-phase inverter bridge module.

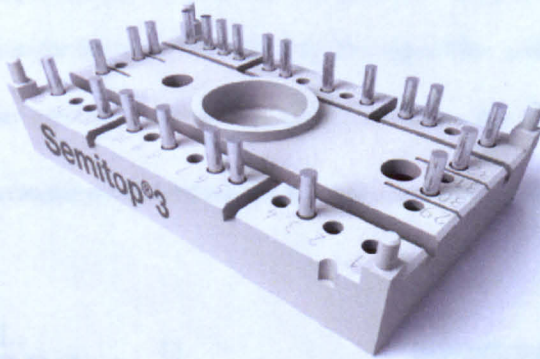


Figure 5.8: The three-phase IGBT inverter bridge module SK35GD126ET used for the inversion stage

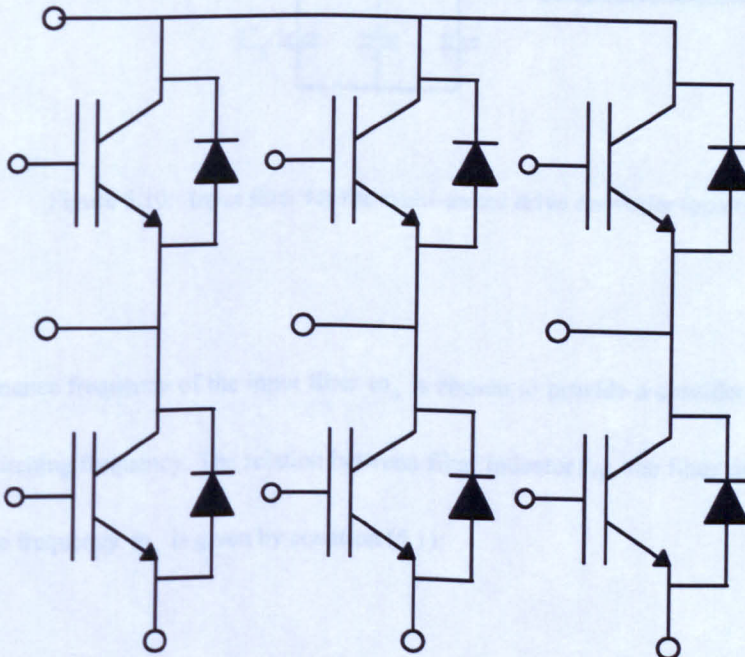


Figure 5.9: Internal circuit of the three-phase inverter bridge module (SK35GD126ET)

5.3.3 Input Filter Design

The multi-motor drive converter topology requires an input filter to remove the high frequency components in the input current. Considering cost and size a simple low-pass LC filter often offers the best solution for the input filter [24, 25]. The input filter configuration for the multi-motor drive converter topology is shown in figure 5.10, where the filter capacitors (C_f) are connected in a star arrangement and inductors (L_f) are connected in series with the supply.

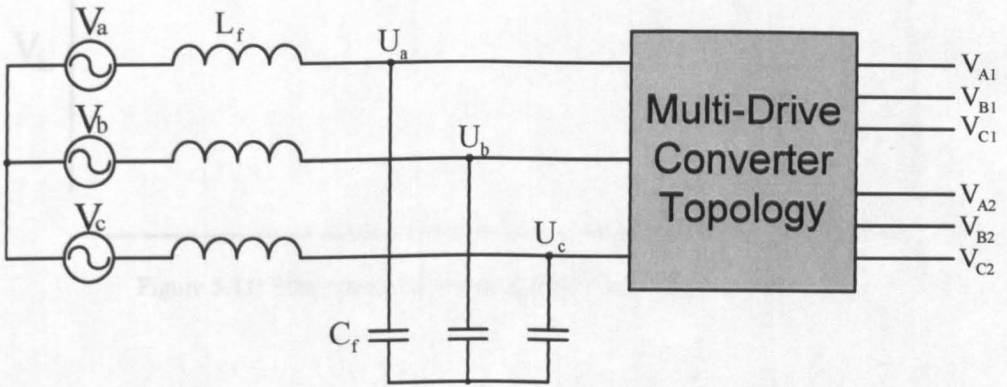


Figure 5.10: Input filter for the multi-motor drive converter topology

The resonance frequency of the input filter ω_o is chosen to provide a considerable attenuation at the switching frequency. The relation between filter inductor L_f , the filter capacitor C_f and resonance frequency ω_o is given by equation (5.1):

$$\omega_o = \frac{1}{\sqrt{L_f \cdot C_f}} \tag{5.1}$$

5.3. Power Converter Design

The transfer function of the input filter can be calculated by using the schematic shown in figure 5.11 [42, 43, 44]. The internal resistance of the inductor is represented by r . This transfer function is used to determine the cut-off frequency of the input filter using the bode plot.

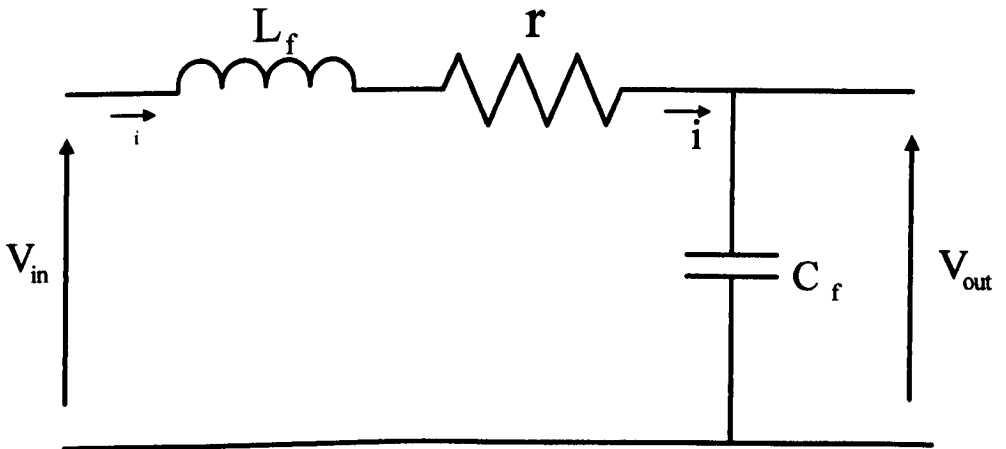


Figure 5.11: Schematic to calculate the transfer function of input filter

The transfer function is the relation between output and input, as defined by equation below:

$$TF = \frac{V_{out}}{V_{in}} \quad (5.2)$$

The input and output voltage can be expressed as:

$$V_{out} = \frac{1}{C_f} \int i dt \quad (5.3)$$

$$V_{in} = L_f \frac{di}{dt} + r \cdot i + \frac{1}{C_f} \int i dt \quad (5.4)$$

5.3. Power Converter Design

Substituting the equation (5.3) and (5.4) in equation (5.2) and applying Laplace Transforms:

$$TF = \frac{1}{L_f C_f} \frac{1}{S^2 + \frac{r}{L_f} S + \frac{1}{L_f C_f}} \quad (5.5)$$

Equation (5.5) represents the general form of the transfer function for input filter and is used to determine the cut-off frequency for the filter design.

In this prototype a variac is used as the source, therefore the inductance of the variac is used rather than additional line inductors. The variac used in this project has inductance 2.426mH and its internal resistance is 2.5Ω. Substituting these values in equation (5.5):

$$TF = \frac{1}{2.426m.C_f} \frac{1}{S^2 + \frac{2.5}{2.426m} S + \frac{1}{2.426m.C_f}} \quad (5.6)$$

The transfer function expressed in equation (5.6) can be plotted for different values of capacitor. MATLAB/Simulink is used to generate the Bode plot from equation (5.6). An important consideration is taken into account that the cut-off frequency of the input filter must be lower than the switching frequency of the input converter. The most suitable value of the capacitor is 2μF for this prototype. By substituting the capacitor value in equation (5.6), the final value of transfer function is expressed by equation (5.7):

$$TF = \frac{(2.061).10^8}{s^2 + 1030.50s + (2.061).10^8} \quad (5.7)$$

5.3. Power Converter Design

Equation (5.7) is used to plot the Bode plot to obtain the frequency response of the input filter as shown in figure 5.12. By analyzing the bode plot, it can be seen that the resonant frequency occurs at 2.28 kHz with an attenuation of 22.9dB. The cut-off frequency is obtained at 3.57 kHz and the attenuation at cut-off frequency is -3.04dB.

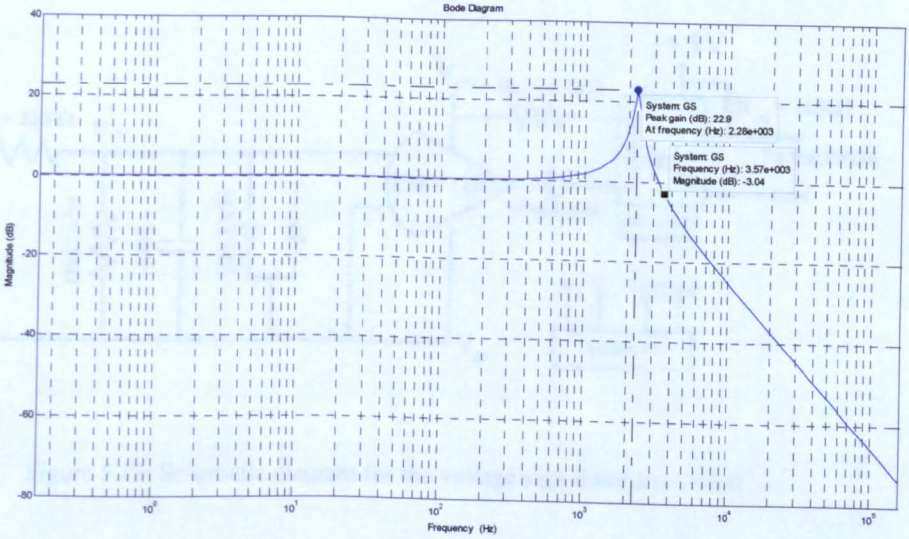


Figure 5.12: Bode plot for input filter transfer function

In order to reduce the stray inductance between the input filter capacitors and the power modules of the multi-drive converter, the input filter capacitors are mounted on the PCB used for the power circuit.

5.3.4 Voltage Sign Detection Circuit

For the converter prototype the relative input voltage magnitude based commutation technique, described in section 2.3.4.2 is used for the rectification stage. This commutation technique requires knowledge of the sign, positive or negative, of each input voltage. Three voltage sign

5.3. Power Converter Design

detection circuits are used to determine the sign of the input line-to-line voltages applied to the bi-directional switches. Figure 5.13 shows a schematic diagram for the voltage sign detection circuit.

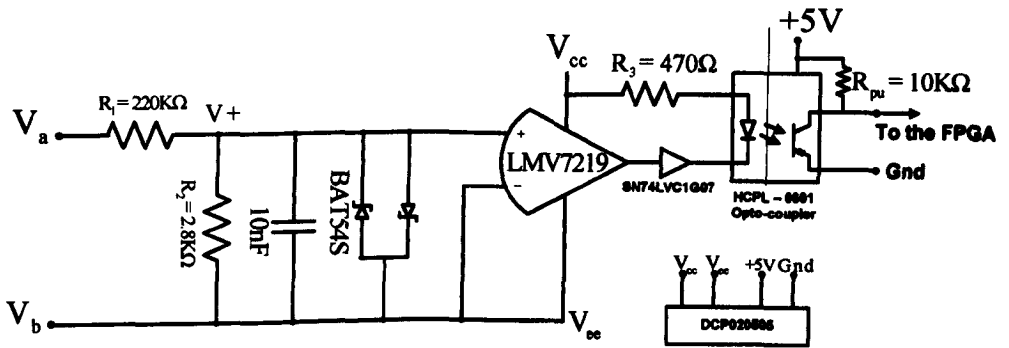


Figure 5.13: Schematic diagram for the voltage sign detection circuit

The input stage of the circuit consists of a potential divider (R_1 and R_2), this generates a voltage (V_+), which is a fraction of the input voltage (V_{ab}). The back-to-back schotky diodes limit the input voltage of the comparator to between $+0.7V$ to $-0.7V$. This voltage is then compared with the comparator ground level (V_b). For the case where $V_a > V_b$, the comparator generates a high logic signal. A capacitor is connected across the inputs of the comparator to filter out high frequency jittering that occurs at the zero crossing of the current.

In this circuit the phase voltage is directly connected to the comparator ground terminal. Therefore, an isolated power supply (DCP020505) is needed in the supply the circuit. A buffer, SN74LVC1G07, is used to drive the opto-coupler which provides the electrical isolation between the input voltage and the control platform.

5.3.5 Over-Voltage Clamp Circuit

A clamp circuit is included in the design to protect the multi-motor drive converter from the over voltages caused by the abnormal conditions, such as input voltage disturbances or a sudden open circuit on the output side. During abnormal or fault condition all the inductive load energy is transferred to clamp capacitors, protecting the converter hardware.

The clamp circuit is built on a PCB, as shown in figure 5.2. The clamp circuit consists of three main components: fast recovery diodes (8EWF12S), clamp capacitors (TS-UP 150 μ F, 450V) and discharge shunt resistors (47K Ω). The 8EWF12S fast recovery diodes were used to construct a rectifier circuit, which has been placed at the bottom layer of the PCB. The rating of each diode is 1200V, 8A. During an over-voltage event, the converter system is shut down and the diodes provide a path to charge up two series connected electrolytic capacitors of 150 μ F, 450V. The energy stored in the clamp capacitors is then dissipated by the resistor (47K Ω) that is connected in parallel with each capacitor.

A voltage detection circuit was built to monitor the clamp circuit's DC-link voltage. The over-voltage detection circuit is shown in figure 5.14. The DC-link voltage of the clamp circuit is measured using a voltage transducer (LEM LV25-P). The output of the transducer is compared to a reference. A maximum value of 700V has been set for this converter. The comparator generates a high logic signal if the clamp circuit's DC-link voltage is larger than 700V. This logic signal then triggers an error signal in the FPGA.

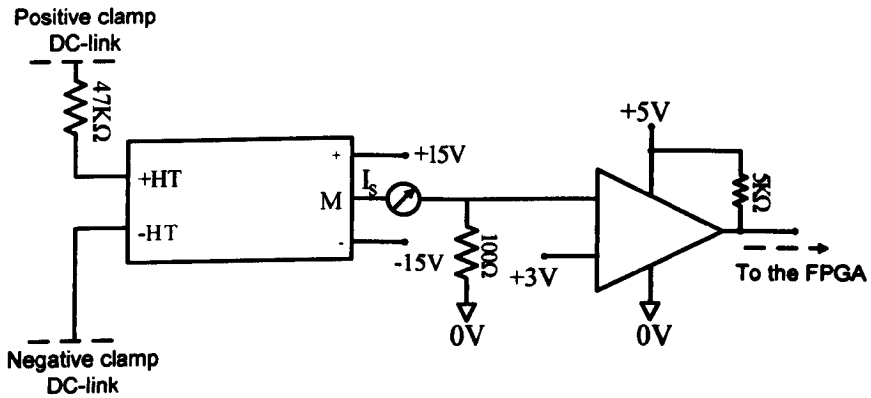


Figure 5.14: The over-voltage detection circuit

5.4 The Control and Interface Circuits

This section describes the control platform for the multi-motor drive converter topology, including the control and interface circuits. The control circuits include the Digital Signal Processing (DSP) and Field Programming Gate Array (FPGA) board. The interface circuits include the Daughter Card (C6713DSK HP1) and Encoder Interface Board. The following sections will give an explanation about each of these boards.

5.4.1 Control Circuits: DSP and FPGA

The control of the multi-motor drive converter topology has been implemented using a Texas Instruments, 32-bit, floating-point digital signal processing (TMS320C6713) [45]. The floating point DSP has some special features like a 32-bit External Memory Interface (EMIF), a 16-bit Host Port Interface (HPI), two 32-bit general purpose timers and a flexible Phase Locked Loop (PLL). These features allow the DSP to connect to the external peripherals such as the FPGA

5.4. The Control and Interface Circuits

and daughter card. With an operating frequency of 225MHz the TMS320C6713 DSP is able to perform a million operations and instructions per second. For this project the TMS320C6713 DSP performs all the modulation calculations and control functions.

To expand the functionality of the DSP a FPGA board powered by the ProASIC A500K050 FPGA is used. Figure 5.15 shows the photograph of FPGA board used for the prototype converter. This FPGA board was designed and developed by the University of Nottingham to control matrix converters for aerospace applications [46]. Due to its flexible design, the same board can be used for many other power converter topologies by making some modifications to the FPGA software.

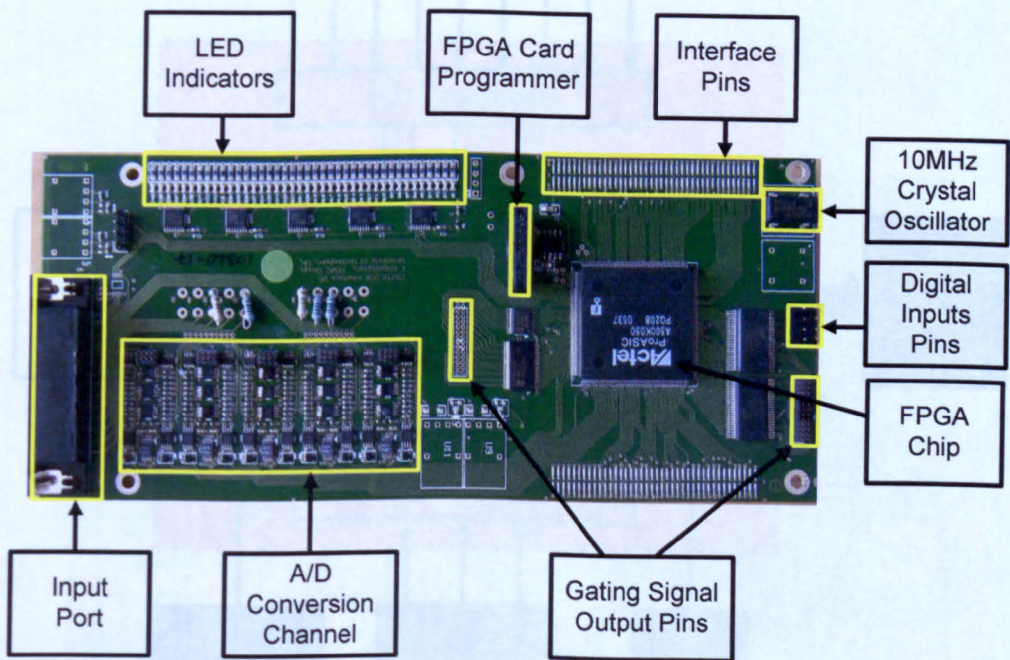


Figure 5.15: The FPGA board used for the prototype converter

5.4. The Control and Interface Circuits

The FPGA board is interfaced to the DSP evaluation board using two 80 pins connectors which are connected on the back of the FPGA board. The analog signals from the power circuit of the converter are connected to the input port of the FPGA board. These analog signals are then converted into digital signals using the A/D conversion channels. The digital signals from the power circuit can directly connected to the digital inputs pins of the FPGA board. The PWM signals from the FPGA board use the output pins connectors to connect the gate drive circuits. The FPGA board also provides the over current protection using trips which can be set from voltage references. Figure 5.16 shows the input and output variables which are connected to FPGA board in this prototype converter.

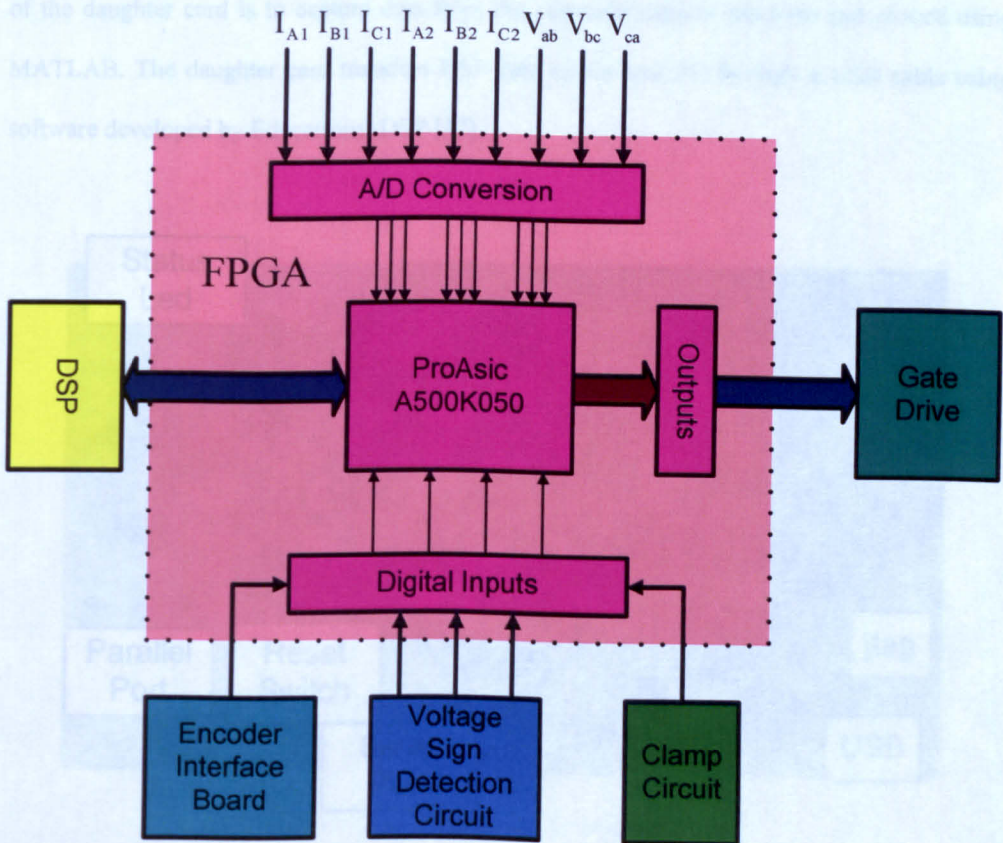


Figure 5.16: The inputs and outputs connected to the FPGA board

5.4. The Control and Interface Circuits

In order to safely commutate the current between the bi-directional switches of the converter, the FPGA is programmed to perform the associated commutation technique. For the prototype converter the relative input voltage magnitude based commutation strategy is used for rectification stage and dead time commutation is used for the inversion stages. The state machines for both commutation strategies have been programmed into the FPGA using VHDL and logic gates.

5.4.2 Host PC Interface Board

The DSK6713HP1 daughter card is used in this project, as shown in figure 5.17. The function of the daughter card is to capture data from the converter control platform and plotted using MATLAB. The daughter card transfers DSP data to the host PC through a USB cable using software developed by Educational DSP [47].

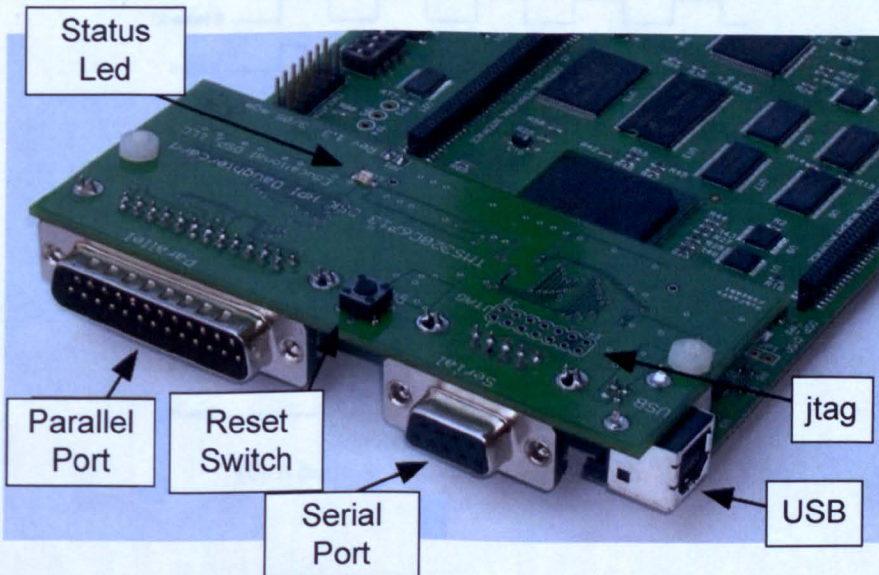


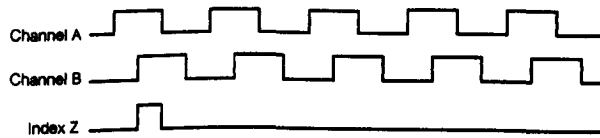
Figure 5.17: The DSK6713 HP1 daughter card

5.4. The Control and Interface Circuits

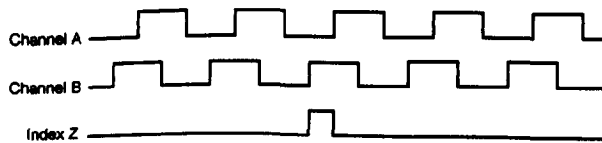
5.4.3 The Encoder Interface Board

An encoder is an electro-mechanical device that can monitor motion or position transforming electro-mechanical rotary movement into a sequence of electrical pulses [48]. The most common type of incremental encoder generate a signal for each incremental change in position of a shaft by scanning photo-electrically a disk to the shaft of the motor which is divided into dark/bright segments. Most of the incremental encoder generates two output signals (A and B) by means of two code tracks with sectors positioned 90° degree out of phase to each other [49].

These two output signals have a unique relationship, for example, if A leads B, then the direction of shaft is clockwise and if B leads A, the direction is anti-clockwise as shown in figure 5.18.



(a) A leads B, Clockwise direction



(b) B leads A, Anti-clockwise direction

Figure 5.18: Incremental encoder signals

5.4. The Control and Interface Circuits

A third output channel, called the zero or reference signal (Z) can be included to supply a single pulse per revolution of encoder. The index signal is used as a reference to establish an absolute position of the motor shaft.

Incremental encoders are susceptible to noise, especially when the encoder cable is long. Noise problems can be reduced by using an encoder those provodes complementary outputs. As shown in figure 5.19, a correct signal will generate two simultaneous outputs. As channel A goes high, \bar{A} goes low. If this doesn't occur, the signal is assumed to be the result of electrical noise and is ignored [50]. Therefore, the complementary signals are transmitted in addition to the channel A, B and Z in order to improve the signal transmission.

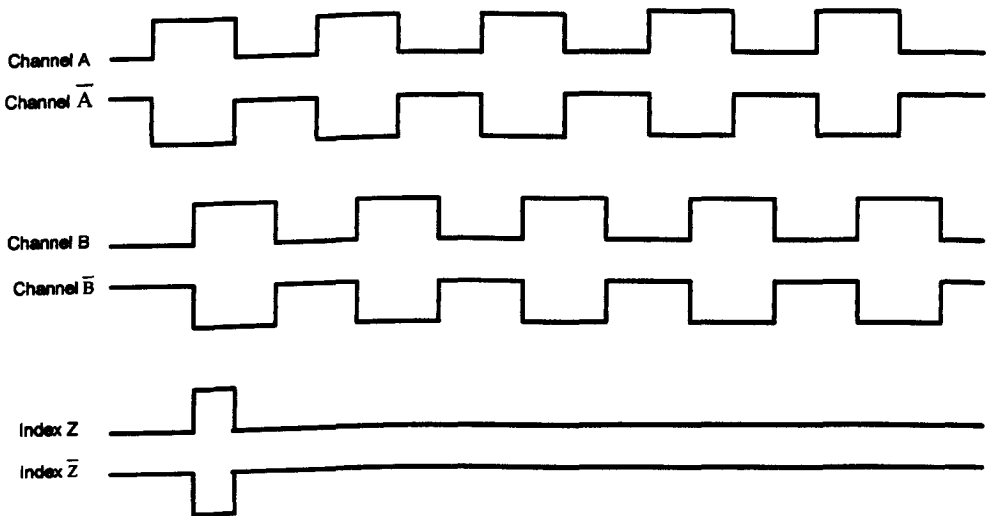


Figure 5.19: Incremental encoder signals with inverted signals

5.4. The Control and Interface Circuits

In this project two induction motors are connected on same shaft. Therefore a single encoder mounts to one motor is used. The encoder generates the six output signals (A, A', B, B', Z, Z'), which are fed to the FPGA card to calculate the rotor position of the motor.

The line diagram of the encoder interface circuit is shown in figure 5.20. The interface circuits consists a Quadruple Differential Line Receiver (SN75173N), which convert encoder output signals (A, A', B, B', Z, Z') to three input signals (A, B and Z) for FPGA card.

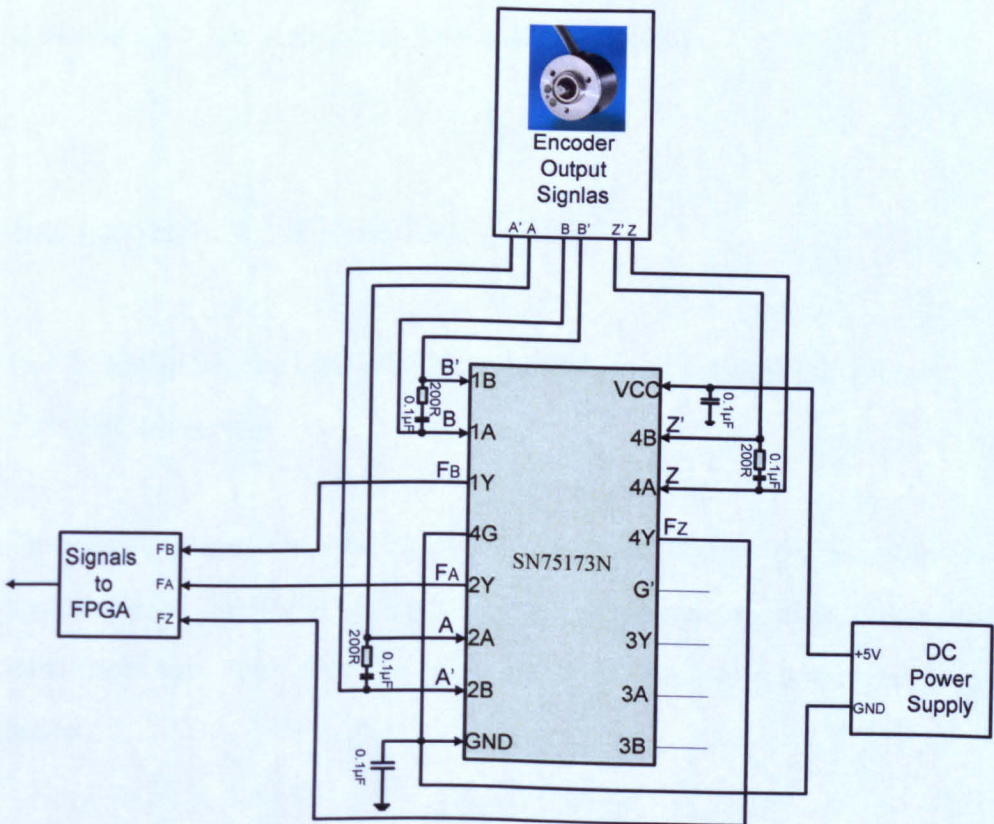


Figure 5.20: Schematic of encoder interface circuit

5.5. Conclusion

5.5 Conclusion

The experimental prototype for the proposed multi-motor drive converter system using a DSP/FPGA control platform has been described. The designs of the gate-drive circuit, the relative input voltage polarity detection circuit, the protection circuit and the encoder interface circuit have been explained.

Chapter 6

Prototype Practical Results

6.1 Introduction

This chapter confirms the validity of the proposed multi-motor drive system using experiment results obtained from a laboratory prototype rated at 7.5 kW, feeding two 3 kW induction motors. The first section of this chapter describes experimental results for the multi-motor drive system with induction motor load. In the next section, the experimental results are presented to prove the effectiveness and feasibility of the proposed multi-motor drive system with the vector control of two induction motors.

6.2 Experimental Results

6.2.1 Multi-Motor Drive System based on a Two-Stage Direct Power Converter

The multi-motor drive converter consists of a single rectification stage shared by two inversion stages. The validity of the multi-motor drive converter is verified by number of experimental tests. Some of the experimental tests are performed and discussed in this chapter.

This section describes the experimental results of the open loop control of the multi-motor drive converter, where an induction motor is connected to each inversion stage as shown in figure 6.1. The experimental result of the multi-motor drive system with two induction motor loads is shown in figure 6.2. The experimental parameters are listed in Appendix-‘E’.

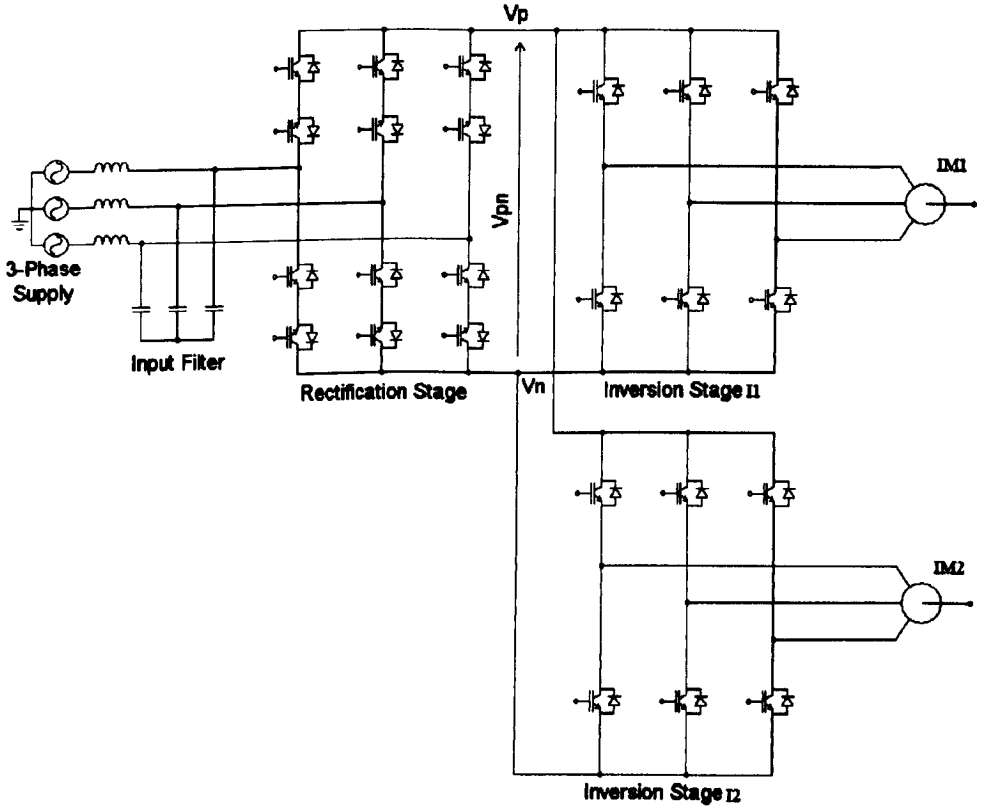
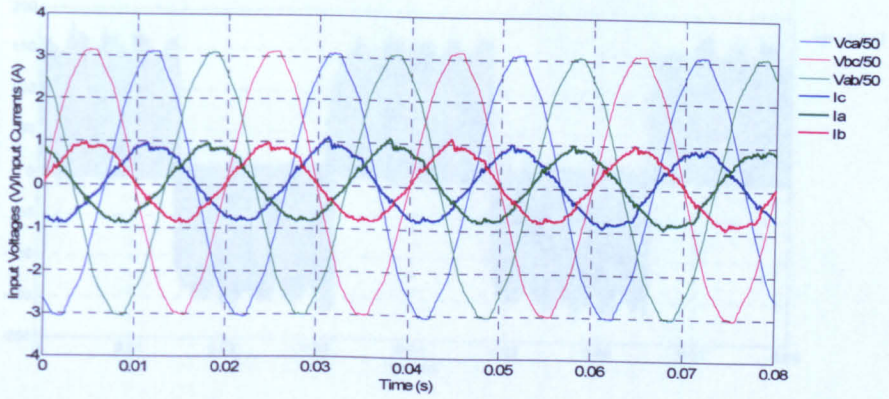


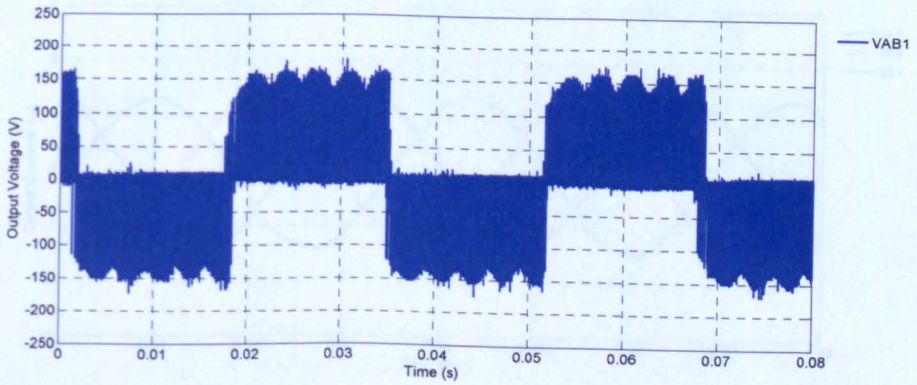
Figure 6.1: Multi-motor drive system with induction motors on each inversion stage

Figure 6.2 shows the experimental results for an input frequency of 50Hz and where the output frequency of inversion stage I1 is 30Hz and I2 is 40Hz.

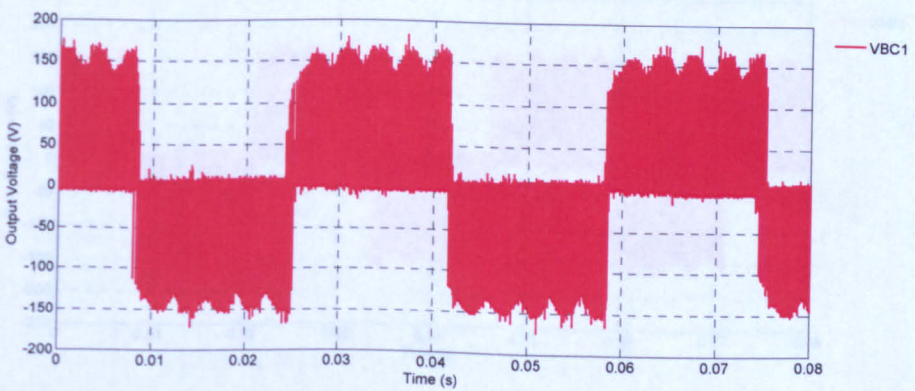
Figure 6.2 (a) shows the three-phase supply voltage and their corresponding line currents. As expected, the input current is sinusoidal and is almost in phase with the input voltage. The output performance of the multi-motor drive converter system with induction motor is shown by the waveforms of the line-to-line output voltages and three-phase output currents for inverter I1 and inverter I2, shown in figure 6.2 (b) to (i).



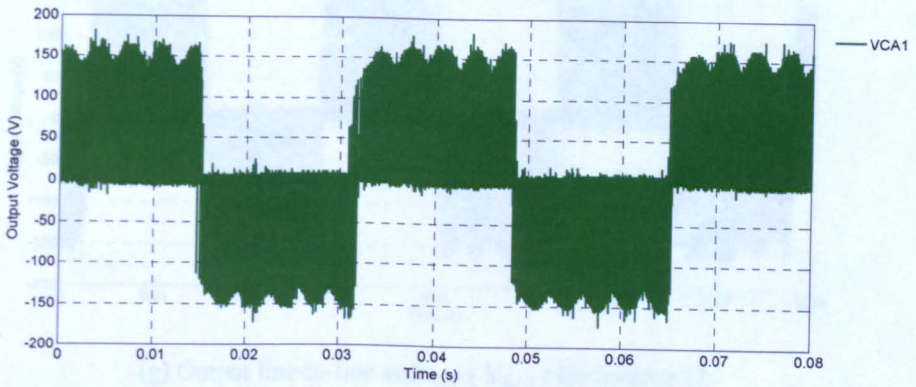
(a) Three-phase input voltages and line currents



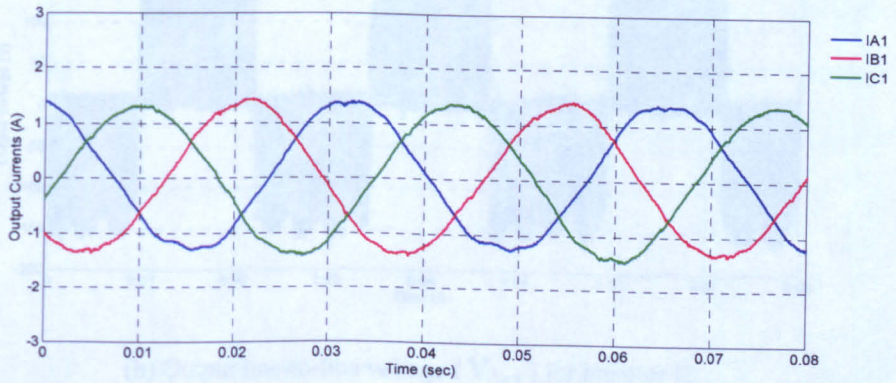
(b) Output line-to-line voltage (V_{AB1}) for inverter I1



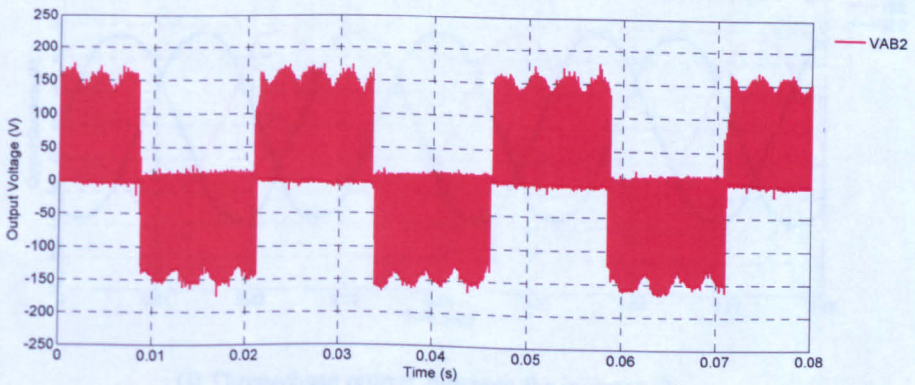
(c) Output line-to-line voltage (V_{BC1}) for inverter I2



(d) Output line-to-line voltage (V_{CA1}) for inverter I1

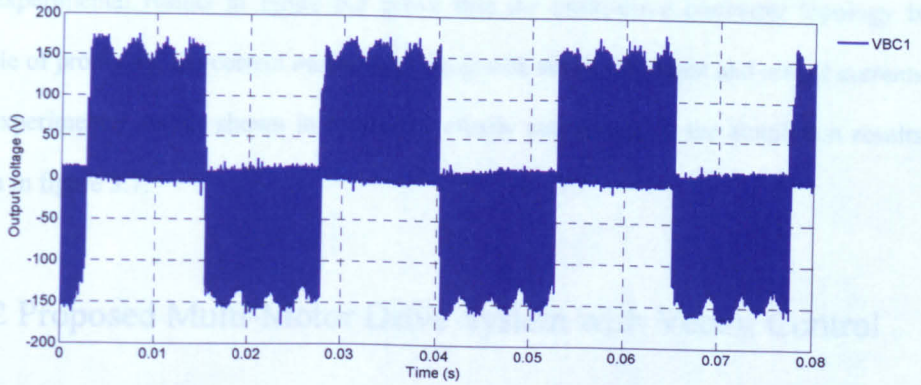


(e) Three-phase output currents for inverter I1

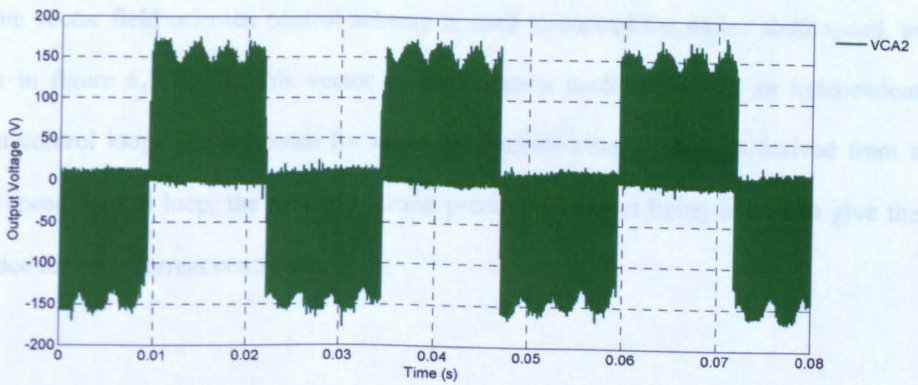


(f) Output line-to-line voltage (V_{AB2}) for inverter I2

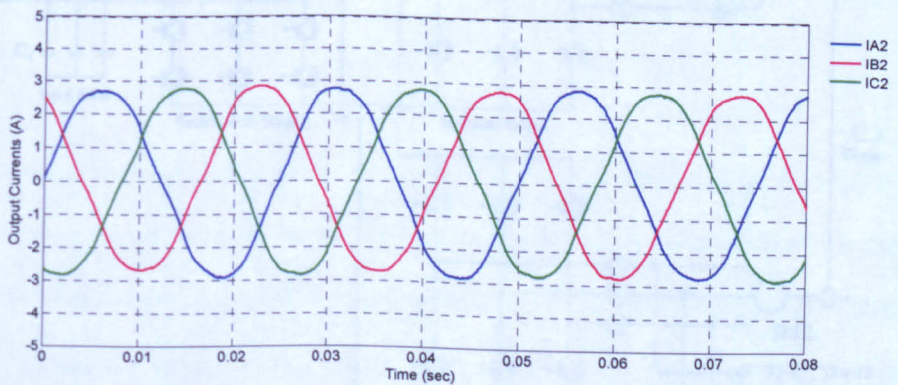
6. 2. Experimental Results



(g) Output line-to-line voltage (V_{BC2}) for inverter I2



(h) Output line-to-line voltage (V_{CA2}) for inverter I2



(i) Three-phase output currents for inverter I2

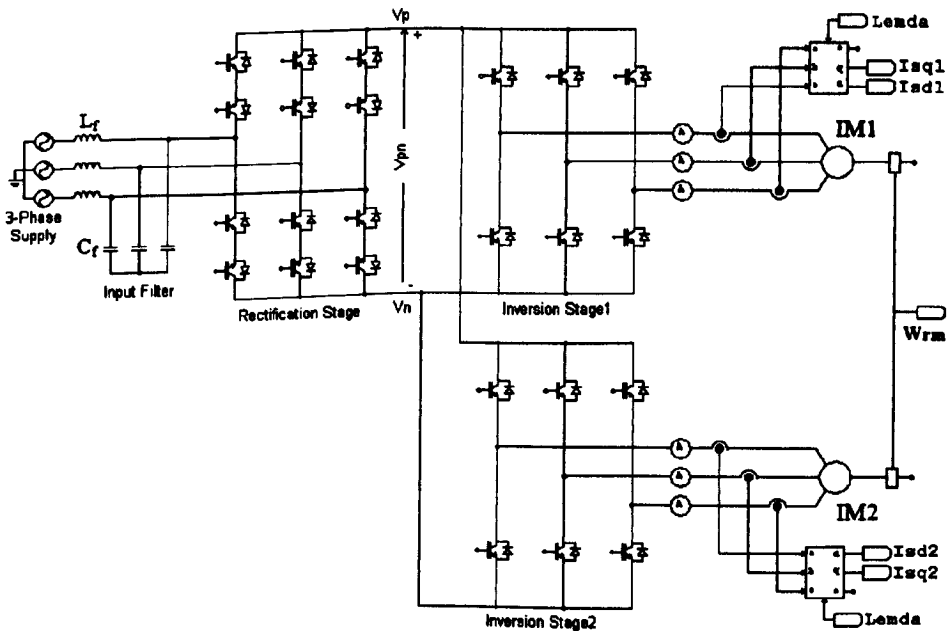
Figure 6.2: Experimental waveforms for the multi-motor drive converter (output frequency for inverter I1 is 30Hz and output frequency for inverter I2 is 40Hz)

6. 2. Experimental Results

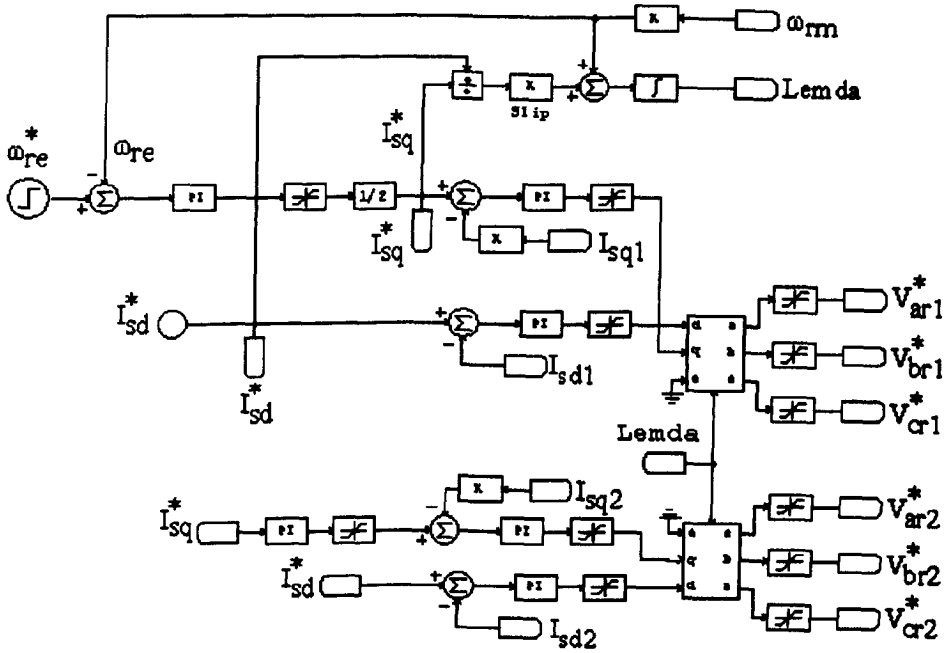
The experimental results in figure 6.2 prove that the multi-drive converter topology is capable of producing the correct output frequency with sinusoidal input and output currents. The experimental results shown in figure 6.2 clearly correspond to the simulation results shown in figure 3.7.

6.2.2 Proposed Multi-Motor Drive System with Vector Control

This section describes the experimental results of the closed loop vector control of the induction motors; two induction motors are connected on same shaft as shown in figure 6.3 (a). The vector field oriented control scheme is used to control the motor shaft speed, as shown in figure 6.3 (b). In this vector control scheme each motor has an independent current control loop. The reference for these two current control loops is derived from a single speed control loop, the required torque producing current being halved to give the reference for each current controller.



(a) The multi-motor drive system



(b) Vector control scheme

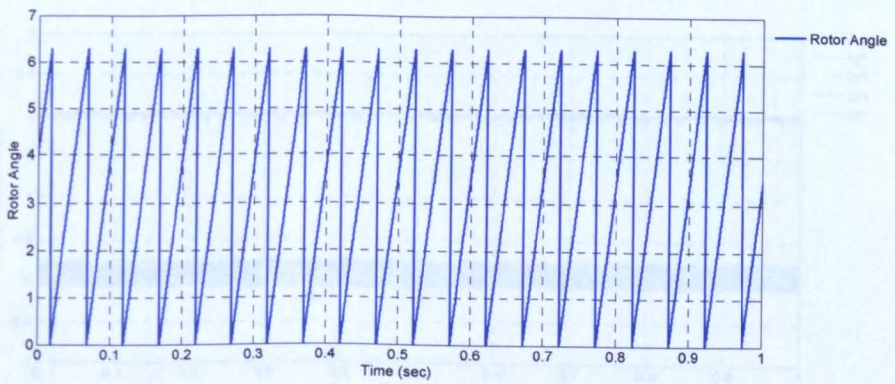
Figure 6.3: The multi-motor drive system with two induction motors connected to the same shaft

The feasibility of the proposed multi-motor drives system with closed loop vector control is verified with experimental test carried out using the laboratory prototype. The experimental results for normal operation of the vector controlled multi-motor drive system are shown in figure 6.4.

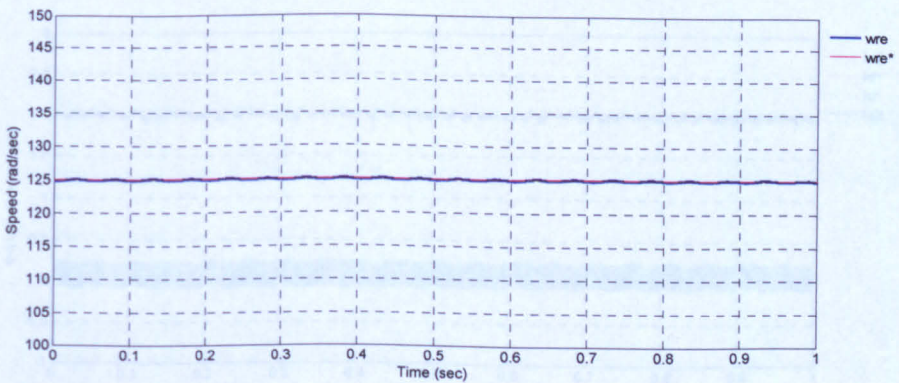
Figure 6.4 (a) shows the rotor angle of the induction motor measured by incremental encoder connected on the motor shaft. This rotor angle is used to calculate the rotor flux angle (λ) to find the actual value of d-q axis currents. Figure 6.4 (b) shows the motors shaft speed at 125rad/sec in steady state operation. The actual speed (ω_{re}) is following the demand speed (ω_{re}^*).

6. 2. Experimental Results

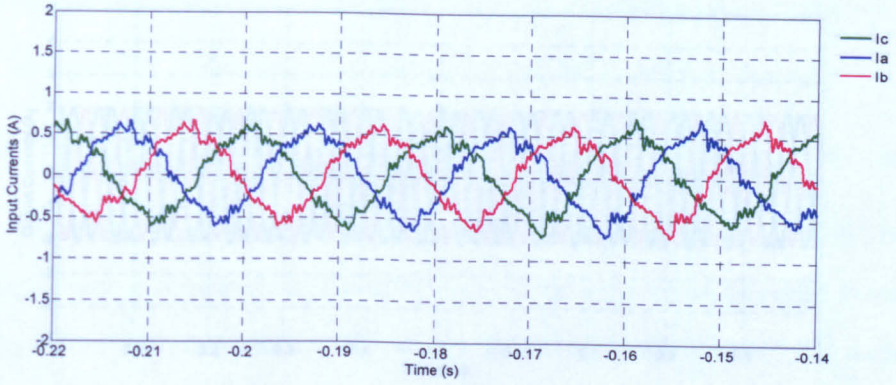
A set of sinusoidal, balanced input currents line current (I_a, I_b, I_c) obtained at the supply side of the converter is shown in figure 6.4 (c). The supply current remains constant during steady state operation. The field producing currents (I_{sd}) and torque producing currents (I_{sq}) for induction motors IM1 and IM2 are shown in figure 6.4 (d) and (e) respectively. The field producing current (I_{sq}) is maintained a constant level during steady state speed. The actual values of the d-q axis currents follow their respective references. The output performance of the multi-motor drive system is shown by the three-phase sinusoidal stator currents for motor IM1 and IM2 in figure 6.4 (f) and (g) respectively.



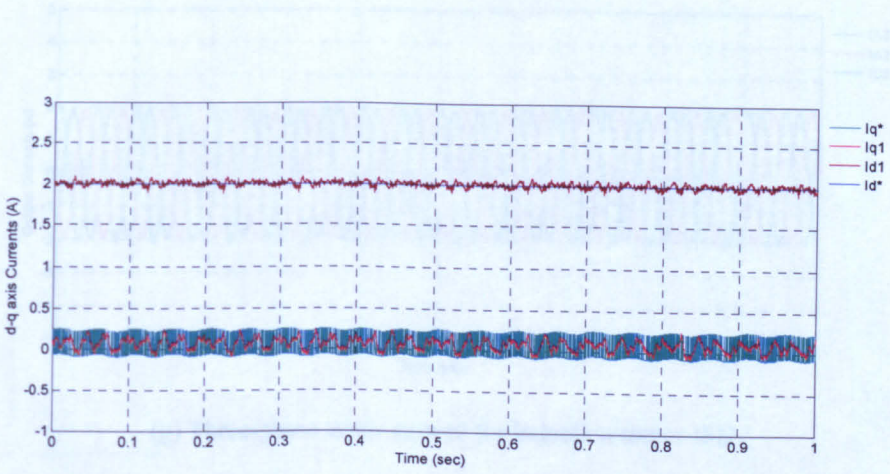
(a) Rotor position (rotor angle) of induction motor



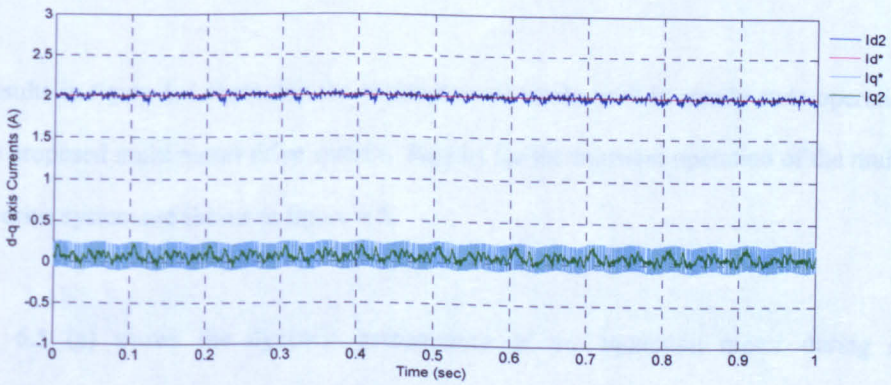
(b) Motor shaft speed



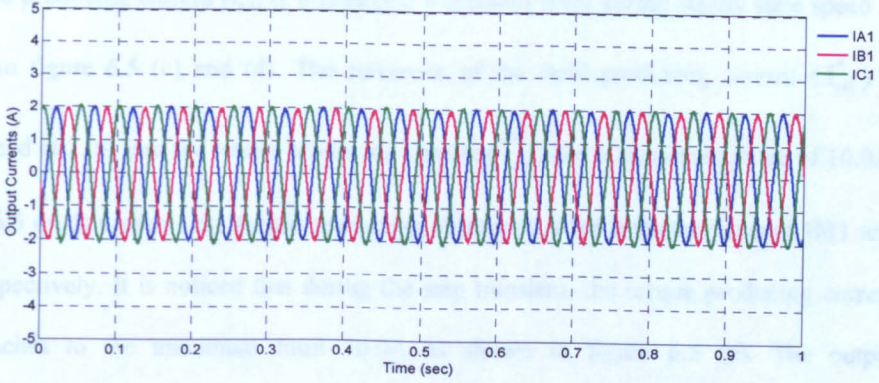
(c) Three-phase input currents



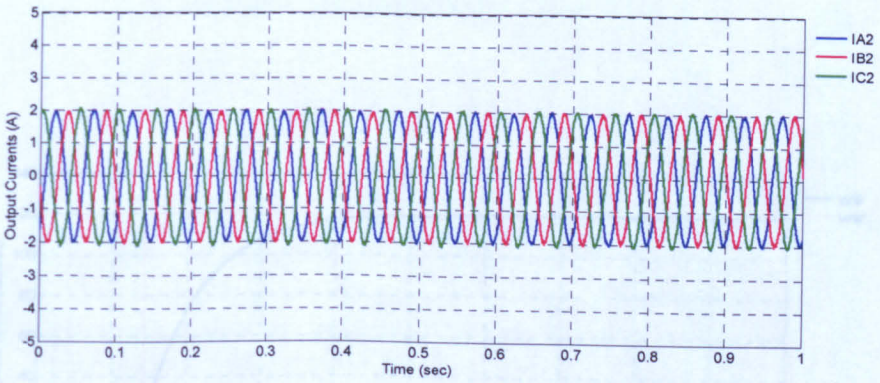
(d) d-q axis current for induction motor IM1



(e) d- q axis current for induction motor IM2



(f) Three-phase stator current for induction motor IM1



(g) Three-phase stator current for induction motor IM2

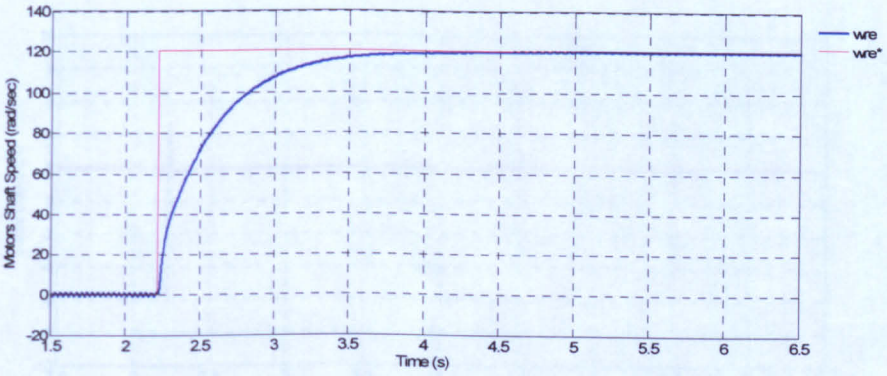
Figure 6.4: Experimental waveforms for the multi-motor drive system with two-induction motors connected on same shaft for steady state operation

The results in figure 6.4 show that the vector control works well in steady state operation for the proposed multi-motor drive system. Results for the transient operation of the multi-motor drive system are shown in figure 6.5.

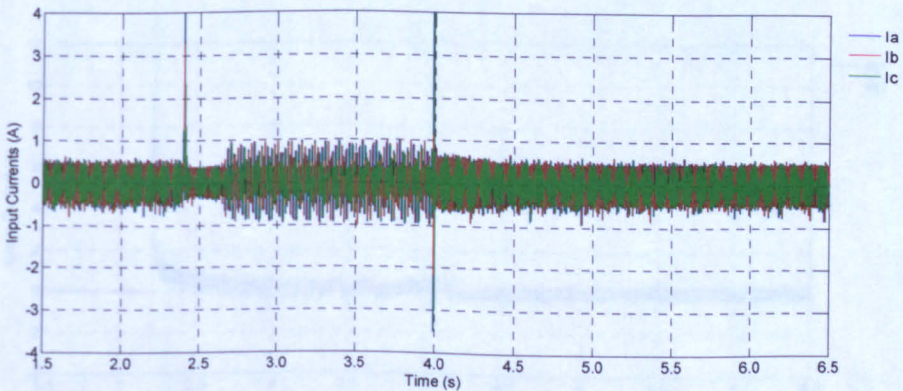
Figure 6.5 (a) shows the dynamic performance of the induction motor during an acceleration from standstill to 120rad/sec with no-load torque. The input currents for the converter are shown in figure 6.5 (b). It is noted that at 2.2 second the motor start accelerating, therefore it requires more supply current until it reaches steady state. The supply currents remain constant during steady state operation.

6. 2. Experimental Results

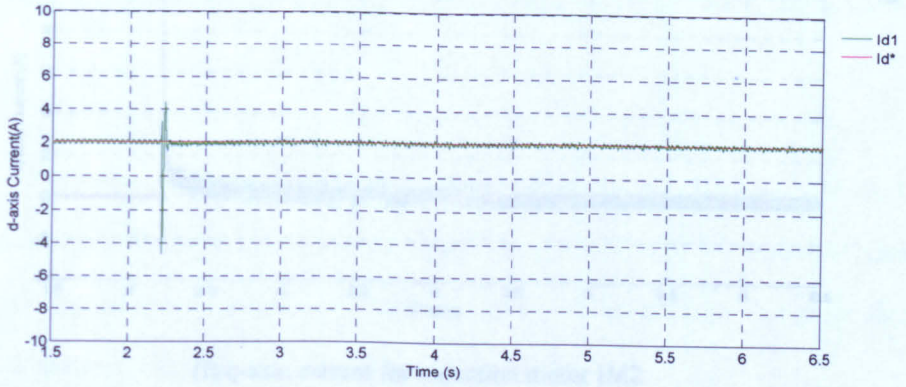
The field producing current (I_{sd}) is maintained a constant level during steady state speed as shown in figure 6.5 (c) and (d). The reference of the field producing current (I_{sd}^*) is maintained at 2.0A and the torque producing current (I_{sq}^*) has a maximum value of 10.0A. Figure 6.5 (e, f) presents the torque producing current (I_{sq}) for induction motors IM1 and IM2 respectively. It is noticed that during the step transient, the torque producing current (I_{sq}) reaches to the maximum limit 10.0A as shown in figure 6.5 (e). The output performance of the multi-motor drive system is shown by the three-phase output currents or stator currents for the induction motors.



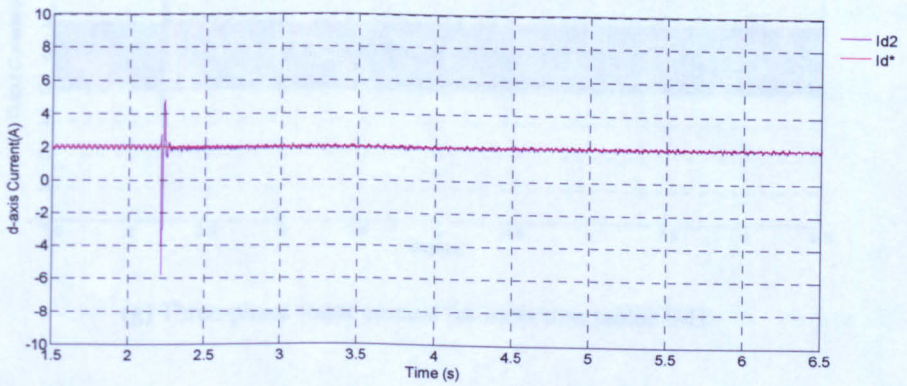
(a) Motor shaft speed



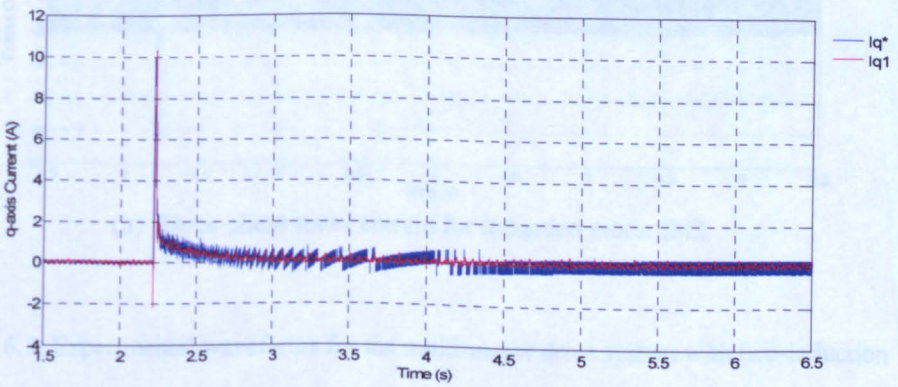
(b) Three-phase input currents



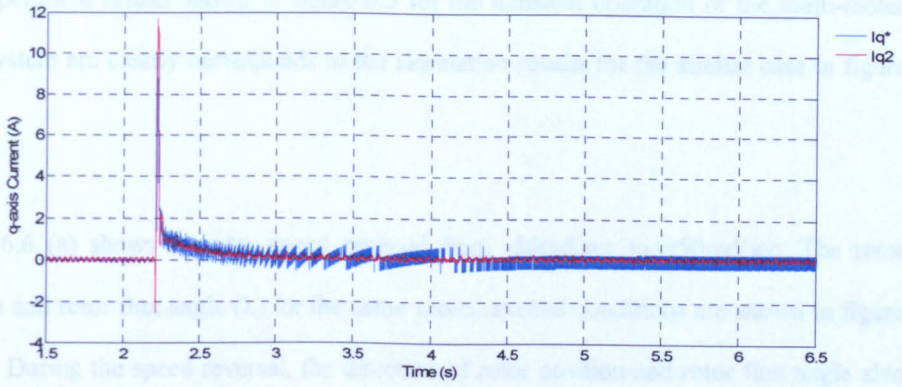
(c) d-axis current for induction motor IM1



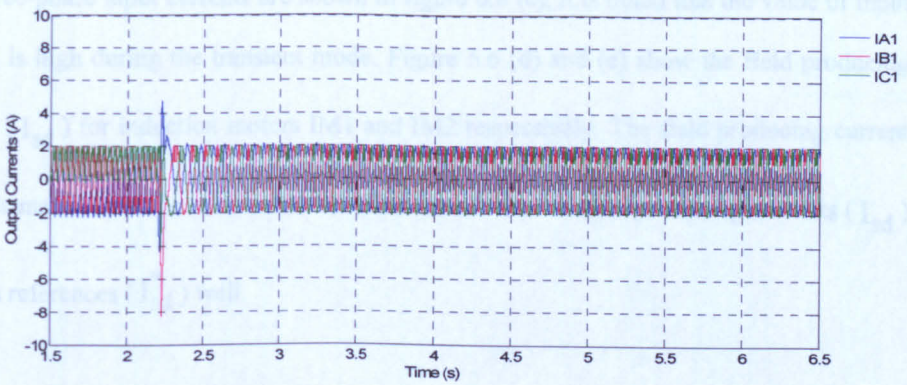
(d) d-axis current for induction motor IM2



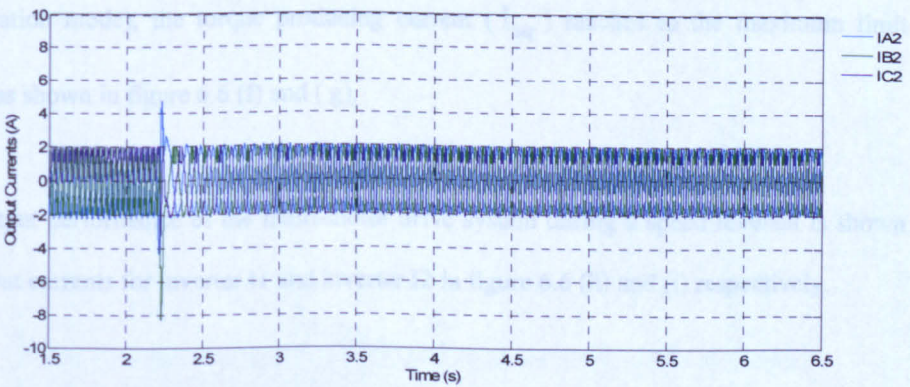
(e) q-axis current for induction motor IM1



(f) q-axis current for induction motor IM2



(g) Three-phase stator current for induction motor IM1



(h) Three-phase stator current for induction motor IM2

Figure 6.5: Experimental waveforms for the multi-motor drive system with two-induction motors connected on same shaft for transient operation

The experiment results shown in figure 6.5 for the transient operation of the multi-motor drive system are clearly corresponds to the simulation results for the similar case in figure 4.22.

Figure 6.6 (a) shows a motor speed reversal from -50rad/sec to +50rad/sec. The rotor position and rotor flux angle (λ) for the same speed reversal conditions are shown in figure 6.6 (b). During the speed reversal, the direction of rotor position and rotor flux angle also change as shown in figure 6.6 (b).

The three-phase input currents are shown in figure 6.6 (c), it is noted that the value of input current is high during the transient mode. Figure 6.6 (d) and (e) show the field producing current (I_{sd}) for induction motors IM1 and IM2 respectively. The field producing current (I_{sd}) is maintained at a constant level. The actual value of field producing currents (I_{sd}) follows references (I_{sd}^*) well.

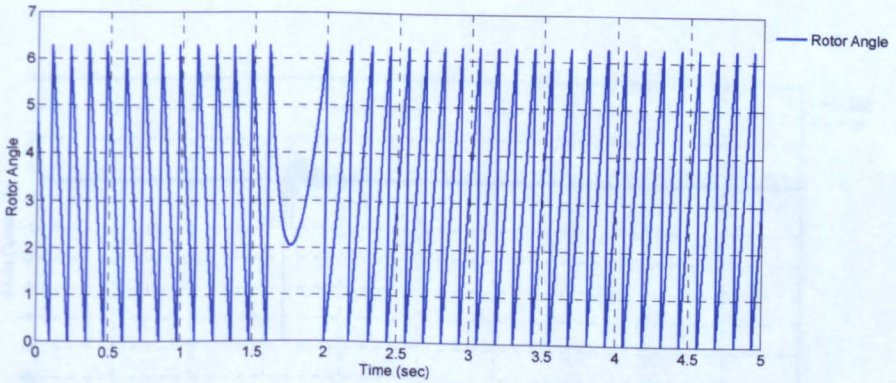
Figure 6.6 (f) and (g) shows the torque producing current (I_{sq}) for induction motors IM1 and IM2 respectively. It is noticed that during the step transient (acceleration and deceleration mode), the torque producing current (I_{sq}) reaches to the maximum limit 10.0A as shown in figure 6.6 (f) and (g).

The output performance of the multi-motor drive system during a speed reversal is shown by output currents for inverter I1 and inverter I2 in figure 6.6 (h) and (i) respectively.

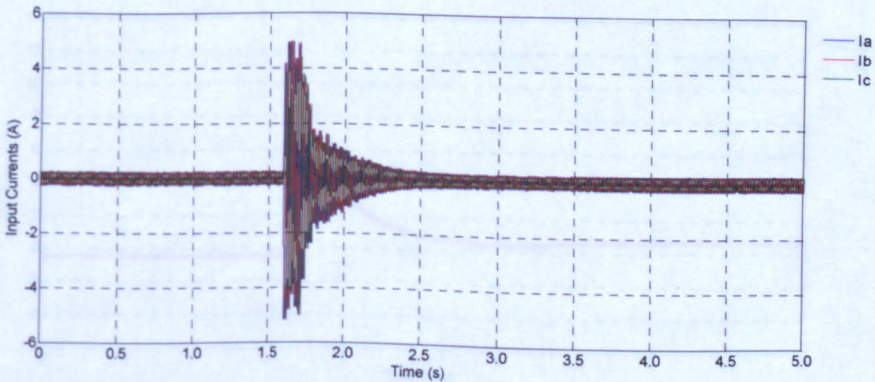
6. 2. Experimental Results



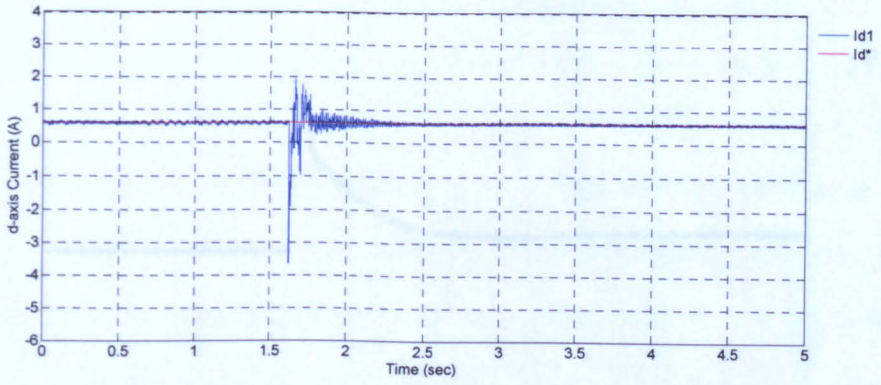
(a) Motors shaft speed



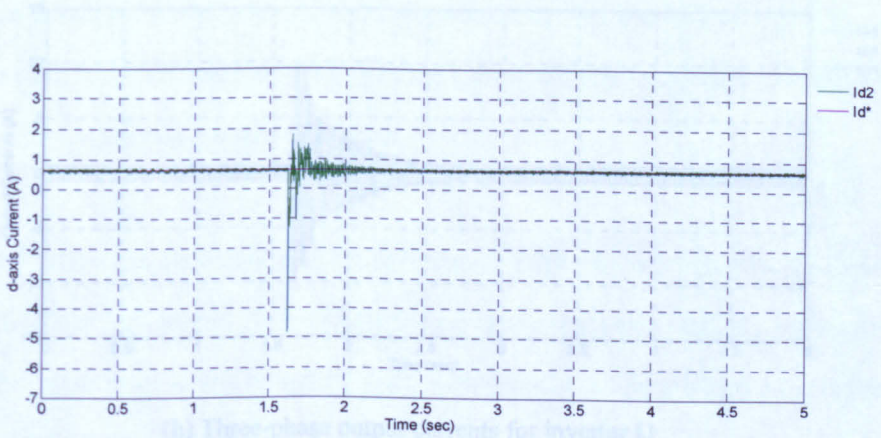
(b) Rotor position (rotor angle) of induction motor



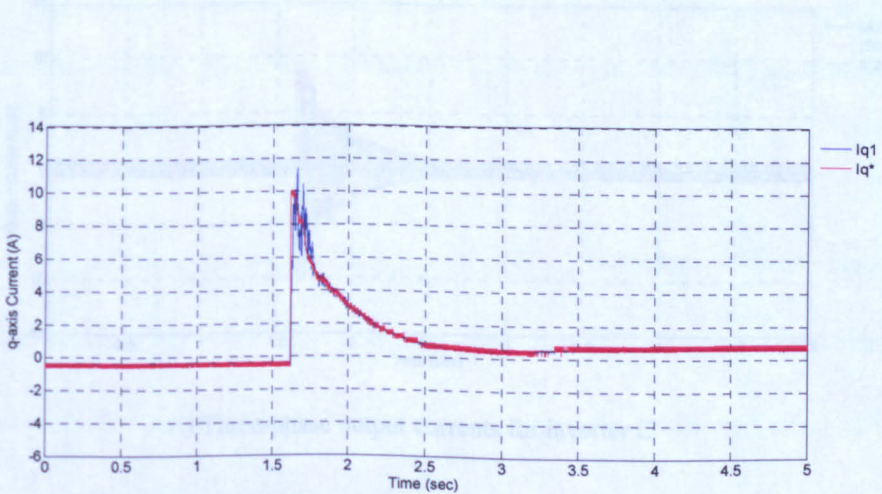
(c) Three-phase input currents



(d) d-axis currents for induction motor IM1

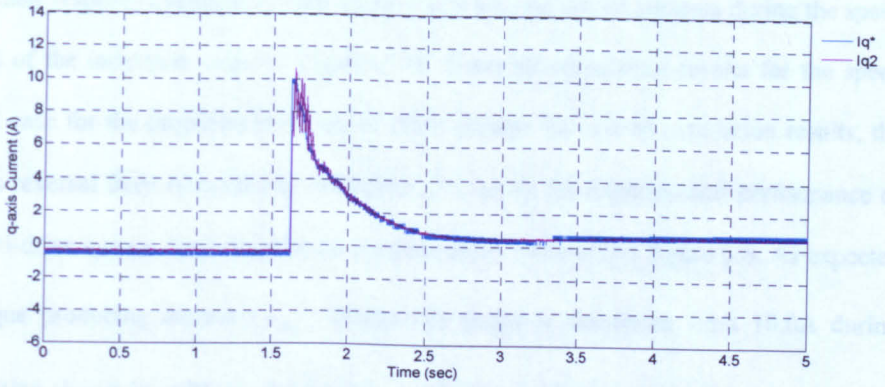


(e) d-axis current for induction motor IM2

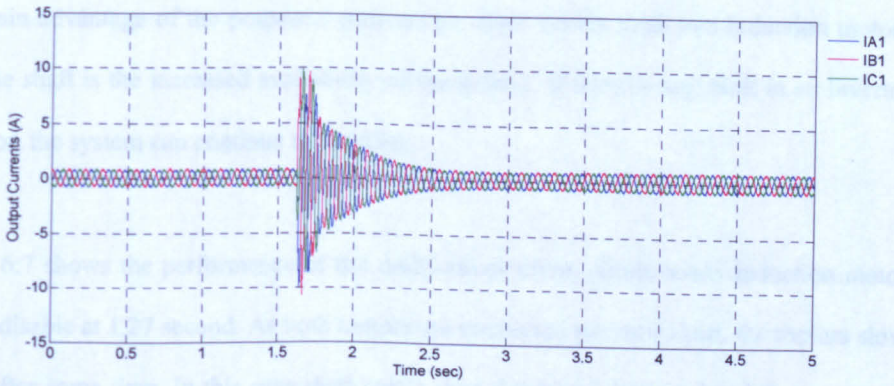


(f) q-axis current for induction motor IM1

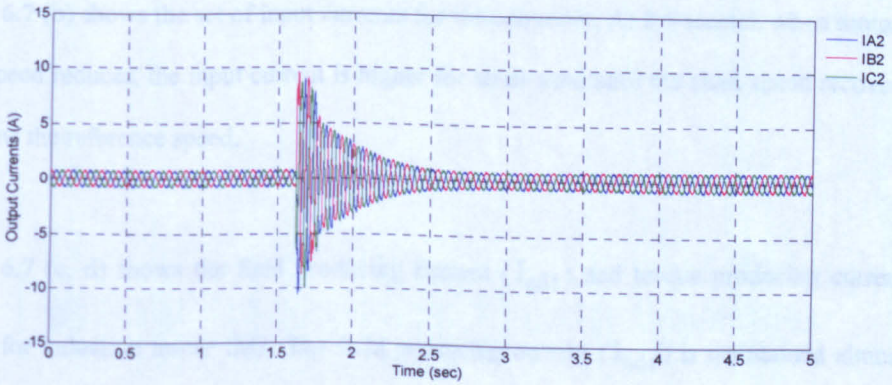
6. 2. Experimental Results



(g) q-axis current for induction motor IM2



(h) Three-phase output currents for inverter I1



(i) Three-phase output currents for inverter I2

Figure 6.6: Experimental waveforms of the multi-motor drive system when speed reversal

6. 2. Experimental Results

The experimental results in figure 6.6 show that the actual speed and d-q axis currents follow their respective references with sinusoidal input and output currents during the speed reversal of the induction motors. Figure 4.26 shows the simulation results for the speed reversal case for the proposed multi-motor drive system. In case of simulation results, the speed is reversal from 62rad/sec to -62rad/sec. To verify the experimental performance of the multi-drive system from negative to positive mode is shown by figure 6.6. As expected the torque producing current (I_{sq}) reaches its negative maximum limit 10.0A during decelerating shown in 4.26 (d) and positive maximum limit during accelerating shown in 6.6 (f).

The main advantage of the proposed multi-motor drive system with two induction motors on same shaft is the increased availability of the system. If there is any fault in an inverter or motor, the system can continue to function.

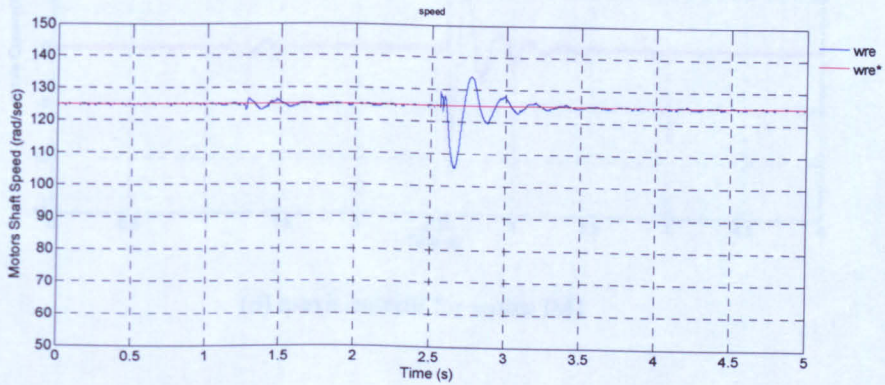
Figure 6.7 shows the performance of the multi-motor drive system when induction motor IM2 is disable at 1.27 second. As both motors are connected on same shaft, the motors slow down after some time. In this case shaft speed slow down at 2.5 second and then recovers to follow the reference value around at 3.1 second.

Figure 6.7 (b) shows the set of input currents for the converter. At 2.5 second, when motors shaft speed reduces, the input current is higher for some time until the shaft speed recovers to follow the reference speed.

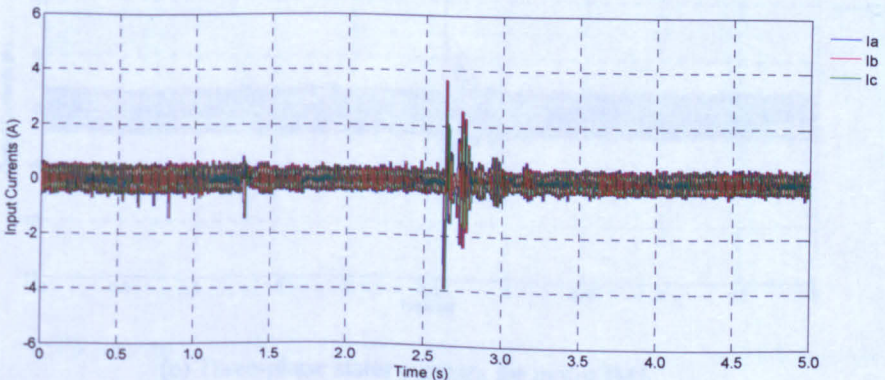
Figure 6.7 (c, d) shows the field producing current (I_{sd1}) and torque producing current (I_{sq1}) for induction motor IM1. The field producing current (I_{sd1}) is maintained almost constant level. The torque producing current (I_{sq1}) reaches the maximum limit of 10.0A at 2.5 second, when motors shaft speed unstable and approaches a zero value. Figure 6.7 (e) shows the three-phase stator currents for motor IM1.

6. 2. Experimental Results

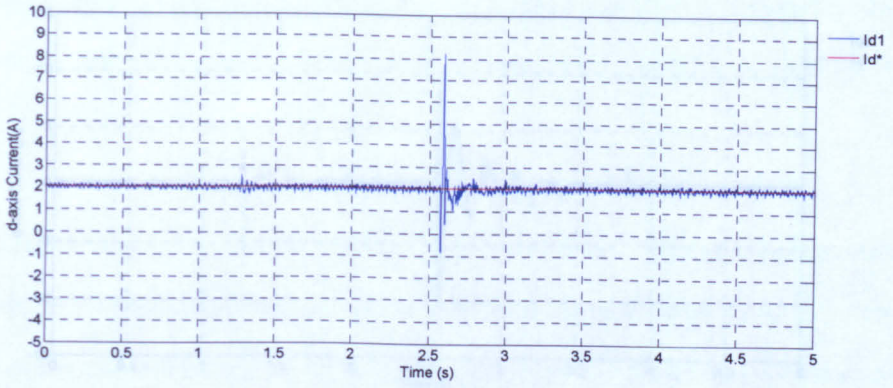
Figure 6.7 (f, g) shows the torque producing current (I_{sq2}) and field producing current (I_{sd2}) for induction motor IM2. The torque producing current (I_{sq2}) reaches the maximum limit 10.0A at 2.5 second and then approaches a zero value. At 1.27 second motor IM2 is disabled, therefore torque producing current (I_{sq2}) remain zero even if shaft speed recover the reference speed by IM1. The field producing current (I_{sd2}) is maintained at a constant level until 1.27 second and after that approaches zero as expected. Figure 6.7 (h) shows the three-phase stator currents for induction motor IM2. These results show that when motor IM2 disabled at 1.27 second, the value of output currents approaches zero.



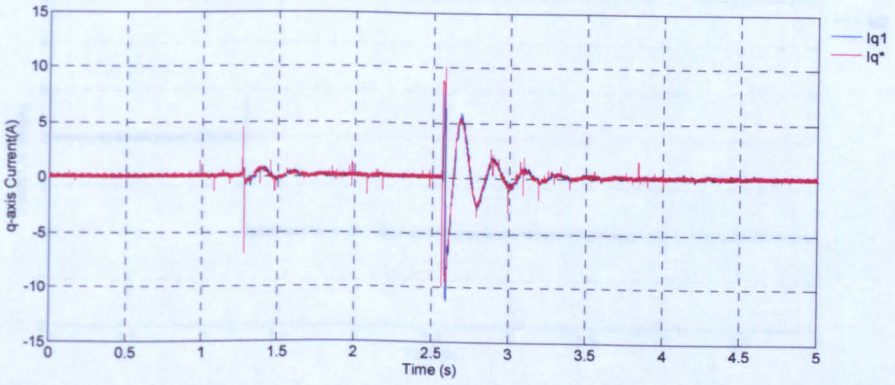
(a) The motors shaft speed



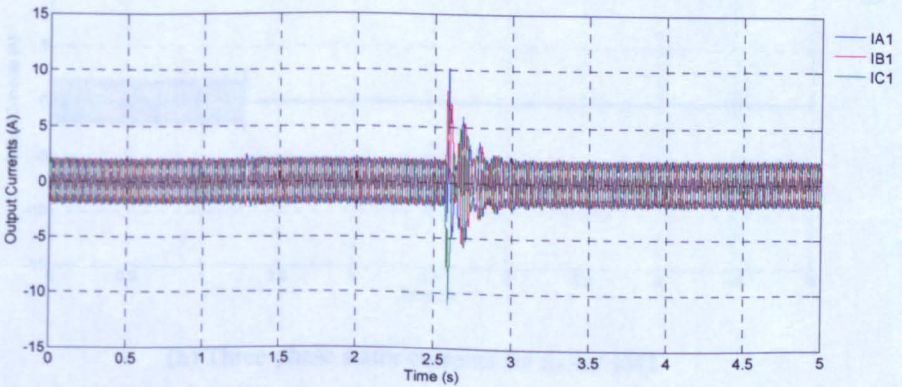
(b) Three-phase input currents



(c) d-axis current for motor IM1



(d) q-axis current for motor IM1



(e) Three-phase stator currents for motor IM1

6. 2. Experimental Results

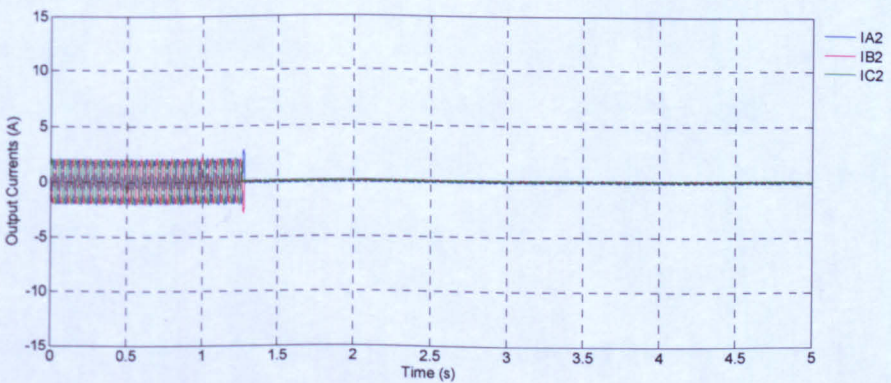
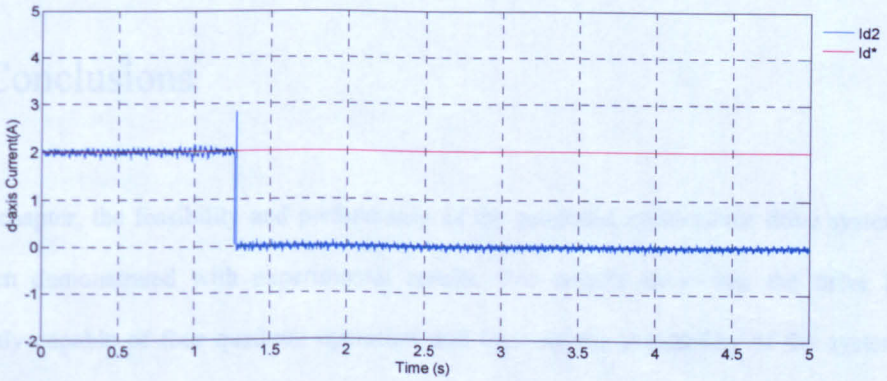
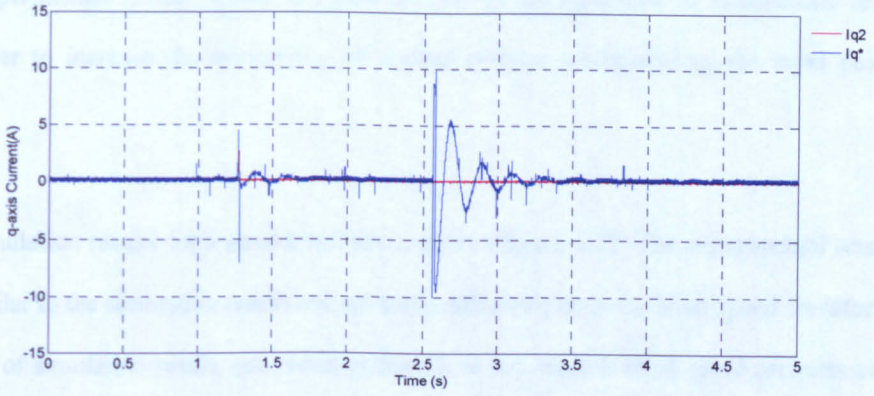


Figure 6.7: Experimental results for the multi-motor drive system when induction motor IM2 is disabled at 1.27 second

The experimental results shown in figure 6.7 proved the capability of multi-motor drive converter to increase the availability of system without compromising the input power quality.

The simulation results for a similar test are shown in figure 4.27. The experimental results are similar to the simulation results except some difference in motor shaft speed waveforms. In case of simulation result, one motor is disable at 0.4 second, shaft speed recovers very quickly without seeing any change in waveform, but this can be visualise properly with experimental waveforms shown in figure 6.7 (a) and same with torque producing currents.

6.3 Conclusions

In this chapter, the feasibility and performance of the proposed multi-motor drive system has been demonstrated with experimental results. The results show that the drive is inherently capable of four quadrant operation and increase the availability of the system with better input and output performance. In this experimental testing the results from the multi-motor drive converter prototype clearly correspond well to the simulation results.

Chapter-7

Conclusions

7.1 Conclusions

In the recent few years, the matrix converter is gaining more attention to academic and industrial researchers as a promising technique for AC to AC power conversion. As discussed in Chapter-2, the conventional matrix converter topology offers the following advantages:

- single stage AC-to-AC power conversion
- sinusoidal input currents and output voltages
- bi-directional power flow
- small passive components, which leads to a potential for good power density

Apart from these benefits the matrix converter has some disadvantages. The voltage transfer ratio is lower than unity (0.866), therefore the circuit has not been considered for standard industrial applications. The converter requires nine bi-directional switches for its operation.

The requirement of large number of bi-directional switches in conventional matrix converter topology increases the cost and complexity of the converter. To overcome this limitation a two-stage direct power converter has been proposed that works in the same way as a conventional matrix converter with reduced number of bi-directional switches.

Another benefit of the two-stage direct power converter over conventional matrix converter is that it offers a cost effective and weight/volume effective multi-motor drive system.

7.1 Introduction

In a multi-motor drive system single rectification stage can be shared by several inversion stages using common DC-link energy storage components. This concept provides a cost effective solution due to sharing of the front end rectifier stage. The use of DC-link capacitors in conventional multi-motor drive system has potential risk due to the high amount of stored energy. Therefore a common DC-link without energy storage components may be an alternative. The two-stage direct power converter offers an attractive option for the multi-motor drive system, which eliminates the use of any energy storage in DC-link.

In this work a multi-motor drive system has been proposed where two induction motors are connected on same shaft. A vector field oriented control system is used to control the induction motors. This type of multi-motor drive system can be used in many industrial and aerospace applications.

In Chapter-2, space vector modulation strategies have been developed for two-stage direct power converter topology. The space vector modulation for multi-motor drive converter topology can be derived from two-stage direct power converter. In Chapter-3 the derivation of space vector modulation strategy for multi-motor drive system has been presented. In this chapter it also shown that by changing the switching pattern it is possible to reduce the size of input filter and switching losses. The operation of the two-stage direct power converter and multi-motor drive converter are shown using simulation results.

In Chapter-4, the proposed multi-motor drive system with indirect vector field oriented control scheme for induction motors control has been presented. This is first time the performance of multi-motor drive system has been tested for two motor connected on same shaft. A modified vector field oriented control scheme has been developed for motors connected on same shaft. The performance of the proposed multi-motor drive system has been shown by simulation results.

7.2 Future Scope

In order to validate the simulation results, the multi-motor drive converter prototype were constructed in Chapter-5 and tested at realistic power levels. The experimental results in Chapter-6 clearly correspond well to the simulation results shown in Chapter 3 and 4.

7.2 Future Scope

The following are some of interesting areas in which further research can be made in order to develop the multi-motor drive system:

- However one of the main advantages of two-stage direct power converter is regeneration capability, but in some applications like aerospace, regeneration is strictly avoided. Therefore research is needed on the detection to avoid the regeneration in two-stage direct power converter topology.
- The implementation of multi-motor drive system that can be tested with PMSM motors

The work carried out in this project has resulted in several conference papers, which are listed in Appendix –‘F’.

Appendix-A

Parameters used in Simulation for Two-Stage Direct Power Converter

- Input

Input Voltages, V_{in_phase} = 240 V

Input Frequency, f_{in} = 50 Hz

- Input Filter

Inductor, L_f = 0.633 mH

Capacitor, C_f = 10 μ F

- Load

Resistor, R_L = 20 Ω

Inductor, L_L = 10mH

- Output

Output Voltage, V_{out_peak} = 270 V

Output Frequency, f_{out} = 60 Hz

- Switching Frequency = 5 KHz

Appendix-B

Parameters used in Simulation for Multi-Motor Drive Converter Topology

- Input

Input Voltages, V_{in_phase} = 240 V

Input Frequency, f_{in} = 50 Hz

- Input Filter

Inductor, L_f = 0.633 mH

Capacitor, C_f = 10 μ F

- Load for Inverter I1

Resistor, R_{L1} = 20 Ω

Inductor, L_{L1} = 10mH

- Load for Inverter I2

Resistor, R_{L2} = 20 Ω

Inductor, L_{L2} = 10mH

- Output for Inverter I1

Output Voltage, V_{out_peak} = 270 V

Output Frequency, f_{out1} = 40 Hz

Output Frequency, f_{out2} = 60 Hz

- Output for Inverter I2

Output Voltage, V_{out_peak} = 270 V

Output Frequency, f_{out2} = 60 Hz

- Switching Frequency = 5 KHz

Appendix-C

Induction Motor Dynamic Equations

A generalized d-q axis dynamic model of the induction motor in the rotating reference frame is used to derive the vector control algorithm. The equations defining the stator and rotor dynamics in a rotating reference frame can be defined as [31]:

$$V_{sd} = R_s I_{sd} + \sigma L_s \frac{d}{dt} I_{sd} - \omega_e \sigma L_s I_{sq} + \frac{L_o}{L_r} \frac{d}{dt} \Psi_{rd} \quad (i)$$

$$V_{sq} = R_s I_{sq} + \sigma L_s \frac{d}{dt} I_{sq} + \omega_e \sigma L_s I_{sd} + \omega_e \frac{L_o}{L_r} \Psi_{rd} \quad (ii)$$

The rotor equations for an induction motor are:

$$0 = \frac{R_r}{L_r} \Psi_{rd} + \frac{d}{dt} \Psi_{rd} - \frac{L_o}{L_r} R_r I_{sd} - \omega_{sl} \Psi_{rq} \quad (iii)$$

$$0 = \frac{R_r}{L_r} \Psi_{rq} + \frac{d}{dt} \Psi_{rq} - \frac{L_o}{L_r} R_r I_{sq} + \omega_{sl} \Psi_{rd} \quad (iv)$$

The stator equations are not useful in the application indirect vector field orientation, therefore only the rotor equations are consider in this analysis. The rotor field orientation is achieved by

Appendix-C

aligning the d-axis with the rotor flux vector, substituting $\Psi_{rq} = 0$ in equations (iii) and (iv).

The field orientation rotor equations will become:

$$0 = \frac{R_r}{L_r} \Psi_{rd} + \frac{d}{dt} \Psi_{rd} - \frac{L_o}{L_r} R_r I_{sd} \quad (v)$$

$$0 = - \frac{L_o}{L_r} R_r I_{sq} + \omega_{sl} \Psi_{rd} \quad (vi)$$

By substituting $\Psi_{rd} = L_o I_{mrd}$, where I_{mrd} is the equivalent magnetising current, equation (iii) and (iv) will become:

$$\frac{L_r}{R_r} \frac{d}{dt} I_{mrd} + I_{mrd} = I_{sd} \quad (vii)$$

$$\omega_{sl} = \left(\frac{R_r}{L_r I_{mrd}} \right) I_{sq} \quad (viii)$$

Equations (vii) and (viii) are known as the vector control equations. Equation (viii) can be written in the form of the rotor time constant (τ_r):

$$\omega_{sl} = \left(\frac{1}{\tau_r I_{mrd}} \right) I_{sq} \quad (ix)$$

where,

$$\tau_r = \frac{L_r}{R_r} \quad (x)$$

Appendix-C

Since, $I_{mrd} = I_{sd}$, equation (ix) becomes,

$$\omega_{sl} = \left(\frac{1}{\tau_r I_{sd}} \right) I_{sq} \quad (xi)$$

Equation (xi) shows that the motor slip frequency is directly proportional to the torque producing current (i_{sq}) and inversely proportional to the rotor time constant (τ_r).

The electromagnetic torque developed by an induction motor can be defined by:

$$T = \frac{2 P L_o^2}{3 2 L_r} I_{sd} I_{sq} \quad (xii)$$

If we define $k_t = \frac{2 P L_o^2}{3 2 L_r}$ equation (xii) will be modified:

$$T = k_t I_{sd} I_{sq} \quad (xiii)$$

Appendix-D

Parameters used in Simulation for Multi-Motor Drive System

- Input

Input Voltages, V_{in_phase} = 240 V

Input Frequency, f_{in} = 50 Hz

- Input Filter

Inductor, L_f = 0.633 mH

Capacitor, C_f = 10 μ F

- Resistive Load

Resistor, R_L = 20 Ω

Inductor, L_L = 10mH

- Switching Frequency = 5 KHz

- Induction Motors Parameters

P = 4

J = 0.01225

B = 0

Lm = 0.1473

Ls = 0.229

Lr = 0.23138

$$R_s = 1.7$$

$$R_r = 2.16$$

- Vector Control

$$I_{sd}^* = 2.0 \text{ A}$$

$$I_{sq}^* \text{ Limit} = 10 \text{ A}$$

$$V_{sq}^* \text{ Limit} = 150 \text{ V}$$

$$V_{sd}^* \text{ Limit} = 150 \text{ V}$$

- Speed Controller

$$k_p = 1.5768$$

$$k_i = 123.9742$$

- Current Controller

$$k_p = 34.5251$$

$$k_i = 28451$$

Appendix-E

Experimental Parameters for Multi-Motor

Drive System

- Input Filter

Inductor, L_f = 2.026 mH

Capacitor, C_f = 2 μ F

- Switching Frequency = 12.5 KHz

- Induction Motor

Name Plate Detail:

Rated Power = 3 kW

Voltage = 415 V

Phase = 3

Frequency = 50 Hz

Current = 5.89 A

Speed = 1435 rpm

Connection = Star

- Speed Controller

k_p = 0.3984

k_i = 0.3846

- Current Controller

$$k_p = 5.10822$$

$$k_i = 5.02276$$

Appendix-F

Published Papers

This work has resulted in the following papers having been published:

- I. Dinesh Kumar, Patrick Wheeler, Jon Clare and Tae-Woong Kim, "Multi-Motor Drive System Based on a Two-Stage Direct Power Conversion Topology for Aerospace Applications," *Proceedings of Power Electronics, Machines and Drives*, pp. 607-610, April 2008.
- II. Dinesh Kumar, Patrick W Wheeler, Jon C Clare and Lee Empringham, "A Multi-Drive System Based on a Two-Stage Matrix Converter," *Proceeding of Power Electronics and Motion Control Conference*, pp. 207-212, Sept. 2008.
- III. Dinesh Kumar, Patrick W Wheeler, Jon C Clare and Tae-Woong Kim, "Weight/Volume Effective Multi-Drive System Based on Two-Stage Matrix Converter," *Proceeding of IEEE Industrial Electronics Conference IECON 2008*, pp. 2782-2787, Nov. 2008.
- IV. Dinesh Kumar, Patrick W Wheeler and Jon C Clare, "A Multi-Drive System Based on Direct Power Converter," *Proceeding of Power Electronics and Application Conference*, on CD-ROM, Sept. 2009.
- V. Dinesh Kumar, Patrick W Wheeler, Jon C Clare and Liliana de Lillo, "Experimental Evolution of the Multi-Drive System Based on Two-Stage Direct Power Converter Topology," *Proceeding of Power Electronics and Motion Control Conference*, on CD-ROM, Sept. 2010.

Appendix-G

List of Symbols

Notation	Meaning
AC	Alternating current
DC	Direct current
SCR	Silicon controlled rectifier
VSI	Voltage source inverter
PWM	Pulse width modulation
ASD	Adjustable speed drives
CSI	Current source inverter
SVM	Space vector modulation
GTO	Gate turn off thyristor
MOSFET	Metal-oxide-semiconductor field-effect transistor
IGBT	Insulated gate bipolar transistor
MC	Matrix converter
SMC	Sparse matrix converter
VSMC	Very sparse matrix converter
USMC	Ultra sparse matrix converter
MCU	Motor control unit
DTC	Direct torque control
IM	Induction motor
DSP	Digital signal processor
FPGA	Field programmable gate array
LC	Inductor plus capacitor
RL	Resistor plus inductor
V	Volt
A	Ampere
Ω	Ohm
H	Henry
Hz	Hertz
V_a, V_b, V_c	Three-phase input voltages
V_A, V_B, V_C	Three output line-to-supply neutral voltages

Appendix-G

V_{ab}, V_{bc}, V_{ca}	Three line-to-line input voltages
V_{AB}, V_{BC}, V_{CA}	Three line-to-line voltages
V_{pn}	DC-link voltage
V_{pn-avg}	Average DC-link voltage
V_i	Input voltages
V_o	Output voltages
$V_{\alpha'}, V_{\beta'}$	Output voltages in α - β reference frame
$V_{\alpha}, V_{\beta}, V_0$	Active voltage vectors inversion stages
$I_{\gamma}, I_{\delta}, I_0$	Active current vectors rectification stage
I_i	Input currents
I_o	Output currents
I_{pn}	DC-link current
I_a, I_b, I_c	Three-phase input currents
I_A, I_B, I_C	Three-phase output currents
I_L	Load current
$d_{\alpha}, d_{\beta}, d_0$	Duty cycles of the inverter voltage vector
$d_{\gamma}, d_{\delta}, d_0$	Duty cycles of the rectifier current vectors
C_f	Input filter capacitor
L_f	Input filter inductor
R_C	Clamp resistor
C_C	Clamp capacitor
R_d	Damping resistor
R_m	Measurement resistor for voltage and current transducer
θ_{out}	The angle of the reference output voltage vector
θ_{in}	The angle of the reference input current vector
$T_{\gamma}, T_{\delta}, T_0$	Switching time of the rectifier current vector
I_{in}	Reference input current vector
V_{out}	Reference output voltage vector
m_R	Modulation index of the rectification stage
m_I	Modulation index of the inversion stage
$T_{\alpha}, T_{\beta}, T_0$	Switching time of the inverter voltage vector
$I_{\alpha'}, I_{\beta'}$	Input currents in α - β reference frame
ϕ	air-gap flux

Appendix-G

Ψ_f	Field flux
Ψ_a	Armature flux
I_f	Field current
I_{sa}, I_{sb}	Stator currents in α - β stationary reference frame
I_{sd}, I_{sq}	Stator currents in d-q rotating reference frame
Ψ_{sa}, Ψ_{sb}	Rotor flux linkage
Ψ_{oa}, Ψ_{ob}	Air gap flux linkage
λ	Rotor flux linkage
σ_r	Leakage co-efficient
ω_{rm}	Mechanical speed
ω_{re}	Electrical speed
ω_{sl}	Slip speed
τ_r	Rotor time constant
τ_m	Motor time constant
τ_s	Armature time constant
R_s	Stator resistance
R_r	Rotor resistance
L_s	Stator inductance
L_r	Rotor inductance
L_o	Mutual inductance
P	Number of poles
J	Motor moment of inertia
B	Friction co-efficient

Bibliography

- [1] P.S. Bimbhra, "Power Electronics," Khanna Publisher, New Delhi, 2000.
- [2] B. K. Bose, "Power electronics – A technology review," *Proceedings of IEEE*, vol. 80, no. 8, pp. 1301 – 1304, Aug. 1992.
- [3] J.M.D. Murphy, F.G. Turnbull, "Power Electronics Control of AC Motors," Pergamon Press, Oxford, 1988.
- [4] L. Malesani, L. Rossetto, P. Tenti, and P. Tomasin, "ac/dc/ac pwm converter with reduced energy storage in the dc link," *IEEE Transactions on Industry Applications*, vol. 31, no. 2, pp. 287 – 292, 1995.
- [5] C. Klumpner, M. Liserre and F. Blaabjerg, "Improved control of an active front end adjustable speed drive with a small dc link capacitor under real grid conditions," *Proc. of IEEE Power Electronics Specialists Conference*, pp. 1156 – 1162, 2004.
- [6] Ned Mohan, Tore M. Undeland, William P. Robbins, "Power Electronics Converters, Application and Design," John Wiley & Sons, Inc, 2003.
- [7] A. Maamoun, "Development of cycloconverters," *IEEE Canadian Conference on Electrical and Computer Engineering*, vol. 1, pp. 521 – 524, 2003.

Bibliography

- [8] C. Klumpner and F. Blaabjerg, "A new cost effective multi-drive solution based on a two-stage direct power conversion topology with reduced input current ripple," *Proc. of IEEE Industry Applications Conference*, vol. 1, pp. 444 –452, 2002.
- [9] J.W. Kolar, M. Baumann, F. Schafmeister, and H. Ertl, "Novel tree-phase ac-dc-ac sparse matrix converter," *Proc. of Applied Power Electronics Conference*, vol. 2, pp. 777 – 791, 2002.
- [10] Dorin O. Neacsu, "Power Switching Converters, Medium and High Voltage," CRC Press, New York, 2006.
- [11] M. Venturini, "A new sine wave in, sine wave out converter technique eliminates reactive elements," *Proc. of POWERCON 7*, pp. 310 – 315, 1980.
- [12] L. De Lillo Liliana, "A matrix converter drive system for an aircraft rudder electro-mechanical actuator," *Tech. Rep., PhD thesis, Department of Electrical and Electronics Engineering, University of Nottingham, 2006.*
- [13] P. Wheeler, J. Clare, L. Empringham, M. Apap, and M. Bland, "Matrix converters," *Power Engineering Journal*, vol. 16, no. 6, pp. 273-282, Dec. 2002.
- [14] J. Holtz and U. Boelkens, "Direct frequency converter with sinusoidal line currents for variable speed ac motors," *IEEE Transactions on Industrial Electronics*, vol. 36, no. 4, pp. 475 – 479, November 1989.
- [15] Y. Minari, K. Shinohara, and R. Ueda, "PWM-rectifier/voltage source inverter without dc link components for induction motor drive," *Proc. of Electric Power Applications*, vol. 140, no. 6, pp. 363 – 368, 1993.

Bibliography

- [16] L. Wei and T.A. Lipo, "A novel matrix converter topology with simple commutation," *Proc. of Industry Applications Society Annual Meeting*, vol. 3, pp. 1749– 1754, 2001.
- [17] Bin Wu, "High Power Converters and AC Drives," A John Wiley & Sons, Inc, Publication, 2005.
- [18] P.C. Krause, O. Wasynczuk, et al , "Analysis of Electric Machinery and Drive Systems," 2nd Edition, IEEE Press, New York, 2002.
- [19] P.W. Wheeler, J. Rodriquez, J.C Clare, L. Empringham, and A. Weinstein, "Matrix Converter- a technology review," *IEEE Trans on Industrial Electronics*, vol. 49, No. 2, pp. 276 – 288, 2002.
- [20] C. Klumpner and Fred Blaabjerg, "Modulation Method for a Multiple Drive System based on a Two-Stage Direct Power Conversion Topology with Reduced Input Current Ripple", *IEEE Transactions on Power Electronics*, pp. 922-929, 2005.
- [21] S. Bernet, T. Matsuo and T.A. Lipo, "A matrix converter using reverse blocking NPN-IGBTs and optimised pulse pattern," *Proceedings of IEEE Power Electronic Specialist Conference*, vol. 1, pp. 107 – 113, 1996.
- [22] P. Nielsen, "The Matrix Converter for an Induction Motor Drive," Technical Report, Ph.D. Thesis, Institute of Energy Technology, Aalborg University, Denmark, 1996.
- [23] R.W. Erickson and O. A. Al-Naseem, "A new family of matrix converters," *Proceedings of IEEE Industrial Electronics Conference*, vol. 2, pp. 1515– 520, 2001.

Bibliography

- [24] P. Wheeler and D. Grant, "Optimized input filter design and low loss switching techniques for a practical matrix converter," *Proceedings of Electric Power Applications*, vol. 144, no. 1, pp. 53 – 60, Jan. 1997
- [25] C. Klumpner, P. Nielsen, I. Boldea and F. Blaabjerg, "A new matrix converter motor (mcm) for industry applications," *IEEE Transactions on Industrial Electronics*, vol. 49, pp. 325 – 335, April 2002.
- [26] P. Nielsen, F. Blaabjerg, and J. K. Pedersen, "New protection issues of a matrix converter—Design considerations for adjustable speed drives," *IEEE Trans. Industrial Application*, vol. 35, pp. 1150–1161, Sept./Oct. 1999.
- [27] L. Wei, T.A. Lipo and H. Chan, "Matrix converter topologies with reduced number of switches," *Proceedings of Power Electronic Specialists Conference*, vol. 1, pp 57 – 63, June 2002.
- [28] M.A. Valenzuela, J. Palma, and R. Sanchez, "DSP based intersectional control in multi-drive systems," *Proc. of IEEE Industry Applications Society Annual Meeting*, vol. 1, pp. 471 – 477, 1997.
- [29] P. Thøgersen, F. Blaabjerg, "Adjustable speed drives in the next decade: The next step in industry and academia," *Proc. of PCIM'00, Intelligent Motion*, pp.95-104, 2000.
- [30] Sanshin Kwak, Hamid A. Toliyat, "Design and performance comparisons of two ultidrive systems with unity power factor," *IEEE Trans. on Power Delivery*, vol.20,No.1, January 2005.

Bibliography

- [31] Kumar Dinesh, Wheeler Patrick, Clare Jon, Kim Tai-Woong, "Weight/Volume Effective Multi-Drive System Based on Two-Stage Matrix Converter," *IECON 08, 2008*, p.p. 2782-2787.
- [32] Hoolboom, G.J, Szabados, B, "Nonpolluting automobiles," *IEEE Transaction on vehicular Technology*, Vol. 43, 1994, No. 4, pp. 1136-1144.
- [33] G Gong, M L Heldwein, U Drogenik, J Miniböck, K Mino, J W Kolar, "Comparative Evaluation of Three Phase High Power Factor AC-DC Converter Concepts for Application in Future More Electric Aircraft," *IEEE Transactions on Industrial Electronics*, vol. 52, #3, Jun 2005.
- [34] P Vas: *Vector Control of AC Machines*, Clarendon Press, Oxford 1990.
- [35] Rakesh Parekh, "AC Induction Motor Fundamentals," AN887, MICROCHIP Technology Inc, DS00887A, 2003.
- [36] B. K. Bose, "Modern Power Electronics and AC Drives," Prentice Hall, 2001.
- [37] M Imayavaramban, "Avoiding Regeneration with a Matrix Converter Drive," Technical Report, PhD thesis, Department of Electrical and Electronics Engineering, University of Nottingham, 2008.
- [38] Meng Lee, "Three-level Neutral-point-clamped Matrix Converter Topology," Technical Report, PhD thesis, Department of Electrical and Electronics Engineering, University of Nottingham, 2009.
- [39] Fuji Electric Device Technology, "Fuji IGBT modules application manuals," Feb. 2004.

Bibliography

- [40] Semikron International, "SK60GM123 IGBT Module Datasheet," June 2007.
- [41] Semikron International, "SK35 GD126 ET Three-Phase Inverter Module Datasheet," July 2006.
- [42] Joseph J. Distefano, III, Allen R. Stubberud, and Ivan J. Williams, "Schaum's Outline of Theory and Problems of Feedback and Control Systems," McGraw-Hill Companies, Inc, USA, 1990.
- [43] Richard C. Dorf and Robert H. Bishop, "Modern Control Systems," Prentice-Hall, Inc, New Jersey, USA, 2001.
- [44] Saul Lopez Arevalo, "Matrix Converter for Frequency Changing Power Supply Applications," Technical Report, PhD thesis, Department of Electrical and Electronics Engineering, University of Nottingham, 2008.
- [45] TMS 320C6713 DSK Technical Reference, Spectrum Digital, INC, November 2003.
- [46] P.W.Wheeler, J.C. Clare, L. Empringham, M. Apap, K. Bradley, C. Whitley and G. Towers, "A matrix converter based permanent magnet motor drive for an aircraft actuator system," *Proceedings of IEEE International Electric Machines and Drives Conference*, vol. 2, pp. 1295 – 1300, June 2004.
- [47] Educational DSP, "Dsk6xxxhpi daughtercard," www.educationaldsp.com, 2007.
- [48] STMicroelectronics: AN 2497 Application Notes, "ST10 electric motor control library: Encoder driver," March 2007.

Bibliography

[49] LC Automation, “Incremental encoders - engineering and function principle”.

[50] SICK Sensor Intelligence, “Basics – Incremental Encoders”.

[51] G. Asher, “Induction Motor Control,” Module lecture handout, University of Nottingham, UK.